5-2012

Diatoms as Recorders of Sea Ice in the Bering and Chukchi Seas: Proxy Development and Application

Beth A. Caisse
University of Massachusetts Amherst, bethc@geo.umass.edu

DIATOMS AS RECORDERS OF SEA ICE IN THE BERING AND CHUKCHI SEAS: PROXY DEVELOPMENT AND APPLICATION

A Dissertation Presented

by

BETH E. CAISSIE

Submitted to the Graduate School of the
University of Massachusetts Amherst in partial fulfillment
of the requirements for the degree of

DOCTOR OF PHILOSOPHY

May 2012

Geosciences

DIATOMS AS RECORDERS OF SEA ICE IN THE BERING AND CHUKCHI SEAS: PROXY DEVELOPMENT AND APPLICATION

A Dissertation Presented

by

BETH E. CAISSIE

Approved as to style and content by:

_____
Julie Brigham-Grette, Chair

_____
R. Mark Leckie, Member

_____
Robert M. DeConto, Member

_____
Jacqueline Grebmeier, Additional Member
Chesapeake Biological Lab
University of Maryland Center for Environmental Science
Solomons, MD

_____
Klaus Nüsslein, Outside Member
Microbiology Department

_____
R. Mark Leckie, Department Head
Geosciences Department

FOR ALLIE,

who dreamed of observing Alaska weather

ACKNOWLEDGMENTS

I am indebted to the many people I have leaned on during my time at UMass Amherst. My advisor, Julie Brigham-Grette, provided me with support throughout the entire process and acted as my cheerleader on many occasions. I am grateful for her encouragement to broaden my dissertation and to take part in diverse opportunities. In particular, I appreciate that she connected me with John Barron (USGS) and Connie Sancetta (Lamont-Doherty Earth Observatory, retired) early on. Both of them opened their homes to me as they taught me diatom taxonomy. None of this work would have been possible without their assistance.

I would like to thank Jackie Grebmeier for inviting me to the Bering Sea in 2006 and allowing me to return to UMass with sea ice and surface sediment samples. I am incredibly fortunate to have been invited back for the Healy 0701 and Shell08 cruises. These cruises improved my research by allowing me to see first-hand what was meant by the ice edge, marginal ice zone, and epontic bloom as well as to witness the amazing diversity of the sea ice ecosystem from diatoms to polar bears.

My research expanded further thanks to my participation as a member of the science party of the Integrated Ocean Drilling Program's Bering Sea Expedition 323, led by Christina Ravelo and Kozo Takahashi.

I thank the rest of my committee: Mark Leckie, Rob De Conto, and Klaus Nüsslein. All of them were happy to discuss scientific questions with me and were incredibly patient and understanding of my tendency to push against deadlines.

Successful field seasons were further aided by the expert navigation and support of the captains and crews of the USCGC Healy, R/V Norseman II, and IODP's JOIDES Resolution. There were a few nail-biting moments on all of these expeditions, but I never doubted for a moment that I was in good hands. The science teams aboard the Healy cruises were unbelievably

welcoming of my geological perspective and I would specifically like to thank Lee Cooper, Karen Frey, Jerry McCormick-Ray, Rebecca Pirtle-Levy, and Carleton Ray for introducing me to Bering Sea ecology, chemical oceanography and sea ice. I would like to thank Jamie Smidt, Sarah-Jane Jackett, and Lisa Crowder for the extra effort they put in to ensure that the data from Exp. 323 was as accurate as possible. I would also like to thank my field assistants, Kenna Wilkie and Kinuyo Kanamaru-Shinn for their collaboration at sea and in the lab.

My data interpretation was aided by a community far broader than my committee. I am thankful for the sedimentological expertise of Jon Woodruff and Ivano Aiello (Moss Landing Marine Lab). I am also grateful to Jon for allowing me to add my samples to the queue for his heavily used gamma counter for lead and cesium dating. My understanding of organic geochemistry was expanded with the help of Steve Petsch, Mea Cook, Kenna Wilkie, and Dave Finklestein. Mike Jercinovic has been more than happy to answer my SEM questions, sputter coat samples, and help me obtain the best images possible. I am especially grateful for the open door policy in the Geosciences Department that allowed me to have spontaneous scientific conversations with Ray Bradley, Dave Boutt, Steve Burns, Isla Casteñeda, and Don Wise throughout my time at UMass. Their expertise certainly improved my lab work and data interpretations. Laurie Brown and Chris Condit have made me feel welcome and supported in the department from day one. I would like to extend a big thanks to them for all of their help. Without the two of them, this journey would have been a lot more difficult.

The Quaternary Lab has been a home for me within the department and I feel especially fortunate to share an office with Donna Francis, a colleague who is always happy to advise me on the biological side of things, motivate me with a pep-talk, or let me know when I'm totally off-base. I would also like to thank Christine Brandon, Liam Bevan, Lesleigh Anderson, Kinuyo Kanamaru-Shinn, Tim Cook, Nick Balascio, and Jeremy Wei for help ranging from Matlab, core

splitting, thin sectioning, scientific banter, and poster making. Undergraduates James Witmer, Cassy Ziemba, Anna Lugosh-Ecker, and Marissa Jenko spent countless hours helping to run grain size samples and make quantitative diatom slides. Without their help, I am certain I would still be doing lab work!

The University Health Services Radiology lab allowed me to x-rays several sediment cores. I thank Helen Drake for her enthusiastic and quick analysis of our cores. I am also thankful to have not one, but two amazing resources for technical questions that arose during my field and lab work. Both John Sweeney and Rick Williams worked with me to modify lab and field equipment to optimize collection of sea ice and diatom settling. I spent many hours with each of them discussing the physics of how things work and I am grateful for their willingness to explain things to me (repeatedly).

Several lines of funding made it possible for me to pursue my PhD. I am grateful for the opportunities to teach at Greenfield Community College, Smith College, and UMass Amherst and I thank Lindy Gougeon, Brian Adams, John Brady, Steve Gaurin, and Julie Brigham-Grette for making this possible. In addition, I communicated my research to middle and high school teachers through the STEM Education Institute. I thank Mort Sternheim for offering me a position with the STEM Polar and STEM-RAYS projects and Marie Silver, Rob Snyder, and Holly Hargraves for their guidance as I developed curricula ideas for teachers.

This work was funded by NSF Office of Polar Programs (NSF-OPP, ARC-1023537) and a Post Expedition Award from the Consortium for Ocean Leadership. I am also grateful to have received a Graduate Research Grant and the Howard Award, both from the Geological Society of America. I am honored to have received the Denise Gaudreau Award from the American Quaternary Association and several awards from the UMass Amherst Department of Geosciences.

Finally, I am especially grateful to my family and friends for the support they've given me. These past six years have not always been easy but I have been surrounded by encouragement and assistance. I've been blessed to have wonderful friends nearby to provide comic relief and a shoulder to lean on. I thank Kate Kelly, Marc Liberatore, Erin Klett, Charlie Herbert, Melody Wright, and Kenna Wilkie for all those times that we shared a coffee, got our kids together, headed out on a ski, or spent the afternoon at the river.

We moved back to Massachusetts to be near my family during graduate school and I am grateful for the time we got to spend close to them. I would like to thank my grandmother, Allie, for digging out her long-retired secretarial skills to set up a filing system for my references. Her lively and insightful comments are sorely missed and I dedicate this dissertation to her memory. My family has always been happy to offer child-care to us, especially before deadlines or while I was at sea. I thank my Mom, Janet Caissie-Williams, for imparting to me her belief in the importance of education, her unwavering support, and her willingness to listen. It is such a gift that my son had such a close relationship with his grandmother as a baby and young child. I thank my step-dad, Ricky for introducing me to earth science as kid and for his solid support through this process. I thank my sisters for believing, without a doubt, that I would finish.

Perhaps the most significant debt of gratitude I have is for my partner, Amy Mayer, and our son, Elias Caissie. I hope that some of the passion I feel for Arctic climate has been imparted to Elias, whose unending questions and energy have often been a welcome break from the lab and writing. I want to sincerely thank Amy for so many things too numerous to mention here, but specifically for her willingness to take on far greater than her share of family responsibilities and for putting up with me being away at sea for months at a time. I am excited for our little family of three to begin our next adventure.

ABSTRACT

DIATOMS AS RECORDERS OF SEA ICE IN THE BERING AND CHUKCHI SEAS: PROXY DEVELOPMENT AND APPLICATION

MAY 2012

BETH E. CAISSIE, B.A., HAMPSHIRE COLLEGE

B.S., UNIVERSITY OF ALASKA FAIRBANKS

M.S., UNIVERSITY OF MASSACHUSETTS AMHERST

Ph.D., UNIVERSITY OF MASSACHUSETTS AMHERST

Directed by: Professor Julie Brigham-Grette

The recent, rapid decline in Arctic summer sea ice extent has prompted questions as to the rates and magnitude of previous sea ice decline and the affect of this physical change on ice-related ecosystems. However, satellite data of sea ice only extends back to 1978, and mapped observations of sea ice prior to the 1970s are sparse at best. Inventories of boreal ecosystems are likewise hampered by a paucity of investigations spanning more than the past few decades. Paleoclimate records of sea ice and related primary productivity are thus integral to understanding how sea ice responds to a changing climate. Here I examine modern sedimentation, decadal-scale climate change in the recent past, and centennial- to millennial-scale changes of the past 400 ka using both qualitative and quantitative diatom data in concert with sedimentology and organic geochemistry.

Diatom taxonomy and corresponding ecological affinities are compiled in this study and updated for the Bering Sea region and then used as recorders of past climate changes. In recent decades, the Pacific Decadal Oscillation and the strength of the Aleutian Low are reflected by subtle changes in sediment diatom assemblages at the Bering Sea shelf-slope break. Farther

back in time, the super-interglacial, marine isotope stage (MIS) 11 (428-390 ka), began in Beringia with extreme productivity due to flooding of the Bering Land Bridge. A moisture-driven advance of Beringian glaciers occurred while eustatic sea level was high, and insolation and seasonality both decreased at the global peak of MIS 11. Atlantic/Pacific teleconnections during MIS 11 include a reversal in Bering Strait throughflow at 410 ka and a relationship between North Atlantic Deep Water Formation and Bering Sea productivity. Finally, concentrations of the biomarker-based sea ice proxy, IP_{25}, are compared to sea ice concentration across the Bering and Chukchi seas. Changes in the concentration of IP_{25} in the sediments may be driven by the length of time that the epontic diatom bloom lasts. When combined with a sediment-based proxy for sea surface temperatures, IP_{25} can be used to reconstruct spring ice concentration.

TABLE OF CONTENTS

LIST OF TABLES

LIST OF FIGURES

CHAPTER 1

INTRODUCTION

1.1 Rationale and Statement of Problem

The natural variability of ice extent has been identified as a priority science question [*Murray et al.*, 2010; *SEARCH*, 2005] because the areal extent of summer Arctic sea ice has been decreasing by more than 10% per decade since 1979 [*Serreze et al.*, 2007; *Stroeve et al.*, 2007]. However, satellite data of sea ice only extends back to 1978, and observations of sea ice prior to the 1970s are sparse at best [*Serreze et al.*, 2007]. Paleoclimate records of sea ice during both glacial and interglacial periods are thus integral to understanding how sea ice responds to a changing climate. Documentation of change, even during the very recent past, is critical to advancing our understanding of how sea ice drives and interacts with the climate system. What is needed to evaluate sea ice change in the past is a quantitative proxy that provides estimates of past sea ice duration and does not confuse sea ice with glacial ice or the transport of terrigenous sediments. This dissertation explores sedimentation in the Bering Sea, establishes the correlation between modern diatoms and sea ice extent, looks down-core at how sea ice fluctuates during a previous super-interglacial period through environmental proxies indicative of this change, and provides the first calibration of an organic biomarker proxy for sea ice. Furthermore, this dissertation offers a solid foundation on which to build a diatom-based sea ice proxy for the Bering Sea.

1.2 Sea Ice Proxies

Over the past several decades, a number of proxies have been proposed for reconstructing sea ice conditions in the Polar Regions. Traditionally, diatom (or other microfossil) assemblages were analyzed and the literature mined for the ecological

requirements of individual species. It was assumed that these modern habitats must have been present in the past for the preserved diatoms to thrive. Principal component analysis was used routinely to determine key relationships within assemblages. The derived factors were mapped and related to oceanographic features such as areas of upwelling, high productivity, currents, seasonal sea ice, or cold water [*Sancetta*, 1983; *Sancetta and Robinson*, 1983]. Over time, this method has been refined statistically to create proxies based on transfer functions that relate satellite-derived sea ice conditions to microfossil data such as,

- a circumpolar Arctic database of dinoflagellate-cysts [*de Vernal et al.*, 2005];
- a regional Antarctic database of diatoms [*Crosta et al.*, 1998]; and
- relative percent abundances of *Fragilariopsis* spp. in the Bering Sea [*Caissie et al.*, 2010].

Recently, several additional proxies have been proposed that are based on the presence or absence of certain microfossils or sedimentological or biogeochemical markers of sea ice including,

- ice rafted debris [*Sakamoto et al.*, 2005], especially silt and clay size terrigenous particles [*Davies et al.*, 2009];
- an ostracode that lives symbiotically with an amphipod in perennial sea ice [*Cronin et al.*, 2010]*;*
- benthic foraminifera adapted to grazing on the underside of sea ice [*Polyak*, 2010]; and
- organic biomarkers created by sea ice diatoms [IP_{25}: *Belt et al.*, 2007; *Sharko*, 2010].

Although not all of the above proxies are used together in a single study, individual proxies, such as ice rafted debris, have allowed researchers to hypothesize that sea ice may

have formed in the central Arctic Basin as far back as the mid to late Eocene [*St. John*, 2008]. Although pre-Quaternary Arctic records are sparse, intervals of possible sea ice coverage have been found in sediment cores recovered from the Lomonosov Ridge (IODP Exp 302, the ACEX expedition) and coastal Arctic locations [*Polyak et al.*, 2010 and references therein]. Specifically, pulses of ice rafted debris are found during the late Miocene [*St. John*, 2008], are the first potential evidence of perennial sea ice recorded in the central Arctic Basin at approximately 14 Ma [*Darby*, 2008; *Frank et al.*, 2008]. However, perennial sea ice reconstructions for the past 14 Ma, like that by Darby [2008], are inconsistent with coastal terrestrial records showing that the entire Arctic was largely forested up until nearly 3 Ma [*Polyak et al.*, 2010, and references therein].

While much attention has been placed on reconstructing the presence or absence of sea ice in the Arctic Basin, specifically whether the Arctic Ocean is covered only seasonally or perennially with ice, it may be even more essential to reconstruct fluctuations between open water, seasonal sea ice and perennial ice at the margins of the Arctic Basin if these data are to be used for proxy-model comparisons providing boundary conditions to the climate modeling community. For example, while the ACEX record does not show any changes in perennial sea ice during the Pliocene [*St. John*, 2008], perhaps due to the dissolution of biogenic particles [*Backman et al.*, 2008], the margins of the Arctic Ocean showed major climatic deterioration at 3 Ma punctuated by extreme warm intervals [*Polyak et al.*, 2010].

The Bering and Chukchi seas are ideal recorders of past sea ice variability because of their location as a gateway between the Arctic and North Pacific oceans and because they are currently covered by sea ice seasonally between 0 and 11 months per year. Additionally, the Bering Sea has been called the “silica ocean” due to the presence of high dissolved silica in its deep waters and the dominance of siliceous microorganisms in surface waters [*Honjo*, 1990].

This makes the region particularly well suited to developing proxy reconstructions based on siliceous microfossils.

The recent IODP Expedition 323 to the Bering Sea provided us with a low-resolution summary of past sea ice in the Bering Sea based on relative proportions of sea ice diatoms and dinoflagellates (Figure 1.1) as well as silt-sized and larger terrigenous grains. At the oldest sites on Bowers Ridge, an increase in sea ice is observed at approximately 2.75 Ma and again at 1.8 Ma. The northwest tip of Bowers Ridge, however, shows low sea ice throughout its 1.2 myr record. Two shelf-slope break sites that extend to almost 2 Ma show an increase in sea ice at approximately 1 Ma, while proxies from the two shortest sites, U1339 at Umnak Plateau and U1345 at the shelf-slope break, reflect oscillations in sea ice on glacial-interglacial timescales over the past 500 ka [*Takahashi et al.*, 2011].

Several shorter cores have been recovered in the Bering Sea that span the Quaternary. Proxies from these cores tend to show both fluctuations in sea ice and in sea level on glacial-interglacial timescales [e.g. *Caissie et al.*, 2010; *Katsuki and Takahashi*, 2005; *Sancetta and Robinson*, 1983]. More specifically, Katsuki and Takahashi [2005] generalize that seasonal sea ice expanded south to Bowers Ridge during glacial periods and that the diatom productivity they observe reflects the interplay between sea level rise, changing coastal proximity, a decrease in Alaskan Stream flow, and a deepening of the mixed layer during glacial intervals [*Katsuki and Takahashi*, 2005]. Similarly, at all Expedition 323 sites, low resolution, multi-proxy comparisons show that in general sea ice was low or absent during interglacial periods of the past 5 Ma. This finding is recorded as low proportions of sea ice diatoms, high proportions of open-water diatoms, high proportions of high productivity dinoflagellates, high proportions of low oxygen foraminifera, and an increase in foraminifera-derived sea surface temperatures. In contrast,

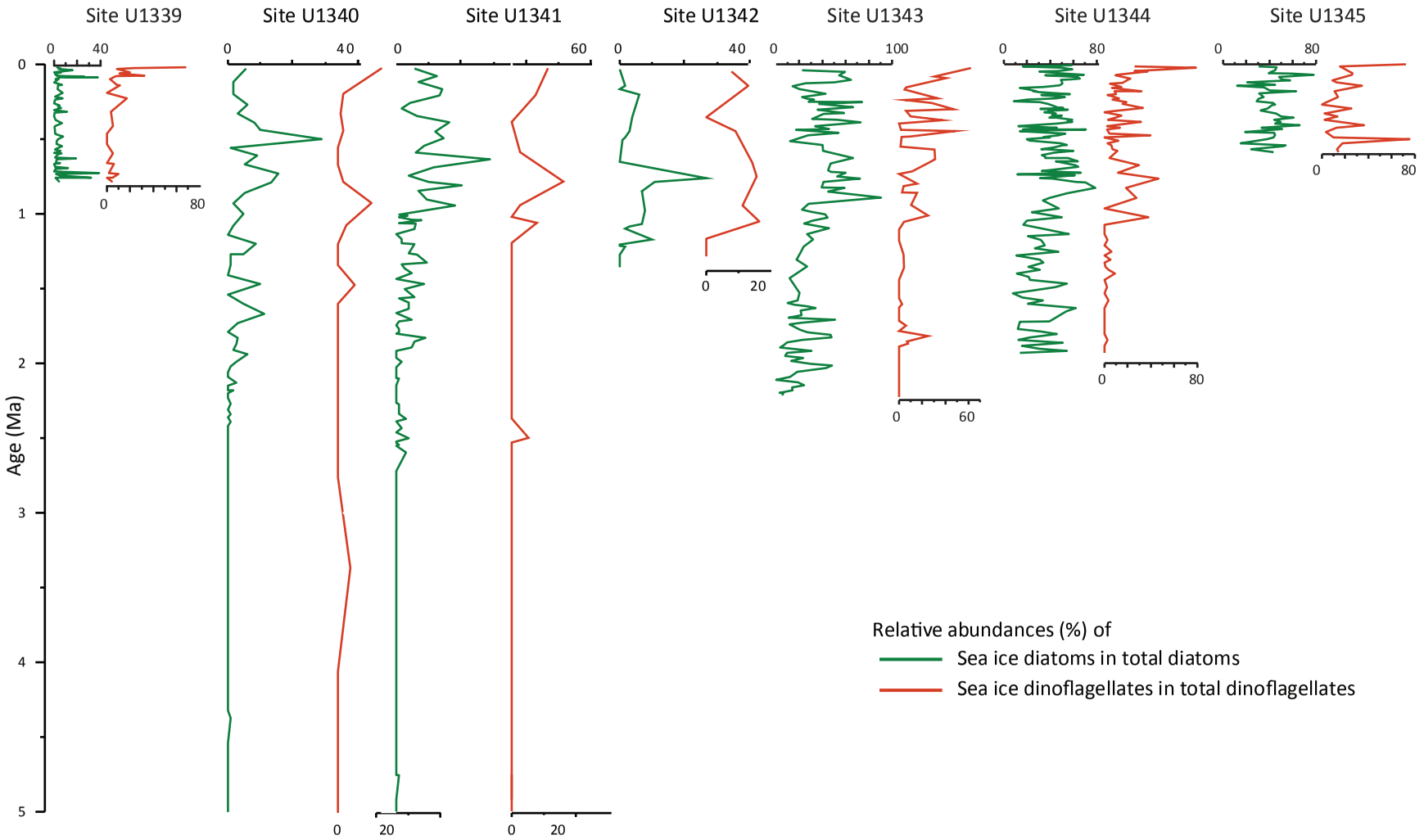

Figure 1.1. Preliminary results from IODP Exp 323 showing the variation in sea ice across the Bering Sea for the past 5 Ma [Takahashi *et al.*, 2011]. Sea ice diatoms include *Thalassiosira antarctica* resting spores, *Thalassiosira hyalina, Bacterosira fragilis, Fragilariopsis cylindrus, Porosira glacialis*, and *Dentonula confervacea*. Sea ice dinoflagellates include only *Islandinium minutum*. Figure modified from Takahashi *et al* [2011].

during glacial periods, calcareous nannofossils decrease and pollen increases at these sites [*Takahashi et al.*, 2011].

These sediment records tell an emerging story of sea ice evolution in the Arctic and more specifically in the Bering and Chukchi seas. What is unknown is:

a) the region-specific, quantitative relationship between a sea ice proxy and annual duration of sea ice;
b) sea ice variability at finer than centennial-scale temporal resolution;
c) sea ice variability at finer than Milankovitch-scale temporal resolution in records older than MIS 5; and
d) the rates at which sea ice retreats and advances, specifically whether it responds gradually or in an abrupt, step-wise fashion to natural climate forcing.

1.3 Dissertation Outline

This dissertation explores the relationship between sediment components, especially diatom assemblages, but also sediment grain size, and an organic biomarker (IP_{25}) and sea ice concentration in the Bering and Chukchi seas. Here I address several of the above topics and document changes in sea surface conditions, with a focus on sea ice, by:

1) analyzing diatom assemblages and diatom accumulation rates across the Bering Sea shelf and comparing them to assemblages from 1969;
2) determining sedimentation rates and the intensity of bioturbation using x-radiographs and lead and cesium isotopes;
3) grouping diatom taxa into environmental niches based on the ecological and statistical literature;

4) analyzing diatom assemblages and grouping taxa down-core in order to reconstruct the sea surface conditions during MIS 11; and
5) using statistical methods to calibrate IP_{25} as a proxy for sea ice concentration in the Bering and Chukchi seas.

The thesis is organized into seven chapters. Chapter One provides a general introduction to sea ice proxies and a history of sea ice in the Arctic followed by a thesis outline. Chapter Two serves as a taxonomic guide to the diatoms observed in the Bering Sea sediments. This chapter is intended to be published as a monograph or "field guide" to Bering Sea diatoms.

The following three chapters are written as manuscripts intended to be submitted for publication in the near future. Chapter Three examines the sediments collected in 1969 and 2006-2007 from four areas of the Bering Sea shelf to see if environmental change observed over the past forty years can be detected. Chapter Four presents the results of a down-core analysis of diatom assemblages and sedimentology deposited during MIS 11 (~425 ka) at the Bering Sea shelf-slope break (IODP Exp. 323 Site U1345). Chapter Five is a statistical analysis of data analyzed by Cecily Sharko and published in her Master's Thesis [*Sharko*, 2010]. This chapter proposes a new calibration of IP_{25}, a biomarker produced by diatoms living in sea ice, to sea ice concentration averaged seasonally over March, April, May, and June. It has been drafted as a manuscript with assistance from co-authors Cecily Sharko Buehler, James J. Kocis, Steven T. Petsch, Julie Brigham-Grette, and Guillaume Massé from the Institut Pierre et Marie Curie.

Chapter Six outlines work in progress and future work that stem from this dissertation. This includes two projects initially proposed as chapters of the dissertation:

1) Diatom Assemblages as a Quantitative Proxy for Sea Ice Duration in the Bering and Chukchi Seas

2) A diatom-based examination of sub-millimeter-scale laminations deposited during the Pliocene at Bowers Ridge, Bering Sea.

Finally, chapter seven summarizes the conclusions drawn from each of the previous chapters.

CHAPTER 2

DIATOMS OF THE BERING SEA SHELF: TAXONOMY AND DISTRIBUTION

2.1 Introduction

This chapter is intended to serve as a "field guide" to the diatoms found in the sediments of the Bering and Chukchi seas. The dominant species in Bering Sea shelf sediments and in older sediments deposited during Marine Isotope Stage 11 (400 ka) at the shelf-slope break are included in this chapter. Each entry includes a summary of the species or genera descriptions. These are previously published formal descriptions compiled with less formal descriptions of species from the literature. What distinguishes this chapter is the region-specific nature of the document, the discussion of ecological niches for each species, and the inclusion of easily searchable tables of morphometric data for major genera. I build on Sancetta's [1982] work by including many sea-ice related species that she did not distinguish, such as the pennate species *Nitzschia frigida* (Figure 2.1) and *Navicula* species, or species that were not yet described in the 1980s (i.e. *Fossula arctica*) and update her [1981] study with new distribution maps.

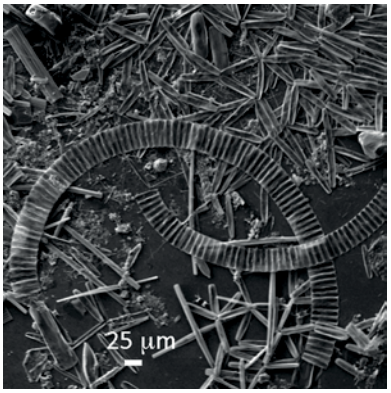

Figure 2.1. Pennate diatoms from the marginal ice zone, including *Fragilariopsis* (ribbons) and *N. frigida* (stars).

A distribution map, light microscope (LM) image, and Scanning Electron Microscope (SEM) image are included for any species that reaches 5% or more of the assemblage at any sample. Other significant species, such as freshwater indicators are also included with summaries of their descriptions and images when possible. Information about the ecological preferences of each taxon is included, when it is known. In addition, the reader is referred to table 4.1 that is included as part of the interpretations in Chapter 4. This table groups the most important species by environmental niche and is compiled from both biological studies and statistical inferences (see Chapter 4 for details). Species are listed on this table under any niche that they have been associated with, but listed in bold type under the most common, or diagnostic niche that they are associated with.

2.2 The Diatom Species of the Bering Sea

2.2.1 *Actinocyclus* Ehrenberg and *Azpeitia* Peragallo species

Both of these genera are members of the family Hemidiscaceae, which has been found in the plankton and also as epiphytes, living attached to plant matter. The main distinguishing characteristic of this family is the pseudonodule, a large circular opening, generally located slightly center-ward of the margin. However, this pseudonodule is commonly difficult to discern in light microscopy. The morphometric data for *Actinocyclus* spp. and *Azpeitia* spp. is included as table 2.1.

2.2.1.1 *Actinocyclus curvatulus* Janisch

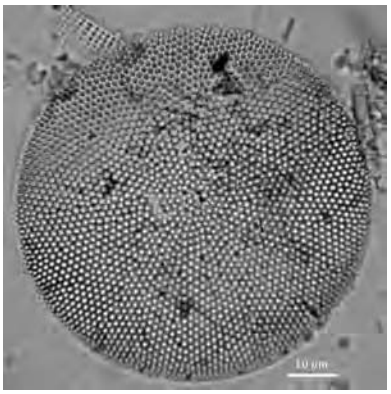

Figure 2.2. LM image of *Actinocyclus curvatulus.*

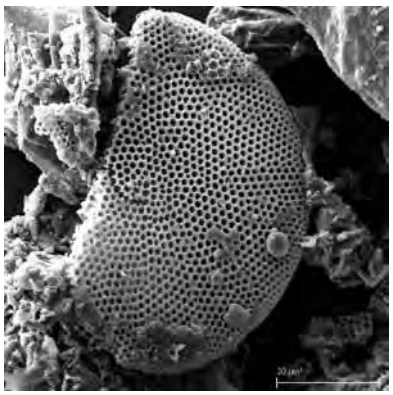

Figure 2.3. SEM image of *Actinocyclus curvatulus.*

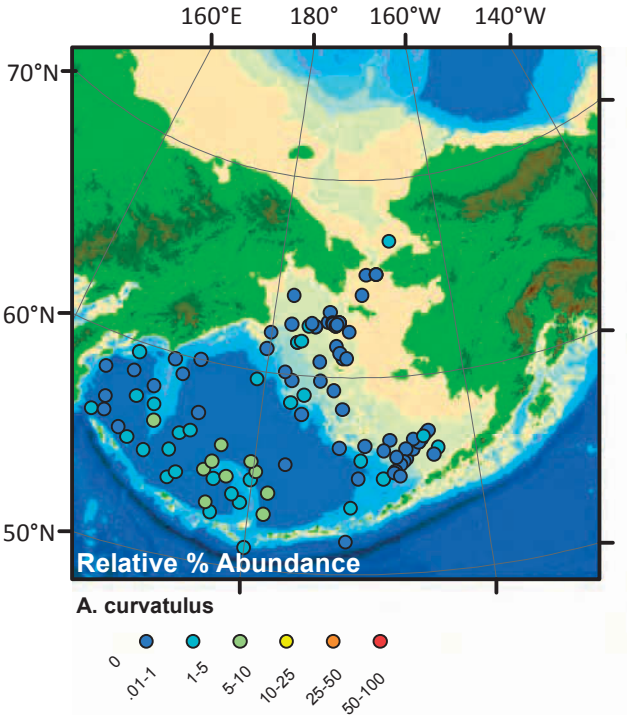

Figure 2.4. Map of *Actinocyclus curvatulus* distribution in the Bering Sea.

This species has been described as a large (~100 µm in diameter), flat, drum shaped valve. There is often a small ring around a "granuliert" center that Sancetta [1982] describes as a slightly dissolved area. The most distinguishing characteristic is the fasciculate arrangement of areolae in clusters that

Table 2.1: Morphometric data for *Actinocyclus* and *Azpeitia* species.

Genus	species	diameter min (µm)	diameter max (µm)	central area	marginal striae per 10 µm min	marginal striae per 10 µm max	processes per 10 µm min	processes per 10 µm max	process type	areolae in 10 µm min at center	areolae in 10 µm max at center	areolae in 10 µm min at margin	areolae in 10 µm max at margin	areolation	pseudonodulus	comments	environmental niche	Reference
Actinocyclus	*curvatulus*	13	160	annulus; sometimes granuliart			12	18	marginal strutted	5	6	8	18	highly fasciculated, curved rows	small, irregular, near mantle	small process at end of the longest row in each fascicle; quincunx arrangement of areolae at margin	found in sea ice; associated with dicothermal species	Hasle and Syvertsen, 1996; Sancetta, 1982
Actinocyclus	*kützingii*	30	70	small annulus	10	12				7	8	7	8	fasciculated with secondary, curved rows	very small, obscure	processes at end of central row of each fascicle; areolae at margin arranged in 2 crossing systems	North Atlantic coastal	Hasle and Syvertsen, 1996
Actinocyclus	*ochotensis*	20	56	small						7	9	4	6		on periphery	large spaces between areolae; areolae may be scattered; areolae become smaller near margin; irregular, outer hyaline ring	pelagic; more common in older sediments	Sancetta, 1982
Azpeitia	*tabularis*	16	70	central process next to a depression			7	12	marginal labiate	6	10	6	10	slightly fasciculated	none	distinct hyaline area at margin	warmer water	Medlin and Priddle, 1990; Sancetta, 1982

sweep out from the center [*Sancetta*, 1982], much like a pinwheel. A small process, with no external tubes or features, is located at the ends of each of the fascicles. Although difficult to see in light microscopy, it is certainly possible. The margin has a quincunx pattern of areolae [*Sancetta*, 1982], however, the margin is often broken off in the sediments. I have found many examples of what looks like *A. curvatulus*, but smaller (~25 µm in diameter). Many questions remain about this species, and it may be that there are several species or varieties included in *A. curvatulus* [*Medlin and Priddle*, 1990]. For this reason I have grouped both large and small varieties into the same taxa.

The pattern of *A. curvatulus* distribution is very similar to that of *Thalassiosira trifulta*, so they are grouped together as indicators of cold, highly stratified, dicothermal water for paleoenvironmental inferences (see table 4.1 for groupings). However, *A. curvatulus* has been found as a member of the plankton blooming near the marginal ice zone [*von Quillfeldt et al.*, 2003].

2.2.1.2 *Actinocyclus ochotensis* Jousé

A. ochotensis is similar to *A. curvatulus*, but it is smaller in diameter (20-56 µm in diameter) and the areolae are widely spaced on the valve face. It is difficult to see the fasciculate pattern of areolation. There is a large, hyaline area in the center

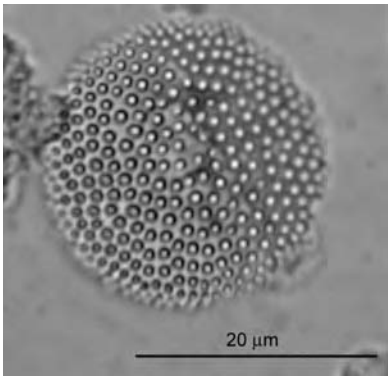

Figure 2.5. LM image of *Actinocyclus ochotensis.*

This is a cold water species and is more prevalent during glacial intervals than interglacials [*Jousé*, 1968]. It is found only over deep water and the spacing between areolae seems to grade into *A. curvatulus*, leading some to propose that there may be an evolutionary relationship between the two *Actinoyclus* species [*Sancetta*, 1982].

2.2.1.3 *Azpeitia tabularis* (Grunow) Fryxell et Sims

Azpeitia species are similar to *Actinocyclus* in that they are flat, drum shaped valves with a pseudonodulus. *A. tabularis* is intermediate in size between *A. curvatulus* and *A. ochotensis*. Areolae are slightly fasciculate or radial. The most distinguishing characteristics are an annulus in

the center with a large, labiate process adjacent to a depression, and a hyaline region between the valve face and the mantle [*Medlin and Priddle*, 1990].

2.2.2 *Bacterosira bathyomphala* (Cleve) Syvertsen et Hasle

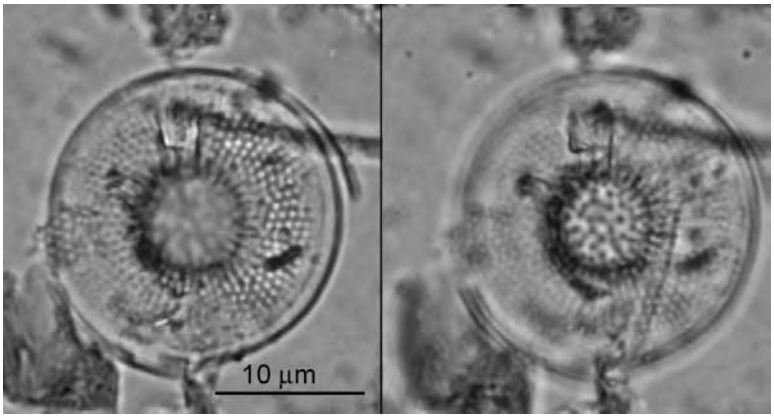

Figure 2.6. LM image of *Bacterosira bathyomphala* at two different focal planes.

B. bathyomphala is the only species in this genus and it is synonymous with *B. fragilis* in older works. There is a varied morphology for this species due to the fact that rarely, vegetative cells and more commonly, heterovalvate resting spores are found in the sediments. The vegetative cell is 18-24 µm in diameter, weakly silicified, and has a cluster of processes in the center and radial ribs (>30 in 10 µm) extending to the margin. At the margin, there is a ring of strutted processes and 1 labiate process [*Hasle and Syvertsen*, 1997]. The hypovalve of the resting spore has a very distinct shape that Sancetta [1982] compared to a sombrero. The center is raised, the middle third is depressed, and the margin rises again like the brim of a hat.

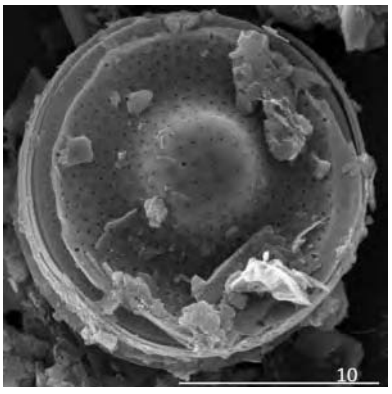

Figure 2.7. SEM image of *Bacterosira bathyomphala.*

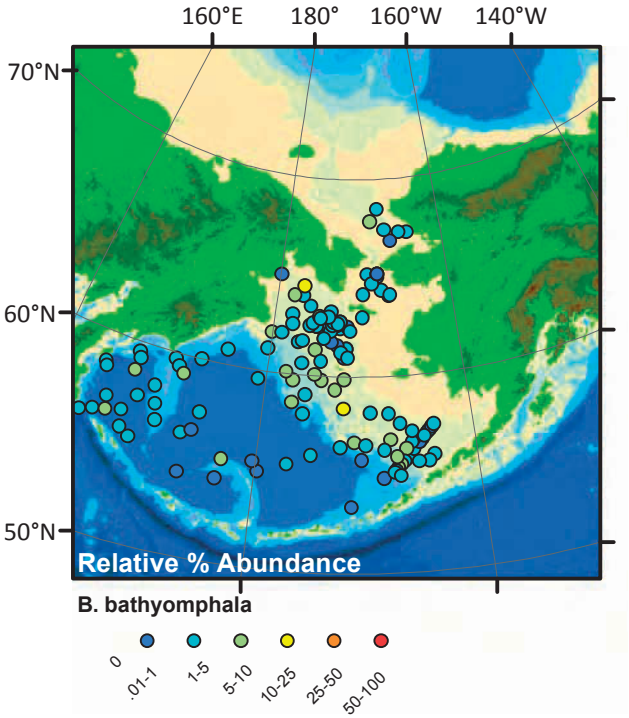

Figure 2.8. Map of *Bacterosira bathyomphala* distribution in the Bering Sea.

Areolae in the central area are often randomly placed and smaller areolae (30 in 10 µm) radiate from the center to the margin [*Medlin and Priddle*, 1990]. These are sometimes not discernable in light microscopy. The epivalve is similar to the hypovalve, but flattened [*Hasle and Syvertsen*, 1997].

B. bathyomphala is found in low abundances in sediment assemblages underlying the seasonal sea-ice zone [*Kazarina and Yushina*, 1999] and is a member of the marginal ice zone flora [*von Quillfeldt et al.*, 2003].

2.2.3 *Hyalochaete Chaetoceros* Ehrenberg *spora*

Considerable variation exists in these common resting spores and unfortunately, the species of *Chaetoceros* can only be definitively identified if the vegetative cell is present because many species make more than one type of resting spore and resting spores of different species are sometimes indistinguishable. Because vegetative cells (Figure 2.10) are not preserved in the sediments, I have chosen to classify *Chaetoceros* RS by their morphology using Suto's morphotaxonomy. The five most common morphotaxa are described below. The morphotaxa are also sometimes difficult to distinguish if only one valve is present because many of the morphotaxa are heterovalvate

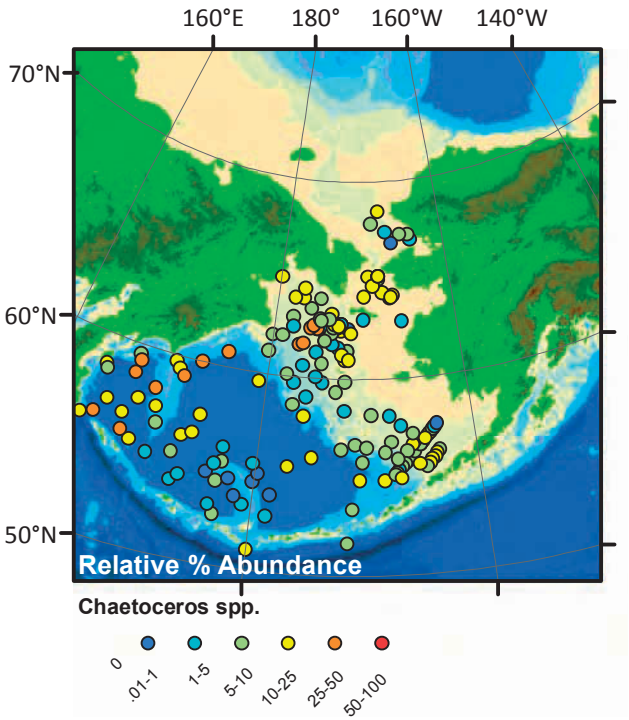

Figure 2.9. Map of *Chaetoceros* RS distribution in the Bering Sea.

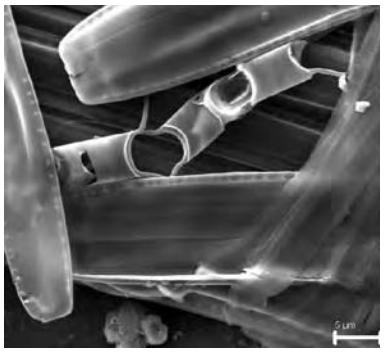

Figure 2.10. SEM image of *Chaetoceros* cell that contains a resting spore. The pennate diatoms around it are *Nitzschia frigida.* This sample was collected in sea ice.

(the hypovalve and epivalve have different morphologies). In cases when a definitive morphotaxa could not be determined, I classified the resting spore as simply *Chaetoceros* sp. RS.

Chaetoceros species are commonly associated with both coastal and open-ocean upwelling [*Lopes et al.*, 2006] or highly productive waters that contain ample amounts of silica [*Kazarina and Yushina*, 1999; *Sancetta*, 1982]. In the North Pacific, *Chaetoceros* found along the coast are associated with summer or fall productivity, but in the open ocean, they're associated with high annual nutrient concentrations [*Lopes et al.*, 2006]. Sancetta [1982] attributes the absence of resting spores in sandy sediments to transport by winnowing. Two *Chaetoceros* species have been found in the marginal ice zone bloom, *C. socialis* (Figure 2.X), and *C. furcellatus.* In fact, the former is one of the most common species found in marginal ice blooms. Further complicating identification, the resting spores of *C. socialis* can be assigned to the morphotaxa *Xanthiopyxis, Gemellodiscus,* or *Vallodiscus. C. furcellatus* resting spores are also assigned to *Gemellodiscus. C. furcellatus* is identifiable if the paired frustules and setae are present [e.g. *Onodera and Takahashi*, 2007], however, this is rare in the sediments. Detailed investigations about *Chaetoceros* RS relationships with environmental variables in the Bering Sea have not been undertaken.

2.2.3.1 Morphotaxa *Dispinodiscus* Suto

Oval to elliptical, generally featureless spore (occasionally the valve face has veins covering it). Epivalve and hypovalve sometimes have different morphologies ranging from flat, to domed or with 2 humps. The defining characteristic is the presence of two small spines near each apex [*Suto*, 2004a].

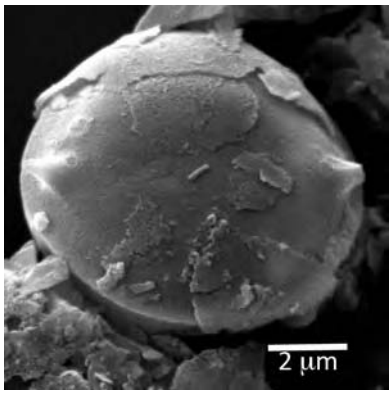

Figure 2.11. SEM image of *Dispinodiscus*. Note, the second spine is has been broken and the spot where the spines attach is under the spore.

2.2.3.2 Morphotaxa *Gemellodiscus* Suto

Gemellodiscus resting spores are circular to oval and generally occur in pairs, though this is not always obvious in the sediments. The valves can be hyaline or covered with spines, but the defining characteristics are long setae extending from the apices (180° apart). These setae

are often broken in the sediments. This is unfortunate because species distinctions are based partly on whether or not these setae are branching, straight, curve back around to overlap one another, or cross and attach to a paired frustule. In girdle-view, the mantle is wide, hyaline, and distinct, often extending above the top of the valve on the apices [*Suto*, 2004c].

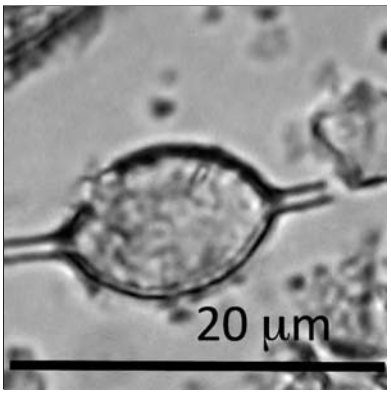

Figure 2.12. LM image of *Gemellodiscus.*

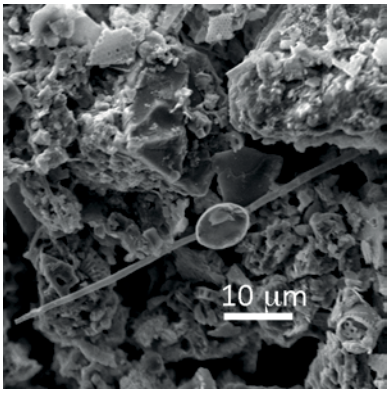

Figure 2.13. SEM image of *Gemellodiscus.*

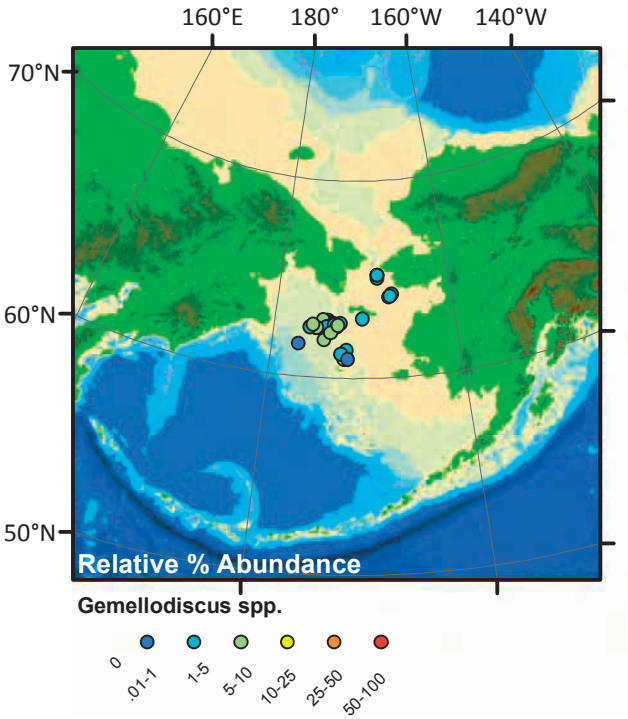

Figure 2.14. Map of *Gemellodiscus* distribution in the Bering Sea.

2.2.3.3 Morphotaxa *Syndendrium* Ehrenberg

Syndendrium is heterovalvate with two or more highly branching processes in the center of the epivalve. In contrast, the hypovalve is generally hyaline with a single ring of puncta around the margin. In some species, the hypovalve also has branching processes. *Syndendrium* was only identified if the processes are seen [*Suto*, 2005b]

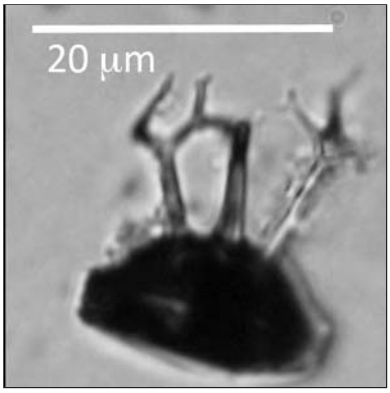

Figure 2.15. LM image of *Syndendrium.*

2.2.3.4 Morphotaxa *Vallodiscus* Suto

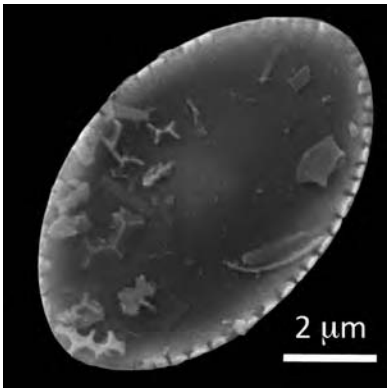

Figure 2.16. SEM image of *Vallodiscus.*

Vallodiscus spores are flat, oval to elliptical, often featureless valves in Bering Sea sediments. They are distinguished by a ring of spines or veins around the margin of the spore. Sometimes the veins branch towards the valve center, but the center remains hyaline [*Suto*, 2005a].

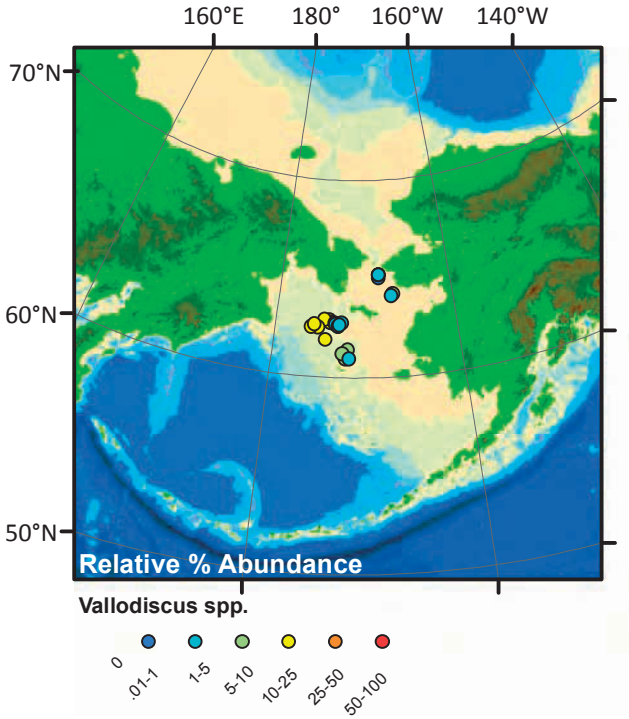

Figure 2.17. Map of *Vallodiscus* distribution in the Bering Sea.

2.2.3.5 Morphotaxa *Xanthiopyxis* Suto

Xanthiopyxis spores occur in many different shapes from round to oval or elliptical; they can be narrow or broad. The defining characteristic is that the valve face is covered by many spines, bristles, or knobs. The mantle and the hypovalve also often contain spines or knobs, but both of these can also be hyaline [*Suto*, 2004b]. Hyaline hypovalves were categorized as *Chaetoceros* sp. RS.

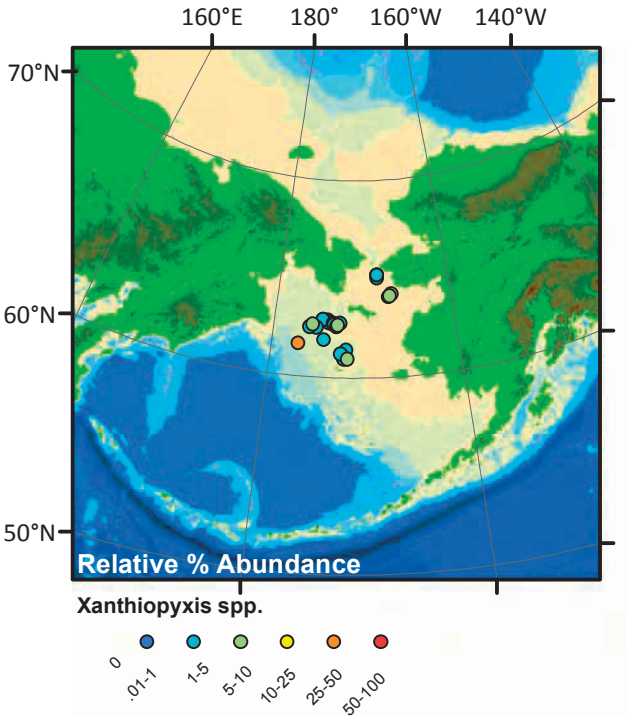

Figure 2.18. Map of *Xanthiopyxis* distribution in the Bering Sea.

2.2.4 *Coscinodiscus* Ehrenberg

Three species of *Coscinodiscus* are found in Bering Sea sediments. None of them occur in high numbers in modern sediments, but down-core relative percentages of these species can be quite large (~50%: [*Sancetta and Silvestri*, 1986]). *Coscinodiscus* spp. are often classified as members of the fall plankton [*Takahashi et al.*, 2002], and the various species have differing temperature preferences [*Sancetta*, 1987]. *C. oculis-iridis* was found associated with fall ice growth [*Gran*, 1904]. There is concern that when *Coscinodiscus* dominates the assemblage either diatom dissolution is great or winnowing was sorting sediments and removing the smaller species [*Kazarina and Yushina*, 1999; *Sancetta*, 1982]. See table 2.2 for morphometric characteristics of the three species found in the Bering Sea.

2.2.4.1 *Coscinodiscus marginatus* Ehrenberg

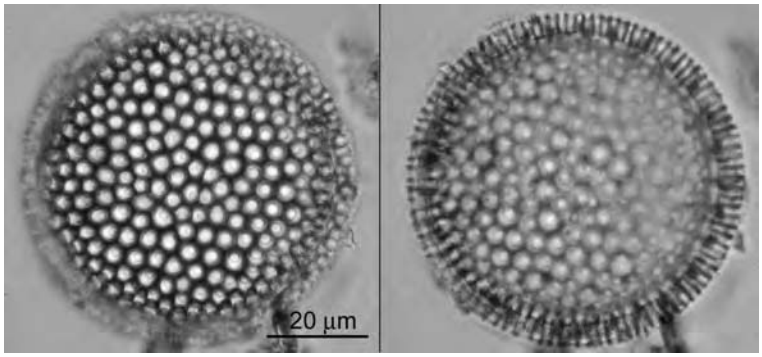

Figure 2.19. LM image of *Coscinodiscus marginatus* in 2 different focal planes.

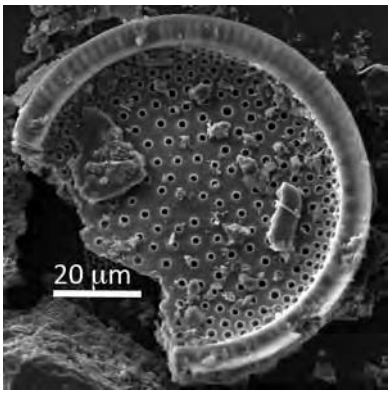

Figure 2.20. SEM image of the interior of *Coscinodiscus marginatus.*

C. marginatus is a coarsely silicified, nearly flat valve. Larger specimens are sometimes depressed in the center. The edges of the valve slopes steeply down towards the margin, which is also flat. This distinctive margin appears striated (though the striations are simply elongated areolae) and is quite wide (up to 4 µm) margin. Areolae have an irregular, radial pattern on the valve face and decrease in size towards the margin. There are no processes visible with light microscopy [*Sancetta*, 1987].

C. marginatus is a member of the temperate zone plankton of the North Pacific (Aizawa et al. 2005), but sediment assemblages have associated this species with the North Boreal Zone

Table 2.2: Morphometric data for *Coscinodiscus* species.

Species	cell shape	cingula	cingula width min	cingula width max	cingula rim edge min	cingula rim edge max	cingula end edge min	cingula end edge max	Central Area	Min Diameter	Max Diameter	height	Areolae shape	Areaolation pattern 1	Areaolation pattern 2	valve center min	valve center max	valve middle third min	valve middle third max	valve mantle min	valve mantle max
Coscinodiscus marginatus	flat/slightly convex; steeply sloping/perpendicular mantle; may be slightly depressed in center	broad, rectangular bands; assymetrical (like canoe upside down)	12	24	3	5	5	8		35	145	10	loculate polygons with "ring of faint poroids" sometimes on inside	irregular radial rows		2	2			3	3
Coscinodiscus radiatus	flat, slopes only in near mantle								may have small hyaline central area (larger forms)	13	100		loculate hexagons w/internal circular foramina; no evidence of velum	radial rows	radial rows less obvious in small specimens	4	5			6	8
Coscinodiscus oculis-iridis	depressed in central half	broad rectangular bands	15	25	4	5	4	8	central rosette of enlarged, elongate areolae (Rarely seen; 10 um wide)	105	180	~20	loculate hexagons w/internal circular foramina; no evidence of velum	radial rows	secondary spiral rows	2	3	1	2	3	3

Table 2.2 continued

Species	areolae comments	margin width min	margin width max	marginal proc comments	strutted processes on valve face	other distinctive features	distribution in N. Pacific	Key distinguishing feature	Reference
Coscinodiscus marginatus		4	6	barely visible, in oblique view, ring of small pores seen among mantle areolae		areolae become elongate near mantle and look like coarse radial striae	late fall in Pacific; common in Gulf of AK	MARGINAL BAND	Sancetta 1987
Coscinodiscus radiatus	areolae may increase in size outward, then decrease significantly at margin	1	2		scattered, in no pattern on small valves (fewer present); at ends of short radial rows on larger valves	areolae elongate near mantle	subtropical gyre	PROCESSES	Sancetta 1987
Coscinodiscus oculis-iridis	areolae increase in size outward, then decrease in outer 1/3 of valve; on mantle areolae arranged in quincunx rows, 3-4 deep			not discerned, in oblique view, ring of small pores seen on mantle above marginal areolae; 1 in 10 um			rare, but present in N Pac and Bering		Sancetta 1987

(Jousé 1968) or areas of high primary productivity (Kazarina 1999). There is some evidence that *C. marginatus* relative percent abundances fluctuate widely with glacial-interglacial cycles [*Sancetta and Silvestri*, 1986].

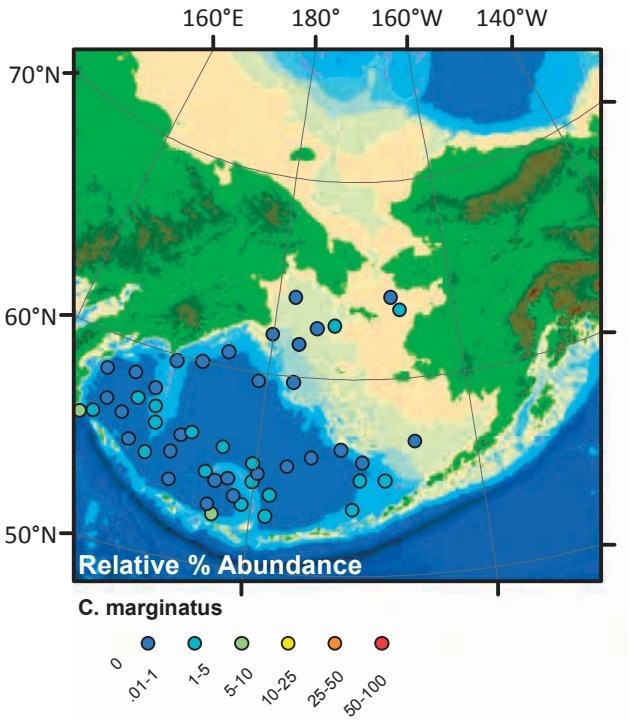

Figure 2.21. Map of *C. marginatus* distribution in the Bering Sea.

2.2.5 *Delphineis* Andrews and *Rhaphoneis* Ehrenberg species

Both of these pennate genera are benthic and are commonly found attached to sand grains within surface and down-core sediments. Both have flat valves that are short in girdle view and broad in valve view. Differences between the genera stem from the characteristics of the sternum (narrow for *Rhaphoneis* and prominent for *Delphineis*). The sternum in *Delphineis* is clear and often enlarges near the apices. In *Rhaphoneis*, uniseriate striae radiate from the narrow sternum. *Rhaphoneis* also has characteristic clusters of small pores at the apices, while *Delphineis* has only 2 pores and a process at each apex. *Rhaphoneis,* in contrast, has a process located between each apex and the valve face [*Medlin and Priddle*, 1990]. See table 2.3 for morphometric data.

2.2.5.1 *Delphineis kippae* Sancetta

D. kippae is relatively coarsely silicified, and the lanceolate outline with rounded capitate apices is distinctive. It has a wide sternum with 4-5 round pores that make up each parallel striae on the valve face. Fewer pores in each striae are present at the apices [*Sancetta*, 1982].

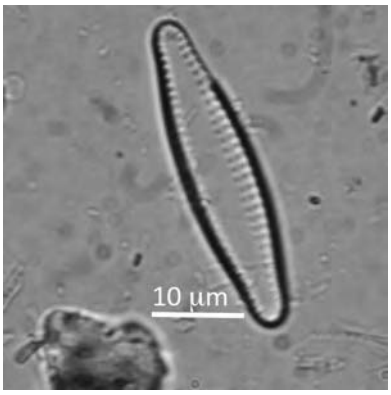

Figure 2.22. LM image of *Delphineis kippae.*

Table 2.3: Morphometric data for *Delphineis* and *Rhaphoneis* species.

Species	Valve shape	Shape of apices	Apical Axis (µm) min	Apical Axis (µm) max	Transapical Axis (µm) min	Transapical Axis (µm) max	Areolae in 10 µm min	Areolae in 10 µm max	Striae in 10 µm min	Striae in 10 µm max	Comments	Reference
Delphineis kippae	elliptical lanceolate	rounded, capitate	30	66	8	9	4	5	10	11	striae curve slightly toward apices; radial at apices; striae in pairs across hyaline axial area	Sancetta, 1982
Delphineis surirella	circular to linear-elliptic or lancet	bluntly rounded	17	53	8	25	7	8	7	12	striae perpendicular to central line; areolae in slightly undulating rows	Hasle and Syvertsen, 1996
Rhaphoneis amphiceros	circular to linear-elliptic	drawn-out/capitate	20	100	18	25			6	7		Hasle and Syvertsen, 1996

2.2.5.2 *Delphineis surirella* (Ehrenberg) G.W. Andrews

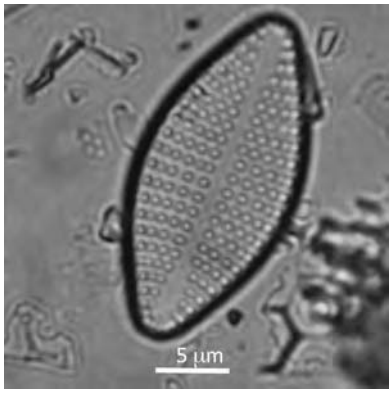

Figure 2.23. LM image of *Delphineis surirella.*

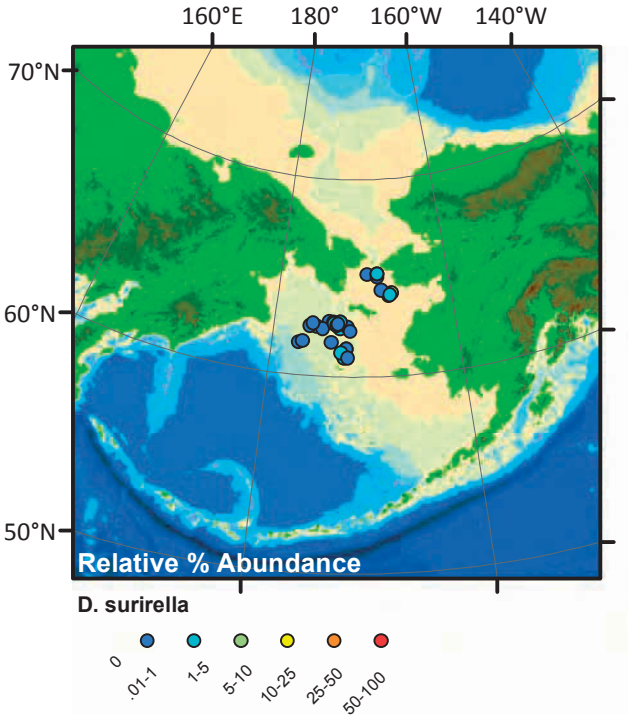

Figure 2.24. Map of *D. surirella* distribution in the Bering Sea.

This is the most common *Delphineis* species found in the Bering Sea surface sediments. This flat, drum shaped frustules has slightly radial uniseriate striae. The sternum is wide, but often has some variability in width between the central area and midpoints of the valve face [*Tomas*, 1996].

2.2.6 *Fossula arctica* Hasle, Syvertsen, et von Quillfeldt

Like *D. kippae, the Fossula arctica* valve is linear to lanceolate with capitate ends. However, it is much more lightly silicified than *D. kippae.* The striae are closer together than in *D. kippae*. Striae range from parallel to slightly radiate at the apices. A very distinct labiate process is found near the epex. This is very clear under the light microscope [*von Quillfeldt*, 2001].

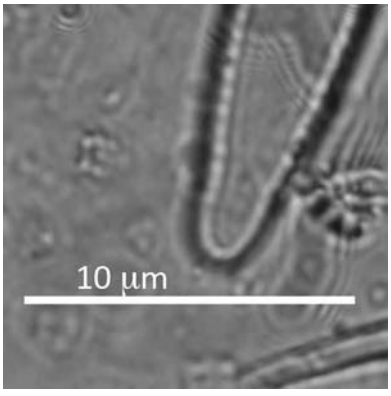

Figure 2.25. LM image of *Fossula arctica.*

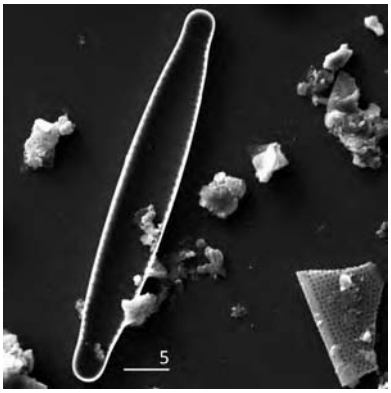

Figure 2.26. SEM image of *Fossula arctica.*

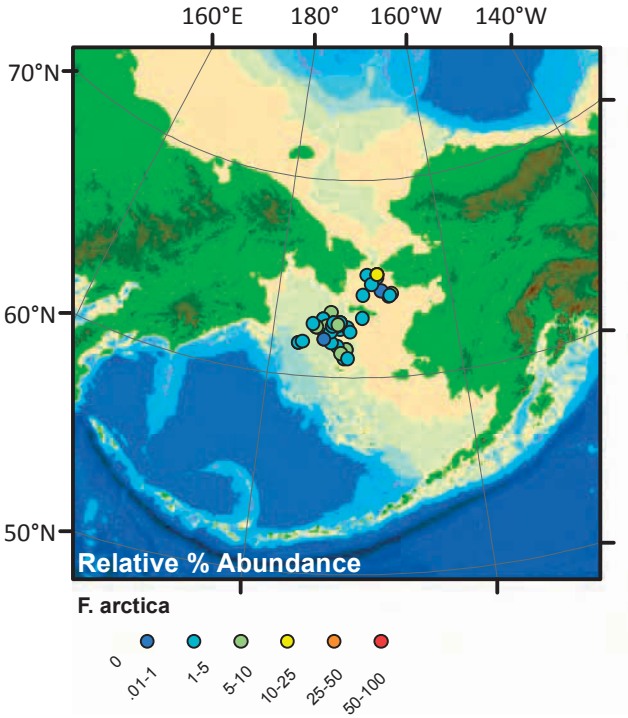

Figure 2.27. Map of *F. arctica* distribution in the Bering Sea.

2.2.7 *Fragilariopsis* Hustedt in Schmidt

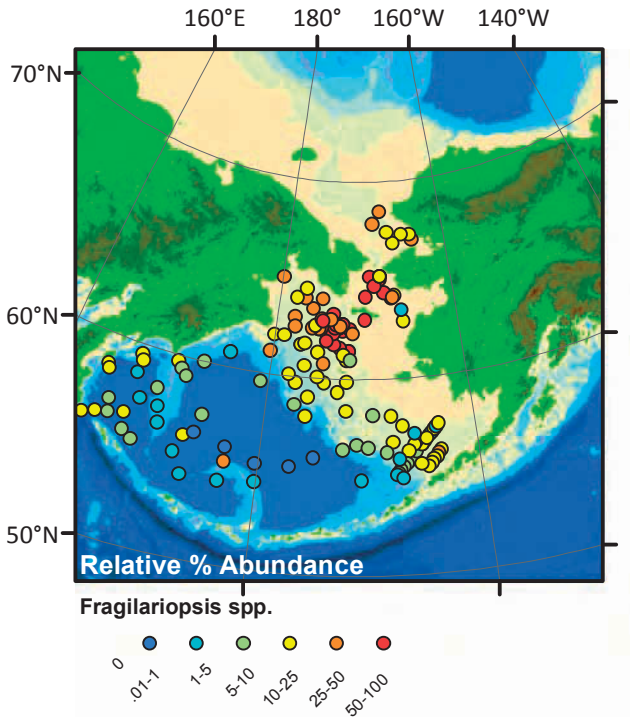

Figure 2.28. Map of *Fragilariopsis* spp. distribution in the Bering Sea.

Fragilariopsis is a pennate genus whose raphe is located in a marginal canal. It forms ribbon colonies and resting spores during various points in its life cycle. Distinguishing characteristics include size and shape of the valve, the presence or absence of a central nodule, and the distribution of fibulae (pore-like structures located along the canal raphe), striae (arrangement of poroids perpendicular to valve length), and poroids (small pores that make up striae) [*Lundholm and Hasle*, 2010].

Fragilariopsis is one of the most abundant species in the marginal ice bloom [*von Quillfeldt et al.*, 2003] and a significant contributor to sediment assemblages. High relative percentages of *Fragilariopsis* spp. have been widely used as a qualitative proxy for sea ice duration, especially in the Bering Sea [*Caissie et al.*, 2010; *Katsuki and Takahashi*, 2005; *Sancetta and Robinson*, 1983]. At least six species of *Fragilariopsis* are found in Bering Sea sediments [*Lundholm and Hasle*, 2010]. These species have slightly different temperature requirements and some are more likely to be found associated with sea ice than others [*Von Quillfeldt*, 2004], but previous work has generally grouped all *Fragilariopsis* species together. Separating these species may improve diatom-based sea ice proxies.

The two most common *Fragilariopsis* species are described below and a table summarizing the morphometric parameters of the other *Fragilariopsis* species found in the Bering Sea is included as table 2.4.

2.2.7.1 *Fragilariopsis cylindrus* (Grunow) Krieger

F. cylindrus is distinguished by its straight, parallel sides and round (almost semi-circular) apices. Striae are parallel and run the full width of the valve. They are made of a mesh of closely spaced poroids. The apices have ribs that are at an oblique angle to the striae (the striae curve around at the ends of the valves), but this feature is sometimes hard to see. This species does not have a central nodule [*Lundholm and Hasle*, 2008; *Sancetta*, 1982; *Tomas*, 1996; *Witkowski et al.*, 2000].

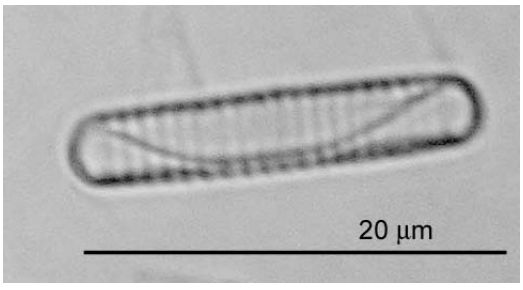

Figure 2.29. LM image of *Fragilariopsis cylindrus.*

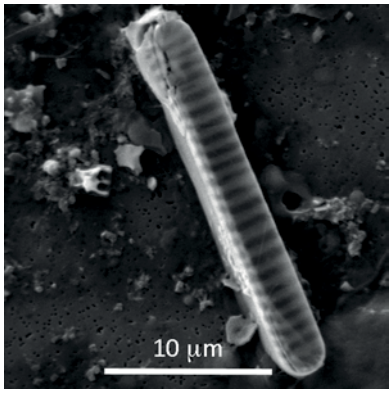

Figure 2.30. SEM image of *Fragilariopsis cylindrus.*

Table 2.4: Morphometric data for *Fragilariopsis* species.

species	valve shape	central nodule	valve width min (µm)	width max	width mean	length min (µm)	length max	length mean	interstriae in 10 µm min	interstriae max	interstriae mean	fibulae in 10 µm min	fibulae max	fibulae mean
Fragilariopsis atlantica	linear-lanceolate, broadly rounded ends, weak heteropolar	yes, wide central interspace w/central nodule, 3 striae wide. Middle striae often widens towards central nodule. In larger spp, central nodule is slightly displaced towards broader end, making valve heteropolar.	7	8	8	20	42	29	18	22	20	as interstriae		
Fragilariopsis bjoernoyaensis		no	2	3		5	8		24	30				28
Fragilariopsis cylindroformis	varies according to length: linear-oblong to elliptical to subcircular				2	3	13							
Fragilariopsis cylindrus	isopolar, straight, parallel margins, rounded apices	no	2	4	3	5	74	20	13	18	15			
Fragilariopsis nana	isopolar, straight, parallel margins, rounded apices	no	1	2	2	4	16	9	14	20	16			
Fragilariopsis oceanica	lanceolate-elliptical; isopolar	yes	5	8	6	9	43	20	12	18	15	12	16	14

Table 2.4 continued

species	rows of poroids	poroids in 10 µm min	poroids max	poroids mean	poroid structure	striae in valvocopula in 10 µm min	striae max	striae mean	stria structure of valvocopula (width x length)	comments	Reference
Fragilariopsis atlantica		29.5	55	37.7	poroids split in 2 sectors	nd	nd	nd	nd	striated valvocopula; The smaller ones are elliptical with obtuse ends; whereas, the larger ones are more linear with one end a little more pointed than the other	Lundholm and Hasle, 2010
Fragilariopsis bjoernoyaensis											Witkowski et al 2000
Fragilariopsis cylindroformis											Hasle & Booth 1984
Fragilariopsis cylindrus	2	50	60	52		39	40	40			Lundholm and Hasle, 2008
Fragilariopsis nana	2-3	60	80	68		nd	nd	nd			Lundholm and Hasle, 2008
Fragilariopsis oceanica		scattered	scattered	scattered	simple	19	28	24	2 parts: proximal 1, distal 1	striated valvocopula	Lundholm and Hasle, 2010

Table 2.4 continued

species	valve shape	central nodule	valve width min (µm)	width max	width mean	length min (µm)	length max	length mean	interstriae in 10 µm min	interstriae max	interstriae mean	fibulae in 10 µm min	fibulae max	fibulae mean
Fragilariopsis pacifica	linear-lanceolate, heteropolar, long narrrow part pointed	yes, seen in LM, but wide space between 2 middle fibulae	7	8	7	27	62	40	16	20	18	as interstriae		
Fragilariopsis pseudonana		no	4	5		4	20		18	22		as interstriae		
Fragilariopsis reginae-jahniae	linear-lanceolate-elliptical, indented at central nodule; isopolar	yes, valve indentation	4	6	5	20	84	43	10	16	13	10	16	12

Table 2.4 continued

species	rows of poroids	poroids in 10 µm min	poroids max	poroids mean	poroid structure	striae in valvocopula in 10 µm min	striae max	striae mean	stria structure of valvocopula (width x length)	comments	Reference
Fragilariopsis pacifica		28.5	35.4	31.4	poroids split in 2 sectors	21	28	24	1 row of striae: 1 2 x 3 5	striated valvocopula	Lundholm and Hasle, 2010
Fragilariopsis pseudonana											Medlin and Priddle, 1990
Fragilariopsis reginae-jahniae		scattered	scattered	scattered	simple	20	26	23	1 row of striae: 2 4 x 2 4 and an unperforated part	striated valvocopula	Lundholm and Hasle, 2010

2.2.7.2 *Fragilariopsis oceanica* (Cleve) Hasle

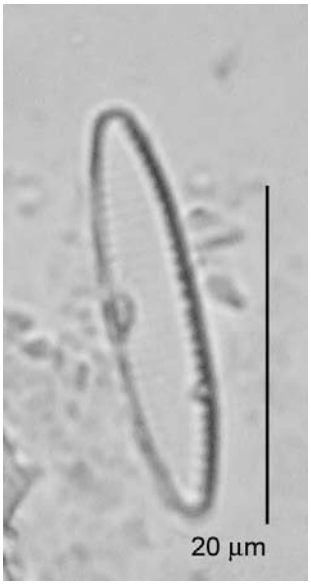

Figure 2.31. LM image of *Fragilariopsis oceanica.*

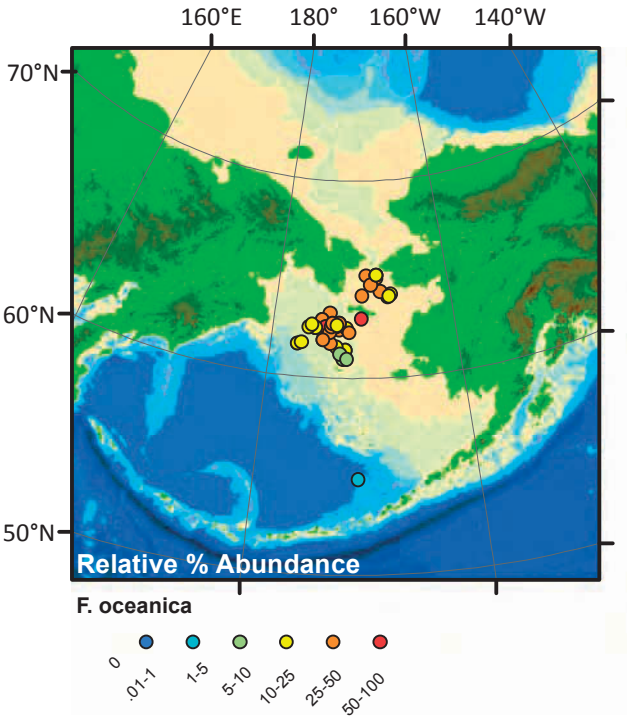

Figure 2.34. Map of *F. oceanica* distribution in the Bering Sea.

Figure 2.32. SEM image of *Fragilariopsis oceanica.*

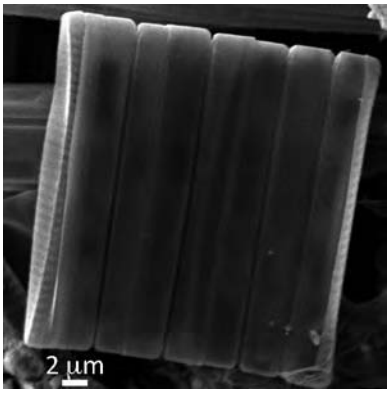

Figure 2.33. SEM image of *Fragilariopsis oceanica* in girdle view.

F. oceanica can be distinguished from *F. cylindrus* by its shape: lanceolate to elliptical. Striae are parallel and run across the full width of the valve, but the poroids that make up the striae are scattered. *F. oceanica* also has a central nodule [*Lundholm and Hasle*, 2010; *Sancetta*, 1982].

2.2.8 *Melosira sol* Dickie

This flat, colony-forming diatom is heavily silicified and commonly bi-layered. The outer layer has radial lamellae that reach the margins, but do not extend all the way to the center of the valve. The inner layer simply contains radial puncta (though this feature is rarely seen). This species tends to be slightly larger (30-96 µm) than *P. sulcata*, but its diameter overlaps largely with *P. sulcata* [*Sancetta*, 1982].

Melosira as a genus has not been extensively studied and very little is known about the true taxonomy of this species. Several other *Melosira* species have been transferred to *Paralia* recently [*Crawford et al.*, 1990]. Its range overlaps with that of *P. sulcata* [*Sancetta*, 1982] and I suspect that this taxon in the Bering Sea is actually a variation or valve type of *P. sulcata*. However, I have separated *Melosira* from *P. sulcata* by valves whose lamellae extend all the way to the margin and which are much more finely spaced than the lamellae in *P. sulcata*.

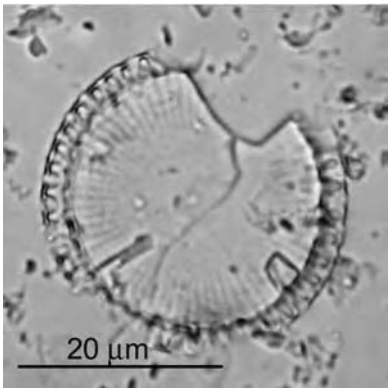

Figure 2.35. LM image of *Melosira sol.*

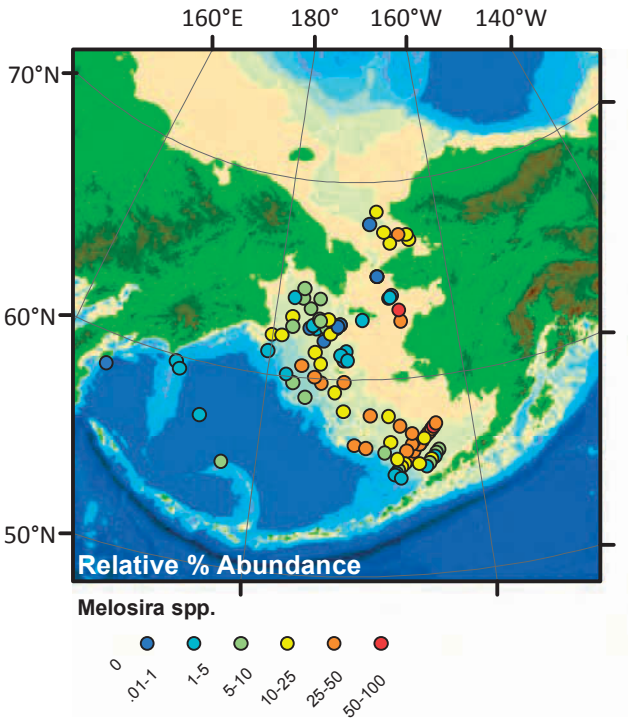

Figure 2.36 Map of *Melosira* species distribution in the Bering Sea.

2.2.9 Naviculoid Species

Diatoms in the pennate family Naviculaceae are quite common in Bering Sea sediments and can be distinguished by the presence of a raphe on both valves that is not subtended by fibulae [*Medlin and Priddle*, 1990]. This is an extremely diverse group that can be identified to the species level (or even finer) in many cases. *Pinnularia quadratarea* is a diverse species with many varieties (see Figures 2.38-2.40). I did not distinguish between varieties. Several of the most common species in the Naviculaceae family are pictured here (Figures 2.37-2.43. Detailed morphometric data can be found in table 2.5.

Figure 2.37. SEM image of *Haslea* sp. and *Navicula* sp. 2 [from *Sancetta,* 1982]

Figure 2.38. SEM image of *Pinnularia quadratarea*

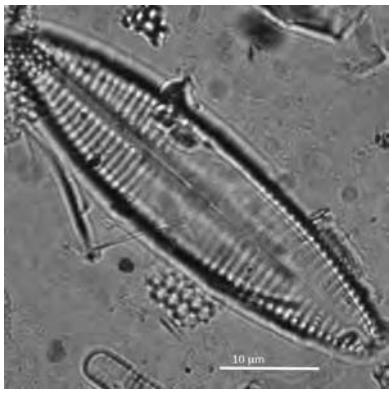

Figure 2.39. LM image of *Pinnularia quadratarea.*

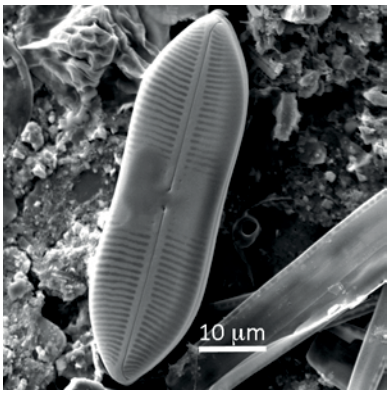

Figure 2.40. SEM image of *Pinnularia quadratarea.*

Figure 2.41. LM image of *Navicula distans*

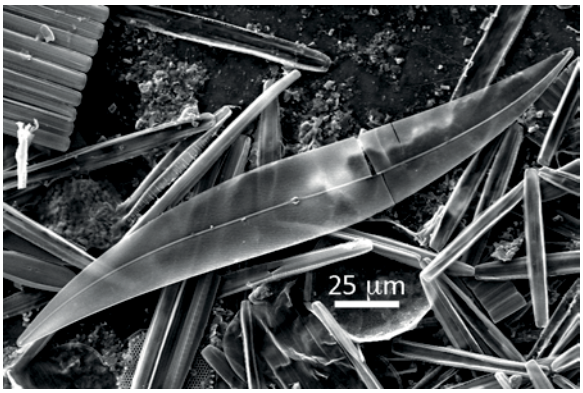

Figure 2.42. SEM image of *Pleurosigma stuxbergii*.

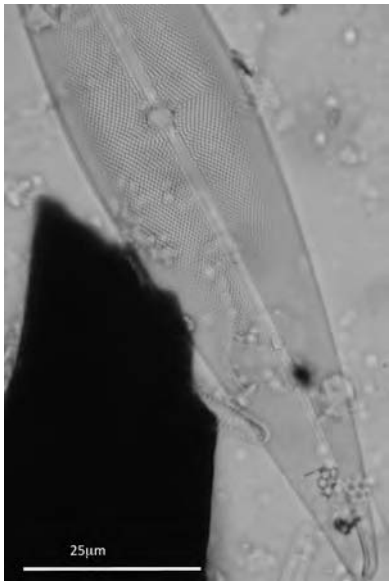

Figure 2.43. LM image of *Pleurosigma stuxbergii*.

Table 2.5: Morphometric data for Naviculoid pennate species.

Genus	species	Valve shape	Raphe characteristics	Apical Axis (µm) min	Apical Axis (µm) max	Transapical Axis (µm) min	Transapical Axis (µm) max	Striae in 10 µm min	Striae in 10 µm max	Striae Type	Striae pattern	Comments	Reference
Diploneis	*litoralis*			26	40	10	12	15	17			raphe canals	Medlin and Priddle, 1990
Diploneis	*smithii*											raphe canals	Medlin and Priddle, 1990; Sancetta, 1982
Gyrosigma	*hudsonii*	sigmoid, lanceolate	straight	78	114	17	21	23	34		transverse and longitudinal striae cross at right angles	longitudinal striae finer and denser than transverse	Medlin and Priddle, 1990
Gyrosigma	*tenuissimum* var. *hyperborea*	slightly sigmoid; linear	straight, but bends slightly towards apices	94	152	5	7	20	30		transverse and longitudinal striae cross at right angles	longitudinal striae finer and denser than transverse	Medlin and Priddle, 1990
Haslea	*crucigeroides*	narrow lanceolate		61	168	8	14	22	24		transverse and longitudinal striae cross at right angles	Pseudostauros	Medlin and Priddle, 1990
Haslea	*vitrea*	narrow lanceolate		131	190	17	20	18	22	dense	transverse and longitudinal striae cross at right angles		Medlin and Priddle, 1990

Table 2.5 continued.

Genus	species	Valve shape	Raphe characteristics	Apical Axis (µm) min	Apical Axis (µm) max	Transapical Axis (µm) min	Transapical Axis (µm) max	Striae in 10 µm min	Striae in 10 µm max	Striae Type	Striae pattern	Comments	Reference
Haslea	*kjellmanii*	broad lanceolate	acute	128	190	27	32	14	16	coarse	transverse and longitudinal striae cross at right angles		Medlin and Priddle, 1990
Navicula	*algida*	lanceolate		34	141	16	51	10	10	areolate		finely areolate at margin	Medlin and Priddle, 1990
Navicula	*directa*	lanceolate		52	137	7	11	9	10		parallel		Medlin and Priddle, 1990
Navicula	*directa* var. *javaica*	linear		65	165	10	12	7	7		uninterrupted	cuneate apices	Medlin and Priddle, 1990
Navicula	*distans*	lanceolate		70	130	14	20	5	6		radiate		Hasle and Syvertsen, 1996
Navicula	*forcipata var. densestriata*	elliptical	lyre-shaped lateral areas around raphe	16	36	6	13	18	24				Medlin and Priddle, 1990
Navicula	*imperfecta*	broad, elliptical		35	115	31	37	7	7		striae interrupted; central striae alternate between long and short		Medlin and Priddle, 1990

Table 2.5 continued.

Genus	species	Valve shape	Raphe characteristics	Apical Axis (µm) min	Apical Axis (µm) max	Transapical Axis (µm) min	Transapical Axis (µm) max	Striae in 10 µm min	Striae in 10 µm max	Striae Type	Striae pattern	Comments	Reference
Navicula	*kariana* var. *detersa*	broad, lanceolate	distinct lateral area	62	113	21	25	10	11	composed of apically elongate linear poroids			Medlin and Priddle, 1990
Navicula	*kryokonites*			19	37	6	11	20	22	areolate			Medlin and Priddle, 1990
Navicula	*kryophila*	broad, lanceolate		42	119	18	40	8	12	multi-seriate			Medlin and Priddle, 1990
Navicula	*novadecipiens*	elliptical	apically asymmetrical, one half is narrower than other	40	88	16	18	12	13	areolate			Medlin and Priddle, 1990
Navicula	*obtusa*	linear		45	117	12	16	10	12	composed of apically elongate linear poroids		concave towards center; butterfly shaped central area	Medlin and Priddle, 1990
Navicula	*oestrupioides*	linear-elliptical	ends curve in opposite directions	33	92	6	7	22	23	areolate			Medlin and Priddle, 1990

Table 2.5 continued.

Genus	species	Valve shape	Raphe characteristics	Apical Axis (µm) min	Apical Axis (µm) max	Transapical Axis (µm) min	Transapical Axis (µm) max	Striae in 10 µm min	Striae in 10 µm max	Striae Type	Striae pattern	Comments	Reference
Navicula	*pellucidula*	broad, elliptical to lanceolate		45	74	18	22	15	15	areolate		central area is narrow transapically; almost looks like stauros	Medlin and Priddle, 1990
Navicula	*recurvata*	lanceolate to elliptcial		29	50	8	9	11	13	composed of apically elongate linear poroids		concave towards center; small, broad axial area	Medlin and Priddle, 1990
Navicula	*solitaria*	linear		22	78	7	8	10	10		uninterrupted	rounded apices	Medlin and Priddle, 1990
Navicula	*superba*	rhombic		44	105	19	25	8	10				Medlin and Priddle, 1990
Navicula	*superba* var. *crassa*	elliptical		40	102	21	25	9	10		interrupted; coarse striae	apices sub-rostrate	Medlin and Priddle, 1990
Navicula	*superba* var. *subacuta*	elliptical		42	98	18	20	8	9		uninterrupted; parallel at center		Medlin and Priddle, 1990
Navicula	*transfuga* var. *septentrionalis*	elliptical		60	67	27	30	12	12		interrupted, dense	apiculate apices	Medlin and Priddle, 1990
Navicula	*transitans*	lanceolate		71	134	16	20	7	9		radiate		Medlin and Priddle, 1990

Table 2.5 continued.

Genus	species	Valve shape	Raphe characteristics	Apical Axis (µm) min	Apical Axis (µm) max	Transapical Axis (µm) min	Transapical Axis (µm) max	Striae in 10 µm min	Striae in 10 µm max	Striae Type	Striae pattern	Comments	Reference
Navicula	*transitans* var. *derasa*	narrow, lanceolate	distinct lateral area	45	93	10	18	9	11	composed of apically elongate linear poroids			Medlin and Priddle, 1990
Navicula	*trigonocephala*	linear		28	62	11	14	10	11				Medlin and Priddle, 1990
Navicula	*trigonocephala* var. *depressa*	linear		50	83	12	13	8	9		interrupted	apiculate apices	Medlin and Priddle, 1990
Navicula	*valida*	narrow, elliptical		33	126	15	26	6	8		striae uninterrupted; central striae alternate between long and short		Medlin and Priddle, 1990
Navicula	*valida* var. *minuta*	elliptical		15	32	11	15	8	9		uninterrupted; radiate at center		Medlin and Priddle, 1990
Pinnularia	*ambigua*	linear-elliptical	broad hyaline areas parallel to raphe	41	75	6	10	7	8	alveolate at margin			Medlin and Priddle, 1990

Table 2.5 continued.

Genus	species	Valve shape	Raphe characteristics	Apical Axis (µm) min	Apical Axis (µm) max	Transapical Axis (µm) min	Transapical Axis (µm) max	Striae in 10 µm min	Striae in 10 µm max	Striae Type	Striae pattern	Comments	Reference
Pinnularia	*quadratarea* var. *bicontracta*	wide at center and again at apices (bicontracted);		41	103	10	15	9	11	multi-seriate		cuneately rounded apices	Medlin and Priddle, 1990
Pinnularia	*quadratarea* var. *capitata*	capitate apices (wider at apices)		54	90	12	15	10	11	multi-seriate			Medlin and Priddle, 1990
Pinnularia	*quadratarea* var. *constricta*	constricted at center; lanceolate ends		35	96	11	19	10	11	multi-seriate	coarse		Medlin and Priddle, 1990
Pinnularia	*quadratarea* var. *cuneata*	elliptical-lanceolate		46	84	16	22	8	9	multi-seriate			Medlin and Priddle, 1990
Pinnularia	*quadratarea* var. *densestriata*	wide at center and again at apices (bicontracted)		32	57	9	10	12	12	multi-seriate		round apices	Medlin and Priddle, 1990
Pinnularia	*quadratarea* var. *dubia*	linear-elliptical		35	62	12	19	9	11	multi-seriate			Medlin and Priddle, 1990

Table 2.5 continued.

Genus	species	Valve shape	Raphe characteristics	Apical Axis (µm) min	Apical Axis (µm) max	Transapical Axis (µm) min	Transapical Axis (µm) max	Striae in 10 µm min	Striae in 10 µm max	Striae Type	Striae pattern	Comments	Reference
Pinnularia	*quadratarea* var. *maxima*	inflated at center		60	119	14	17	8	9	multi-seriate			Medlin and Priddle, 1990
Pinnularia	*quadratarea* var. *minor*	constricted at center		23	41	8	10	13	14	multi-seriate	finely striate		Medlin and Priddle, 1990
Pinnularia	*quadratarea* var. *subglabra*	lanceolate		65	94	15	20	8	9	multi-seriate			Medlin and Priddle, 1990
Pinnularia	*semiinflata*	linear, but with an asymmetrical bulge in the center		22	70	8	10	13	14	alveolate/ multi-seriate			Medlin and Priddle, 1990
Pleurosigma	*siberica*	slightly sigmoid; linear		140	230	12	12	26	27				Medlin and Priddle, 1990
Pleurosigma	*stuxbergii* var. *rhomboides*	strongly sigmoid, lanceolate, broad		83	166	26	33	22	26		transverse and longitudinal striae cross at oblique angles		Medlin and Priddle, 1990
Stauroneis												central area expanded into a stauros	Medlin and Priddle, 1990

2.2.10 *Neodenticula seminae* (Simonsen et Kanaya) Akiba et Yanagisawa

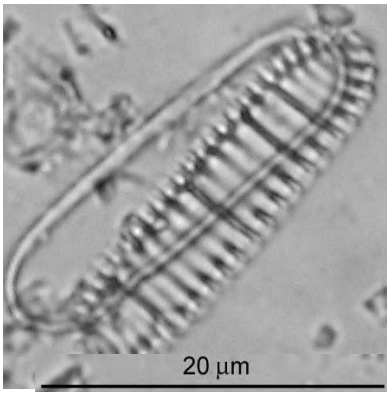

Figure 2.44. LM image of *Neodenticula seminae.*

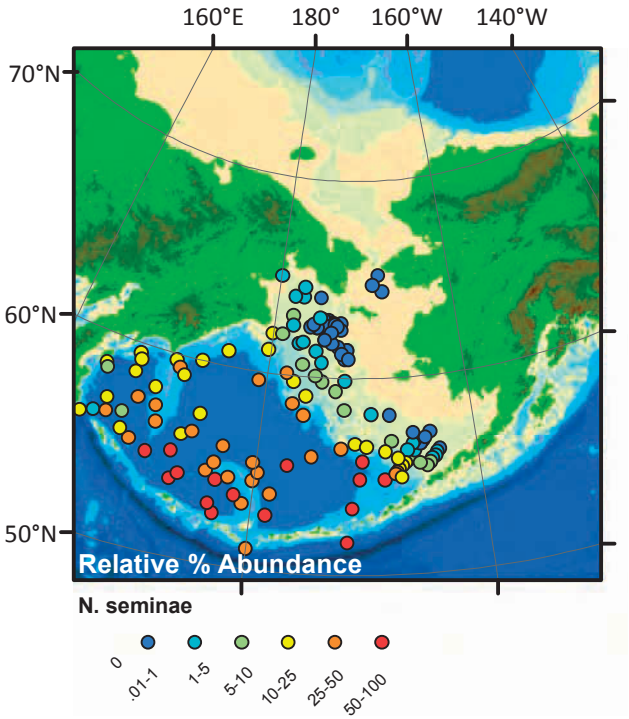

Figure 2.45 Map of *N. seminae* distribution in the Bering Sea.

This species is a small, heavily silicified pennate diatom that is distinguished by parallel pseudosepta that thicken or fork at the ends. One to three secondary pseudosepta run parallel between them. Although the pseudosepta are parallel for the most part, they do curve slightly towards the margins. *N. seminae* can be distinuguished from the Pliocene species *Neodentiucla kamtschatica* by the presence of the pseudosepta.

N. seminae is associated with high salinity, deep waters [*Kazarina and Yushina*, 1999] in the North Pacific, where it is a predominant member of the phytoplankton [*Takahashi et al.*, 2002]. *N. seminae* is endemic to the low nutrient, Pacific water above 42° N[*Sancetta*, 1982] and so it has been used as an indicator of Alaskan Stream water [*Caissie et al.*, 2010; *Katsuki and Takahashi*, 2005; *Sancetta*, 1982]. However, abundances of *N. seminae* varies in the North Pacific on glacial-interglacial time scales [*Sancetta and Silvestri*, 1984], so a reduction in *N. seminae* can indicate either a reduction in Pacific inflow to the Bering Sea or a reduction in the abundance of *N. seminae* in the North Pacific. Because it is heavily silicified, high relative proportions may alternatively indicate dissolution [*Sancetta*, 1982].

It is worth noting that the extinction of *N. seminae* in the North Atlantic occurred around

800 ka, and is used as a datum for the North Atlantic diatom biostratigraphy [*Koc and Flower*, 1998], but this species recently has resurfaced in the North Atlantic. This new appearance has been circumscribed to Arctic summer ice retreat allowing *N. seminae* to migrate through the Arctic Ocean to the North Atlantic [*Reid et al.*, 2007].

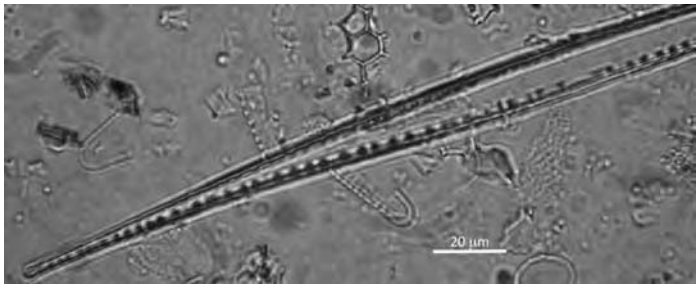

Figure 2.46. LM image of *Nitzschia laevissima.*

2.2.11 *Nitzschia* Hassall species

Nitzschia is a pennate diatom with a full raphe located on the valve margin or near the center of the valve. Frustules can be either linear or sigmoid and *Nitzschia* species may form colonies or live solitarily. A distinguishing characteristic is the presence of fibulae, which subtend the raphe and look like bars on the edges of the valves. Another distinguishing characteristic is the presence or absence of a central nodule. In many cases, *Nitzschia* could not be distinguished to the species level due to difficulty in identifying key characteristics under the light microscope [*Medlin and Priddle*, 1990], although species are assigned whenever possible. Detailed morphometric data [*Medlin and Hasle*, 1990] can be found in table 2.6.

2.2.11.1 *Nitzschia frigida* Grunow

This *Nitzschia* species has sub-parallel, linear to linear lanceolate edges and a central nodule that looks like a longer fibulae at the center of the margin. It is weakly silicified and the striae appear discontinuously across the valve face [*Medlin and Priddle*, 1990]

N. frigida is a common diatom in the epontic bloom [*von Quillfeldt et al.*, 2003] and has been reported from fast ice in the Arctic [*Medlin and Hasle*, 1990]. It is the only *Nitzschia* species whose relative percent abundances was over 5%

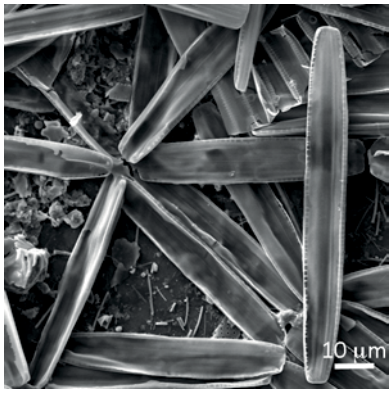

Figure 2.47. SEM image of *Nitzschia frigida.*

Table 2.6: Morphometric data for *Nitzschia* species.

Species	Apical Axis (µm) min	Apical Axis (µm) max	Transapical Axis (µm) min	Transapical Axis (µm) max	Fibulae in 10 µm min	Fibulae in 10 µm max	Striae in 10 µm min	Striae in 10 µm max	Striae resolvable in LM?	central nodule	Reference
Nitzschia frigida	45	75	4.5	7.5	7	9	45	50	n	y	Medlin and Priddle, 1990
Nitzschia neofrigida	60	109	6	7	6	8	40		r	y	Medlin and Priddle, 1990
Nitzschia polaris	50	169	5	7	5	8	40		p	y	Medlin and Priddle, 1990
Nitzschia promare	31	45	4	5.5	8	12	45	50	n	y	Medlin and Priddle, 1990
Nitzschia scabra	108	220	7	10	2	3	mottled			n	Medlin and Priddle, 1990
Nitzschia arctica	90	155	7	8	8	10	24	26	y	y	Medlin and Priddle, 1990
Nitzschia brebissonii var. *borealis*	120	170	6	8	7	8	12	18	y	n	Medlin and Priddle, 1990
Nitzschia laevissima	115	170	6	6.5	6	8	40		v	y	Medlin and Priddle, 1990
Hantzschia weyprechtii	55	75	6	7	9	11	33	35	y	y	Medlin and Priddle, 1990

Striae resolvable in LM?

N = not resolvable with LM

R = barely resolvable with LM

P = not present on valve face, hyaline

V = striae appearance varies from hyaline to isolated areolae to 40 in 10 µm

Y = resolvable

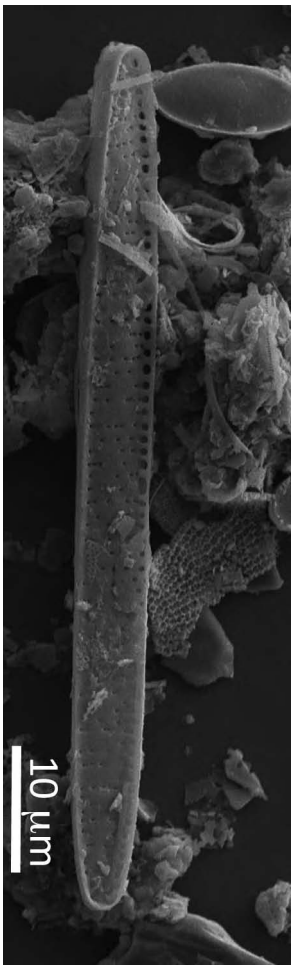

Figure 2.48. SEM image of *Nitzschia frigida.*

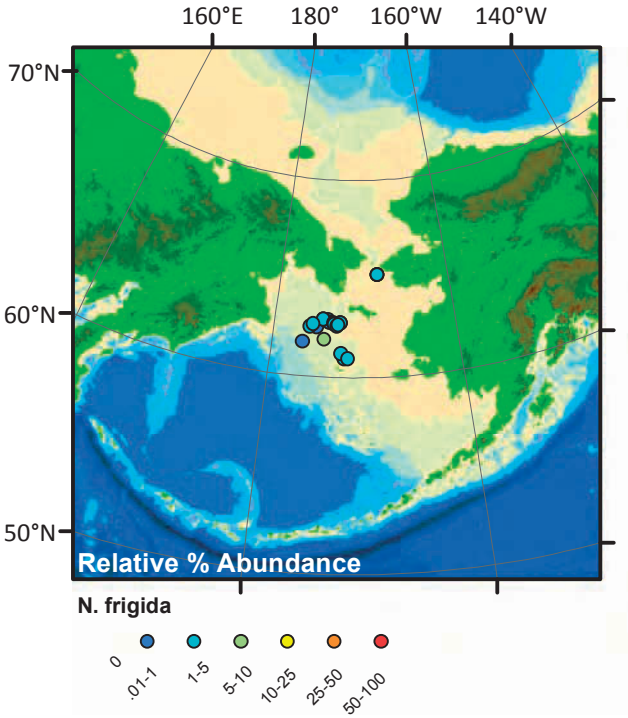

Figure 2.49 Map of *N. frigida* distribution in the Bering Sea.

2.2.12 *Paralia sulcata* (Ehrenberg) Cleve

P. sulcata is a small, heavily silicified, colony forming pennate diatom. It is characterized by radial ribs on the central third of the valve face [*Sancetta*, 1982]. These ribs sometimes resemble wedges of an orange. It is heterovalvate and has at least two types of valves that are morphologically distinct. Separation valves are the outer-most valves in a colony. They

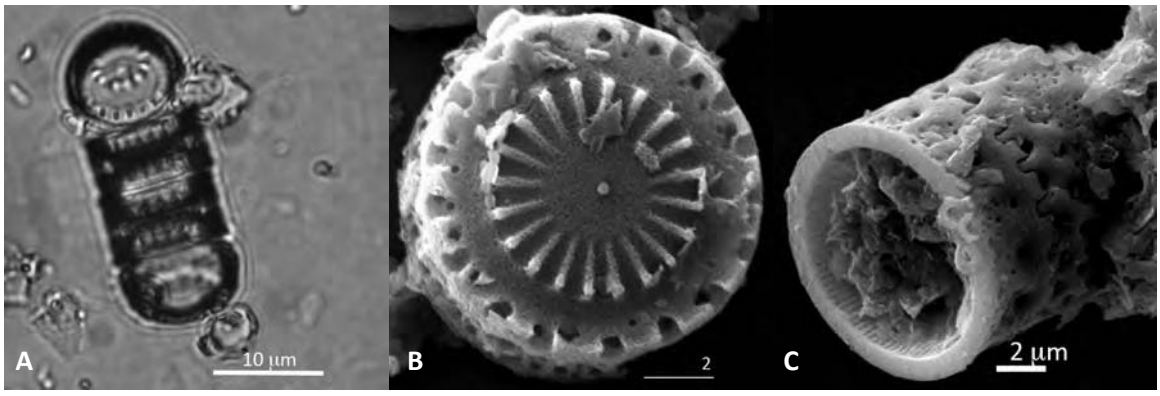

Figure 2.50. a) LM image of *P. sulcata*. This image shows both the girdle and valve view. b) SEM image of *P. sulcata* valve. c) Girdle view of *P. sulcata* showing interlocking ridges and grooves.

are convex. The radial ribs are small, close to the center, and do not have as much relief as those in the linking valves [*Sims and Crawford*, 2002]. Linking valves are flat discs with high, radial ridges and grooves that connect to neighboring valves. The margin also has linking spines or prongs [*Sims and Crawford*, 2002].

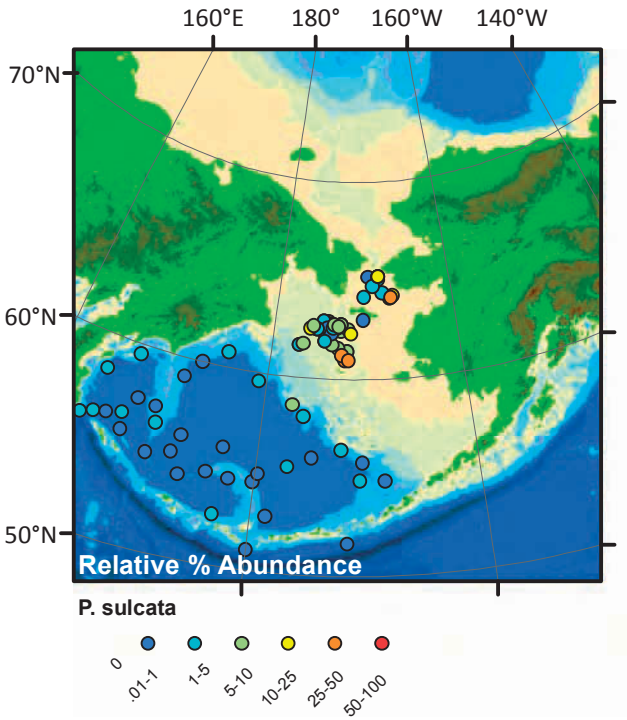

Figure 2.51 Map of *P. sulcata* distribution in the Bering Sea.

There are many morphologies of *P. sulcata*. In addition to the heterovalvate colonies, valves for solitary planktic forms of *P. sulcata* look different from the benthic forms. I have tried to separate different valve types when possible. I am also suspicious that diatoms that have been previously identified as *Melosira sol* are actually *P. sulcata.* Little taxonomic information exists for *M. sol*, and some forms of *P. sulcata* have previously been misidentified as *Melosira* species [*Crawford et al.*, 1990].

P. sulcata can be either planktic or benthic [*Kariya et al.*, 2010] and is associated with river deltas. Its Bering Sea range overlaps that of *Melosira sol* [*Sancetta*, 1982]. It is a member of the marginal ice zone assemblage [*von Quillfeldt et al.*, 2003], but has also been reported as living on the underside of multiyear ice (Horner 1985). Pushkar [1999] asserts that *P. sulcata* indicates water shallower than 20 m. Its high abundances in the Bering Strait may mean that it is adapted to moving water [*Sancetta*, 1982]. *P. sulcata* thrives in water that is warmer than 3° C [*Zong*, 1997], with low light [*Blasco et al.*, 1980] and low salinity [*Ryu et al.*, 2008].

2.2.13 *Rhizosolenia hebetata* J.W. Bailey

Rhizosolenia is an unusual looking centric species that is long and conical with one or two very long processes. It is always seen in girdle view. There are two varieties of *R. hebetata*

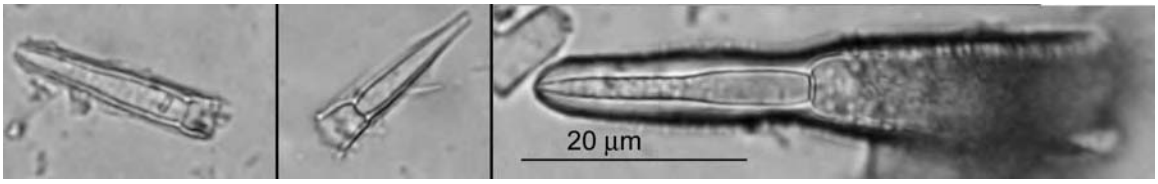

Figure 2.52. LM image of *Rhizosolenia hebetata* f. *hebetata.*

that are both heavily silicified. *R. hebetata* f. *hebetata* is distinctive. The otaria covers the entire process and there are no claspers at the base of the process, which has a rounded tip. *R. hebetata* var. *semispina* has a long process that tapers into a narrow tube. It has pointed otaria that extend up to 3 µm up the base of the process [*Medlin and Priddle*, 1990].

R. hebetata is part of the open ocean plankton [*Lopes et al.*, 2006] and part of the Bering Basin assemblage [*Sancetta*, 1981]. It occurs in high numbers on Bowers ridge [*Sancetta*, 1982] and has been found as part of the summer bloom in upwelling zones near the Aleutian Islands [*Aizawa et al.*, 2005]. Sancetta [1982] points out that this heavily silicified diatom may be found in areas where winnowing is prevalent.

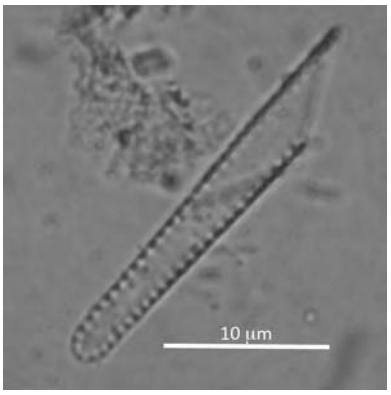

Figure 2.53. LM image of *Thalassionema nitzschioides.*

2.2.14 *Thalassionema nitzschioides* (Grunow) H. et M. Peragallo

T. nitzschioides is a variably long pennate diatom (10 – 110 µm long and 2-3 µm wide). Its valves are linear with parallel margins and it has bluntly rounded, isopolar apices. There are distinctive marginal pores along the edges (10-12 per 10 µm), and a labiate process is located at each apex [*Hasle*, 2001].

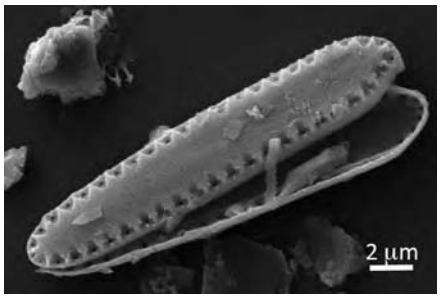

Figure 2.54. SEM image of *T. nitzschioides.*

T. nitzschioides is a cosmopolitan species that has been found under zones of upwelling [*Sancetta*, 1982], in the marginal ice zone [*von Quillfeldt et al.*, 2003], and associated with warm water in the North Pacific [*Lopes et al.*, 2006]. This makes defining an ecological niche difficult at best, although the species shows considerable variation in relative percent abundances over time.

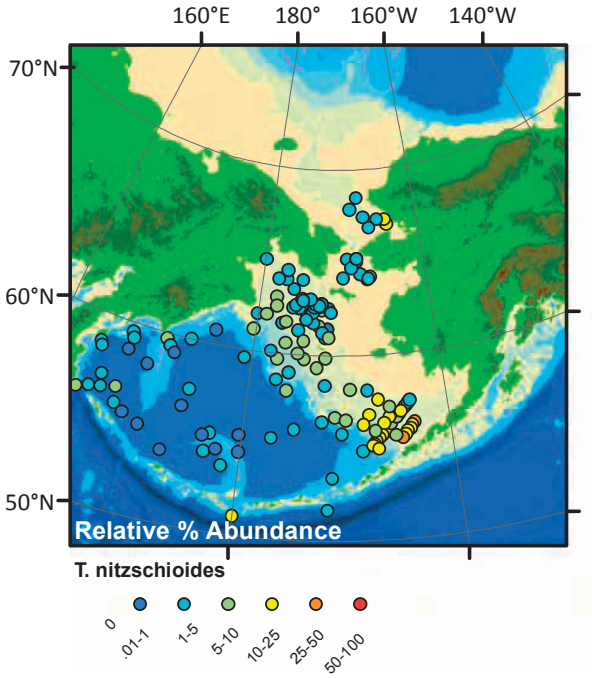

Figure 2.55 Map of *T. nitzschioides* distribution in the Bering Sea.

2.2.15 *Thalassiosira* Cleve species

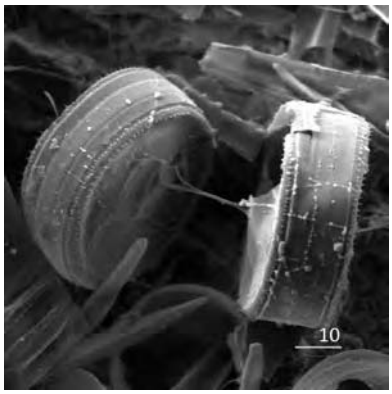

Figure 2.56. SEM image of 2 *Thalassiosira hyalina* frustules attached to each other by chiton threads.

Individual *Thalassiosira* specimens attach to each other using threads extending from strutted processes arranged on the valve face (Figure 2.56). The arrangement of the strutted processes, marginal processes, and labiate processes are the main distinguishing factors for this genus. Valve size and density of areolae are of secondary importance [*Hasle and Syvertsen*, 1997]. Table 2.7 lists the morphometric data for most of the taxa included in the *Thalassiosira* genus.

Thalassiosira is, by far, the genus with the most diversity in Bering Sea sediments with 31 different taxa identified in surface and down-core sediments. Species fill widely varied environmental niches including sea ice, upwelling zones, highly stratified water, cold water, and warm water [*Barron et al.*, 2009; *Fryxell and Hasle*, 1972; *Horner*, 1985; *Lopes et al.*, 2006; *Saitoh and Taniguchi*, 1978; *Sancetta*, 1982; *Shiga and Koizumi*, 2000; *von Quillfeldt et al.*, 2003].

Table 2.7: Morphometric data for *Thalassiosira* species. Abbreviations: strutted process (SP), labiate process (LP), occluded process (OP)

Species	# central processes	location of central processes	central areola or annulus??	# of rings of marginal processes	Min Diameter (µm)	Max Diameter (µm)	Areaolation pattern 1	Areaolation pattern 2	Areaolation pattern 3	areolae/10 µm							marginal processes in 10 µm min	marginal processes in 10 µm max
										valve face min	valve face max	valve mantle min	valve mantle max	marginal min	marginal max	comments		
T. allenii	1		no	1	5	20	straight	eccentric	radial rows slightly fasciculated	18	24	30	40	6		mantle areolae 1/2 size of those on valve face		
T. angulata	1		no	1	12	39	eccentric	sometimes straight or sectors		8	18	14	24	3				
T. anguste-lineata	1 -9 in each arc	in arcs in a ring some distance from valve center		1	14	78	linear	eccentric	fasciculate	8	18						3	6
T. antarctica var. *borealis*	cluster (2-7)	center		2-3	18	43	radial	bifurcate	occasionally lightly fasciculate	20	24						8	
T. baltica	cluster (2-9)	center		2	20	120	fasciculate			10	20						6	7
T. binata	1	next to large central areola	yes	1	4	18	radial	eccentric		30	40	30	40	5	13	total		

Table 2.7 continued

Species	marginal processes comments	marginal ribs	external/internal process tubes	# labiate processes	location of labiate processes	strutted processes on valve face	occluded processes	other distinctive features	distribution	Reference
T. allenii				1	takes place of marginal strut proc				warm water to temperate	Hasle and Syvertsen 1997
T. angulata	long external tubes; wide apart; 1 areolae from margin		long external tubes on processes	1	close to marginal SP				Subarctic to temperate	Hasle and Syvertsen 1997; Medlin and Priddle, 1990
T. anguste-lineata			conspicuous external tubes on marginal sp					sometimes dificult to discern central sp in coarsely areolate inds.	Subarctic to temperate	Hasle and Syvertsen 1997; Medlin and Priddle, 1990
T. antarctica var. *borealis*	SP barely distinguishalbe w/LM			1	large, near mantle			RS--primary valve flattened, secondary valve highly arched, SP on valve face; distinguish from T. gravida because it has 1 or 2 SP in center, and 1 or 2 marginal rows of SP; areolae is coarser too	northern cold water to temperate	Hasle and Syvertsen 1997; Medlin and Priddle, 1990
T. baltica				3 or 4	on valve mantle				brackish water (Baltic Sea/Arctic Oc)	Hasle and Syvertsen 1997; Medlin and Priddle, 1990
T. binata				1	between 2 marginal SP			smaller, more finely areolate than T. nord	warm water to temperate	Hasle and Fryxell, 1977

Table 2.7 continued

Species	# central processes	location of central processes	central areola or annulus??	# of rings of marginal processes	Min Diameter (µm)	Max Diameter (µm)	Areaolation pattern 1	Areaolation pattern 2	Areaolation pattern 3	areolae/10 µm							marginal processes in 10 µm min	marginal processes in 10 µm max
										valve face min	valve face max	valve mantle min	valve mantle max	marginal min	marginal max	comments		
T. bioculata	1				20	60	fasciculated	radial ribs		16	20						5	7
T. bulbosa RS	1			1	2	16	heavily silicified			20	26	20	26	?				
T. bulbosa vegetative cell	1		f	1	2	16	lightly silicified			36	42	36	42	5				
T. conferta	1		relatively prominent	1	4	23	radial rows	in sectors in larger specimens		25	27	25	27	3	5	apart		
T. constricta	cluster of 3-12	center		1	18	28				40	60						3	5
T. curviseriata	1 or 2	next to annulus	off center annulus		5	14				26	30						2	3

Table 2.7 continued

Species	marginal processes comments	marginal ribs	external/internal process tubes	# labiate processes	location of labiate processes	strutted processes on valve face	occluded processes	other distinctive features	distribution	Reference
T. bioculata	µm apart		long internal parts of marginal proc seen in LM	1	slightly off center			"forms low, heavily silicified semiendogenous RS w/convex, coarsely areolated primary and secondary valves"	northern cold water to temperate/high arctic	Hasle and Syvertsen 1997; Medlin and Priddle, 1990
T. bulbosa RS									northern, cold water/high arctic	Medlin and Priddle, 1990
T. bulbosa vegetative cell	low bulb shaped outer parts			1	between 2 marginal SPes				northern, cold water/high arctic	Hasle and Syvertsen 1997; Medlin and Priddle, 1990
T. conferta				1	v. small between 2 larger marginal SPes			small labiate distiguishes it from T. nord	Subarctic to temperate	Hasle and Syvertsen 1997; Medlin and Priddle, 1990; Hasle and Fryxell, 1977
T. constricta	wider apart than T. hyalina			1	midway between 2 SP			RS very different from veg	northern cold water to temperate	Medlin and Priddle, 1990
T. curviseriata	conspicuous w/ 2 opposing wings			1	close to marginal SP				cosmopolitan, not polar reg	Hasle and Syvertsen 1997

Table 2.7 continued

Species	# central processes	location of central processes	central areola or annulus??	# of rings of marginal processes	Min Diameter (µm)	Max Diameter (µm)	Areaolation pattern 1	Areaolation pattern 2	Areaolation pattern 3	areolae/10 µm							marginal processes in 10 µm min	marginal processes in 10 µm max
										valve face min	valve face max	valve mantle min	valve mantle max	marginal min	marginal max	comments		
T. decipiens	1			1	9	40	eccentric	radial rows occasionally		8	12	10	15	4	6			
T. delicatula	1			4?	9	30	radial rows	slight fasciculation in larger sp		22	26						4	5
T. diporocyclus	1			2	12	24	fasciculate			24	31						3	4
T. eccentrica	1	next to central areola	surrounded by ring of 7 areolae	3	15	110	eccentric	tends to fasciculation		5	11						2	5
T. endoseriata	4 to 14	in an irregular ring, each process takes the place of an areola in the middle row of a sector			20	60				11	18						5	6
T. gravida	numerous	center			17	62	radial rows			20							5	10

Table 2.7 continued

Species	marginal processes comments	marginal ribs	external/internal process tubes	# labiate processes	location of labiate processes	strutted processes on valve face	occluded processes	other distinctive features	distribution	Reference
T. decipiens				1	prominent; between 2 marginal SPes					Sancetta 1982
T. delicatula						alternating in 3 rings, external parts conspicuous, but shorter than those of OP	in a ring between valve face and mantle		cosmopolitan, not polar reg	Hasle and Syvertsen 1997
T. diporocyclus	µm apart		no external tubes	1	in peripheral ring				warm water to temperate	Hasle and Syvertsen 1997
T. eccentrica	2 rings w/short external tubes; 1 ring of spines farther away from margin					scattered			cosmopolitan, not polar reg	Fryxell and Hasle 1972
T. endoseriata				1	1/4 the distance from the margin to the center				warm water	Hasle and Syvertsen 1997
T. gravida				1	large	numerous scattered across face and mantle		no RS	Subarctic to temperate	Hasle and Syvertsen 1997; Medlin and Priddle, 1990

Table 2.7 continued

Species	# central processes	location of central processes	central areola or annulus??	# of rings of marginal processes	Min Diameter (µm)	Max Diameter (µm)	Areaolation pattern 1	Areaolation pattern 2	Areaolation pattern 3	areolae/10 µm							marginal processes in 10 µm min	marginal processes in 10 µm max
										valve face min	valve face max	valve mantle min	valve mantle max	marginal min	marginal max	comments		
T. guillardii	0-3	subcentral	yes	1	4	14	not resolved w/LM	slightly raised ribs radiate from annulus		30	40	70	80				7	8
T. hendeyi	1			3	42	110	straight tangential rows			5	6						5	6
T. hispida	1			1	15	25				18		24	26	5				
T. hyalina	cluster (2-15)	center		1	16	45	radial rows or ribs, mantle areolated			13	24						5	9
T. hyperborea	ring	subcentral			16	70	radial rows			8	18						3	5
T. kushirensis	1 -8 in no pattern	subcentral		1	8	35				15	24						7	8

Table 2.7 continued

Species	marginal processes comments	marginal ribs	external/internal process tubes	# labiate processes	location of labiate processes	strutted processes on valve face	occluded processes	other distinctive features	distribution	Reference
T. guillardii	regularly spaced			1	replaces SP					Hasle and Syvertsen 1997
T. hendeyi	small SP, not resolved w/LM							low, wavy marginal ridge	warm water to temperate	Hasle and Syvertsen 1997
T. hispida									northern, cold water to temperate	Medlin and Priddle, 1990
T. hyalina			conspicuous external tubes on marginal proc	1	replaces marginal SP			well-areolated valves = RS	northern cold water to temperate/high arctic	Hasle and Syvertsen 1997
T. hyperborea									brackish water (Baltic Sea/Arctic Oc)	Hasle and Syvertsen 1997; Medlin and Priddle, 1990
T. kushirensis	coarse	coarse interstriae		1				at least 4 varieties	Japanese waters; N Atlantic waters	Medlin and Priddle, 1990

Table 2.7 continued

Species	# central processes	location of central processes	central areola or annulus??	# of rings of marginal processes	Min Diameter (µm)	Max Diameter (µm)	Areaolation pattern 1	Areaolation pattern 2	Areaolation pattern 3	areolae/10 µm							marginal processes in 10 µm min	marginal processes in 10 µm max
										valve face min	valve face max	valve mantle min	valve mantle max	marginal min	marginal max	comments		
T. leptopus	0		central areola larger than others	2 to 3	26	165	straight tangential rows			4	7					areolae smaller on mantle and irregularly arranged	3	8
T. mala	1	off-center		1	4	10	visible by focusing on central part of valve face			25	30	50		4	10			
T. mediterranea	2-8 radial rays extend 1/2 way to margin, each ends w/ SP	subcentral	yes	1	6	20	not resolved w/ LM			30							3	6
T. minima	2, sometimes 1, occasionally 3!	subcentral			5	15				30	40						3	6
T. minuscula	1			1	10	27	barely visible w/LM			32	48	32	48	3	4	apart		

Table 2.7 continued

Species	marginal processes comments	marginal ribs	external/internal process tubes	# labiate processes	location of labiate processes	strutted processes on valve face	occluded processes	other distinctive features	distribution	Reference
T. leptopus	marginal proc not visible in LM, 1 ring of coarse proc farther from margin: 1 large LP and evenly spaced coarse, short occluded proc									Hasle and Syvertsen 1997
T. mala			inconspicuous external tubes	1	midway between 2 marginal SP				warm water to temperate	Hasle and Syvertsen 1997
T. mediterranea	close to valve margin			1	midway between 2 SP				warm water to temperate	Hasle and Syvertsen 1997
T. minima				1	close to 1 marginal SP			subcentral proc distinct w/short, external tubes	cosmopolitan, not polar reg	Hasle and Syvertsen 1997
T. minuscula			no external tubes	1	close to 1 or 2 SP, distal from valve margin				warm water to temperate	Hasle and Syvertsen 1997

Table 2.7 continued

Species	# central processes	location of central processes	central areola or annulus??	# of rings of marginal processes	Min Diameter (µm)	Max Diameter (µm)	Areaolation pattern 1	Areaolation pattern 2	Areaolation pattern 3	areolae/10 µm							marginal processes in 10 µm min	marginal processes in 10 µm max
										valve face min	valve face max	valve mantle min	valve mantle max	marginal min	marginal max	comments		
T. nordenskioeldii	1	close to annulus	yes	1	10	50	delicate			14	18	14	18	3				
T. oceanica	1			1	3	12	not visible in LM	radial ribs or poroid areolae		40	60	40	60	3	4			
T. oestrupii var. *oestrupii*	1	nearly central			7	60	sublinear			6	12						1	2
T. oestrupii var. *venrickae*	1				6	39	distinct eccentric pattern			6	11						4	7
T. pacifica	1	next to annulus	yes	1	7	46	linear	eccentric	fasciculate	10	19	20	28	4	7			
T. partheneia	1			1	6	14	not visible in LM	radial ribs or poroid areolae		40	60	40	60	3	5			

Table 2.7 continued

Species	marginal processes comments	marginal ribs	external/internal process tubes	# labiate processes	location of labiate processes	strutted processes on valve face	occluded processes	other distinctive features	distribution	Reference
T. nordenskioeldii	1/3 way in from margin		very long, prominent	1	variable w/in ring of marginal proc			slanting valve mantle	northern, cold water to temperate	Hasle and Syvertsen 1997; Medlin and Priddle, 1990
T. oceanica	distinct; close to margin		short external tubes	1	close to 1 SP			widely spaced marginal processes and location of lab process	warm water	Hasle and Syvertsen 1997
T. oestrupii var. *oestrupii*	µm apart			1	2 or 3 areolae away from center				warm water to temperate	Hasle and Syvertsen 1997
T. oestrupii var. *venrickae*	µm apart			1	2 or 3 areolae away from center			distinguished by distinct eccentric areola pattern & widely separated marginal SP	warm water to temperate	Hasle and Syvertsen 1997
T. pacifica		yes	distinct, coarse external tubes	1	replaces a marginal SP			ribbed margin	Subarctic to temperate	Hasle and Syvertsen 1997; Medlin and Priddle, 1990
T. partheneia			internal parts longer than inconspicuous external parts	1	equidistant between 2 SP			shape of SP and location of LP	warm water	Hasle and Syvertsen 1997

Table 2.7 continued

Species	# central processes	location of central processes	central areola or annulus??	# of rings of marginal processes	Min Diameter (µm)	Max Diameter (µm)	Areaolation pattern 1	Areaolation pattern 2	Areaolation pattern 3	areolae/10 µm							marginal processes in 10 µm min	marginal processes in 10 µm max
										valve face min	valve face max	valve mantle min	valve mantle max	marginal min	marginal max	comments		
T. poroseriata	1 to 8	on a straight, curved, or zigzag line	at end of line		14	38	radial	fasciculated	weakly silicified	11	16						1	2
T. proschkinae	1	close to LP			3	12	eccentric			25	30						ca. 1.5	
T. pseudonana	0		sometimes	1	2	6	not revealed w/LM	radial ribs		50	70						6	14
T. punctigera	1			1	40	186	fasciculate			10	23	10	23	4	5	mostly		
T. rotula	cluster	center			8	55	radial ribs	poorly developed except on mantle		18	24						12	15
T. simonsenii	1	next to sm. Areola		2	30	59	straight tangential rows			4	5						5	6
T. subtilis	1	subcentral		1	15	32	fasciculate			30		30		3	4	apart		

Table 2.7 continued

Species	marginal processes comments	marginal ribs	external/internal process tubes	# labiate processes	location of labiate processes	strutted processes on valve face	occluded processes	other distinctive features	distribution	Reference
T. poroseriata				1	in line w/ central processes away from margin				Subarctic to temperate	Hasle and Syvertsen 1997; Medlin and Priddle, 1990
T. proschkinae	µm apart			1	close to center			marginal SP not as widely spaced	cosmopolitan	Hasle and Syvertsen 1997
T. pseudonana				1	midway between 2 SP					Hasle and Syvertsen 1997
T. punctigera	small, densely spaced; close to margin	yes	short external tubes				larger than SP; farther from margin, longer	Licea has more widely spaced marginal SP; lundiana has SP scattered on valve face in 2 marginal rings, finer areolation	warm water to temperate	Hasle and Syvertsen 1997
T. rotula								may be same as T. gravida, but temperature dependent	cosmopolitan	Hasle and Syvertsen 1997
T. simonsenii	small SP, not readily visible w/LM	yes		2	long tubes		yes		warm water to temperate	Hasle and Syvertsen 1997
T. subtilis			no external tubes	1	distal from margin	yes, scattered			warm water to temperate	Hasle and Syvertsen 1997

Table 2.7 continued

Species	# central processes	location of central processes	central areola or annulus??	# of rings of marginal processes	Min Diameter (µm)	Max Diameter (µm)	Areaolation pattern 1	Areaolation pattern 2	Areaolation pattern 3	areolae/10 µm							marginal processes in 10 µm min	marginal processes in 10 µm max
										valve face min	valve face max	valve mantle min	valve mantle max	marginal min	marginal max	comments		
T. symmetrica	1 ring	center	central areola slightly larger than other, surrounded by rosette of 7 areolae	1	30	88	eccentric			5	7			6	8		4	6
T. trifulta	1 to 8	in 1 or 2 lines in center			16	58	straight	slightly curved tangential rows	coarsely silicified	5	7						2	
T. weissflogii	2-28 in irregular ring	subcentral		1	5	32	irregular, small/not well defined			30	40						9	16

Table 2.7 continued

Species	marginal processes comments	marginal ribs	external/internal process tubes	# labiate processes	location of labiate processes	strutted processes on valve face	occluded processes	other distinctive features	distribution	Reference
T. symmetrica	not visible in LM			2	2 LP 170 degrees apart on margin					Fryxell and Hasle 1972
T. trifulta				1	8 or 9 areolae from center; closer to mantle than to center				southern cold water	Hasle and Syvertsen 1997
T. weissflogii				1	very large, replaces SP				fresh to brackish water; cosmopolitan ?	Hasle and Syvertsen 1997

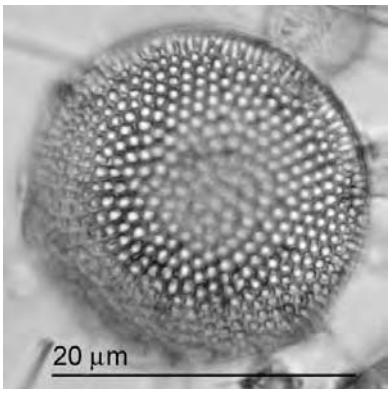

Figure 2.57. LM image of *Thalassiosira antarcitca* RS.

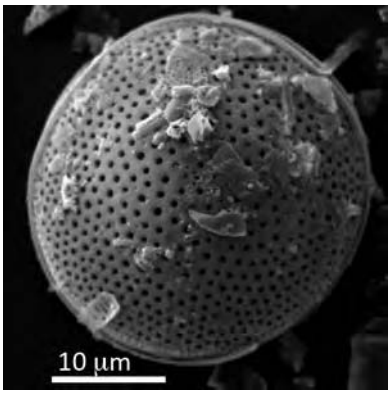

Figure 2.58. SEM image of *Thalassiosira antarcitca* RS.

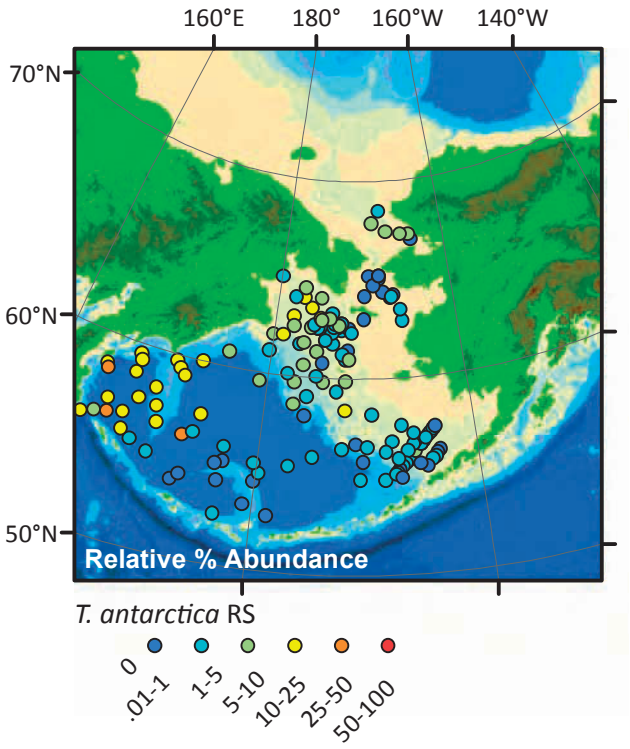

Figure 2.59 Map of *T. antarctica* RS distribution in the Bering Sea.

2.2.15.1 Thalassiosira antarctica var. borealis G. Fryxell, Doucette, and Hubbard spora

There has been much confusion in the literature about this taxa, which is a bipolar species, but was described separately in the Antarctic and the Arctic. Additionally, the resting spore was described and named (*Coscinodiscus* subglobosus) before either vegetative cell was described. Even today, resting spores of *T. antarctica* var. *borealis* are sometimes classified as *T. gravida* RS. However, *T. gravida* does not form resting spores [*Hasle and Syvertsen*, 1997].

In addition, there are multiple morphologies of this taxa due to the fact that there are three types of resting spores formed by *T. antarctica* and some of these resting spores are heterovalvate. In general, the valves are small to mid-sized and domed. Areolae are arranged in radial rows or irregularly and there are approximately 7 areolae in 10 µm. The hypovalve sometimes has a cluster of strutted processes in the center of the valve and/or scattered over the surface of the valve face. However, the epivalve of exogenous and semiendogenous resting

spores are flattened and do not generally have processes on the valve face [*Heimdal*, 1971; *Medlin and Priddle*, 1990; *Sancetta*, 1982; *Syvertsen*, 1979].

The ecology of *T. antarctica* var. *borealis* is not well known, but it has been observed as a member of the plankton living near the marginal ice zone [*von Quillfeldt et al.*, 2003], especially in coastal waters, or waters with temperatures between -1° and 4 ° C [*J A Barron et al.*, 2009; *Shiga and Koizumi*, 2000]. In addition, the resting spores have been associated with thick pack ice, and may be transported great distances [*Horner*, 1985]. Sancetta [1981] pointed out that the highest abundances of *T. antarctica* mimic those of *Chaetoceros* RS, which may indicate that it is associated with upwellilng, high productivity, or the sea ice margin [*Sancetta*, 1981]. In Antarctica, the southern version of this bipolar species is well known as a fall phytoplankton that grows as light declines and sea ice expands [*Cunningham and Leventer*, 1998]. It may be that the boreal version has similar affinities.

2.2.15.2 *Thalassiosira hyalina* (Grunow) Gran

T. hyalina is a distinctive species with flat, finely, radially areolate valves. There is a cluster of strutted processes in the center and a ring of fairly closely spaced short marginal processes. A labiate process replaces a marginal process. This species can be distinguished from *T. gravida*, which has strutted processes across the valve face [*Medlin and Priddle*, 1990; *Tomas*, 1996].

T. hyalina is associated with the marginal ice zone and has been reported to bloom in ice leads [*Gran*, 1904] or in the plankton surrounding the ice [*Schandelmeier and Alexander*, 1981].

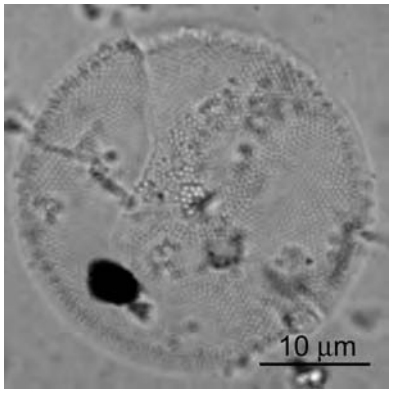

Figure 2.60. LM image of *Thalassiosira hyalina.*

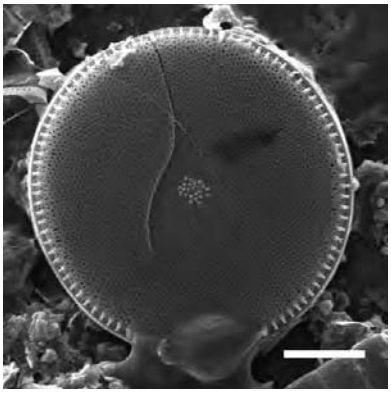

Figure 2.61. SEM image of *Thalassiosira hyalina.*

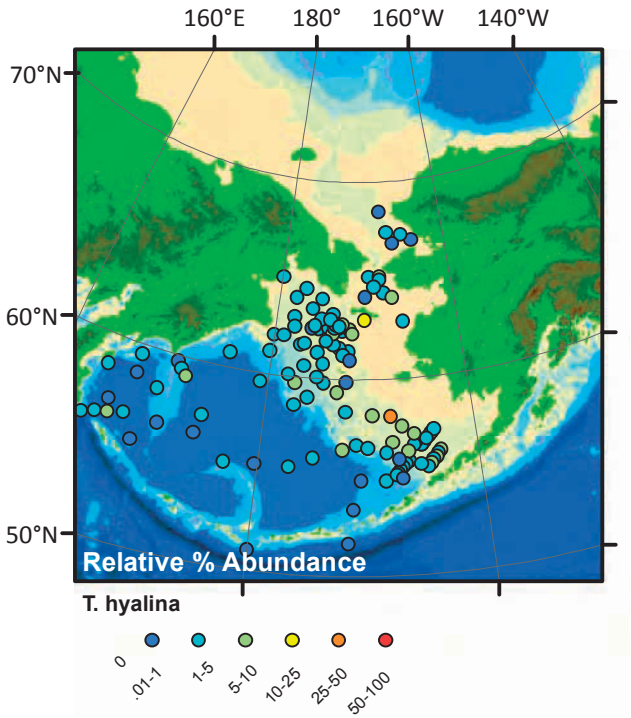

Figure 2.62 Map of *T. hyalina* distribution in the Bering Sea.

2.2.15.3 *Thalassiosira nordenskioeldii* Cleve

T. nordenskioeldii is a stunning diatom that is slightly depressed in the center with one central strutted process. It has a labiate process located within the ring of marginal processes. The most distinctive feature is a ring of spines and processes about 2/3 of the way between the central area and the margin [*Medlin and Priddle*, 1990].

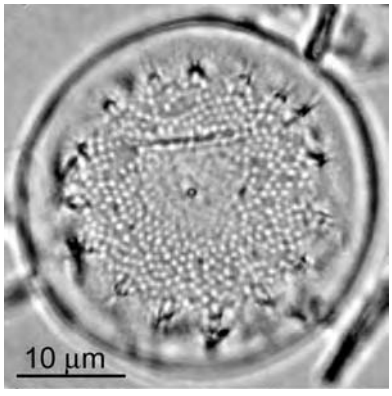

Figure 2.63. LM image of *Thalassiosira nordenskioeldii.*

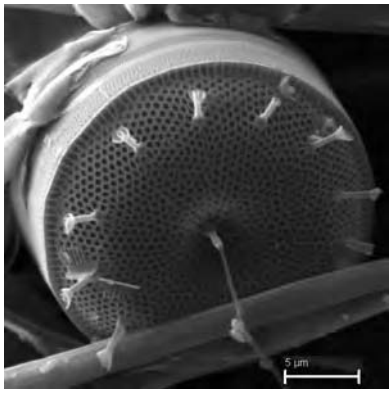

Figure 2.64. SEM image of *Thalassiosira nordenskioeldii.*

This species is a member of the plankton that forms large masses in early spring associated with the marginal ice zone and has been observed blooming at the margin of the ice (Clev, 1896) and in the early spring bloom [*Schandelmeier and Alexander*, 1981; *von Quillfeldt et al.*, 2003].

2.2.15.4 *Thalassiosira* Cleve species < 10 µm

Small *Thalassiosira* species occasionally accounted for more than 10% of the sediment diatom assemblages. These individuals were all smaller than 10 µm in diameter and so did not have features clear enough to separate into separate species. This group may include the following species: *T. binata, T. bulbosa, T. mala, T. mediterranea, T. minima, T. miniscula,* and *T. pacifica.* Many of these species are

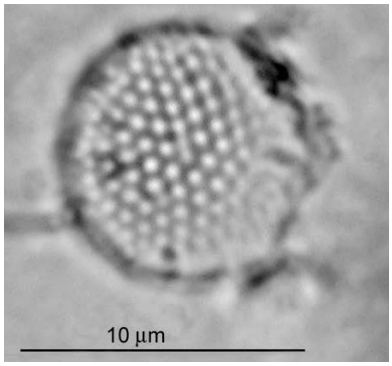

Figure 2.66. LM image of a small *Thalassiosira* species.

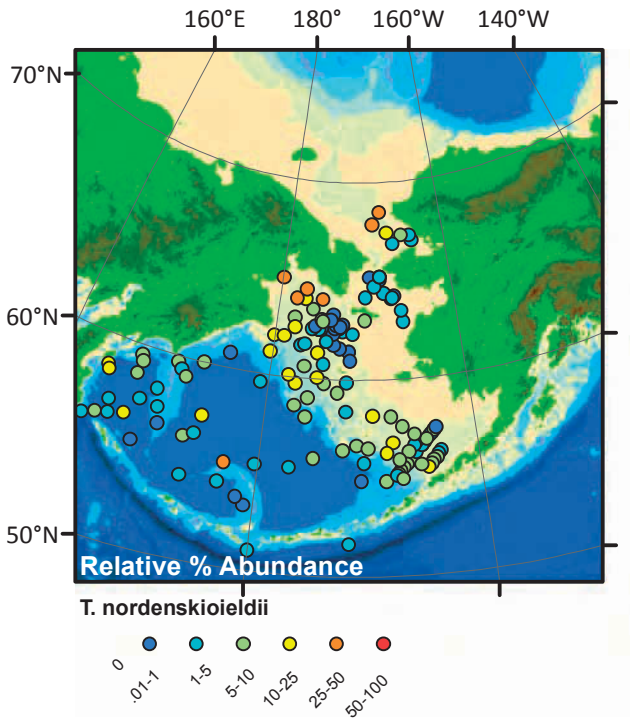

Figure 2.65 Map of *T. nordenskioeldii* distribution in the Bering Sea.

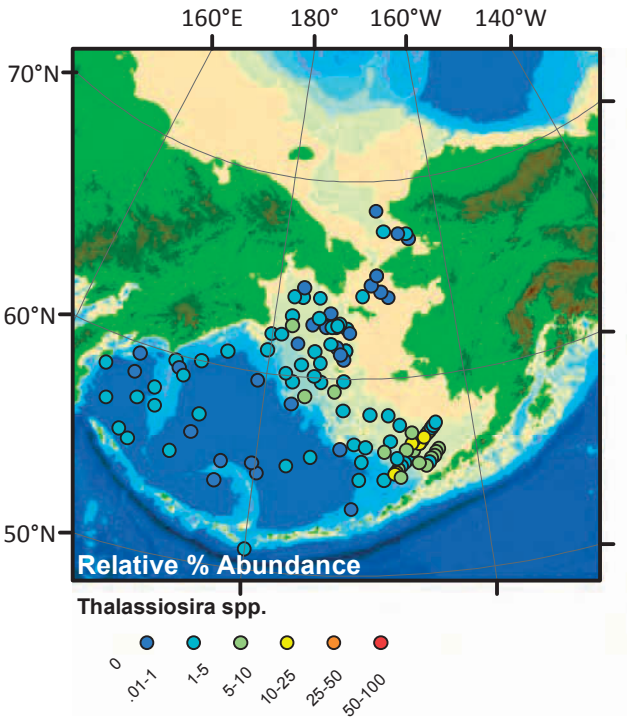

Figure 2.67 Map of small *Thalassiosira* species distribution in the Bering Sea.

associated with warmer water [*Aizawa et al.*, 2005], and small *Thalassiosira* spp. track upwelling in the North Pacific [*Lopes et al.*, 2006], so although this is likely an amalgamation of species, some relevant paleoecological information can still be extracted.

2.2.15.5 *Thalassiosira trifulta* Fryxell

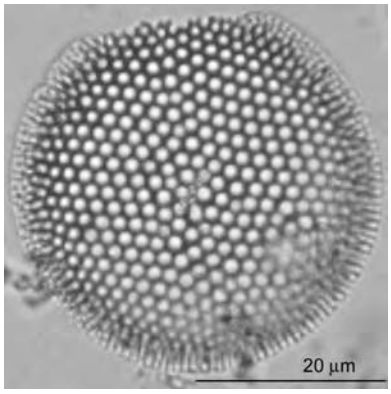

Figure 2.68. LM image of *Thalassiosira trifulta.*

The *T. trifulta* group is distinctive due to its large areolae that range from 5-6 per 10 µm. This species displays considerable variation when viewed using a scanning electron microscope (SEM), so is often described as a species group. I have not used the SEM to distinguish between species, so *T. oestrupii* is the only member of the *T. trifulta* group that has been classified separately (see section 2.2.15.6).

T. trifulta is a flat valve with large, hexagonal areolae arranged in radial, linear, or eccentric patterns across the valve face. Generally *T. trifulta* has 3 strutted processes in the valve center, but sometimes there are as few as 2 or as many as 5 or 6 arranged in 1 or 2 lines. The central strutted process has three struts which can sometimes be seen under the light microscope. One labiate process is located a few areolae away from the margin [*Medlin and Priddle*, 1990].

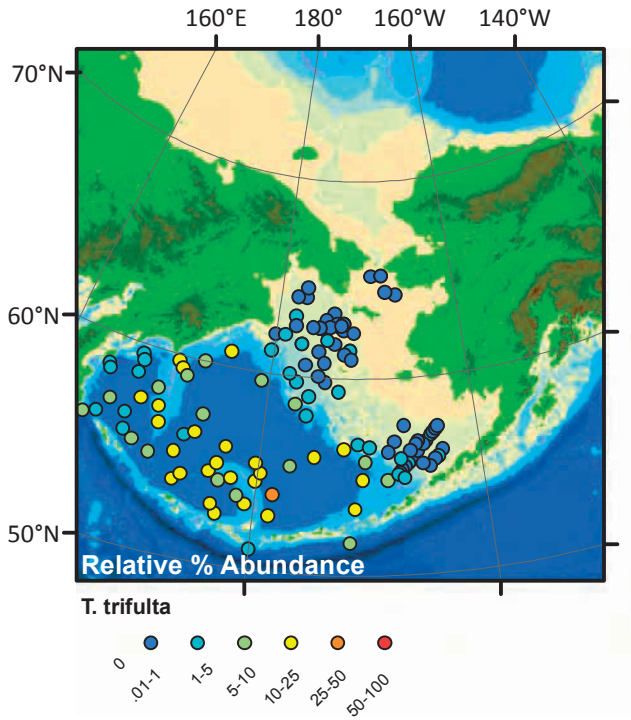

Figure 2.69 Map of *T. trifulta* distribution in the Bering Sea.

T. trifulta is associated with *A. curvatulus* and cold, low salinity, highly stratified water that forms after the sea ice melts. It is also prevalent in the cold, productive gyre of the Bering Sea, while Kazarina [1999] associates it with high salinity deep waters and Sancetta [*Sancetta*, 1982] associates it with highly productivity water of the basin gyres.

2.2.15.6 Other *Thalassiosira* Species

Several other common *Thalassiosira* species are pictured here. Detailed morphometric data can be found in table 2.7.

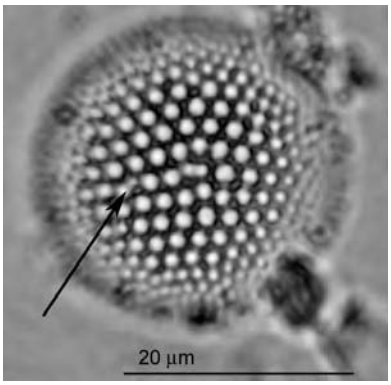

Figure 2.70. LM image of *T. oestrupii* (Ostenfeld) Hasle which has 1 central strutted process and 1 labiate process (LP) 2-3 areolae away. The arrow points to the LP.

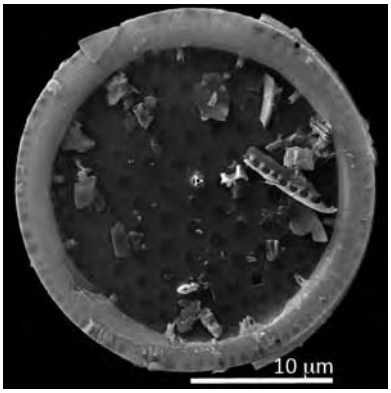

Figure 2.73. SEM image of *T. oestrupii.* The processes are clearer here.

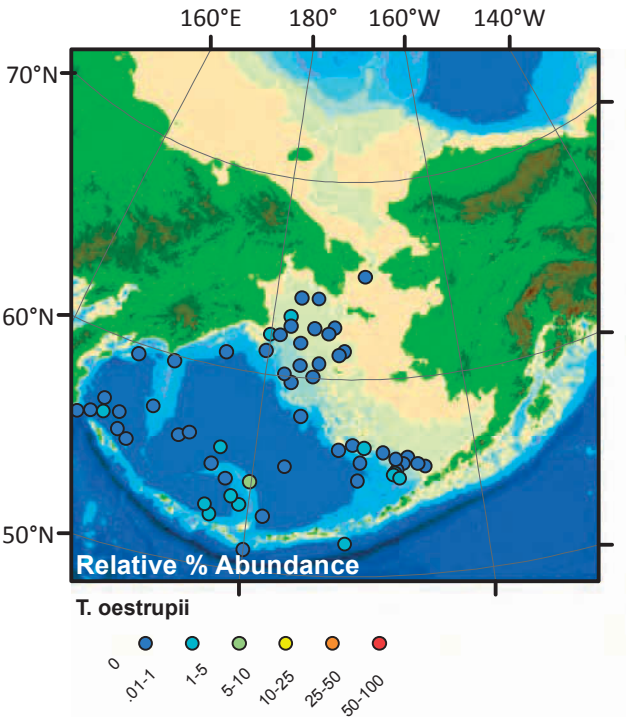

Figure 2.71 Map of *T. oestrupii* distribution in the Bering Sea.

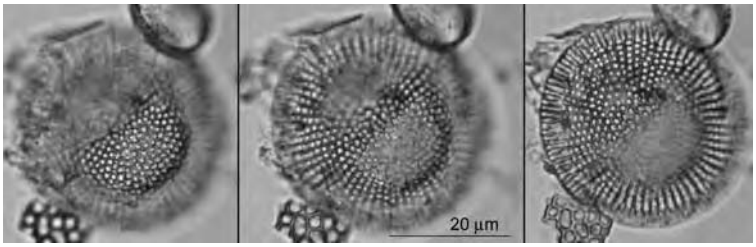

Figure 2.72. LM image of *Thalassiosira hyperborea* (Grunow) Hasle in three focal plains.

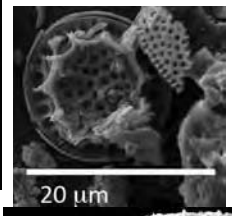

Figure 2.74. SEM image of *T. jouseae* Akiba This is a fossil species that occurs in sediments older than ~300-400 ka [*Barron and Gladenkov*, 1995].

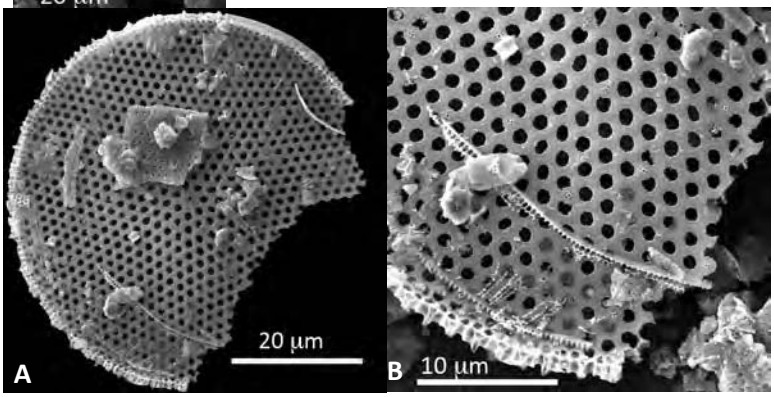

Figure 2.75. a) and b) SEM images of *T. eccentrica* (Ehrenberg) Cleve. Panel b shows the strutted processes covering the valve face.

2.2.16 Other pennate species

Many other pennate species were found in the sediments. These species occur as single individuals in a sample. Several of these minor species are pictured here.

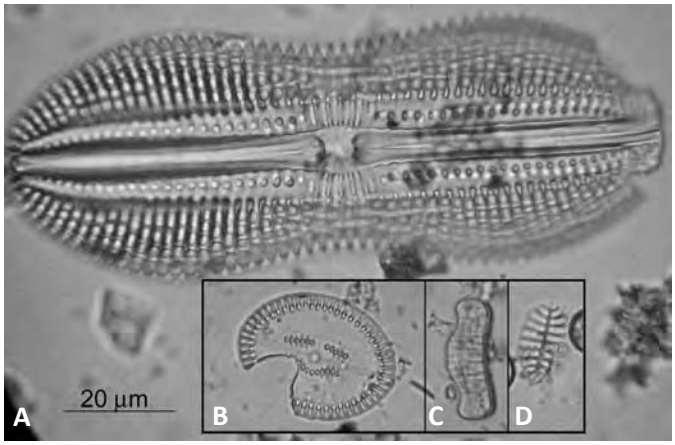

Figure 2.76. LM images of a) *Diploneis smithii* (Brébisson in W. Smith) Cleve b) and c) Unknown pennates, and d) *Cocconeis* Ehrenberg

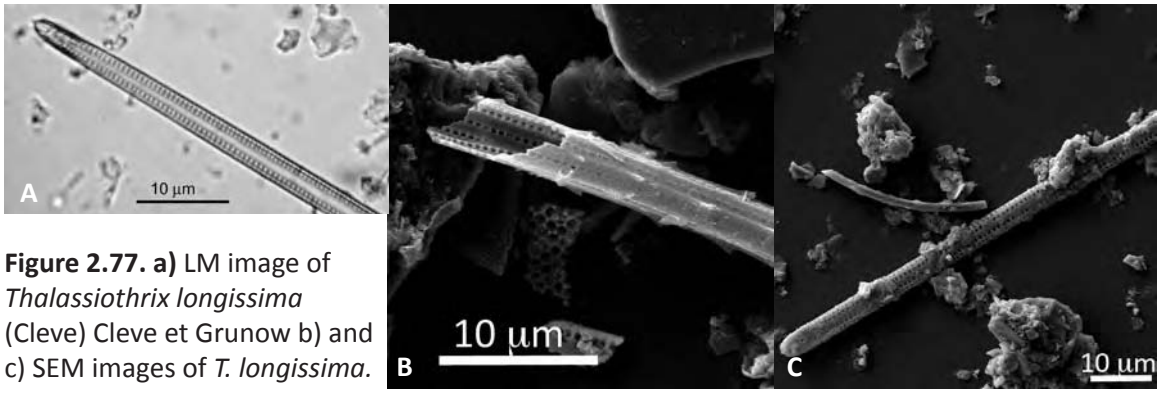

Figure 2.77. a) LM image of *Thalassiothrix longissima* (Cleve) Cleve et Grunow b) and c) SEM images of *T. longissima.*

2.2.17 Other centric species

There are several other centric species that do not make up more than 5% of any assemblage, but which may be important ecologically. Some of these species are pictured to the right and on the next page.

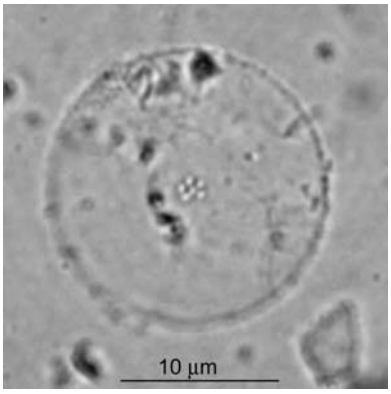

Figure 2.78. LM of *Pseudoposira elegans* Shushukova-Poretskaya

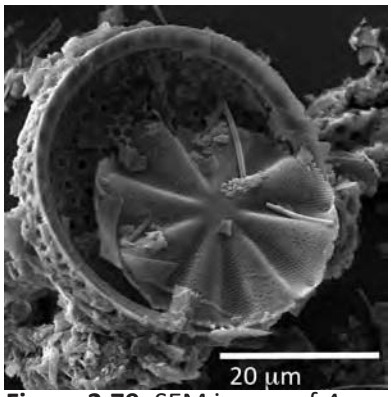

Figure 2.79. SEM image of *Actinoptychus* Ehrenberg resting inside a *Stephanopyxis turris* (Greville et Walker-Arnott) Ralfs valve.

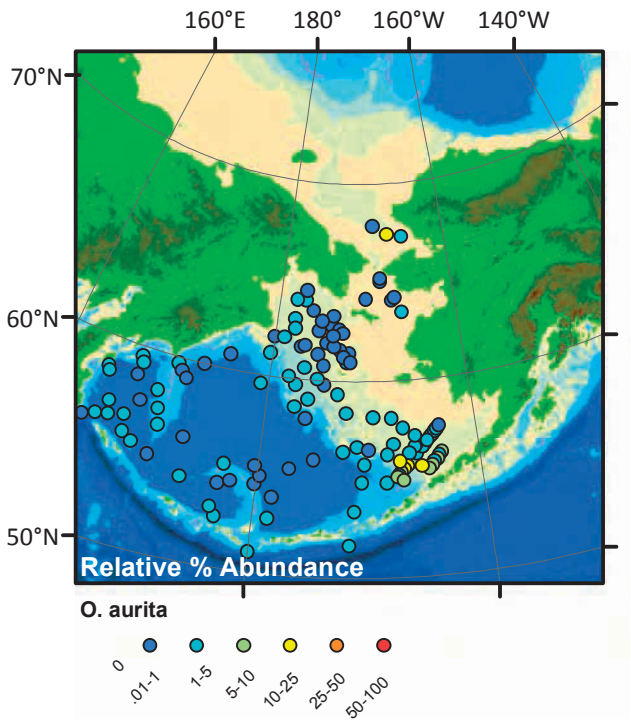

Figure 2.80 Map of *O. aurita* distribution in the Bering Sea.

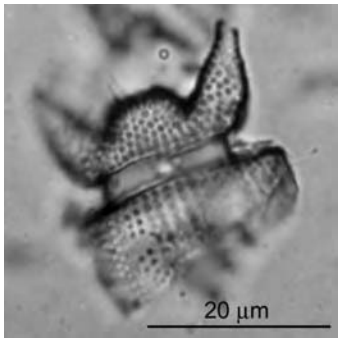

Figure 2.81. LM of *Odontella aurita* (Lyngbye) Agardh.

2.2.18 Freshwater species

Both species in this grouping belong to the Stephanodiscaceae family, which is one of the dominant fresh water families, present in lakes and slow moving rivers [*Håkansson*, 2002]; however, a few *Cyclotella* species are found in brackish and neritic environments (e.g. *C. stylorum*) [*Hasle and Syvertsen*, 1997]. These brackish species are not included in this grouping.

2.2.18.1 *Cyclotella ocellata* Pantocsek

C. ocellata is one of the smallest species encountered, often less than 10 µm in diameter, but ranging up to ~17 µm. It is a round, species with a mostly flat valve face. The most characteristic feature is the presence of three large papillae with corresponding depressions that sometimes connect the papillae in a y-shaped depression. Håkansson [2002] shows that this species can have up to five papillae, but I have only found species with three. Striae extend from the midway point of the valve face to the margin.

2.2.18.2 *Puncticulata radiosa* (Lemmermann) Håkansson

This is a very distinctive centric diatom with a flat valve face (~25 µm in diameter). The central area contains areolae arranged in loose concentric circles around the center. The middle third of the valve is covered by radially arranged ribs that sometimes bifurcate midway. These ribs may be striae [*Håkansson*, 2002]. Marginal processes are located at the end of each rib, approximately 4 µm from the valve edge.

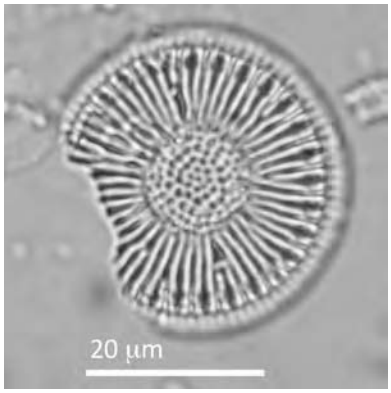

Figure 2.82. LM of *Puncticulata radiosa.*

CHAPTER 3

SIXTY YEARS OF SEA-ICE DRIVEN DIATOM ASSEMBLAGE CHANGES ON THE BERING SEA SHELF: A SIGNAL SUBDUED BY BIOTURBATION

3.1 Abstract

Components of the Bering Sea ecosystem ranging from commercially important fisheries to phytoplankton have been impacted by regime shift in the Pacific Decadal Oscillation (PDO) and changes in the intensity of the Aleutian Low over the past 60 years. The changes in these climate drivers are clearly recorded in sediment diatom assemblages. Diatom assemblages from core-tops collected in 1969 compared with core-tops collected in 2006 and 2007 show a significant change in one area of the Bering Sea shelf. This local change is largely due to variations in sea ice, perhaps brought on by an earlier melt season. In addition to comparing the two time-slices, magnetic susceptibility, grain size, and diatom assemblages were analyzed down-core in short (8-20 cm) Haps cores collected from four areas on the Bering Sea shelf. These short sediment sequences are moderately bioturbated, but still reflect shifting environmental conditions since 1950. Down-core, changes in diatom assemblages and accumulation rate are subtle, but appear to track changes the PDO index and strength of the Aleutian Low back to 1950. A core collected from the shelf slope break of the Bering Sea shows that during the positive phase of the PDO, the so-called green belt experienced higher productivity and warmer sea surface temperatures with reduced sea ice. Surface sediments on the Bering Sea shelf reflect modern conditions and are appropriate for future use in proxy calibration. Additionally, surface cores contain a record of decadal-scale environmental change that has been largely untapped for study.

3.2 Introduction

Recent environmental change in the Bering Sea includes regime shifts in the Pacific Decadal Oscillation [*Bond*, 2003; *Mantua et al.*, 1997], and corresponding changes in air and bottom water temperatures and sea ice [*Grebmeier et al.*, 2006b]. More recently an increase in the number of days that sea ice is present along the shelf-slope break has been detected [*Grebmeier et al.*, 2010] despite continued rapidly decreasing seasonal sea ice in the Chukchi Sea and Arctic Ocean [*Serreze et al.*, 2007]. These physical changes have manifest biological changes [*Grebmeier*, 2012] including a northward migration of pelagic fish from the southern Bering Sea [*Grebmeier et al.*, 2006b] and shifts in the timing and duration of sea-ice related primary productivity and the spring bloom [*Stabeno et al.*, 2001].

However, long term records of climate change in the Bering Sea span 30 or 40 years at most and are based either on repeated sampling of stations over decades [e.g. *Grebmeier et al.*, 2006b] or the satellite record [e.g. *Serreze et al.*, 2007]. Although there are a few records of Bering Sea climate change based on growth bands in coralline algae [*Halfar et al.*, 2011] and the geochemistry of a short gravity core [*Lu et al.*, 2005], few studies have looked at Bering Sea sediments in high resolution to recreate the climate of the very recent past. Additionally, questions remain about whether the bioturbated shelf sediments can be used as a proxy for a rapidly changing environmental parameter, such as sea ice, or if they even represent modern conditions.

Here we look in detail at diatom assemblages, grain size, magnetic susceptibility, and lead and cesium isotopes in four areas of the Bering Sea shelf (Figure 3.1). We show that surface sediments record modern deposition and are subject to moderate levels of bioturbation. Perhaps because environmental changes have, in some cases, been quite extreme in the region, the sediments record subtle differences between two time-slices (1969 vs. 2006/2007) and

down-core the highly bioturbated record of change has been muted, but not completely obscured.

3.3 Study Location

3.3.1 Hydrography and Productivity of the Bering Sea Shelf

Pacific water enters the marginal sea through deep passes in the Aleutian Islands and circulates cyclonically around the deep basin of the Bering Sea before moving onto the shelf and flowing northward through the Bering Strait. Acceleration of currents along the 100 m isobath [*Stabeno et al.*, 1999] and tidal movements drive upwelling through canyons along the shelf-slope break [*Kowalik*, 1999]. On the shelf, there are three distinct water masses. The Anadyr Water is confined to the western part of the shelf. It is the coldest and has the highest salinity of the three water masses. Alaska Coastal Water, in the east, is fresher, warmer, and has a lower nutrient concentration. These two water masses make up the bulk of the flow through the Bering Strait [*Codispoti et al.*, 2009]. The third water mass is the Bering Shelf Water, which is

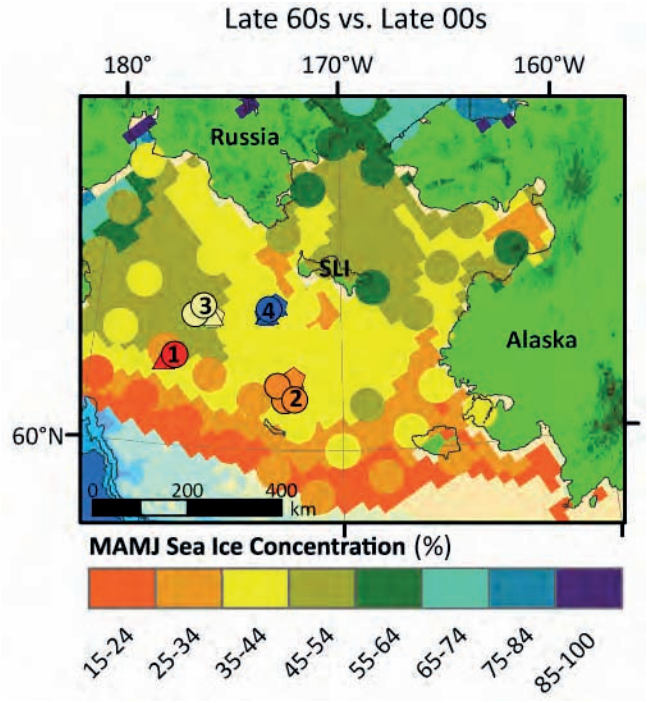

Figure 3.1. Study area showing sample locations and sea ice concentration. Colored contours show average MAMJ sea ice concentrations for 1998-2007 derived from the SSM-I passive microwave sensor data [Cavalieri et al., 1996]. Large dots show average MAMJ sea ice concentrations for 1960-1969 derived from the Chapman and Walsh [1991] dataset. Circles denote samples collected in 1969, pentagons are samples collected in 2006, and triangles are samples collected in 2007. SLI = St Lawrence Island. Each of the four Areas mentioned in the text are numbered and color coded. Area 1 = red; Area 2 = orange; Area 3 = buff; Area 4 = blue.

intermediate to Anadyr and Alaska Coastal Water in terms of temperature and salinity [*Grebmeier et al.*, 2006a].

Sea ice is seasonally present across the entire shelf and influences the salinity and temperature of these water masses. In general, sea ice forms along the coast in the northern Bering Sea and is moved southward by prevailing winds. Coincidently, winter cyclonic storms enter the Bering Sea from the south and effectively move sea ice back to the north. This means that in years when the Aleutian Low is intensified, sea ice extent is low [*Overland and Pease*, 1982]. Salinity is high in polynyas to the lee of islands where ice forms and low near the shelf-slope break where the ice melts [*Stabeno et al.*, 1999]. Sea ice also influences the timing and intensity of primary productivity in the Bering Sea. The seasonal succession of diatom productivity on the Bering Sea shelf begins with the epontic, or under/within ice bloom when photosynthetically active radiation (PAR) reaching the base of the ice becomes strong enough to initiate photosynthesis. As soon as the sea ice begins to break up, the epontic bloom is replaced by the marginal ice bloom [*Alexander and Niebauer*, 1981; *Schandelmeier and Alexander*, 1981], which is strongest in years when the marginal ice zone reaches the zone of upwelling along the shelf slope break, the so-called "Green Belt" [*Springer et al.*, 1996]. These two ice-related blooms are followed by the spring phytoplankton bloom and lower summer and fall diatom productivity [*von Quillfeldt*, 2000]. Diatom productivity is limited by light early in the season and nutrients later on [*Gradinger*, 2009; *Niebauer et al.*, 1995]. Because sea ice plays an important role in influencing both light and nutrients [*Stabeno et al.*, 2001] and changes in sea ice duration and extent have a significant impact on diatom productivity[*Grebmeier*, 2012], reductions or increases in primary productivity should be reflected either by a change in diatom assemblages or in diatom accumulation rates in the sediments.

3.3.2 Regional Climatological Teleconnections

The Pacific Decadal Oscillation (PDO) is an index of climate variability, much like the El Niño Southern Oscillation (ENSO). In contrast to ENSO, the PDO is persistent for several decades as opposed to several years. It primarily impacts the North Pacific and North Atlantic [*Mantua et al.*, 1997] and is one of the primary controls on climate in the Bering Sea. Positive values of the PDO correspond to warm winters with increased productivity [*Bond*, 2003], an intensified Aleutian Low, and high salmon catches [*Mantua et al.*, 1997]. Regime shift from negative to positive values occurred in 1925 and 1977. A regime shift to negative values occurred in 1947 [*Mantua et al.*, 1997]. In 1998, a secondary shift in sea level pressure and sea surface temperatures occurred again, but its signature is a departure from previous PDO regime shifts [*Bond*, 2003]. Grebmeier and co-authors [2006b] attribute increasing air and bottom water temperatures and an earlier onset of the melt season to changes in both the PDO and the Arctic Oscillation. They observe a northward migration of pelagic fish from the southern Bering Sea and a decline in the benthic infaunal biomass that supports large predators such as sea ducks, whales, and walrus [*Grebmeier et al.*, 2006b]. Such changes in benthic and pelagic ecosystems are a response to changes in organic carbon export from the surface waters [*Grebmeier*, 2012].

3.4 Materials and Methods

3.4.1 Sediment Samples

3.4.1.1 Sediments collected in 2006 and 2007

Haps sediment cores [modified from the design *Kanneworff and Nicolaisen*, 1973] were collected on board the icebreaker USCGC Healy in May and June of 2006 and 2007 (cruises HLY0601 and HLY0702). The Haps corer is designed to preserve the sediment water interface

and in many cases, the water was clear when it was brought on deck, indicating that we were successfully recovering the most recent sedimentation. The cores, which range in length from 13 to 18 cm, were extruded in 1 cm intervals, bagged, and refrigerated until analysis. In 2006, several Haps cores were subsampled using a PVC pipe inserted through the center of the full Haps. Many stations were sampled twice during each cruise and most of the stations occupied in 2006 were revisited in 2007.

3.4.1.2 Sediments collected in 1969

In the late summer of 1969, the R/V Thomas G. Thompson (cruise TT42) and USCGC Northwind (cruise NW69) visited the Bering Sea, taking gravity cores along the ships' tracks. Both ships also collected piston cores at select stations. Smear slides were made from these core tops (1-2 cm) and examined for diatom taxonomy [*Sancetta*, 1982] and ecological distribution [*Sancetta*, 1981]. It is possible that some of the smear slide samples from these older cores were actually taken from the piston cores, but based on the nature of the studies that they were obtained for it is more likely that all smear slides were made from the gravity cores. We assume that the smear slides include sediments representative of late 1960s deposition.

3.4.1.3. The Four Areas

For this study, four Areas were delineated south of St. Lawrence Island across the Bering Sea shelf. Area 1 is located near the shelf-slope break in the present-day "Green Belt" [*Springer et al.*, 1996]. Area 2 is in shallower water southeast of Area 1. It is likely overlaid by Bering Shelf Water. Area 3 is also in shallow water, northeast of Area 1. It may be overlaid by Anadyr Water or Bering Shelf Water. Area 4 is southwest of Saint Lawrence Island and is similarly overlain by Anadyr and Bering Shelf Water.

In each of these four areas, sediments collected in 1969 were located near (<25 km) Haps core stations collected almost 40 years later (Figure 3.1). Diatom assemblages were re-counted from seven of these archived smear slides. We also looked at diatom assemblages down-core at Area 1 (Site HLY0702 DBSB/145) to detect changes in recent productivity and at grain size, magnetic susceptibility, and x-radiographs from several other short cores across the shelf to characterize sedimentation and bioturbation (see Table 3.1 for station information and a list of which stations were assigned to each Area).

Table 3.1: Station Information and Associated Areas

Station	Latitude	Longitude	Water Depth	Date Collected	Sample Type	Depth	Area
Hly 0702 DBSB/164	61.613	-177.122	119	6/15/2007	Haps	0-13	1
Sancetta TT42-147	61.698	-176.6883	109	9/9/1969	smear slide	0-1	1
Hly 0601 NEC5/1	61.384	-171.951	57	5/9/2006	Haps	0-18	2
Hly 0702 NEC5/1	61.382	-171.962	60	5/18/2007	Haps	0-1	2
Sancetta TT42-117	60.945	-172.252	65	9/6/1969	smear slide	0-1	2
Sancetta TT42-24	61.21	-172.533	67	8/24/1969	smear slide	0-1	2
Sancetta TT42-67	60.962	-171.842	63	8/29/1969	smear slide	0-1	2
Hly 0601 DLN4/24	62.511	-175.293	81	5/15/2006	Haps	0-1	3
Hly 0702 DLN4/8	62.513	-175.3	81	5/20/2007	Haps	0-1	3
Hly 0702 DLN4/145	62.513	-175.3	80	6/12/2007	Haps	0-1	3
Sancetta NW69-27	62.5	-176	nd	6/15/1969	smear slide	0-1	3
Sancetta TT42-40	62.663	-175.645	84	8/26/1969	smear slide	0-1	3
Hly 0601 SWC3/18	62.582	-173.069	59	5/14/2006	Haps	0-1	4
Hly 0702 SWC3/24	62.582	-173.087	63	5/23/2007	Haps	0-1	4
Hly 0702 SWC3/116	62.577	-173.065	64	6/7/2007	Haps	0-1	4
Hly 0601 SWC3a/29	62.756	-172.714	60	5/17/2006	Haps	0-16	4
Hly 0601 SWC3a/90	62.758	-172.711	60	5/29/2006	Haps	0-1	4
Hly 0702 SWC3a/33	62.755	-172.7	62	5/25/2007	Haps	0-1	4
Sancetta TT42-37	62.655	-172.957	64	8/26/1969	smear slide	0-1	4

3.4.2 Sedimentology

3.4.2.1 Down core X-Radiographs and Magnetic Susceptibility

All subsampled Haps cores collected during Healy 0601 were split along the core axis and x-rayed at the UMass Amherst University Health Services to determine sediment density. Cores were laid 101 cm from the beam and x-rays were taken using 60-70 kV and 5 mAs beam characteristics. X-radiographs were scanned at 2400 dpi to create digital images of the cores. Magnetic susceptibility was measured on these same cores in 0.5 cm intervals using a Bartington Magnetic Susceptibility Meter Model MS2.

3.4.2.2 Grain Size

Grain size was measured on samples collected in 2006 and 2007 using the Coulter LS200 laser diffraction particle analyzer. Pretreatment of sediments follows Sakamoto's [2005] procedure; however, samples were not centrifuged between chemical treatments to avoid losing very fine sediments. Instead chemical volumes were adjusted so that each treatment was neutralized before the next chemical was added. Pretreatment was necessary to remove organics, carbonates, biogenic opal, and to disperse clay particles. This allows the determination of patterns in sedimentation of terrigenous grains without influence from biogenic particles.

3.4.3 Age Dating

Samples were initially taken in 3 cm intervals down the length of a Haps core from Area 1, HLY 0702 DBSB/164 (hereafter DBSB). Sediments were dried in an 80° C oven, homogenized, and crushed using a mortar and pestle. A Canberra GL2020R low-energy Germanium gamma well detector with low-background cryostats was used to measure lead and cesium isotopes in each sample. Count times averaged 2-3 days until the standard error was appropriately small.

Pb-214 was assumed to be in secular equilibrium, and used as a proxy for supported ^{210}Pb (Figure 3.2). Unsupported (atmosphere-derived) ^{210}Pb was calculated as the difference between ^{210}Pb and ^{214}Pb. After a small ^{137}Cs peak was located, the core was resampled at 1 cm intervals above and below this peak and analyzed using an identical protocol.

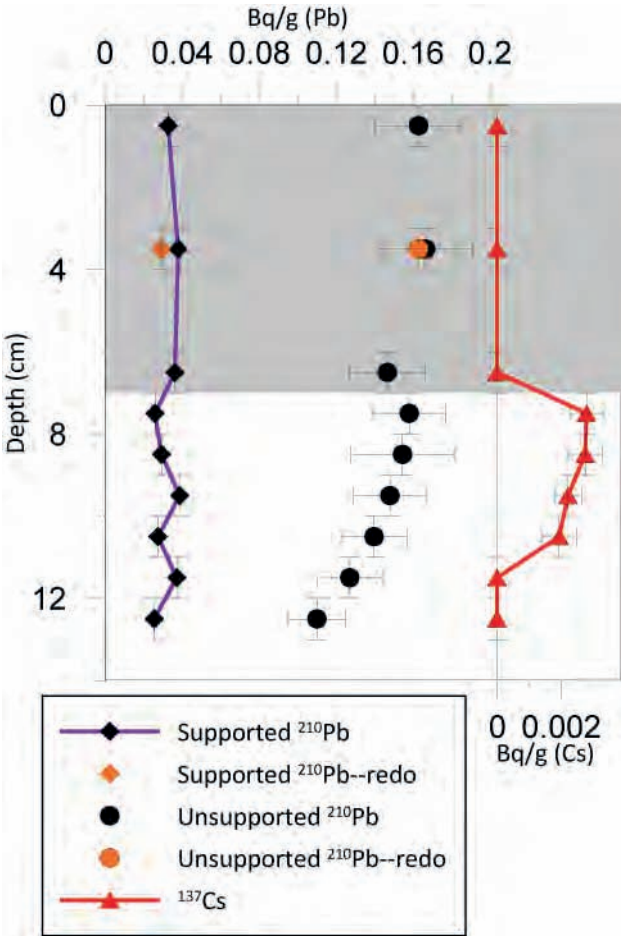

Figure 3.2. Down-core profiles of lead and cesium isotopes for HLY 0702 DBSB/145 (Area 1). The grey box indicates the mixed layer in the core. Unsupported ^{210}Pb was calculated as the difference between total ^{210}Pb and ^{214}Pb. A replicate sample was run at 3.5 cm. This is shown in orange on the plot.

3.4.4 Diatom Assemblages

Quantitative diatom slides were prepared according to the method described in Scherer [1994]. Cover slips were mounted on cleaned microscope slides using hyrax in toulene (refractive index: 1.7135). This method allows for a direct comparison of diatom flux to the sediments between samples. At least 300 diatom valves in at least three random transects across the slide were identified using an Olympus BH-2 transmitted light microscope at a magnification of 1250x [see *Armand et al.*, 2005; *Sancetta*, 1979; *Sancetta and Silvestri*, 1986; *Scherer*, 1994]. The transects were measured using a stage micrometer. Partial valves were counted according to the methods of Schrader and Gersonde [1978]. All diatoms were identified

to the species level when possible following published taxonomic descriptions and images [*Hasle and Heimdal*, 1968; *Koizumi*, 1973; *Lundholm and Hasle*, 2008; 2010; *Medlin and Hasle*, 1990; *Medlin and Priddle*, 1990; *Onodera and Takahashi*, 2007; *Sancetta*, 1982; 1987; *Syvertsen*, 1979; *Tomas*, 1996; *Witkowski et al.*, 2000]. All resting spores of *Hyalochaete Chaetoceros* were grouped together into one taxon. Diatom counts were transformed into relative percent abundances. Absolute abundances (diatoms per gram sediment) were calculated following the methods of Scherer [1994].

The previously published diatom counts from the 1969 sediments were not used because Sancetta [1981] grouped together several key species and neglected others because their taxonomy was unknown. For example, Sancetta [*Sancetta*, 1982] grouped all *Fragilariopsis* species together, but today we know that there are at least six different *Fragilariopsis* species present in the Bering Sea with varying affinities for sea ice [*Lundholm and Hasle*, 2010]. Most pennate diatoms were grouped (both neritic species and ice-related species), although these two types of pennate diatoms record very different depositional environments. Many *Chaetoceros* RS were not counted because its taxonomy was unknown at the time [*Sancetta*, 1982], and at least one important, sea-ice related species has been described since these counts were published (i.e. *Fossula arctica* [*Hasle et al.*, 1996]).

The archived diatom slides made from sediment collected in 1969 were not originally prepared as quantitative slides, but simply as smear slides [*Sancetta*, 1981], so it is not possible to calculate the absolute abundance of diatoms in these samples. Only relative percent abundance data can be obtained. However, diatom counting was carried out the same as above with at least 300 valves counted in at least three transects in each sample.

Diatom assemblages were compared using the analysis of similarity (ANOSIM) measure described in Clarke [1993]. This is a statistical test that can be used to determine if there are

differences between populations. There is no assumption of independence and no limit on the number of variables (i.e. taxa) associated with each sample. R is the test statistic (unrelated to r^2 values) and is based on the ranked similarities between stations. By definition, R will fall between 0 and 1, with values close to zero indicating that the null hypothesis cannot be rejected [*Clarke*, 1993]. The two-way ANOSIM was used to test the nested null hypotheses:

1) There is no difference between diatom assemblages at Areas 1 through 4.

2) There is no difference between diatom assemblages for samples collected in 1969 vs. samples collected in 2006-2007.

One-way ANOSIM was then used to test the null hypothesis that there is no difference between diatom assemblages at the two time slices within each area.

3.5 Results

3.5.1 Sedimentology

Visual inspection of microscope slides made from core tops and short cores reveals that the sediments are composed primarily of a mix of diatoms, terrigenous clay and silt, and lesser amounts of tephra shards, and sand grains. Silicoflagellates are common, as are sponge spicules. Occasional coccolithophorids are found. Chains (>3 frustules) of colony forming diatoms, such as *Paralia sulcata, Fragilariopsis* spp., and *Fossula arctica*, are found in all four areas in both new and old samples.

Short cores contain massive, mixed sediments, and x-radiographs reveal few sedimentary structures. What structures are present appear to be related to sediment processing by infauna (see Figure 3.3. black arrow). The most obvious component of the short cores are several different species of bivalves located throughout the cores, but worm tubes are also visible in some core x-rays (Figure 3.3).

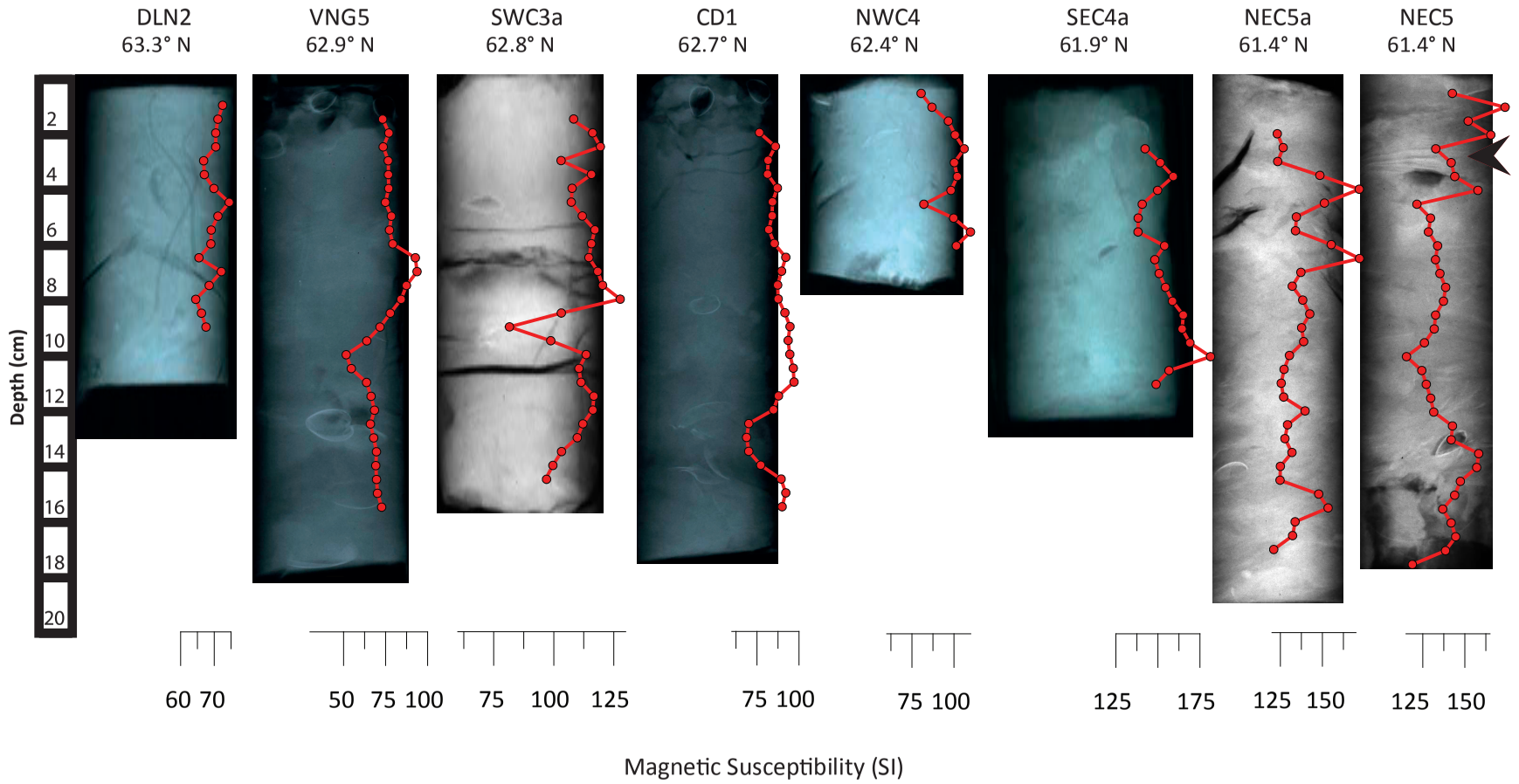

Figure 3.3. X-ray images of short HAPS cores collected during the Healy 0601 cruise. The dominant features of these images are the massive character of the sediments and presence of bivalves and burrows throughout. Magnetic susceptibility for each core is plotted on top of the core image. Cores are arranged in decreasing latitude from left to right.

Surface and down-core sediments vary in size from 0.3 µm (clay) to 200 µm (very fine sand). Grain size profiles show relatively poorly mixed sediments with broad peaks centered around 40 µm (silt). There is only a subtle change down-core in grain size. At Area 2, HLY0601 NEC5, the mode becomes more defined between 1 and 2 cm and is associated with laminations directly above a bivalve shell (Figure 3.4).

Magnetic susceptibility varies between 60 and 175 SI down-core in all short cores and decreases with increasing latitude. Visually, the magnetic susceptibility traces for NEC5 and NEC5a (Area 1) share many trends, but not all. NEC5a was sampled 20 days after NEC5 and 3.8 km away from the original station. Similarly, SWC3a (Area 4) also shares some similarity with the cores in Area 1. However, the variability in these cores is high and there does not appear to be any robust trends in magnetic susceptibility over time. No other obvious correlation exists between sites based on changes in magnetic susceptibility or sediment characteristics (Figure 3.3).

3.5.2 Age Model for HLY 0702 DBSB/145 (Area 1)

Unsupported ^{210}Pb shows little variation in the top 7-9 cm of DBSB, and decreases linearly below 7 cm, although it does not reach values equivalent to supported ^{210}Pb (Figure 3.2). Unsupported ^{210}Pb is present throughout the core, therefore, we are unable to create a reliable age model based on ^{210}Pb; however, because the half life of ^{210}Pb is 22.3 years, the entirety of the core must be younger than ~150 years [*Preiss et al.*, 1996].

^{137}Cs shows a broad (3 cm thick) peak between 7.0 cm and 11.0 cm (Figure 3.2). We assigned 1963, the year that ^{137}Cs peaked in the atmosphere [*Thomson et al.*, 2002], to the median depth of the ^{137}Cs peak, which is 9.5 cm. Using a linear sedimentation rate of 0.22 cm per year, ages were assigned to samples downcore. This method assigns a year of 2007 to the

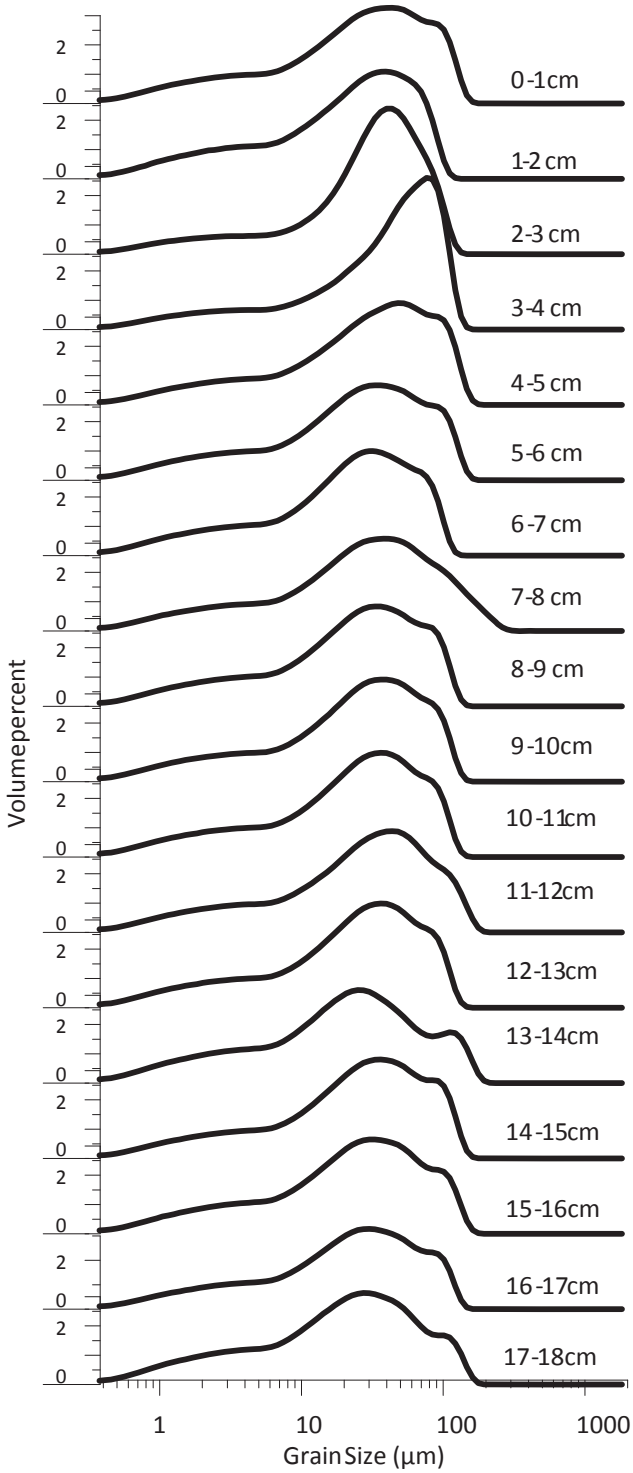

Figure 3.4. Plots showing grain size down-core in Healy 0601 NEC5/001. Volume percent for each trace ranges from approximately 0 to 3%, but the axes are overlapping. Each trace represents the grain size distribution in a 1 cm slice from the core.

top of the core (the year the core was taken), 1975 to the base of the mixed layer, and 1949 to the base of the core (12.5 cm).

3.5.3 Diatom assemblages

3.5.3.1 Diatom Assemblages in Surface Sediments

The major diatom species found in sediments across the southern Bering Sea shelf include resting spores of *Chaetoceros* species (hereafter, *Chaetoceros* RS), *Fragilariopsis cylindrus, Fragilariopsis oceanica, Paralia sulcata,* and *Thalassionema nitzschioides* with minor contributions from *Delphineis surirella, Fossula arctica, Thalassiosira antarctica* resting spores (RS), *Thalassiosira hyalina, Melosira sol, Thalassiosira nordenskioeldii,* and *Navicula* sp. (Figure 3.5). Two-way analysis of similarity (ANOSIM) [*Clarke*, 1993] shows that overall, the four different areas have significantly different diatom assemblages (R: 0.56, p=0.0016, but the two ages of samples (1969 vs. 2006/2007) do not have significantly different diatom assemblages (R = 0.11, p = 0.36). When the similarity in each area is analyzed separately, only Area 2 shows a significant difference in diatom assemblages for the two different ages (R = 0.75, p = 0.093) at a 90% confidence level. This is shown graphically in a non-metric multi-dimensional scaling diagram which is unit-less, but shows the relative similarity between samples (Figure 3.6). In this figure, samples with similar diatom assemblages plot close together, while samples with less similar diatom assemblages plot farther away from each other. Clusters of samples indicate a population of similar diatom assemblages. When the diatom assemblages are transformed to presence or absence data, which puts a very high weight on minor species, ANOSIM shows that both the four different areas and the two different ages of stations have significantly different diatom assemblages (R = 0.3, p = 0.06, and R: 0.5, p=0.02 respectively) at a 90% confidence level.

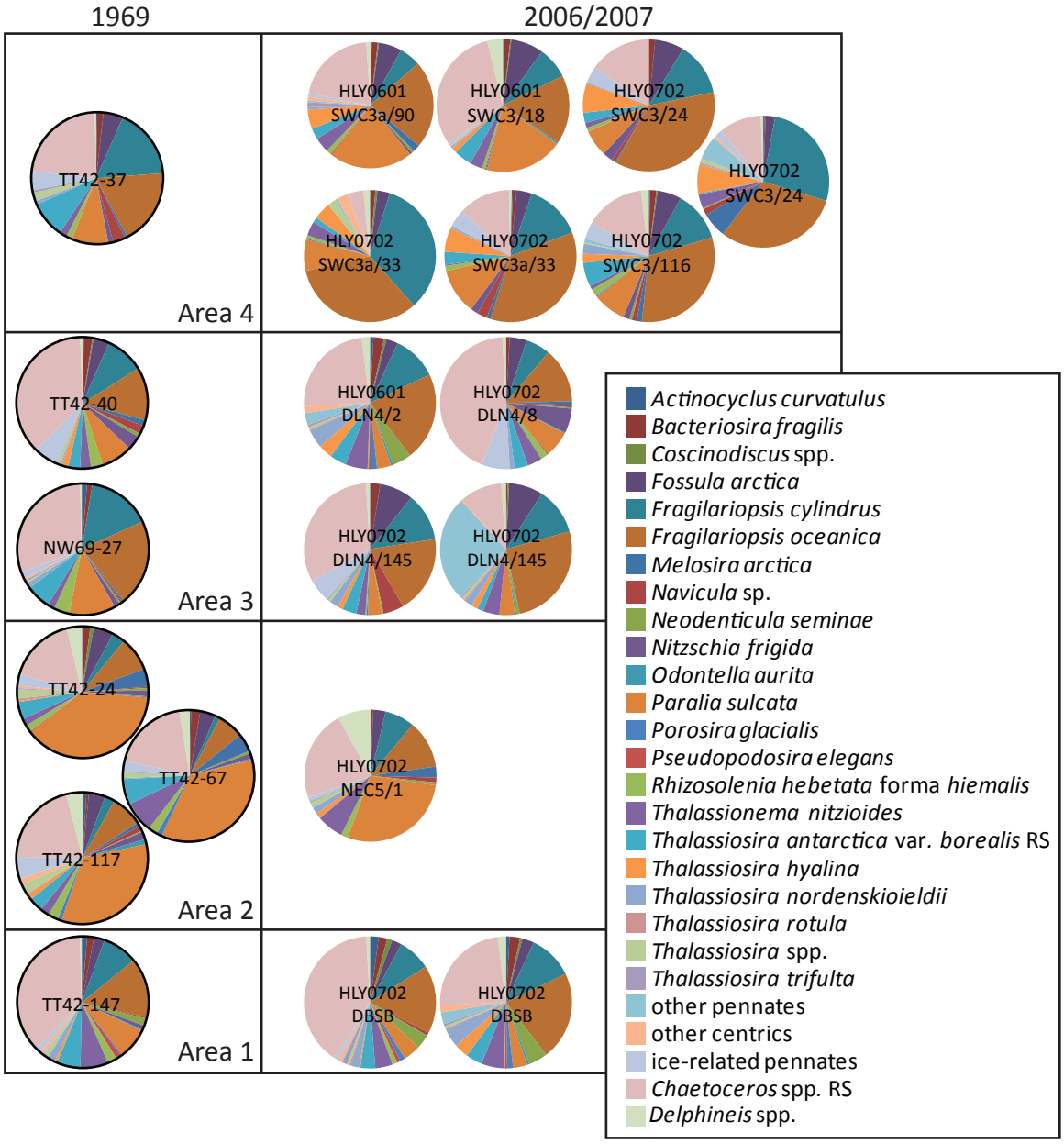

Figure 3.5. Pie charts showing the differences in diatom assemblages between samples and between years. Samples collected in 1969 are outlined in black and located in the first column, samples collected in either 2006 or 2007 are in the second column. Each row denotes an area as described in the text. Note that several samples were counted twice and several areas were visited more than once.

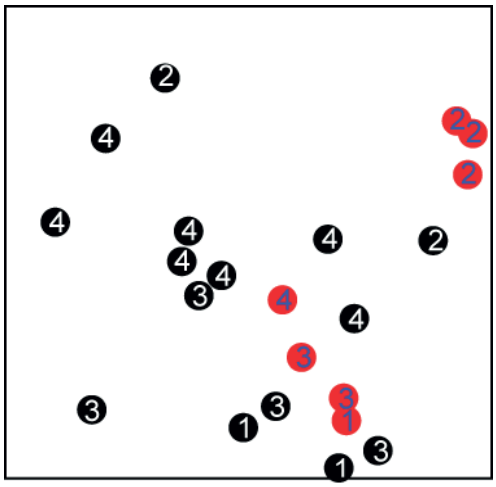

Figure 3.6. Graphical representation of non-metric multi-dimensional scaling. Both axes represent similarity coeffients, which are relative measures of similarity. Since these are only relative measures, the axes are value-less. Stations are labeled according to Area (1-4). See the map in Figure 3.1 for locations of the different areas. The colors denote whether they were collected in 1969 (red) or 2006-2007 (black). Stations that plot close together in this figure have very similar assemblages whereas stations that plot far apart have less similar assemblages. An ANOSIM test shows that there is a significant difference in diatom assemblages at the 4 areas, but no difference between samples collected in the different years. The exception to this is Area 2, where there is a difference in assemblages collected in the different years. This is seen in the plot by all the 1969 (red) stations plotting close together, but far from the Area 2 recent (black) stations. Stress, which is a measure of the scatter between observed and expected similarity rank, is 0.13, which indicates that this graphical representation is a reasonable portrayal of real ecological difference [Clarke, 1993].

3.5.3.2 Down-core changes in diatom assemblages

The diatom species that dominate the down-core assemblages are similar to those that dominate the surface sediments. They include *Chaetoceros* RS, *T. nitzschioides,* and, *F. oceanica* with minor contributions from *T. nordenskioeldii, T. antarctica* RS, *F. cylindrus, F. arctica, P. sulcata,* and *N. seminae.* The variability stems mainly from alternations between relative percent abundances of *F. oceanica* and *Chaetoceros* RS. A small increase in *T. nitzschioides* occurs in ~1971.

Diatom accumulation rates vary down-core at Area 1 between 40 and 100 million valves per gram of sediment. Increases in diatom accumulation rate down-core are often associated with higher relative percent abundances of *Chaetoceros* RS. The main components of the diatom assemblage from the Area 1 sample collected in 1969, TT42-147, are very similar to those in the assemblage at DBSB today and in the past ~80 years (Figure 3.7).

3.6 Discussion

3.6.1 Modern Deposition on the Bering Sea Shelf

Modern deposition is often assumed in proxy development studies that compare core-top sediments to current climatological conditions [e.g. *de Vernal et al.*, 2001; *Pichon et al.*, 1987; *Sancetta*, 1981], however, sedimentation regimes are complex and shelf areas may have regions of deposition and regions of non-deposition or erosion quite close to one another. On the Bering Sea shelf, diatom preservation, grain size analysis, and lead and cesium dating confirm that the top 1 cm of sediments in the four areas examined was deposited within the past 35 years.

3.6.1.1 Diatom Colony Preservation

Several types of diatoms form colonies by attaching to each other in various ways. Three types of colony-forming diatoms were found in every sample we examined: *P. sulcata, Fragilariopsis* spp., and *F. arctica. P. sulcata* forms colonies by linking siliceous grooves and ridges on its valve face with corresponding grooves and ridges on a neighboring valve face [*Round et al.*, 1990]. Such connections would be expected to be quite refractory in the sediments and so these colonies would likely be found far down-core. However, *Fragilariopsis spp.* and *F. arctica* form colonies by excreting a mucilage pad along the surface of the valve that

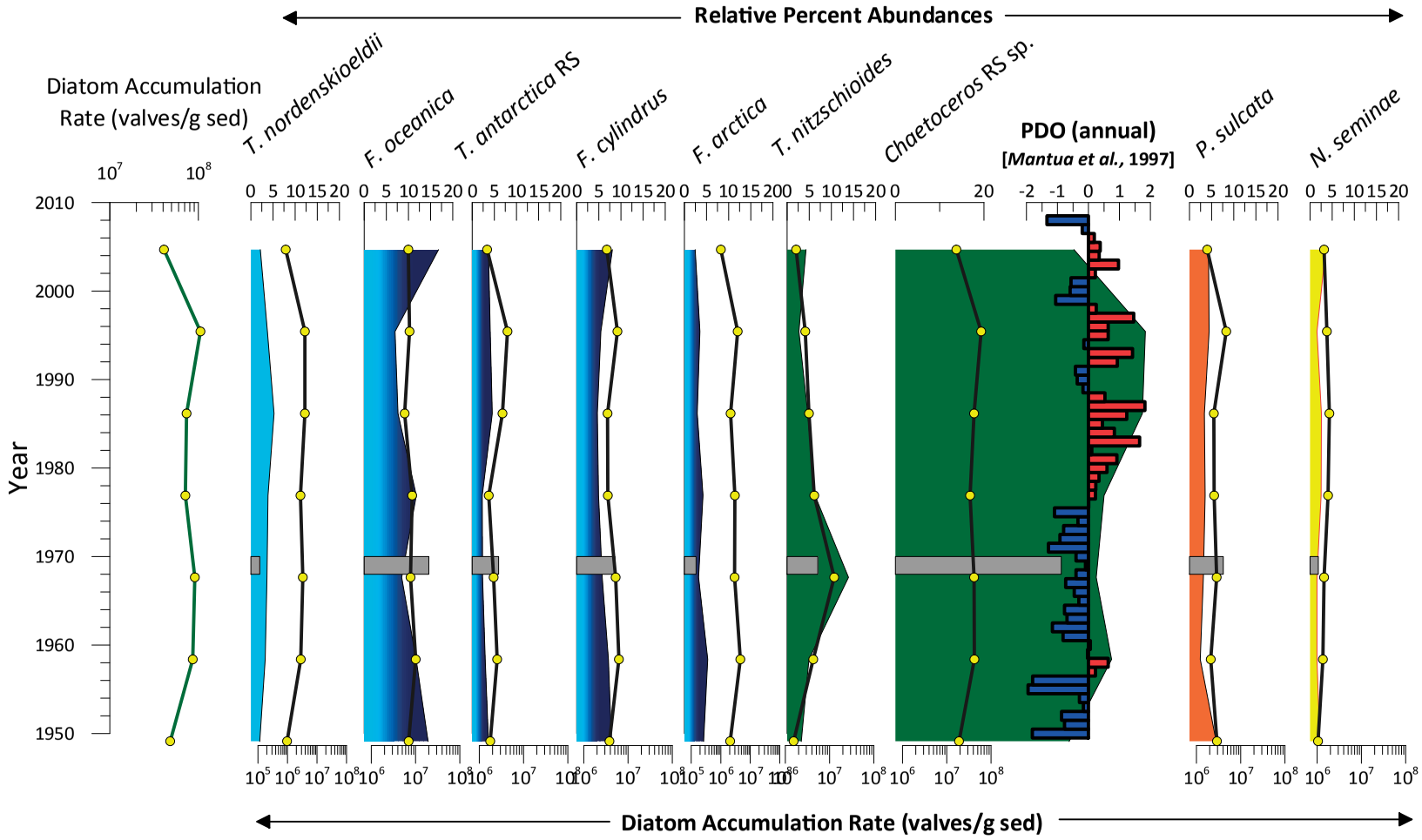

Figure 3.7. Down-core changes in diatom assemblages at HLY 0702 DBSB/145. Both diatom accumlation rate (bottom axis, line plots), and relative percent abundances (top axis, area plots) are shown for major (> 10%) diatom taxa. Also shown are relative percent abundances in the nearby station TT 42-147, collected in 1969 (grey bars). The Pacific Decadal Oscillation Index is plotted above relative percent abundance of *Chaetoceros* RS. Red bars indicate positive values of the PDO, blue are negative values [*Mantua, et al.,* 1997].

attaches the frustule to a neighboring frustule. This pad is presumed to be made of polysaccharides [*Round et al.*, 1990] and would probably be quite labile in the sediments. Every sample has occurrences of long ribbon colonies of *Fragilariopsis spp.* and *F. arctica,* therefore, we conclude that these species had been recently deposited, and perhaps even deposited from the bloom of the year they were collected.

3.6.1.2 Grain Size and Sorting

Detailed grain size analysis of these sediments and from other core tops in the region shows that sediments on the Bering Sea shelf tend to consist of either poorly sorted clay and silt or well sorted silt and sand [*Caissie et al.,* in prep. See figure 6.5]. However, all four areas in this study are composed of poorly sorted clay and silt (Figure 3.8), which are generally reflective of

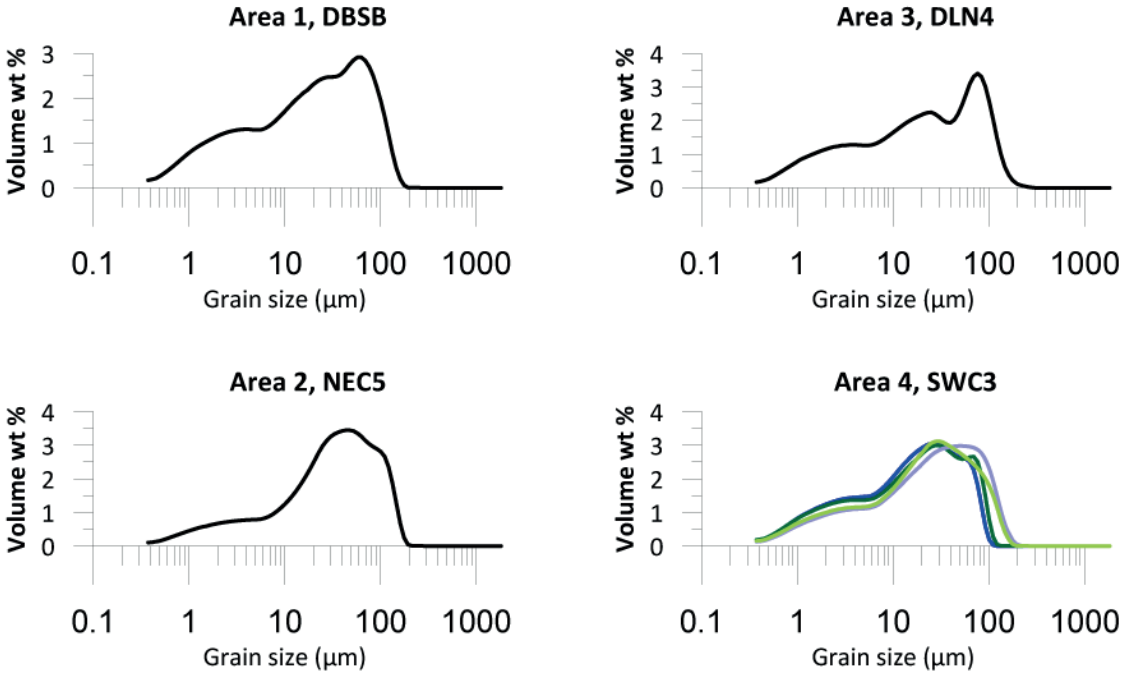

Figure 3.8. Grain size profiles for each area examined on the Bering Sea shelf. The different color traces in Area 4 refer to samples collected in slightly different locations or different years (2006 or 2007) and are included to demonstrate reproducibility and accuracy within a single area.

pelagic deposition [*Gardner et al.*, 1980]. One area north of St Lawrence Island was rejected from this study because the granulometric analysis indicated the sediments were very well sorted sand, which may be a sign of winnowing or transport by strong currents [*Gardner et al.*, 1980].

3.6.1.3 Bioturbation and Radiogenic Isotopes

Lead and cesium isotopes also indicate modern deposition. The presence of unsupported ^{210}Pb throughout core DBSB (Figure 3.2) indicates that the entire core was deposited within the past ~150 years [*Nittrouer et al.*, 1979]. This is further supported by recent ^{210}Pb dating of 12 cores in the Bering Sea which showed unsupported ^{210}Pb across the shelf [*Oguri et al.*, 2012], indicating wide-spread, recent deposition of sediments in the Bering Sea.

Bioturbation on the Bering Sea shelf has been estimated to range from 6 to 10 cm, with less bioturbation occurring under the Alaska Coastal Waters [*Grebmeier and McRoy*, 1989] and up to 35 cm down on the Chukchi Sea shelf [*Cooper et al.*, 2009]. Bioturbation occurs due to sediment processing by worms, bivalves, and other infauna [*Grebmeier and McRoy*, 1989], but larger organisms can also mix the sediments. Grey whale and walrus foraging leaves pits in the Bering and Chukchi seas that extend up to 10 m long, but are generally only 10 cm deep. Older, current-reworked grey whale pits have been observed up to 40 cm deep. Nelson et al [1993] show that resuspension of sediments in the Bering and Chukchi seas is significant due to mammal feeding. They estimate that whales resuspend twice as much sediment as the Yukon River carries into the Bering Sea and walruses resuspend almost 20 times as much sediment as the Yukon River carries. Much of this sediment simply falls back to the sea floor, but the finest materials may get carried north by currents [*Nelson et al.*, 1993]. Walrus feeding is patchy across the shelf. Walrus are carried on ice floes from which they periodically dive off of to forage, much

like a conveyor belt [*Ray et al.*, 2006]. Whale feeding, on the other hand, appears to be restricted to the sandy, poorly sorted sediments north of St. Lawrence Island [*Grebmeier*, 2012; *Johnson and Nelson*, 1984] or the Bering Strait [*Grebmeier et al.*, 2006b]. Although not every part of the Bering Sea is scavenged in a season, bioturbation has a significant impact on both the stratigraphic integrity of the sediments and on sediment aeration and nutrient dynamics [*Ray et al.*, 2006].

In bioturbated sediments, a marker horizon, such as a tephra layer or anthropogenic isotope peak, is both flattened and spread upward over time. When a second marker horizon is added to the sediments relatively close together, bioturbation can merge the two markers into one broad trace [*Robbins*, 1986]. At DBSB, there is a sub-surface ^{137}Cs peak, similar to other cores studied across the Bering and Chukchi seas [*Cooper et al.*, 2005; *Cooper et al.*, 2009; *Oguri et al.*, 2012; *Pirtle-Levy et al.*, 2009]. In addition to using cesium as a dating tool, we can say that because there is no detectable ^{137}Cs in the core top, most of the sediments above 7 cm were deposited after 1963, and there is not a significant amount of upward mixing of ^{137}Cs. It is also possible that the peak we see is a merger of the two commonly observed cesium peaks, 1986 (the Chernobyl disaster) and 1963 (the nuclear test ban treaty) [e.g. *Thomson et al.*, 2002], which would indicate much higher sedimentation rates at the shelf-slope break.

Additional variables support the notion that Bering Sea sediments have been deposited recently and at high sedimentation rates. These include the presence of the short-lived cosmogenic isotope, ^{7}Be, in Bering and Chukchi sediments [*Cooper et al.*, 2005], as well as abundant chlorophyll-*a* preserved up to 10 cm deep in Haps cores [*Pirtle-Levy et al.*, 2009]. In this study, however, we focus on sediment variables that could be evaluated many years after sediment collection so that archived sediments could be used for proxy development.

3.6.1 Down-core Records of Magnetic Susceptibility and Grain Size

Downcore x-radiographs, granulometric analysis, magnetic susceptibility, and sedimentology all point to highly bioturbated sediments across the shelf. None of these sediment qualities can be used to correlate cores to each other as is commonly done with deep sea sediments. Rather all of the sediment characteristics appear to be directly related to sediment processing by infauna. In addition, biological observations indicate that nuculid bivalves have become the dominant bivalve on the Bering Sea shelf in the past 40 years [*Grebmeier*, 2012; *Grebmeier et al.*, 2006b; *Merrill et al.*, 2010], and these are the dominant bivalves seen in core x-rays (Figure 3.3).

3.6.2 Diatom Assemblage Change Down-Core in Area 1

Although DBSB shows a sub-surface peak in ^{137}Cs, down-core changes in diatom assemblages are subtle (Figure 3.7). This could be for one of two reasons. Either there has been no change in diatom sediment assemblages since the 1950s, or bioturbation has effectively mixed the sediments such that the signal of environmental change is muted. The largest variations we observe are between the relative percent abundances of the marginal ice zone species, *Fragilariopsis oceanica* [*von Quillfeldt et al.*, 2003] and *Chaetoceros* RS, a high productivity indicator [*Lopes et al.*, 2006; *Sancetta*, 1982]. A peak in both relative percentages and accumulation of the cosmopolitan species *Thalassionema nitzschioides* occurs in ~1968.

From 2003-2008, there was a decrease in chlorophyll-*a* concentration in the water column [*Grebmeier et al.*, 2010] in roughly the same area as DBSB. This decrease is presumably due to decreasing diatom productivity driven by an increase in the number of days that ice is present in the area [*Grebmeier*, 2012; *Grebmeier et al.*, 2010]. A possible decrease in diatom

accumulation rate in the sediments since 1990 reflects this observation and hints that the sediments down-core are subtly reflecting changes in sea surface conditions (Figure 3.7).

Lu and others [2005] examined organic geochemistry in a short multicore close to Area 1, but farther off the shelf. Their down-core profiles in organic geochemistry also show very muted variability, but they assert that the sediments record warming between 1920 and 1950 as well as between 1980 and 1999. These warmings are recorded as oxidized sediments with decreased terrigenous organic matter and increased marine-sourced organic matter [*Lu et al.*, 2005]. Compellingly, their second interval of warming corresponds with the interval in DBSB with the lowest relative percentages of *F. oceanica,* the highest relative proportions of *Chaetoceros* RS, and slightly higher diatom accumulation rates. These diatom changes indicate a reduction in marginal sea ice and an increase in diatom productivity. The timing of these changes may be related to regime shift in the PDO in 1977, which brought about warmer winters and an intensified Aleutian Low [*Mantua et al.*, 1997] which would have prevented southward sea ice growth [*Overland and Pease*, 1982]. Historically, records of Aleutian Low strength only extend back to 1924. A recent proxy record of Aleutian Low strength from coralline algae suggests that prior to the twentieth century, the strength of the Aleutian Low is more strongly correlated with salmon abundance than the PDO is. A strong Aleutian Low increases cloudiness and wind strength in the Bering Sea [*Halfar et al.*, 2011] and this increase in mixing, coupled with shade, promotes diatom growth [*Tozzi et al.*, 2004]. Increased productivity from ~1978 to 2000 is reflected as increases in *Chaetoceros* RS and diatom accumulation rates at DBSB.

3.6.4 Diatom Assemblage Change between Time Slices

Although ANOSIM showed no significant differences in the diatom assemblages at most areas, there are subtle qualitative changes in specific taxa that can be seen graphically (Figure 3.9). We plot the relationship between relative percent abundance of major taxa in 1969 on the x-axis vs. the same taxa in 2006 and 2007 on the y-axis. A 1:1 line is plotted as well. Values that plot below this line are species that have decreased since 1969, and values above the line are species that have increased.

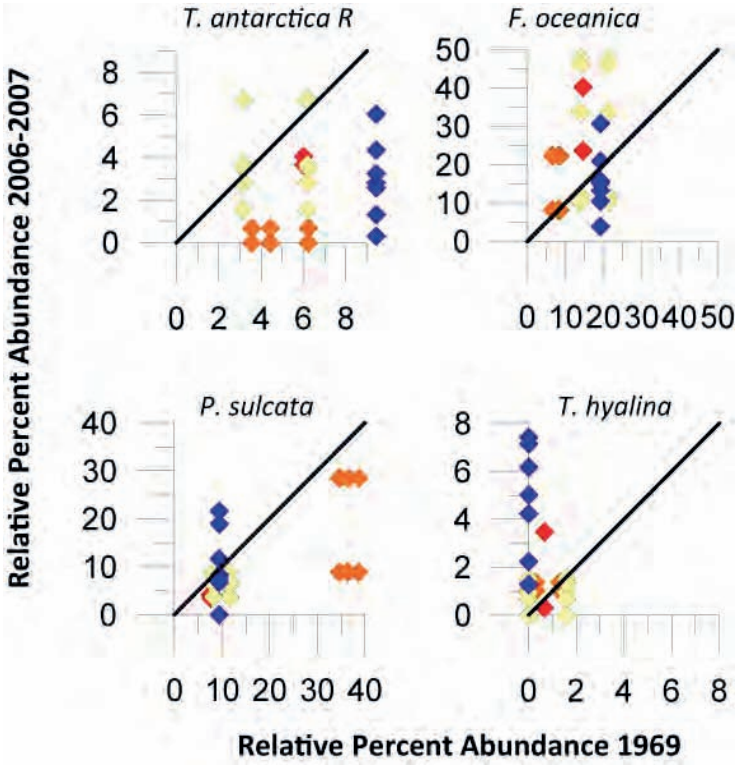

Figure 3.9. Plots showing the change in relative percent abundances of diatom species between 1969 and 2006/2007. Percent abundance in 1969 is plotted on the x-axes and percent abundance in 2006-2007 is plotted on the y-axes. 1:1 lines are drawn in each plot. Dots above this line indicate samples that have seen an increase in this species over the past 40 years, dots below the lines are samples that have seen a decrease in the species. Dots are color coded by area as indicated on Figure 3.1. Area 1=red, Area 2=orange, Area 3=yellow, Area 4=blue.

Area 1 is located within the highly productive green belt along the shelf-slope break. Diatom accumulation rate here is the highest of all four areas (Figure 3.10). In years when the marginal ice zone advances as far as the shelf-slope break, productivity is higher in the early spring due to upwelling that brings nutrients from the deep Bering basin up to the surface here. Despite Arctic-wide decreases in sea ice duration and extent, the green belt has seen an increase in the number of days that sea ice is present each year [*Grebmeier et al.*, 2010] (Figure 3.1). Coincident with this is a decrease in chlorophyll-*a* [*Grebmeier et al.*, 2010]. At area 1, we see slight decreases in *T. antarctica* RS and epontic species, but increases in marginal ice zone species and *F. oceanica.* This might indicate a shift in sea ice dynamics from a system with thicker, more continuous ice to one where the ice has already begun to break up when the ecosystem is no longer light limited.

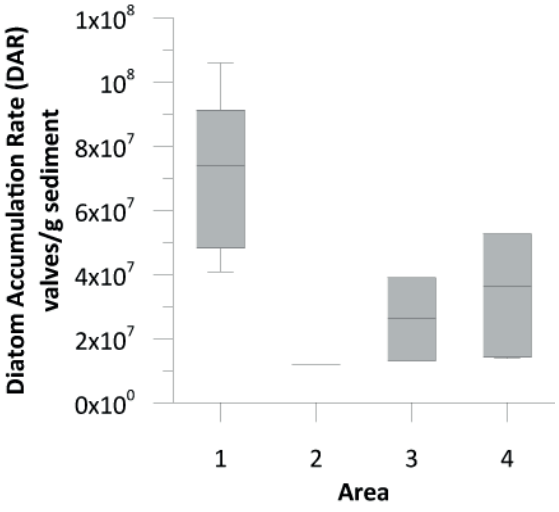

Figure 3.10. Box plots showing diatom accumulation rate at each area (1-4) examined on the Bering Sea Shelf. Area locations can be found on Figure 3.1. Boxes are drawn to the upper and lower quartiles with the median expressed as the line in the center of the box. The whiskers extend to the maximum and minimum values. There are no outlier values. Area 2 only has one quantitative sample, so there is no box plot.

ANOSIM does show a significant change in diatom assemblages at area 2 (Figure 3.6). There is a decrease in epontic species, *Thalassiosira antarctica,* and the neritic species *Paralia sulcata.* This is similar to what was seen in Area 1, but with an additional decrease in the transport of neritic species to the site. These changes can also be ascribed to changing ice dynamics.

Area 3 is between the greenbelt and the St. Lawrence Island polynya. Its diatom assemblage shows no change at all between years, but rather has a wide spread in relative percent abundances of all major species. This area is influenced by Anadyr water and shifting locations of the Anadyr water may be responsible for the large differences in the diatom assemblages between nearby sites.

Area 4 is located in the highly-studied "cold pool" [*Grebmeier et al.*, 2006b; *Merrill et al.*, 2010; *Sigler et al.*, 2011]. The cold pool is located in the St. Lawrence Island Polynya, an area of high productivity and nutrients, but which drives higher productivity in areas "down-stream" such as the green belt [*Grebmeier and Barry*, 2006]. Area 4 has the second highest diatom accumulation rates (Figure 3.10), supporting the notion that diatom accumulation rates do track primary productivity and can be used to approximate surface productivity. Biological investigations of the cold pool show that infaunal biomass has variably decreased [*Grebmeier et al.*, 2006b] or increased [*Merrill et al.*, 2010] since the 1970s depending on the sampling density and temporal variability in sampling. Both studies agree that there has been a shift in bivalve communities to one dominated by *Nuculana radiata* [*Grebmeier*, 2012; *Grebmeier et al.*, 2006b; *Merrill et al.*, 2010]. We see an insignificant decrease in *T. antarctica* RS, and increase in *T. hyalina*, which again points to a possible increase in species associated with the marginal ice zone bloom and decreased transport from coastal regions to the site.

3.7 Conclusions

Multiple lines of evidence support our hypothesis that the top 1 cm of sediments on the Bering Sea shelf represents several years to decades of deposition and not hundreds to thousands of years. We suggest that studies using the top 1 cm of Bering and Chukchi shelf

sediments for proxy calibration compare sediment characteristics to 10 to 30 years of climate data.

Recent climate changes in the region, including changes in the Pacific Decadal Oscillation and the strength of the Aleutian Low are reflected as subtle changes in diatom assemblages down-core. During the positive phase of the PDO, and interval of a deepened Aleutian Low, sediments at the shelf-slope break recorded an increase in diatom productivity and a decrease in sea ice concentration. We hypothesize that due to bioturbation, the signal is muted, and suggest that further study of short cores in higher resolution is necessary to determine if these changes can be seen in other areas of the Bering Sea shelf that are potentially more sensitive to change or resistant to bioturbation. In addition, there is evidence that these climate changes can be seen in sediments collected several decades apart. Although most areas examined show no change, Area 2 shows a decrease in neritic species transported to the site, possibly by sea ice and a decline in sub-ice productivity early in the spring. This area is targeted as the next location to look for down-core change.

CHAPTER 4

SEA SURFACE CONDITIONS DURING MARINE ISOTOPE STAGES 12 TO 10 AT NAVARIN CANYON IN THE BERING SEA (IODP SITE U1345)

4.1 Abstract

Records of terrestrial-marine coupling during past warming intervals are essential for understanding climate system dynamics. The Bering Sea is ideally situated to record how opening or closing the Pacific-Arctic ocean gateway (Bering Strait) impacts primary productivity, sea ice, and sediment transport; however, very little is known about this region prior to 125 ka. IODP Expedition 323 to the Bering Sea offered the unparalleled chance to look in detail at time periods deeper than had previously retrieved using gravity and piston cores. Here we present a diatom assemblage record for Marine Isotope Stages 12-10 from Site U1345A located near the shelf-slope break. MIS 11 is bracketed by highly productive laminated intervals that may have been triggered by flooding of the Beringian shelf. The site was near the marginal ice zone and therefore experienced seasonal sea ice throughout both the glacial and interglacial stages. A Middle Pleistocene glaciation previously known only from Beringian highstands transported poorly sorted, terrigenous material, fresh water diatoms, and neritic (coastal) diatoms off the shelf when global eustatic sea level was at its peak. This localized glaciation was driven by decreasing insolation, reduced seasonality, and high moisture availability due to high sea level, ice-free summers and high humidity between 410 and 400 ka. Sudden decreases in upwelling and North Pacific diatom indicators at 410 ka suggest that flow through the Bering Strait may have been reversed temporarily due to changes in North Atlantic Deep Water formation. Although future work is required to confirm this reversal, the diatom assemblages at U1345 include multiple lines of evidence for Atlantic-Pacific teleconnections during MIS 11.

4.2 Introduction

Predictions and modeling of future climate change require a detailed understanding of how the climate system works. Reconstructions of previous warm intervals can shed light on interhemispheric teleconnections. The most recent interglacial period when orbital conditions were similar to today was approximately 400 ka during the extremely long interglacial known as marine isotope stage (MIS) 11. Eccentricity was low, obliquity was high and the amplitude of precessional changes was low [*Loutre and Berger*, 2003]. In addition, CO_2 concentration averaged approximately 275 ppm, which is similar to pre-industrial levels [*EPICA community members*, 2004]. The transition from MIS 12 into MIS 11 has been compared to the last deglaciation [*Dickson et al.*, 2009] and extreme warmth during MIS 11 is considered an analog for future warmth [*Droxler et al.*, 2003; *Loutre and Berger*, 2003], although the natural course of interglacial warmth today has been disrupted by anthropogenic forcing [*IPCC*, 2007].

Globally, MIS 11 is easily recognizable in the sediment record by an abrupt and distinct transition from high to low $\delta^{18}O$ values at the MIS 12/11 boundary and subsequent prolonged low values of $\delta^{18}O$ during MIS 11 [*Lisiecki and Raymo*, 2005]. Furthermore, MIS 11 was unique in the Polar Regions. Antarctica experienced temperatures 2° C warmer than pre-industrial temperatures [*Jouzel et al.*, 2007], and boreal forest extended across Greenland, which may have been largely ice free [*de Vernal and Hillaire-Marcel*, 2008]. Large lakes in Siberia were anomalously productive and record warmer air and lake temperatures than today. Lake Baikal was 2° C warmer [*Prokopenko et al.*, 2010] and Lake El'gygytgyn was 4° C warmer [*Lozhkin et al.*, in prep]. MIS 11 is also unique in Beringia because Beringian glaciers advanced while sea level was still high [*Brigham-Grette et al.*, 2001; *Huston et al.*, 1990; *Kaufman et al.*, 2001; *Pushkar et al.*, 1999]. This implies that parts of Beringia were glaciated rapidly as high latitude insolation fell in the northern hemisphere, but before global sea level dropped in response to the buildup of

large ice sheets reaching lower latitudes. Late MIS 11 ice (i.e., leading to the Nome River Glaciation in MIS 10) is widely believed to be the last of the most extensive glaciations in Beringia [*Brigham-Grette et al.*, 2001; *Gualtieri and Brigham-Grette*, 2001; *Kaufman et al.*, 1991; *Manley et al.*, 2001].

Despite the work done on land to characterize the warmth of MIS 11, very little is known about this interval from the marine record, especially in the North Pacific region. Modeling studies describe several mechanisms for linking the Atlantic and Pacific through oceanic heat transport on glacial-interglacial scales [*DeBoer and Nof*, 2004; *Hu et al.*, 2010], however, there have been no tests of these modeling studies using proxy data older than 30 ka. Furthermore, the location of the Bering Sea marginal ice zone advanced and retreated hundreds of kilometers during the past three glacial-interglacial cycles [*Caissie et al.*, 2010; *Katsuki and Takahashi*, 2005; *Sancetta and Robinson*, 1983]; however, sea surface and intermediate water variability before MIS 5 is unknown.

This investigation of terrestrial-marine coupling at the shelf-slope break during the transition from MIS 12 to 10 is the first study of this interval in the subarctic Pacific (Figure 4.1). We use sedimentology and diatom assemblages as proxies for sea ice, sea surface conditions, and shelf to basin transport. These proxy records show changes in sea ice and glacial ice that are in sync with insolation changes at high northern latitudes. An interval of productivity occurs at the glacial termination (Termination V) that is both short-lived and intense. We put these changes seen in the Bering Sea in the context of global records of MIS 11 that explore questions of sea level rise and the influence of thermohaline circulation on prolonging interglacial warmth.

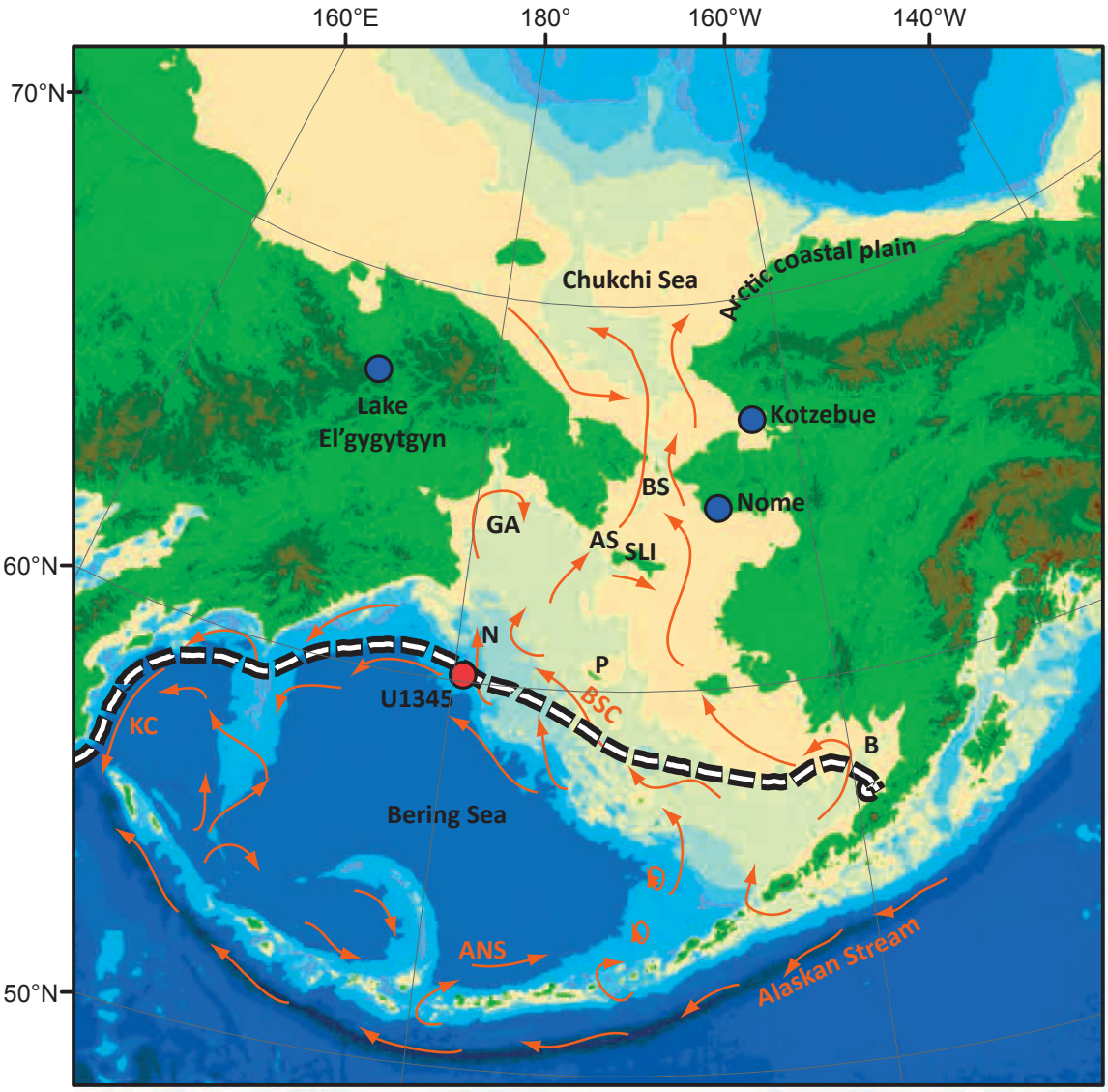

Figure 4.1. Map of the Beringia. Locations of place names from the text are labeled: Aleutian North Slope Current (ANS), Anadyr Strait (A), Bristol Bay (B), Bering Strait (BS), Bering Slope Current (BSC), Gulf of Anadyr (GA), Kamchatka Current (KC), Navarin Canyon (N), Pribilof Islands (P), St. Lawrence Island (SLI). The white and black dashed line is the modern maximum extent of sea ice [*Cavalieri et al.,* 1996]. Currents are in orange and are modified from Stabeno [1999]. Base map is modified from Manley [2002].

4.3 Background

4.3.1 Global Sea Level during MIS 11

The maximum height of sea level during MIS 11 is an open question with estimates ranging from more than 20 m above present sea level (apsl) [*Kindler and Hearty*, 2000] to 0 m apsl [*Rohling et al.*, 2010]. The discrepancy may stem from large differences between global eustatic [*Bowen*, 2010] or ice-volume averages [*McManus et al.*, 2003] and regional geomorphological or micropaleontological evidence [*van Hengstum et al.*, 2009]. Regional isostatic adjustment due to glacial loading and unloading is also perhaps not as insignificant as previously assumed and regional highstands may record higher than expected sea levels if glacial isostasy has not been accounted for even at places that were never glaciated [*Raymo and Mitrovica*, 2012; *Raymo et al.*, 2011]. The recent work by Raymo and Mitrovica suggests that eustatic sea level during MIS 11 was 6-13 m apsl [*Raymo and Mitrovica*, 2012].

Regardless of the ultimate height of sea level, the transition from MIS 12 to MIS 11 was the greatest change in sea level of the last 500 ka [*Rohling et al.*, 1998]; sea level rose from -140 m to its present level or higher [*Bowen*, 2010]. Up to three highstands occurred during MIS 11 [*Kindler and Hearty*, 2000], the highest at the second June insolation peak at 65°N. This highstand is referred to as MIS 11.3 and occurs 406 ka [*Bassinot et al.*, 1994]. Sea levels above modern require partial or complete collapse of the Greenland ice sheet (up to 6 m) [*de Vernal and Hillaire-Marcel*, 2008] and/or the West Antarctic Ice Sheet [*Scherer et al.*, 1998], but not the East Antarctic Ice Sheet [*Raymo and Mitrovica*, 2012]. Recent drilling in Antarctica failed to find evidence for West Antarctic Ice Sheet collapse during MIS 11 and East Antarctica appears stable; however, small changes in these ice sheets may have contributed up to 5 m of sea level rise [*EPICA community members*, 2004].

4.3.2 Sea Level Variation in Beringia

Beringia refers to both the terrestrial and marine regions north of the Aleutian Islands that stretch to the shelf-slope break in the East Siberia, Chukchi, and Beaufort seas (Figure 4.1). On land, Beringia extends from the Lena River in Siberia to the Mackenzie River in Canada. Large portions of the Beringian shelf are exposed when sea level drops below -50 m [*Hopkins*, 1959] and this subareal expanse stretches more than 1000 km from north to south during glacial periods (Figure 4.2) . In contrast, as sea level rises at glacial terminations the expansive continental shelf is flooded, introducing fresh nutrients into the southern Bering Sea [i.e. *Bertrand et al.*, 2000; *Ternois et al.*, 2001] and re-establishing the connection between the Pacific and Atlantic oceans through Bering Strait.

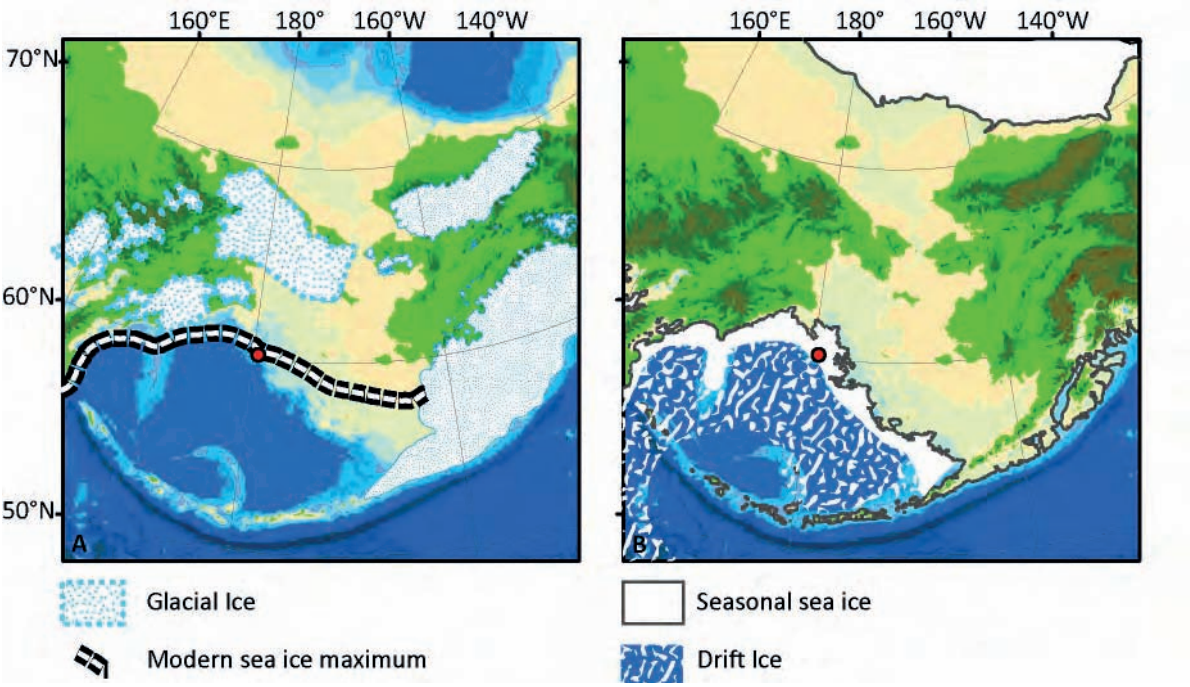

Figure 4.2. Maximum glacial and sea ice extents in Beringia. A. depicts the maximum glacial ice in Beringia as inferred from terminal and lateral moraines. This is not intended to show the maximum extent during a particular glaciation, but rather the maximum possible extent of glacial ice. These moraines are likely from several different major glaciations. The white and black dashed line is the modern maximum extent of sea ice [Cavalieri et al., 1996]. B. depicts the approximate pattern of sea ice during glacial stages [Katsuki and Takahashi, 2005]. The dark grey contour is -140 m, the approximate sea level during MIS 12 [Rohling et al., 2010]. Base map is modified from Manley [2002].

4.3.3 Beringian Hydrography

Today, water circulates cyclonically in the deep basins of the Bering Sea (Figure 4.1). Site U1345 is influenced by the northwest flowing Bering Slope Current, which is derived from the Alaskan Stream. The Alaskan Stream flows westward, south of the Aleutians and turns northward to enter the Bering Sea through deep channels in the western Aleutian Islands. North of the Aleutian Islands, this now eastward flowing water is called the Aleutian North Slope Current. Interactions with the shelf turn this current to the northwest where it becomes the Bering Slope Current [*Stabeno et al.*, 1999]. Tidal forces and eddies in the Bering Slope Current drive upwelling through Navarin Canyon and other interfluves along the shelf-slope break [*Kowalik*, 1999]. The resulting cold water and nutrients brought to the sea surface, coupled with the presence of seasonal sea ice, drive the high productivity found today in the so called "Green Belt" [*Springer et al.*, 1996] along the shelf-slope break. North of the site, low salinity, high nutrient shelf waters [*Cooper et al.*, 1997] primarily flow north through the Bering Strait to the Arctic Basin [*Schumacher and Stabeno*, 1998].

Major changes in currents may have occurred throughout MIS 12 to 10 due to sea level rise and fall, the strength of North Atlantic Deep Water (NADW) formation, and the intensity of winds originating in the Southern Ocean [e.g. *DeBoer and Nof*, 2004; *Hu et al.*, 2010]. Specifically, as sea level rose after MIS 12, the connection between the Pacific and the Atlantic was reestablished. De Boer and Nof [2004] suggest that under these high sea level conditions, if freshwater is suddenly released into the North Atlantic, the Bering Strait might act as an "exhaust valve" allowing fresh water from the North Atlantic to flow into the Arctic Ocean and then flow south through the Bering Strait, thus preventing a shut-down in thermohaline circulation [*DeBoer and Nof*, 2004]. Hu et al. [2010] suggest that when sea level is fluctuating

near the sill depth of Bering Strait, this gateway can modulate widespread climate changes. When Bering Strait is open and North Pacific water is transported to the North Atlantic, the less saline Pacific water can freshen the North Atlantic and slow meridional overturning, subsequently cooling the North Atlantic, but warming the North Pacific. This North Atlantic cooling causes the buildup of ice sheets and global sea level drops, closing Bering Strait. A closed Bering Strait concentrates fresher waters in the North Pacific and more saline waters in the North Atlantic. A more saline Atlantic means that stratification is low and meridional overturning is increased. This increases oceanic heat transport to the North Atlantic, triggers warming in the North Atlantic and ultimately ice sheets retreat and sea level rises reconnecting the Pacific with the Atlantic [*Hu et al.*, 2010].

4.4 Methods

4.4.1 Study Area and Sampling

The Integrated Ocean Drilling Program's Expedition 323, Site U1345, is located on an interfluve ridge near the shelf-slope break in the Bering Sea (Figure 4.1). Navarin Canyon, one of the largest submarine canyons in the world [*Normack and Carlson*, 2003] is located just to the northwest of the site. Sediments were retrieved from ~1008 m of water, placing the site at the center of the modern day oxygen minimum zone [*Takahashi et al.*, 2011]. We focus on this site because of its proximity to the modern marginal ice zone in the Bering Sea and anticipated high sedimentation rates.

Site U1345 was drilled five times during Exp. 323 and cores from four of these holes were described onboard the JOIDES Resolution. This study focuses on 3 cores, all from Hole A. There are core gaps between each of these cores and missing time is depicted on all figures. In addition to the original analyses presented here, we refer to the shipboard core descriptions

and physical properties data [*Takahashi et al.*, 2011] in our interpretations. Depths are reported in CCSF-A, a correlated depth scale that allows for direct comparison between drill holes. Units are meters below sea floor (mbsf). A small syringe was used to collect approximately 1 cc of sediment from U1345A every 50 cm (~1500 yr resolution) between 108.86 m and 137.25 mbsf.

4.4.2 Age Model

The age model (Figure 4.3) is based on the shipboard age model which was developed using magnetostratigraphy and biostratigraphy. First and last appearance datums for diatoms and radiolarians make up the majority of the biostratigraphic markers. As there were no magnetic reversals observed at this site, magnetic susceptibility was used to correlate approximate depths of marine isotope stages between sites [*Takahashi et al.*, 2011]. Oxygen isotope measurements taken on three benthic foraminifera species, *Uvigerina peregrina, Nonionella labradorica,* and *Globobullimina affinis* [*Cook, et al.,* in prep.], were then used to tune site U1345 to the global marine benthic foraminiferal isotope stack [*Lisiecki and Raymo*, 2005] (Figure 4.3). Based on this combined age model, MIS 11 begins in the core at 130 mbsf. Sedimentation rate during MIS 11 is 29 cm/kyrs and during MIS 10, it is 50 cm/kyrs [*Cook, et al.,* in prep.]. Although we are reasonably confident about this age model, sample resolution was not high enough to determine patterns in millennial scale changes at the site or compare our record to others that examine MIS 11 at sub-millennial scale resolution.

4.4.3 Diatom Analysis

In order to quantify the number of diatom valves deposited per gram of sediment, diatom slides were prepared according to the method described in Scherer [1994]. Cover slips were mounted on cleaned microscope slides using hyrax in toulene (refractive index: 1.7135). This method allows for a direct comparison of diatom flux to the sediments between samples. At least 300

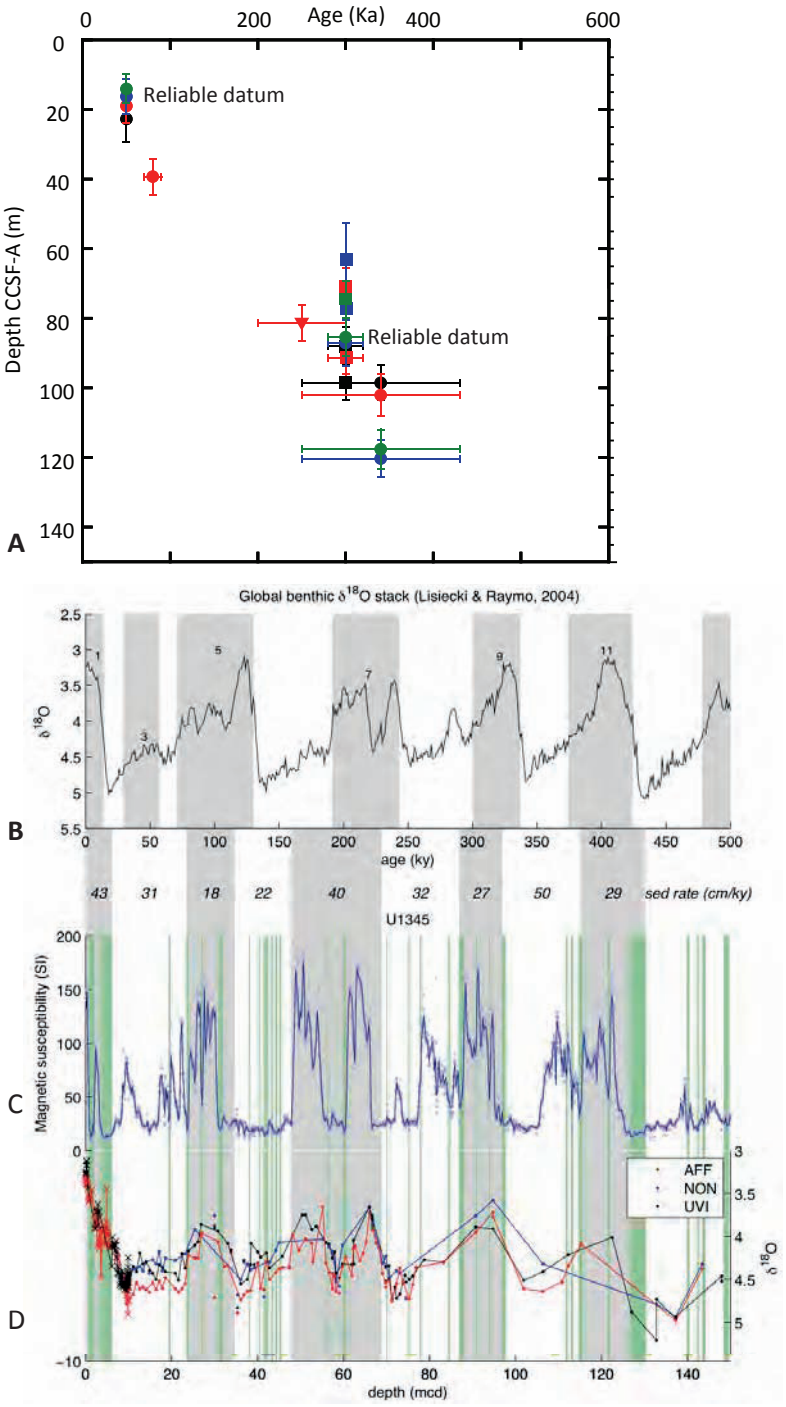

Figure 4.3. Age Model for U1345. a) Shipboard biostratigraphic data. Colors denote the Hole that each datum was recorded in: U1345A (red), U1345C (green), U1345D (blue), and U1345E (black). Dots are radiolarian datums, boxes are diatoms, and triangles are silicoflagellates. b) Each interglacial period is shaded grey and the marine isotope stage number is indicated for the LR04 oxygen isotope stack [*Lisiecki and Raymo*, 2005]. c) Magnetic susceptibility [*Takahashi et al.*, 2011]. d) Oxygen isotope data from the benthic foraminifera, *Uvigerina peregrina* (black), *Nonionella labradorica* (blue), and *Globobulimina affinis* (red). Crosses at the top of the record are measurements from HLY02-02-3JPC, a piston core taken near U1345. The grey bars are estimates for how the interglacials correspond to the LR04 stack [*Cook, M.S.* in prep].

diatom valves in at least three random transects across the slide were identified using a light microscope at a magnification of 1250x [see *Armand et al.*, 2005; *Sancetta*, 1979; *Sancetta and Silvestri*, 1986; *Scherer*, 1994]. The portion of the slide that was examined was measured using a stage micrometer. Partial valves were counted according to the methods of Schrader and Gersonde [1978]. All diatoms were identified to the species level when possible following published taxonomic descriptions and images [*Hasle and Heimdal*, 1968; *Koizumi*, 1973; *Lundholm and Hasle*, 2008; 2010; *Medlin and Hasle*, 1990; *Medlin and Priddle*, 1990; *Onodera and Takahashi*, 2007; *Sancetta*, 1982; 1987; *Syvertsen*, 1979; *Tomas*, 1996; *Witkowski et al.*, 2000]. Morphotaxa of *Hyalochaete Chaetoceros* resting spores were also identified using Suto's taxonomy [*Suto*, 2003; 2004a; b; c; 2005a]. Diatom counts were transformed into relative percent abundances. Absolute abundances (diatoms per gram sediment) were calculated following the methods of Scherer [1994]. Diatom taxa were then grouped according to ecological niche (Table 4.1) based on biological observations [*Aizawa et al.*, 2005; *Fryxell and Hasle*, 1972; *Håkansson*, 2002; *Horner*, 1985; *Saitoh and Taniguchi*, 1978; *Schandelmeier and Alexander*, 1981; *von Quillfeldt*, 2001; *von Quillfeldt et al.*, 2003] and statistical associations [*Barron et al.*, 2009; *Caissie et al.*, 2010; *Hay et al.*, 2007; *Katsuki and Takahashi*, 2005; *Lopes et al.*, 2006; *McQuoid and Hobson*, 2001; *Sancetta*, 1981; 1982; *Sancetta and Robinson*, 1983; *Sancetta and Silvestri*, 1986; *Shiga and Koizumi*, 2000]. In cases where a diatom species was reported to fit into more than one environmental niche, it was grouped into the niche where it was most commonly recognized in the literature.

4.5 Results

4.5.1 Sedimentology

The sediments at Site U1345A, Cores 12-14 are primarily clays and silts with varying amounts of diatoms, sand, and tephra throughout. The proportion of diatoms relative to terrigenous or volcanigenic grains is highest during laminated intervals. Vesiculated tephra shards were seen in every diatom slide analyzed. There are several discrete sand layers, especially in Core 14, and shell fragments are also abundant in Core 14. Subrounded to rounded clasts (granule to pebble) occur frequently throughout the interval. We combined clast and sand layer data from Holes A, C, D, and E at Site U1345 when examining their distribution (Figure 4.4).

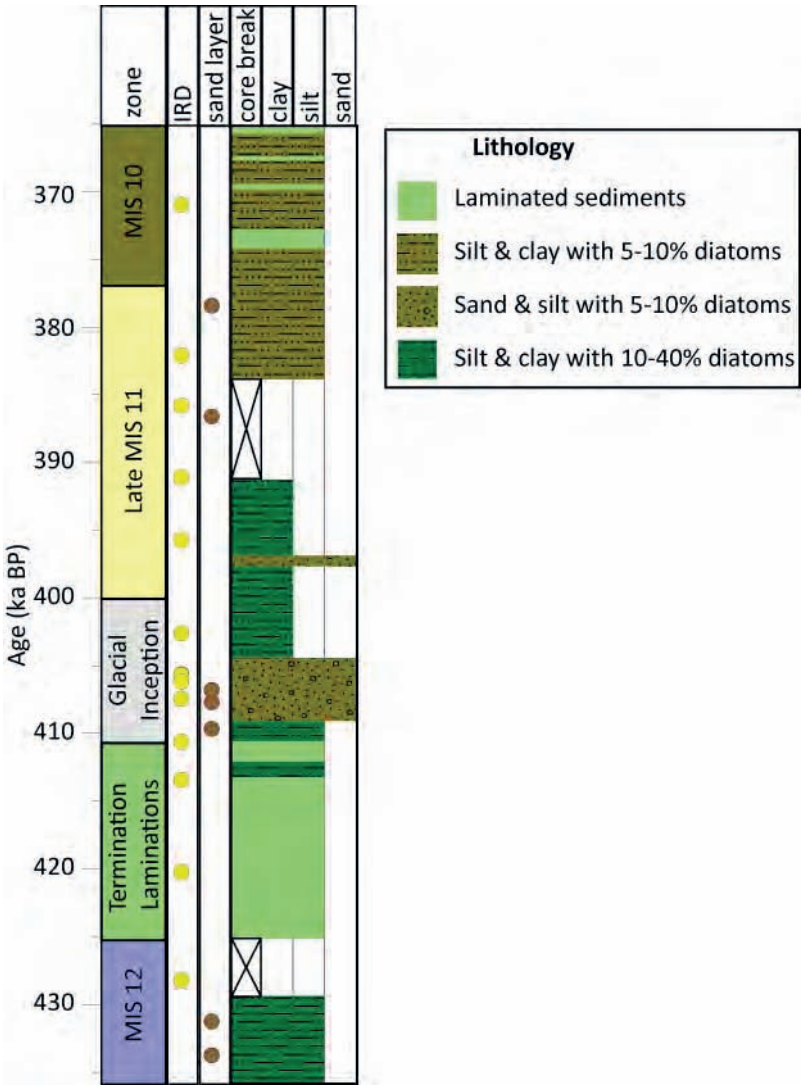

Figure 4.4. Lithostratigraphic column for U1345A. The generalized zones described in the text are delineated to the left of ice rafted debris (yellow dots) and sand layers (maroon dots). IRD and sand layers are a compilation of these features in all four holes at U1345. Core gaps are depicted by x's. The width of the lithologic column varies according to grain size with coarser sediments drawn as wider boxes. Colors depict varying amounts of diatoms relative to terrigenous grains in the sediment. Laminations are depicted as pale green bars.

In general the sediments are massive with centimeter–scale dark or coarse grained mottles. However, laminated

Table 4.1: Bering Sea diatom species grouped by environmental niche. In cases where a species appears in more than one niche, the grouping used in this study is highlighted in bold.

Modern Seasonal Succession			
Epontic	**Marginal Ice Zone (MIZ)**	**Both Epontic and MIZ**	**Summer Bloom**
Melosira arctica	***Bacterosira bathyomphala***	*Actinocyclus curvatulus*	***Coscinodiscus* spp.**
Navicula transitrans	*Chaetoceros furcellatus*	***Fossula arctica***	***Leptocylindrus* sp.**
Nitzschia frigida	*Chaetoceros socialis*	***Fragilariopsis cylindrus***	***Rhizosolenia* spp.**
	Leptocylindrus sp.	***Fragilariopsis oceanica***	
	Odontella aurita	***Navicula pelagica***	
	Paralia sulcata	**Naviculoid pennates**	
	Porosira glacialis	***Nitzschia* spp.**	
	Staurosirella pinnata	***Pinnularia quadratarea***	
	Thalassionema nitzschioides	***Thalassiosira antarctica***	
	Thalassiosira angulata	***Thalassiosira gravida***	
	Thalassiosira baltica		
	Thalassiosira decipiens		
	Thalassiosira hyalina		
	Thalassiosira hyperborea		
	Thalassiosira nordenskioeldii		
	Thalassiosira pacifica		

Continued on next page

Table 4.1 continued

Water Mass Tracers				*Shelf to Basin Transport*	
Dicothermal	**Upwelling**	**Alaska Stream**	**Warmer Water**	**Neritic**	**Fresh Water**
Actinocyclus curvatulus	***Chaetoceros* spp.**	***Neodenticula seminae***	***Azpeitia tabularis***	***Actinoptychus senarius***	***Cyclotella ocellata***
Thalassiosira trifulta	***Odontella aurita***		***Stellarimia* sp.**	***Amphora* sp.**	*Cyclotella stylorum*
	Thalassionema nitzschioides		*Thalassionema nitzschioides*	***Cyclotella stylorum***	*Staurosirella pinnata*
	Thalassiosira pacifica		***Thalassiosira eccentrica***	***Delphineis spp.***	***Stephanodiscus* sp.**
	***Thalassiosira* spp. small**		***Thalassiosira oestrupii***	***Dentonula confervacea***	
	Thalassiothrix longissima		***Thalassiosira symmetrica***	***Diploneis smithii***	
				Naviculoid pennates	
				Odontella aurita	
				Paralia sulcata	
				Rhaphoneis amphiceros	
				Stephanopyxis turris	
				Thalassiosira angulata	
				Thalassiosira decipiens	
				Thalassiosira eccentrica	

intervals bracket MIS 11 (Figure 4.4). Termination V is characterized by a 3.5 m thick laminated interval, estimated to span 12 ka (see Table 4.2 for depths and ages). During the transition from MIS 11 to MIS 10, a series of four thinner laminated intervals occurs. Each interval lasts between .3 and 1.6 ka, with 2 to 6 ka between intervals (Table 4.2). Laminations are millimeter-scale alternations of black, olive gray, and light brown sediments. In addition to containing a high proportion of diatoms, the laminated intervals also contain high relative proportions of calcareous nannofossils and foraminifera. The majority of these intervals display horizontal, parallel laminations; however, a 7 cm interval during the termination lamination is highly disturbed, showing recumbent folds in the laminations [*Takahashi et al.*, 2011]. This interval was not sampled. In general, the upper and lower boundaries of laminated intervals are gradational; however the boundaries between individual lamina are sharp [*Takahashi et al.*, 2011].

Table 4.2: Distribution of Laminated Intervals during MIS 12 to MIS 10

Lamination	Depth	Age	Duration (kyrs)	Kyrs to next lamination
MIS 10.4	111.25-111.01	365.8-365.3	.5	N/A
MIS 10.3	112.23-112.06	367.7-367.4	.3	2.2
MIS 10.2	113.31-113.06	369.9-369.4	.5	2.7
MIS 10.1	115.53-114.75	374.4-372.8	1.6	6.1
Termination	140.07-126.52	425.1-413.2	11.9	62.6

4.5.2 Diatoms

4.5.2.1 Diatom Assemblages

A total of 102 different taxa were identified during MIS 12 to 10 in U1345. Individual samples include between 26 and 46 taxa each with an average of 37 taxa. Laminated intervals contain fewer taxa than bioturbated intervals do. This decrease in diversity is confirmed using the Margalef, Simpson, and Shannon indices which all show similar downcore profiles (Figure 4.5). The Margalef index is a measure of species richness [*Maurer and McGill*, 2011]. It shows a decrease in the number of taxa beginning at the onset of the laminated interval at Termination

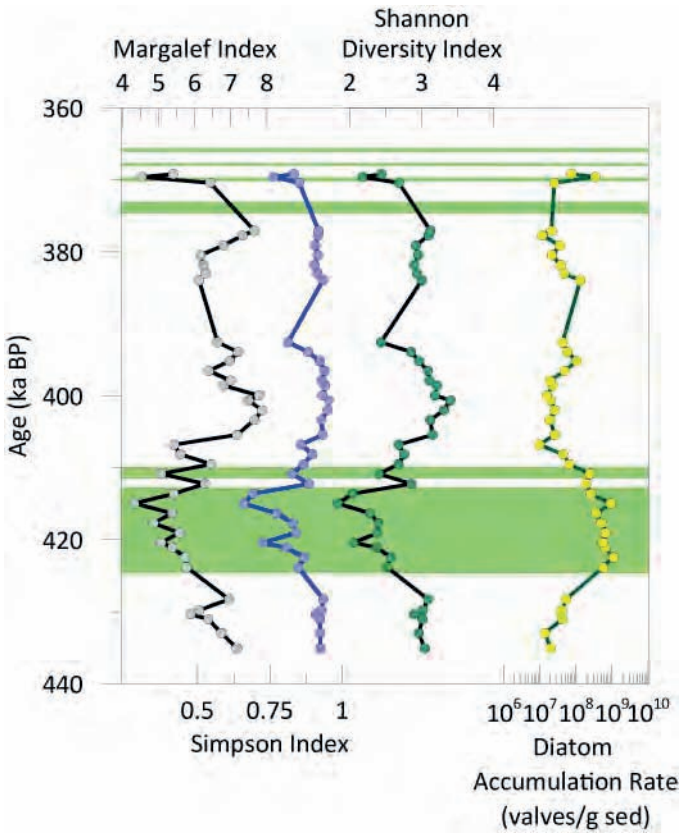

Figure 4.5. The Margalef, Simpson, and Shannon diversity indices plotted with diatom accumulation rate. Laminated intervals are shown as green bars.

V, and remaining low until ~407 ka. Instead of species richness, the Simpson index measures the evenness of the sample. Values close to 1 indicate that all taxa contain an equal number of individuals, while values close to 0 indicate that one species dominates the assemblage [*Maurer and McGill*, 2011]. In general, the Simpson index is close to 1 throughout the core indicating a rather even distribution of diatom valves across all taxa; however, during the laminated intervals (both at Termination V and during early MIS 10), the Simpson index drops reflecting the dominance by *Chaetoceros* RS during these intervals (Figure 4.5). It does not come close to 0, which would likely indicate a strong dissolution signal. The Shannon diversity index measures both species richness and evenness [*Maurer and McGill*, 2011]. Correspondingly, it is low during the laminated intervals, high during MIS 12 and peaks at 400 ka (Figure 4.5).

Diatom accumulation rate varies between 10^7 and 10^9 diatoms deposited per gram of sediment with values an order of magnitude higher during laminated intervals than during massive intervals (Figure 4.6). The diatom assemblage is dominated by *Chaetoceros* and *Thalassiosira antarctica* resting spores (RS), with lesser contributions from *Fragilariopsis*

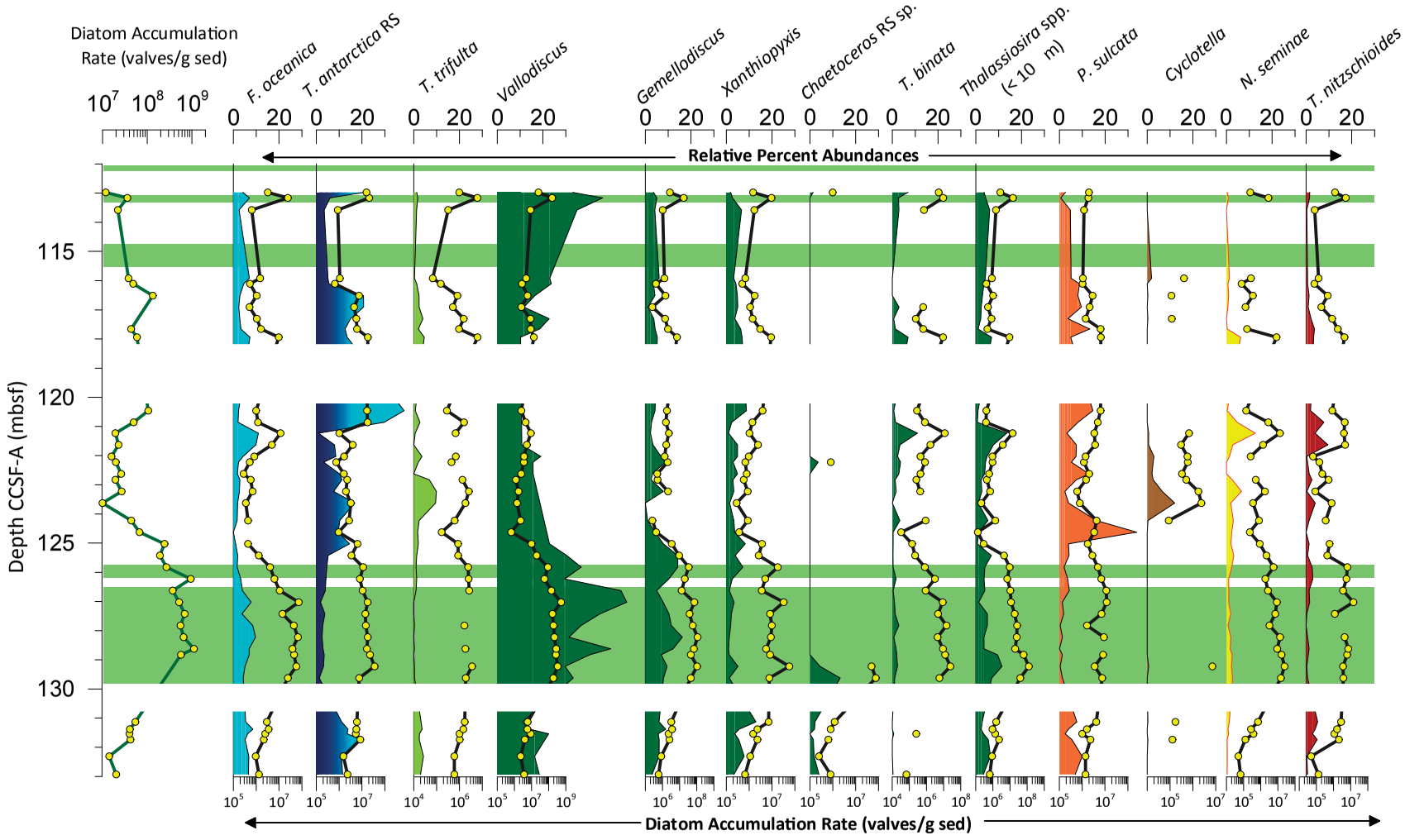

Figure 4.6. Diatom accumulation rate (dots) and relative percent abundances (area plots) for the most common diatoms at U1345. Percent abundance plots are colored according to the ecological niche that each diatom was placed into (see fig. 4.5). Laminated intervals (green bars) are included for reference and core gaps are denoted as breaks in the plots.

oceanica, Cyclotella spp., *Thalassiosira binata,* small (<10 µm in diameter) *Thalassiosira* species, *Thalassiosira trifulta, Neodenticula seminae,* and *Paralia sulcata* (Figure 4.6).

Relative percent abundances of *Chaetoceros* RS are highest (up to 69% at 415 ka/127.03 mbsf) during the laminated intervals and, in general, mimic the pattern of both diatom accumulation rate and insolation at 65° N [*Berger and Loutre*, 1991] (Figure 4.6). *Thalassiosira antarctica* RS, in contrast, are lowest during the laminated intervals (as low at 1%) and higher during MIS 12 and between 407 ka and 380 ka (124.69 and 116.77 mbsf). This taxon peaks at 38% relative abundance at 393 ka (120.58 mbsf; Figure 4.6).

Relative percent abundances of the characteristic marginal ice zone species, *Fragilariopsis oceanica* [*Caissie et al.*, 2010; *Saitoh and Taniguchi*, 1978; *Sancetta*, 1982; *von Quillfeldt et al.*, 2003], oscillate between ~10% and less than 3% of the diatom assemblage. Between 412 and 400 ka (126.15 and 122.63 mbsf), *F. oceanica* remains low for an extended period. The neritic species and moving water indicator, *P. sulcata* is low until 408 ka (124.98 mbsf) when it begins to rise to 34% relative abundance at 407 ka (124.67 mbsf). *P. sulcata* remains moderately high (~10%) for the rest of the record*. C. ocellata* is the dominant taxa in the fresh water group and the variability in its abundances are discussed below. *T. trifulta* follows a very similar distribution to the fresh water group and *C. ocellata*. It is relatively high (~4%) during MIS 12, is virtually absent from the sediments during the Termination V lamination, and then increases again until a peak of 10% relative abundance at 403 ka (123.62 mbsf). *Thalassiosira binata* and other small (<10 µm in diameter) *Thalassiosira* species have similar distributions with low abundances throughout the record (< 6%) except for a small peak between 394 and 399 ka. Small *Thalassiosira* species also have a second peak of 11% relative abundance just after the onset of the Termination V laminations (420-425 ka). The relative

percent abundances of *N. seminae* are discussed below. The largest peak in *N. seminae* at 395 ka also corresponds with an increase in *Thalassionema nitzschioides* (Figure 4.6).

4.5.2.2 Diatom Proxies

Diatoms, like many organisms, thrive under a specific range of environmental conditions or optima and this optima is different for each species. For this reason, diatom assemblages are excellent paleoceanographic indicators [*Smol*, 2002]. Table 4.1 delineates which species were grouped together into specific environmental niches. Our interpretations of the paleoceanographic sea surface conditions at the Bering Sea shelf-slope break during MIS 12 to 10 are based on changes in these 8 groups and the variability of *Neodenticula seminae*, an indicator of the Alaskan Stream and North Pacific water [*Katsuki and Takahashi*, 2005; *Sancetta*, 1982] (Figure 4.7).

4.5.2.2.1 Sea Ice Species

Epontic diatoms are those that bloom attached to the underside of sea ice or within brine channels in the ice. This initial spring bloom occurs below the ice as soon as enough light penetrates to initiate photosynthesis in the Bering Sea and can occur as early as March [*Alexander and Chapman*, 1981]. The centric diatom, *Melosira arctica,* and pennate diatoms, *Nitzschia frigida* and *Navicula transitrans* are among the major components of the epontic diatom bloom [*von Quillfeldt et al.*, 2003] and are all found in the sediments at U1345A,although they make up a minor proportion of the sediment diatom assemblage.

A second ice-associated bloom occurs as sea ice begins to break up on the Bering Sea shelf. This bloom is referred to as the marginal ice zone bloom and many of its members are common species in the sediment assemblage including the pennate diatom, *Staurosirella pinata* (=*Fragilaria* cf. *pinata*), and the centric diatoms, *Bacterosira bathyomphala* and several

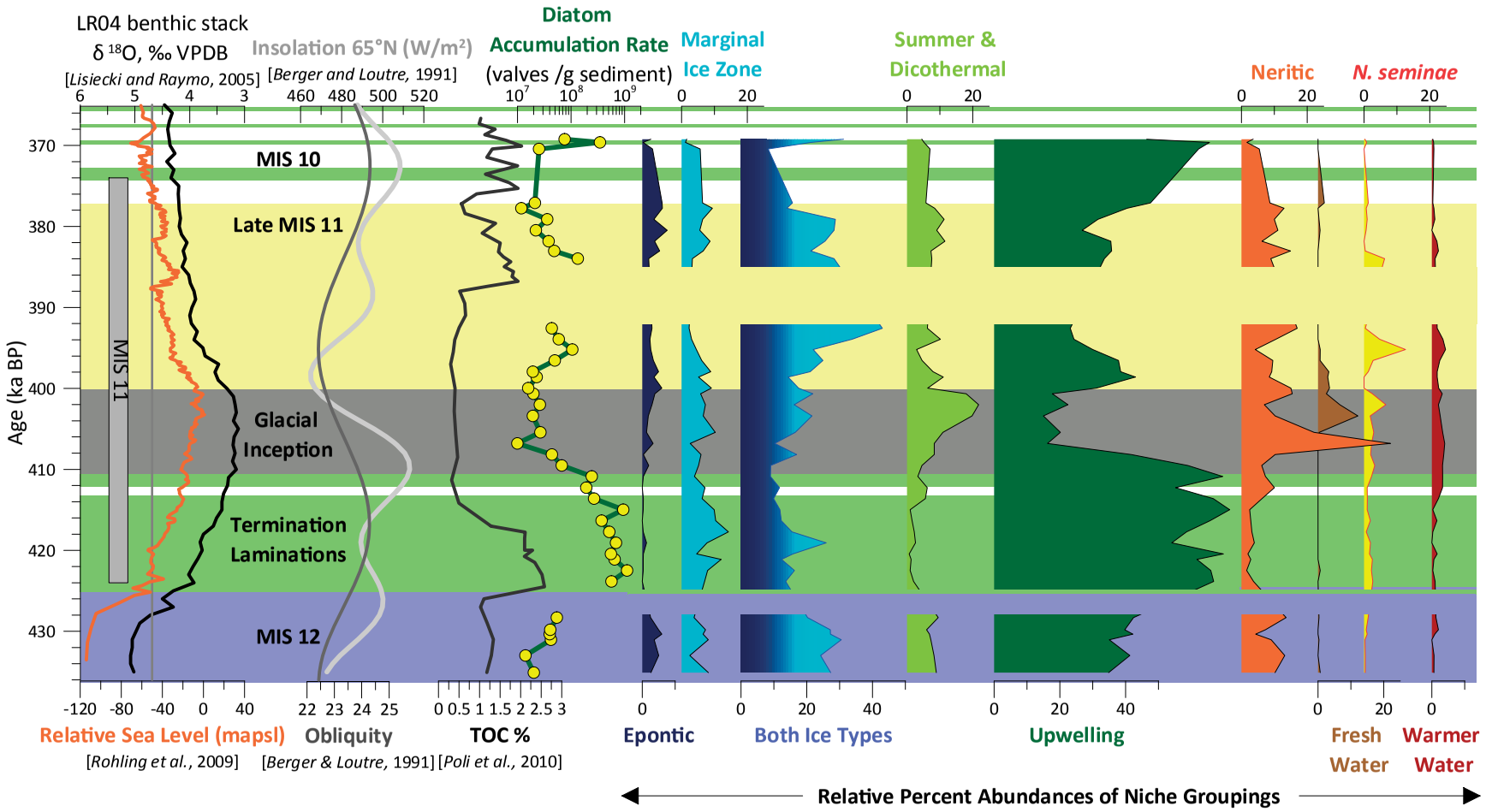

Figure 4.7. Global eustatic sea level, the LR04 $\delta^{18}O$ stack from benthic foraminifera, insolation at 65° N, and relative percent abundances of diatoms grouped and color coded by species niche. A vertical grey line ine is drawn at -50 m apsl through the eustatic sea level curve. This depth is the approximate sill depth of Bering Strait. Colored bars refer to zones of MIS 11 mentioned in the text.

Thalassiosira species including *Thalassiosira antarctica* resting spores [*Schandelmeier and Alexander*, 1981; *Shiga and Koizumi*, 2000; *von Quillfeldt et al.*, 2003]. *T. antarctica* RS have been classified in various ways in the past and their ecology is not well understood. However, *T. antarctica* is a member of the marginal ice zone flora [*von Quillfeldt et al.*, 2003] and was the only organism in thick pack ice [*Horner*, 1985]. The resting spores are associated with coastal or ice-margin waters that range from −1 to 4 °C and have relatively low salinity (25–34‰) [*Barron et al.*, 2009; *Shiga and Koizumi*, 2000]. In Antarctica *T. antarctica* blooms in concert with frazil and platelet ice growth [*Pike et al.*, 2009]. This has not yet been observed in the Arctic, though it is a possibility.

Several diatom species are present in both types of sea ice blooms, and so while they are indicators of ice presence, they cannot be used to distinguish between types of sea ice. These species are grouped under "both ice types" and include such common diatoms as *Fragilariopsis oceanica, Fragilariopsis cylindrus, Fossula arctica,* and many Naviculoid pennate diatoms [*Saitoh and Taniguchi*, 1978; *Sancetta*, 1981; *Schandelmeier and Alexander*, 1981; *von Quillfeldt*, 2001; *von Quillfeldt et al.*, 2003].

Epontic species are present in low relative percent abundances (< 8%) throughout much of the record, but there is a marked absence of them during the laminated interval from 425 to 413 ka (129.96-126.45 mbsf). Marginal ice zone species fluctuate between 4% and 14% throughout the record and do not show any trends in abundance changes. The grouping of species found both within the ice and in the water surrounding ice, however, is roughly anticorrelated with June top of the atmosphere insolation at 65°N [*Berger and Loutre*, 1991] with high abundances of this group occurring during periods of low insolation. High relative abundances of this group vary between 20% and 30% and occur during MIS 12 from 435 to 425 ka (132.90 to 129.96 mbsf) and during the end of MIS 11 from 390 to 380 ka (119.70 to 116.77

mbsf). Additional peaks in the "both ice types" group occur at 419 ka (128.21 mbsf) and 369 ka (112.86 mbsf). Low relative abundances (~10%) occur throughout much of MIS 11 (Figure 4.7).

4.5.2.2.2 Warmer Water Species

Diatoms associated with warmer water or classified as members of temperate to subtropical assemblages are rare in this record; however, they are present. This group includes *Azpeitia tabularis, Thalassiosira eccentrica, Thalassiosira oestrupii,* and *Thalassiosira symmetrica.* [*Fryxell and Hasle*, 1972; *Lopes et al.*; *Sancetta*; *Sancetta and Silvestri*, 1986].

Relative abundances of warmer water species are quite low throughout the record (<5%), and are highest (3-4%) during the peak of MIS 11, from 414 to 394 ka (126.74 to 120.87 mbsf) (Figure 4.7).

4.5.2.2.3 Alaskan Stream Species

Neodenticula seminae is often used as a tracer of North Pacific water, in particular the Alaskan Stream [e.g. *Caissie et al.*, 2010; *Katsuki and Takahashi*, 2005]. But its distribution also varies on glacial-interglacial time scales within the Pacific Ocean [*Sancetta and Silvestri*, 1984]. It is adapted to the low productivity of the North Pacific gyre and is heavily silicified which could lead to high proportions of *N. seminae* reflecting simply dissolution of finely silicified diatoms [*Sancetta*, 1981; 1982]. *N. seminae* is used here as a tracer of Pacific water with the above caveats.

N. seminae begins to increase at 431 ka, more than 5 ka before the termination lamination. It remains stable at ~2% relative percent abundance between 425 and 403 ka (129.96-123.63 mbsf), then peaks at 13% at 395 ka (121.17 mbsf). *N. seminae* remains low through MIS 10 (Figure 4.8).

4.5.2.2.4 Upwelling Species

Chaetoceros resting spores are the dominant taxa included in the upwelling group. *Chaetoceros* RS have been used as indicators of high productivity [e.g. *Caissie et al.*, 2010] and are found in locations influenced by intense upwelling [*Lopes et al.*, 2006; *Sancetta*, 1982]. In addition, *Chaetoceros socialis* can be a common member of the marginal ice zone bloom [*von Quillfeldt*, 2001] and a dominant member of the sub ice bloom [*Melnikov et al.*, 2002]. *Chaetoceros furcellatus* is also associated with the marginal ice zone bloom [*von Quillfeldt*, 2001]. Unfortunately, the morphology of *Chaetoceros* resting spores is quite variable, and they cannot be classified definitively without the labile vegetative cell also present [*Tomas*, 1996]. *Odontella aurita, Thalassionema nitzschioides* are also included in the upwelling group although they too are associated with the marginal ice zone [*von Quillfeldt et al.*, 2003], areas of high productivity [*Aizawa et al.*, 2005], and upwelling [*Lopes et al.*, 2006; *Sancetta*, 1982]. It may be that the combination of upwelling and ice melt at the shelf slope break in the Bering Sea is responsible for statistical correlation between these two environmental niches. The spring-blooming *Thalassiosira pacifica* and small (<10 µm) *Thalassiosira* species round out the upwelling group due to their associations with high

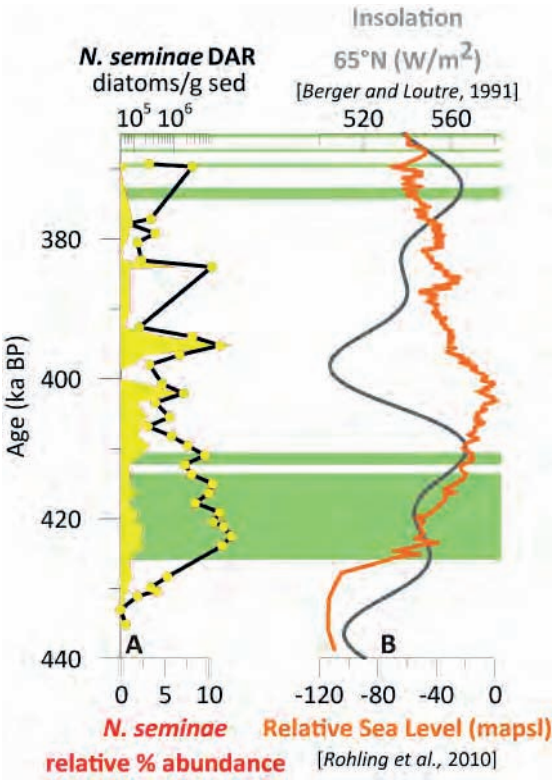

Figure 4.8. Abundances of Neodenticula seminae and sea level. Panel A shows both accumulation rates and relative percent abundances of N. seminae. Panel B shows insolation in grey and eustatic sea level in orange. Laminated intervals are shown in green.

productivity and upwelling specifically in the Bering Sea and North Pacific [*Aizawa et al.*, 2005; *Hay et al.*, 2007; *Katsuki and Takahashi*, 2005; *Lopes et al.*, 2006; *McQuoid and Hobson*, 2001; *Saitoh and Taniguchi*, 1978].

Upwelling species are roughly correlated with insolation [*Berger and Loutre*, 1991] with highest relative abundances (60-70%) occurring during high levels of insolation. An exception to this is the interval between 400 and 390 ka when upwelling species are moderately high (30-40%) and insolation is at its lowest. The lowest relative abundances (15-20%) of upwelling species occurs as insolation declines between 407 and 402 ka (124.69 to 123.22 mbsf). Upwelling species are high during both the Termination V laminations and during the MIS 10 laminations (Figure 4.7).

4.5.2.2.5 Dicothermal Water Indicators and Late Summer Species

Dicothermal water is characterized by a cold layer of water found between warmer surface and deeper water. It is stable because of very low salinity the surface layer above it. In the Sea of Okhotsk and the Bering Sea, the dicothermal layer is often associated with melting sea ice. The highest abundances of *Thalassiosira trifulta* are found blooming in this highly stratified, cold water in the Sea of Okhotsk today [*Sancetta*, 1981; *Sancetta and Silvestri*, 1986].

Actinocyclus curvatulus has been observed living in water surrounding sea ice [*von Quillfeldt et al.*, 2003]; however, it is neither a common member of the marginal ice zone flora, nor is its spatial distribution in the Bering Sea consistent with the distribution of sea ice [*Sancetta*, 1982]. Its relative percent abundances are more closely associated with those of *T. trifulta* [*Sancetta*, 1982], and so it was grouped with *T. trifulta* as an indicator of dicothermal water.

Genera present in the Bering Sea during late summer (*Coscinodiscus, Leptocylindrus,* and *Rhizosolenia*) [*Aizawa et al.*, 2005; *Lopes et al.*, 2006; *von Quillfeldt et al.*, 2003] tend to covary with the dicothermal water indicators, so the two groups were merged for comparison with other diatom groups.

These two groups are highest (10% relative abundance) at ~402 ka (123.22 mbsf) as insolation is declining. This peak is coeval with an intermediate peak in *N. seminae* and occurs immediately following a peak in neritic species. Dicothermal water indicators and summer species are lowest (< 1%) during the termination lamination (425-406 ka; 126.45 to 124.39 mbsf). Intermediate relative abundances (1% to 5%) occur during MIS 12 and from 399 ka (122.34 mbsf) to the top of the record (369 ka/112.86 mbsf) (Figure 4.7).

4.5.2.2.6 Shelf to Basin Transport Indicators

Freshwater species are rare, but present in the record. They include the centric species *Cyclotella ocellata* and *Puncticulata radiosa* [*Håkansson*, 2002]. Additional freshwater diatoms found in the record are species found in sea ice (*S. pinnata*)[*von Quillfeldt et al.*, 2003] or in the neritic zone (*Cyclotella stylorum)* [*Barron et al.*, 2009] and so these species were placed in the marginal ice zone and neritic groups respectively.

The dominant species in the neritic group is *Paralia sulcata,* which is an interesting species because it can be either planktic or benthic [*Kariya et al.*, 2010] and is associated both with river deltas and the sea ice species, *Melosira arctica* [*Sancetta*, 1982]. It is a member of the marginal ice zone assemblage [*von Quillfeldt et al.*, 2003] and Pushkar [1999] asserts that *P. sulcata* indicates water shallower than 20 m. Its high abundances in Bering Strait may mean that it is adapted to moving water [*Sancetta*, 1982]. *P. sulcata* thrives in water that is warmer than 3 degrees [*Zong*, 1997], with low light [*Blasco et al.*, 1980] and low salinity [*Ryu et al.*, 2008].

The fresh water group is notably absent from much of the core, but prevalent between 405 and 395 ka (124.10 and 121.17); it reaches its highest relative percent abundance (12%) at 403 ka (123.62 mbsf). Neritic species, on the other hand maintain ~10% relative abundance throughout the core except for a short interval between 408 ka and 405 ka (124.98 mbsf to 124.10 mbsf) when they increase to 45% of the assemblage (Figure 4.7).

4.6 Discussion

The study interval can be broken into five zones based on changes in diatom assemblages and lithology (Figure 4.7). These zones reflect changing sea ice, glacial ice, sea level, and SST and correspond to events recognized elsewhere in ice cores and marine and lake sediments.

4.6.1 Marine Isotope Stage 12

The oldest zone stretches from the beginning of the record to 425 ka and reflects conditions at the end of MIS 12. Although diatom accumulation rate is quite low, this period is characterized by a relatively diverse assemblage (Figure 4.5) with moderate amounts of sea ice, upwelling, and dicothermal species (Figure 4.7) indicating seasonal sea ice with highly stratified waters during the ice-melt season. Sea level was low during this interval [*Rohling et al.*, 2010], placing U1345 proximal to the Beringian coast (Figure 4.2), however, fresh water species are absent and there are moderate relative percentages of neritic species indicating relatively low amounts of shelf to basin transport. There is little evidence of pebbles or very poorly sorted sediments, but two sand layers may be evidence of either glacial ice rafted debris (IRD) coming from the Aleutians or Beringia or of sediment reworking (Figure 4.4). With the Beringian shelf exposed, the continent was relatively arid and glacial ice may have been restricted to mountain-valley glaciers, similar to conditions during the last glacial maximum [e.g. *Glushkova*, 2001].

These small, distant glaciers would not have produced large amounts of ice bergs, but may have contributed some ice that brought sand grains to the shelf-slope break.

This finding is in contrast to the North Atlantic where MIS 12 is characterized as an intense glacial period with ice rafted debris found as far south as Bermuda [*Poli et al.*, 2000]. Similar to the Bering Sea, the North Atlantic was highly stratified with significantly reduced NADW production [*Poli et al.*, 2010]. This high stratification effectively trapped high nutrient concentrations below 2000 m [*Thunell et al.*, 2002] in contrast to today when only the Pacific is underlain by nutrient-rich waters [*Thunell et al.*, 2002]. High stratification appears to have led to lowered productivity in both the Atlantic and Pacific.

Towards the end of MIS 12, both relative percent and absolute abundances of *N. seminae* begins to increase (Figure 4.8). Two factors control *N. seminae* abundance: increasing *N. seminae* in the North Pacific, or increasing the influence of Pacific water at U1345. Because sea level has not yet begun to rise, it is more likely that the increase in *N. seminae* is due to this species increasing in the Pacific just before Termination V. This precedes any other record of deglaciation in the region, but occurs in sync with an increase in insolation.

4.6.2 Termination V Laminations (425-411 ka)

Termination V, the transition from MIS 12 to MIS 11 is placed at 428-422 ka. During the first half of the termination, productivity in Lake Baikal begins to increase at about 429 ka [*Prokopenko et al.*, 2010], and in Antarctica, flux of terrigenous dust decreases at this time, reflecting perhaps a decrease in Southern Ocean winds. Sea ice and CO_2 don't change until later [*Wolff et al.*, 2006]. The first half of Termination V is not expressed at U1345 (part of it is missing due to a core gap), but the second half stands out. At 425 ka, a thick laminated interval is deposited indicating that the bottom water at 1000 m in the Bering Sea was dysoxic. This

laminated interval also overlaps with the warmest, most humid, least continental period recorded in the sediments at Lake Baikal (420-405 ka) which was surrounded by boreal forest at the time [*Prokopenko et al.*, 2010].

The diatom assemblage in the laminated interval (425-407) suggests extremely productive water with reduced sea ice. It is unlikely that there was an early spring, epontic bloom. In contrast to terrestrial records, SSTs were slightly warmer than MIS 12, but this was not the warmest part of the record. Upwelling was intense along the shelf-slope break.

Coincidentally, global eustatic sea level rises above the estimated Bering Strait sill depth (-50 m) at 425 ka. It is plausible that increased nutrient availability drove high primary productivity as floods scoured fresh organic matter from the submerging continental shelf [*Bertrand et al.*, 2000]. This mechanism has been suggested to explain increasing productivity during the last deglaciation in the Sea of Okhotsk [*Shiga and Koizumi*, 2000] and during MIS 11 in the North Atlantic [*Poli et al.*, 2010] and also may have contributed to dysoxia by ramping up nutrient recycling, bacterial respiration and decomposition of organic matter in the Bering Sea.

Alternatively, higher productivity may have been driven by an increase in micronutrients such as iron. Several mechanisms have been proposed for higher nutrient concentrations during the last deglaciation including weakening of North Pacific stratification or enhanced surface nutrient utilization [*Brunelle et al.*, 2007] or an increase in volcanic activity contributing iron to the surface waters [*Huybers and Langmuir*, 2009]. Such mechanisms may have been important during Termination V as well.

In the North Atlantic, episodic increases in productivity occur at this time and NADW formation intensifies (Figure 4.7). Ventilation of NADW generally continues to increase from 424 to 410 ka [*Chaisson et al.*, 2002; *Dickson et al.*, 2009; *Poli et al.*, 2010] to its strongest and then weakens over the course of the interglacial [*Thunell et al.*, 2002]. At the same time NADW

ventilation is increasing, the strength of Southern Ocean winds is decreasing [*Wolff et al.*, 2006] and mega-droughts are occurring in the US Southwest. These droughts have been ascribed to a shift in aridity as the westerlies moved poleward [*Fawcett et al.*, 2011]. Shifting the westerlies may also have increased humidity farther north in Beringia [*Seager et al.*, 2007]. Evidence for intensified upwelling in the Bering Sea, further suggests teleconnections between NADW formation, the strength of the southern winds, upwelling in the North Pacific, and northward flow through Bering Strait [e.g. *DeBoer and Nof*, 2004].

4.6.3 Peak MIS 11 (411-400 ka)

At approximately 410 ka, several lines of evidence point toward a reorganization of Bering Sea circulation in concert with deep ocean circulation and heat transport between the North Atlantic and Antarctica. Proxy evidence for NADW ventilation (decreases in $CaCO_3$ % and $\delta^{13}C$) indicates that between 412 and 392 ka, NADW formation decreased for short periods (< 1 ka) [*Poli et al.*, 2010]. Terrigenous metals, which may reflect Patagonian wind strength, increase slightly around 411 ka in the EPICA Dome C ice core [*Wolff et al.*, 2006]. At the California margin, redwoods are prominent reflecting warm, humid conditions [*Lyle et al.*, 2001] and productivity sharply decreases in the Bering Sea returning oxygenated waters to 1000 m. Epontic blooms resume and *N. seminae* sharply decreases in absolute abundance (Figure 4.8), indicating reduced influence from the Pacific Ocean. Together, these events point towards a possible switch in Bering Strait flow from northward to southward at 411 ka [e.g. *DeBoer and Nof*, 2004]. Further evidence for this was found on St. Lawrence Island where Arctic mollusks suggest that flow through Bering Strait was reversed during the Middle Pleistocene [*Hopkins*, 1972] bringing Arctic mollusks to the Gulf of Anadyr while warmer Pacific water continued to flow northward and mix with Arctic water at Anadyr Strait.

Peak interglacial conditions occur shortly after this apparent temporary reversal in Bering Strait throughflow. During 11.3, temperatures were the highest in Antarctica (407 ka) [*Pol*, 2011] and global ice volume was the lowest (402 ka) [*Lisiecki and Raymo*, 2005] that they have been for the past 500 kyrs. Modern barrier reefs were formed in the tropics, and carbonate dissolution was wide spread in the deep waters of both the Atlantic and the Pacific [*Thunell et al.*, 2002]. On the continents and in the Pacific Ocean, proxy data points to air and sea surface temperatures warmer than today [*de Vernal and Hillaire-Marcel*, 2008; *Lozhkin et al.*, in prep; *Lyle et al.*, 2001; *Prokopenko et al.*, 2010; *Raynaud et al.*, 2005; *Tarasov et al.*, 2011; *Tzedakis*, 2010] and Lake Baikal and Lake El'gygytgyn were highly productive [*Lozhkin et al.*, in prep; *Prokopenko et al.*, 2010; *Tarasov et al.*, 2011]. In contrast, the Blake Plateau in the North Atlantic had low organic matter flux to the sediments [*Poli et al.*, 2010] as did the California margin [*Lyle et al.*, 2001], indicating that El Nino-like conditions may have been present at MIS 11.3.

At U1345, the diatom assemblages largely support these previous studies. Relative percentages of warm water species are the highest in the record as are dicothermal species and those that bloom in late summer. In contrast, DAR and relative percent abundances of both sea ice and upwelling species are low (Figure 4.7). Summers were warm with highly stratified water; sea ice occurred seasonally, perhaps lasting a bit longer than during Termination V, and upwelling was reduced at the shelf-slope break, which limited diatom productivity.

4.6.3.1 Glacial Inception in Beringia

Although global sea level was near its maximum, and much of the world was experiencing peak MIS 11 conditions, there is evidence that the high latitudes were already cooling. Insolation at 65° N began to decline at 410 ka [*Berger and Loutre*, 1991], cooling begins

at 407 ka in Antarctica, expressed both isotopically and as an expansion of sea ice [*Pol*, 2011], and millennial scale cooling events are recorded at Lake Baikal [*Prokopenko et al.*, 2010]. By 405 ka, Lake Baikal begins to shift towards a dryer, more continental climate [*Prokopenko et al.*, 2010] and several lines of evidence point to glacial inception occurring in Beringia.

Although their fluctuations are small, warm water species begin to decline at 408 ka. This is followed by a significant increase in neritic species at 407 ka and then the highest relative percentages of fresh water species at the site. There are several ways that these species could have been carried out to 1000 m of water over the shelf-slope break at this time of high sea level when U1345 was more than 300 km from the coast:

1) turbidites or strong density currents on the shelf,
2) sediment reworking and winnowing,
3) sea ice, or
4) glacial ice.

Sancetta and Robinson [1983] argue that benthic pennate species were transported out of shallow water by rivers and turbidity currents during glacial periods, but they do not consider ice as a transport mechanism [*Sancetta and Robinson*, 1983].

The sedimentology of the core does not show any evidence of fining up sequences or evidence of turbidite deposition [*Takahashi et al.*, 2011] and multiple terrigenous grain sizes indicates that the sediments are relatively poorly sorted. If winnowing were a dominant transport mechanism, the sediments should be well sorted. The dominant neritic diatom, *P. sulcata* may be adapted to moving water associated with river deltas. The peak in *P. sulcata* relative percentages may be reflective of a paleo river channel near U1345; however sea level is at a maximum, so U1345 would have been quite far from any river delta. We question whether density currents and sediment reworking are the dominant transport mechanisms during this

time. However, there is not sufficient data at present to rule out a change (strengthening/directional change) in bottom currents as a method of sediment transport, especially in light of the possibility of southward Bering Strait thru flow.

Sea ice could bring neritic diatoms out to deeper waters as it preferentially entrains silt and clay size particles [*Reimnitz et al.*, 1998]. However, if there was an increase in sea ice, we would expect to see a significant increase in sea ice diatoms during this interval. Instead we see a small increase in sea ice related species, primarily epontic species. During this time, the marginal ice zone assemblage is dominated by *T. antarctica* RS which is a taxon primarily found in coastal, low salinity areas [*Barron et al.*, 2009; *Shiga and Koizumi*, 2000], so its presence may simply be indicative of increased shelf to basin transport.

The fourth transport mechanism, glacial ice, is effective at carrying terrigenous and near shore particles far from land. We do not have detailed grain size data for this interval to check the sorting and mode of sediments; however, shipboard data shows an increase in the presence of large, isolated clasts, interpreted as ice rafted debris, a cluster of sand layers, a thick interval of silty sand (Figure 4.4), and an increase in natural gamma radiation [*Takahashi et al.*, 2011], a proxy for clay content [*Carter*, 2005]. The increase in multiple sizes of terrigenous grains coupled with the high percentages of fresh water and neritic species (Figure 4.9) favors transport by ice bergs that could carry unsorted sediments from both the shelf and the exposed continent out to the shelf slope break; although certainly a combination of transport mechanisms may be occurring.

Diversity is highest at 400 ka, perhaps due to the multiple contributions of diatoms from fresh water on the shelf, the coast, and pelagic deposition. Additionally the assemblage during this interval is very similar to the assemblage found in sediments from the Anvillian Transgression 800 km northeast of U1345 near Kotzebue [*Pushkar et al.*, 1999]. Pushkar [1999]

describes the assemblage as reflecting very warm SSTs and high river run off bringing fresh water diatoms out to sea. He relates the prevalence of *P. sulcata* here to a lowering of salinity also due to high run off from the continents [*Pushkar et al.*, 1999]. We do not find support for the assertion that sea ice was significantly reduced or absent during the Anvillian Transgression [*Kaufman and Brigham-Grette*, 1993; *Pushkar et al.*, 1999]. In fact, relative percentages of sea ice diatoms are similar to those during MIS 12 and 10.

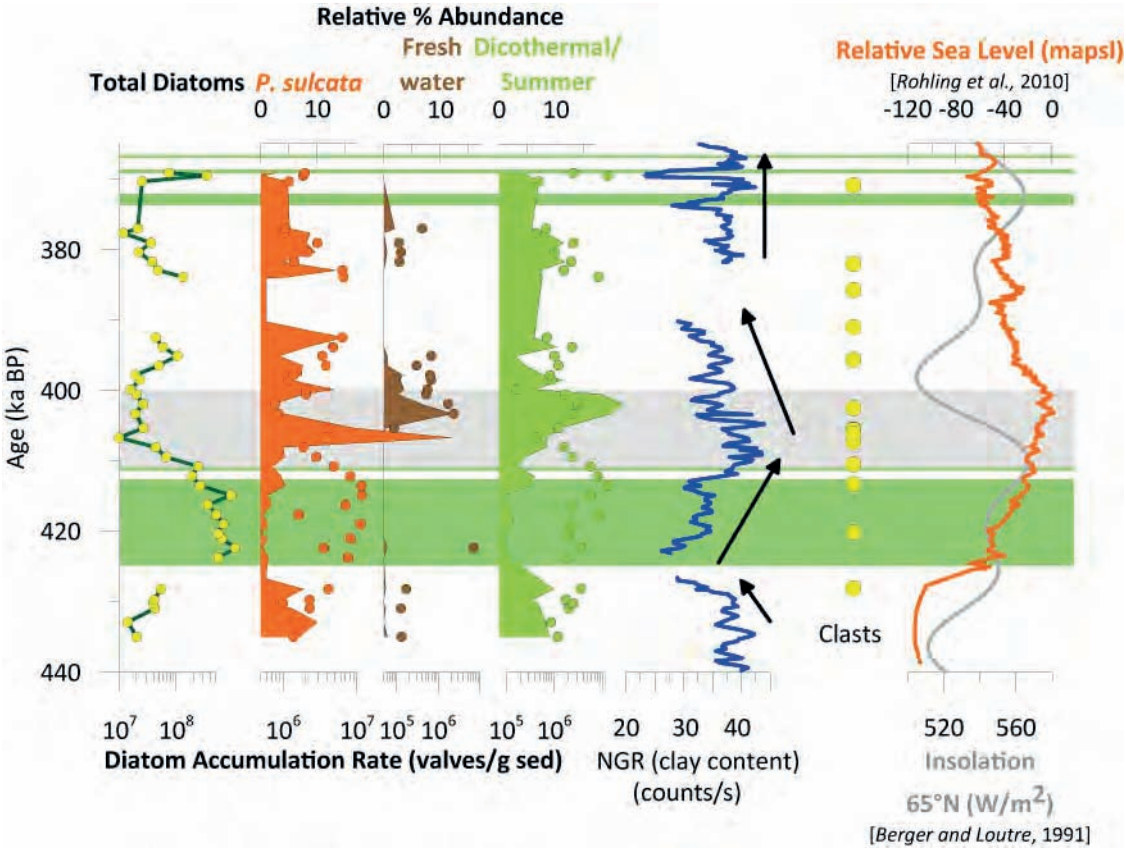

Figure 4.9. Proxy indicators of shelf to basin transport. Panel A shows the total diatom accumulation rate. Area plots depict relative percent abundance of B. P. sulcata, C. fresh water species and D. dicothermal or summer blooming species. Dots overlying the area plots indicate the diatom accumulation rate of the same species. E. The blue line is natural gamma radiation, a proxy for clay content. Panel F depicts isolated clasts (IRD) for all holes at U1345, plotted as yellow circles. G. Global eustatic sea level is shown in orange and insolation at 65° N is grey. The grey bar spans 411-400 ka, the interval of glacial inception in Beringia. Laminated intervals are shown in green.

Although this transgression has not been precisely dated on land, it has been placed in MIS 11 [*Kaufman et al.*, 1991; *Miller et al.*, 2009]. The current height of these uplifted marine deposits suggest that relative sea level may have been 9-25 m apsl [*Kaufman et al.*, 1991; *Pushkar et al.*, 1999]. Adjusting for glacial isostasy [*Raymo and Mitrovica*, 2012], these high stands actually might reflect eustatic sea levels very close to modern height or up to 10 m apsl. Additionally, SSTs during this transgression were warmer than today near Kotzebue [*Pushkar et al.*, 1999] and similar to today farther north on the Arctic coastal plain [*Kaufman and Brigham-Grette*, 1993].

4.6.3.2 Nome River Glaciation

Glacial deposits from the most extensive Beringian glaciation rest upon Anvillian and correlative transgressive marine sediments from St. Lawrence Island [*Gualtieri and Brigham-Grette*, 2001; *Hopkins*, 1972] to the Pribilof Islands [*Hopkins*, 1966] and from the Alaska Arctic coastal plain [*Kaufman and Brigham-Grette*, 1993], south to Kotzebue [*Huston et al.*, 1990], Nome [*Kaufman*, 1992], and Bristol Bay [*Kaufman et al.*, 2001]. Mollusks and pollen in the glaciomarine sediments reflect a tundra environment on St. Lawrence Island and temperatures similar to today [*Hopkins*, 1972]. The middle to top of one of these glaciomarine deposits, the Baldwin Silt, contains colder marine microfossils revealing that the warmer Pacific influence was cut off though sea level remained high enough for marine deposition near Kotzebue. Sea ice and freshwater diatoms deposited by glacial outwash are common [*Pushkar et al.*, 1999]. This indicates that Beringian ice advanced more than 200 km from the Brooks Range to Kotzebue Sound and reached its maximum extent while sea level was still high [*Huston et al.*, 1990].

Evidence for glacial ice at U1345 supports the notion of glaciation during MIS11 initiated by decreasing insolation coupled with a proximal moisture source for snow buildup: the flooded

Beringian shelf. [*Huston et al.*, 1990; *Pushkar et al.*, 1999]. This "snow gun" hypothesis has been invoked for other high latitude glaciations [*Miller and De Vernal*, 1992]; however, Beringia is uniquely situated. Once sea level began to drop, Beringia became more continental and arid [*Prokopenko et al.*, 2010] and the moisture source for these glaciers was quickly cut off.

4.6.4 Late MIS 11 (400-377 ka)

Evidence of the Nome River Glaciation is short lived at U1345 (<10 ka). By 400 ka, the high percentages of fresh water, late summer and dicothermal species have been replaced with the highest proportions of sea ice species coupled with the highest percentages of the North Pacific tracer, *N. seminae.* Warm water species continue decrease from 400 to 377 ka. These patterns reflect general cooling worldwide [*de Abreu et al.*, 2005; *Prokopenko et al.*, 2010; *Raynaud et al.*, 2005] and decreasing sea level [*Rohling et al.*, 2010]. Sea level is still high enough though to allow *N. seminae* to reach the shelf slope break, but significant parts of the Beringian continental shelf are exposed, cutting off the moisture supply for the Nome River Glaciation [*Pushkar et al.*, 1999]. Subaerial and glaciofluvial deposits above the Nome River and correlative glaciations indicate that Beringian ice retreated, while climate remained cold or grew colder. Ice wedges and evidence of permafrost are also common [*Huston et al.*, 1990; *Pushkar et al.*, 1999] above Nome River glaciation deposits.

At 388 ka a pulse of organic matter is deposited in the North Atlantic [*Poli et al.*, 2010] (Figure 4.5). It is unfortunate that there is a core break during this critical interval at U1345, however, the data we have indicate somewhat increased sea ice and productivity at the same time as the organic carbon pulse occurs in the North Atlantic is high [*Poli et al.*, 2010] (Figure 4.7). We proposed that at 425 ka, a change in nutrient recycling due to flooding of Bering Strait drove increased primary productivity in both the Atlantic and Pacific. It is tantalizing to note that

this secondary increase in productivity also occurs at a time when global sea level was fluctuating around -50 mapsl [*Rohling et al.*, 2010] (see grey line at -50 m on Fig 4.7) and may be again related to shelf to basin nutrient dynamics [e.g. *Bertrand et al.*, 2000]. The teleconnection between productivity in the Bering Sea and the North Atlantic at this time suggests that sea level fluctuation driven by the closure of Bering Strait may also be occurring at the end of MIS 11 as well as during the last glacial maximum [*Hu et al.*, 2010].

4.6.5 MIS 10

At ~377, MIS 11 transitions to MIS 10. Laminations reflecting high productivity and reduced oxygen in the intermediate waters are again deposited. This interval is quite different from MIS 12 and is characterized by a low diversity assemblage, dominated by upwelling indicators, a moderate amount of sea ice indicators, and low amounts of all other diatoms.

4.7 Conclusions

The shelf-slope break in the Bering Sea (Site U1345A) records changes in diatom assemblage during the transition from MIS 12 to MIS 11. Assemblage turnovers occur at 425 ka, 410 ka, 400 ka, and 377 ka, and reflecting changes in upwelling, sea ice, glacial ice, and potentially even current direction.

Upwelling was robust during the termination laminations and MIS 10 laminations, and moderate during late MIS 11. Productivity increases in the Bering Sea occur coeval with high productivity pulses in the North Atlantic and may be related to sea level rise and flooding of Bering Strait.

Beringia was glaciated briefly while sea level was at its highest point. This glaciation appears to have been driven by unusually humid conditions at a time when insolation and obliquity are decreasing. It is recorded in the sediments as an increase in unsorted sediments

ranging from clay to pebbles, and maxima in fresh water and neritic diatom relative percent abundances.

There are no major changes in sea ice throughout the transition from MIS 12 to MIS 11 to MIS 10, although there are minor changes. Notably, there are no epontic species during Termination V. U1345 appears to have been near the marginal ice zone throughout this interval.

When NADW is high in the North Atlantic, productivity is high in the Bering Sea. A short-term decrease in NADW strength at 410 ka may have triggered a reversal in the flow of water through Bering Strait. Reductions in upwelling and North Pacific species as well as geomorphologic evidence of Arctic mollusk range extensions to the south [*Hopkins*, 1967] support the notion of reversed flow. Future work to specifically test this hypothesis is necessary and MIS 11 may be an appropriate time interval to focus such a study.

CHAPTER 5

A MODERN CALIBRATION OF IP_{25} WITH SEA ICE CONCENTRATION AND SEA SURFACE TEMPERATURE IN THE BERING AND CHUKCHI SEAS

5.1 Abstract

In recent years, due to greenhouse gas emissions, there has been a remarkable decrease in Arctic sea ice extent and duration, but what is unknown is the sensitivity of sea ice to previous, orbitally-driven warmings. To address this question, a quantitative proxy for sea ice concentration is urgently needed. Here we examine the organic biomarker called IP_{25}, which has been proposed as a proxy for the presence of seasonal sea ice. We report IP_{25} concentration measured in a suite of surface sediment samples in the Bering and Chukchi seas and their correlation to spring (MAMJ: March, April, May, June) sea ice concentration and spring environmental variables. We use principal component and stepwise regression analysis to develop a quantitative relationship between MAMJ sea ice concentration, IP_{25} concentration and MAMJ sea surface temperature. This calibration will allow quantitative down core reconstructions of past sea ice presence and duration, which can be used as realistic boundary conditions in climate model simulations.

5.2 Introduction

Sea ice plays a critical role in high latitude marine carbon cycling [*Lee et al.*, 2008], is one of the main drivers of thermohaline circulation by its control on deep and intermediate water formation [*Thomas and Dieckmann*, 2003], and its reduction exerts a positive feedback to climate warming due to the albedo effect [*Holland et al.*, 2006]. As such, it is essential for both climate modellers interested in future sea ice projections and paleoclimate workers to

understand how sea ice has varied in the past, especially during major climate transitions such as glacial terminations and inceptions.

Traditionally, researchers have looked to the sediments to develop proxies in order to reconstruct the oscillation between ice free, seasonally ice covered, and perennially ice covered intervals. These include ice rafted debris [*Davies et al.*, 2009; *Sakamoto et al.*, 2005] and microfossil assemblages, especially dinoflagellate cyst and diatom, in conjunction with principal component analysis (PCA) or transfer functions [*de Vernal et al.*, 2001; *Sancetta and Robinson*, 1983]. Recently, an organic biomarker, IP_{25}, has been proposed as a new proxy for sea ice [*Belt et al.*, 2007]. IP_{25} is a monounsaturated Highly Branched Isoprenoid (HBI) found in sea ice and sediments underlying sea ice, but is conspicuously absent from open water and sediments under open water [*Belt et al.*, 2007]. Culture experiments have confirmed that a restricted number of species belonging to the genera *Haslea, Navicula,* and *Pleurosigma* synthesize HBIs [*Damsté et al.*, 2004], but although these genera are represented in the sea ice, further work is needed to confirm the exact source of IP_{25} amongst the sympagic flora [*Massé et al.*, 2011]. Despite not knowing the exact diatom source species, Belt and co-investigators [2008], used compound specific isotopic techniques, to further confirm a sea ice origin for $IP_{25.}$ Since then several studies have confirmed its usefulness in providing qualitative estimates of past sea ice occurrences [*Massé et al.*, 2008; *Müller et al.*, 2009; *Vare et al.*, 2009]. However, a set of calibration studies would greatly contribute to extending the usefulness of this novel proxy by, in turn, providing a tool for robust and quantitative sea ice estimates directly useable in modeling studies. A first attempt was made by Müller and co-workers by comparing IP_{25} (sea ice) and sterol (open water) abundances in surface sediment collected in the Fram Strait and Greenland seas[*Müller et al.*, 2011].

In this study, we have determined IP_{25} abundances in a series of surface sediments collected across both the Chukchi and Bering seas. We then compared our IP_{25} abundances with modern day sea ice concentration in an attempt to provide a quantitative calibration of the proxy for these areas.

5.3 Background

The Bering and Chukchi seas are an ideal location to base a proxy-calibration linking IP_{25} and spring sea ice conditions (Figure 5.1) because primary productivity here is dominated by diatoms [*Takahashi et al.*, 2002]. At least two separate sea-ice related diatom blooms occur in the region (both the epontic or under ice bloom and marginal ice zone bloom) [*Alexander and Niebauer*, 1981] and therefore, we expected the sediments to contain ample reservoirs of IP_{25}.

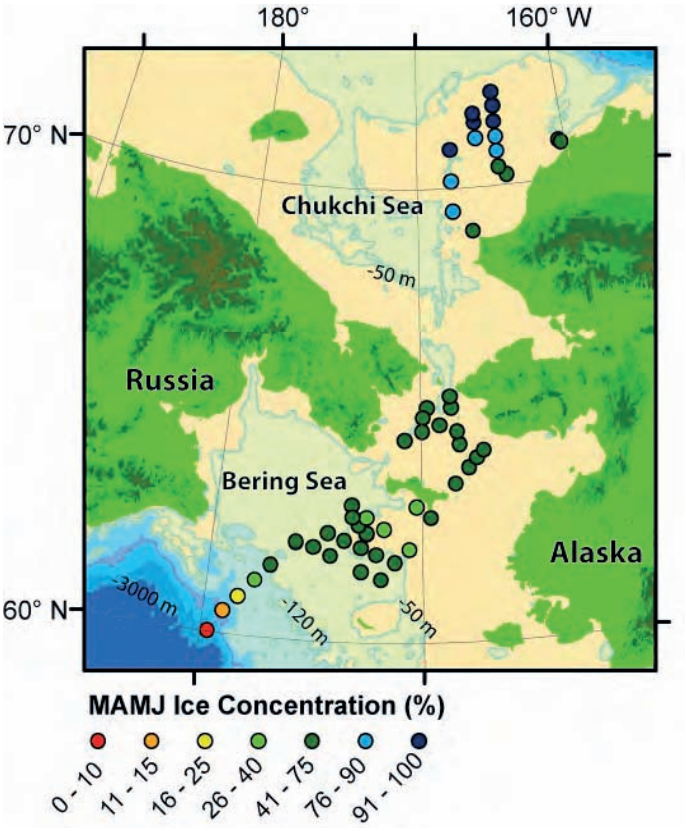

Figure 5.1. Stations colored according to spring (March, April, May, June) sea ice concentration derived from passive microwave sensors (Cavalieri et al., 2008). Bathymetry shading is at -50 m (depth to flood Bering Strait), -120 m (depth to sea level during the Last Glacial Maximum), -250 m, -500 m. Depths below 500 m are colored in increasing shades of blue every 1000 m.

The suspected IP_{25}-producing species (e.g. *Haslea* spp.) are ubiquitous, though minor (<1%), components of the sediment assemblages across the study area. These pennate diatoms bloom during spring when the light is

intense enough to sustain photosynthesis under sea ice [*Horner and Schrader*, 1982] and are not initially nutrient-limited as nutrient pulses occur as sea ice melts [*Alexander and Chapman*, 1981], through ice-edge upwelling [*Alexander and Niebauer*, 1981], and from upwelling along the Bering Sea shelf-slope break [*Stabeno et al.*, 2001]. Although the initiation of these blooms is likely not nutrient limited, there is evidence that the nutrient availability decreases as the blooms progresses, impacting the total mass of organic matter exported from sea ice [*Gradinger*, 2009]. The epontic bloom begins in March and lasts until sea ice begins to break up. In the Bering Sea, this may be less than a month, while in the Chukchi Sea, this may be up to three months [*Alexander and Chapman*, 1981]. Cores retrieved from sea ice include brown layers, up to 30 cm thick, of benthic diatoms attached to the base of the ice and extending up through brine channels within the ice [*von Quillfeldt et al.*, 2003]. At the end of the first sea ice-related bloom, these pennate diatoms are succeeded by other sea-ice associated species, such as *Fragilariopsis cylindrus* and *Thalassiosira hyalina*, in a later, brief, and highly-productive, sea-ice margin bloom that occurs as the ice breaks up [*Alexander and Chapman*, 1981]. These later-blooming species are not suspected to biosynthesize IP_{25}.

5.4 Data and Methods

5.4.1 Sediment sampling

The top 1 cm of sediments was taken from a Van Veen grab aboard the USCGC Healy (HLY 0701) in the Bering Sea and aboard the R/V Norseman II (Shell08) in the Chukchi Sea. Sediments were stored in the dark in combusted glassware and frozen until analysis. Although the undisturbed sediments from a small multi-corer are often considered preferable to sediments from a Van Veen grab, we took care to remove the most top sediments before opening the Van Veen grab. Additionally, Pirtle-Levy and co-authors recently showed no

significant difference between samples retrieved from the sediment water interface preserved in Haps cores and the top sediments from a Van Veen grab [*Pirtle-Levy et al.*, 2009].

5.4.2 Environmental Variables

Sea ice concentration was obtained from the National Snow and Ice Data Center (NSIDC dataset 0051) and derived from the Defense Meteorological Satellite Program (DMSP) -F11 and –F13 Special Sensor Microwave/Imagers (SSM/I) [*Cavalieri et al.*, 1996]. March, April, May, June (MAMJ) sea ice concentration for 1998-2007 was interpolated for each station and spring averages were calculated using ArcGIS. SST was derived from the NOAA National Centers for Environmental Prediction (NCEP) analysis of both climate models and observations [*Reynolds et al.*, 2002]. Spring averages were computed online at the IRI/LDEO Climate Data Library (http://iridl.ldeo.columbia.edu/SOURCES/.NOAA/.NCEP/.EMC/.CMB/.GLOBAL/.Reyn_SmithOIv2/). The remaining environmental variables were interpolated from the World Ocean Atlas 2009 [*Antonov et al.*, 2010; *Garcia et al.*, 2010] and were downloaded from http://iridl.ldeo.columbia.edu/expert/SOURCES/.NOAA/.NODC/.WOA09.

5.4.3 Elemental and Grain Size Analysis

Total nitrogen (TN) content was measured on 7 mg aliquots of dry sediment in tin weighing boats using a Costech ECS140 Elemental Analyzer (EA). Total organic carbon (TOC) content was determined by a similar procedure, using silver weighing boats, and dissolving inorganic carbon in the samples with sulfurous acid prior to EA analysis. Acetanilide standards were analyzed with both sets of samples. Sediment was processed for grain size analysis following the protocol of Sakamoto et al [2005] and analyzed on a Coulter LS200 laser diffraction particle analyzer.

5.4.4 Lipid Purification and Analysis

Sediment samples were freeze-dried and homogenized. An internal standard (10 µl of 10 µg/ml 7-hexyl nonadecane) was added to the dry sediment for quantification on a gas chromatograph and mass spectrometer (GC/MS). Lipids were extracted from the sediment samples with three rinses of 3 ml of 2:1 DCM:Methanol. Two ml of methanol, 2 ml of hexane, and 1 ml of water were added to each dried lipid extract, shaking vigorously between each. The hydrocarbon-bearing hexane layer was transferred from the top of each sample onto its own hexane conditioned silica gel column with three rinses of 2 ml of hexane, shaking vigorously between each rinse. Further purification of the hydrocarbon fraction was performed according to methods described by Belt and others [2007]. An Agilent 7890A gas chromatograph (GC) and 5975C mass spectrometer (MS) were used to perform GC/MS analysis of the final purified extract. The GC oven temperature was programmed to start at 40^{o}C, increase 10^{o}C/min until 300^{o}C and held at that final temperature for 10 min. IP_{25} in samples was quantified using a ratio of the abundance of the 350 ion from IP_{25} and the 266 ion from the internal standard (7-hexyl nonadecane) [*Belt et al.*, 2007; *Massé et al.*, 2008; *Vare et al.*, 2009].

5.5 Results and Discussion

5.5.1 Environmental and Sedimentological Data

The 59 stations in this study are located along spring (MAMJ) environmental gradients of SST (-2° to 2° C), sea surface salinity (SSS) (30 to 33 PSS), nitrate (3 to 18 µmol/l), phosphate (0 to 2 µmol/l), and sea ice concentration (6% to 93%) (Figure 5.1). Based on published averages of sedimentation rates (0.6 to 0.9 cm per year) [*Grebmeier*, 1993; *Pirtle-Levy et al.*, 2009] and bioturbation depths (10 cm) [*Grebmeier*, 1993], the top 1 cm of sediment integrates approximately 10 years of deposition. Therefore, all satellite- and model-derived variables are

averaged across the 10 year period immediately preceding sampling (1998-2007). We focus on spring environmental variables since March, April, May, and June are the months that presumed IP_{25}-producing diatoms are blooming in the study area [*Alexander and Chapman*, 1981].

We measured IP_{25}, TOC, TN and grain-size (GS) in each surface sample [see *Sharko*, 2010]. IP_{25} is present in all surface samples and its concentration is reported as normalized to TOC concentration (µg/gTOC). Spatially, IP_{25} concentration shows a striking increase as spring sea ice concentration increases (Figure 5.2) with IP_{25} values an order of magnitude higher in the Chukchi Sea (400-2000 µg/gTOC) than in the Bering Sea (40-300 µg/gTOC). These values, in turn, are one to two orders of magnitude higher than in the North Atlantic [*Müller et al.*, 2011], also a seasonally ice covered region.

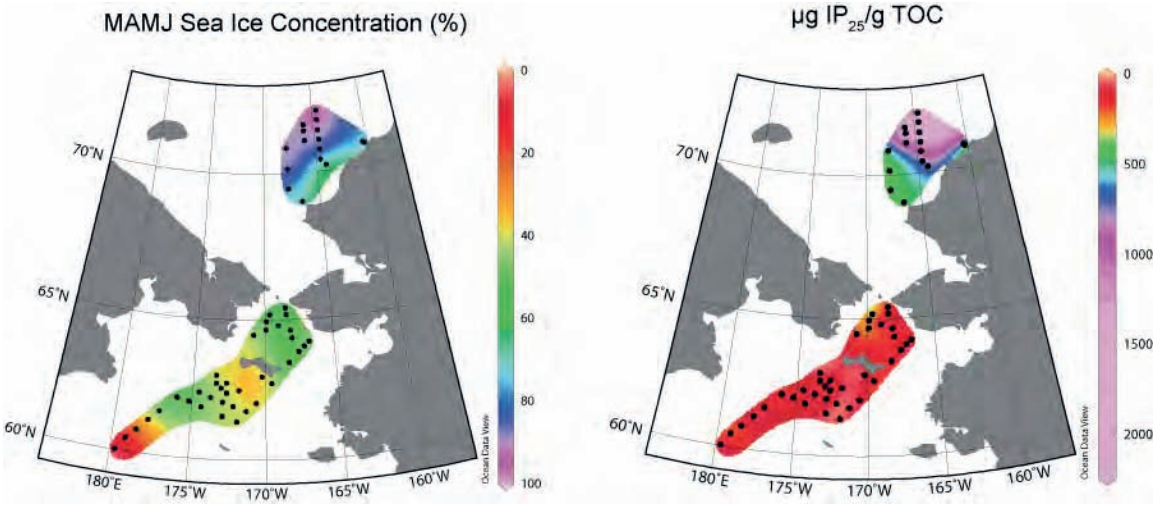

Figure 5.2. Spring sea ice concentration (expressed as % ice) compared to IP25 concentration across the study area. Maps are contoured using Ocean Data View 4's DIVA gridding algorithm (Schlitzer, 2011). Note that IP25 is contoured non-linearly as the concentrations increase exponentially. Increases in each variable are denoted by cooler colors. Black circles depict sample locations.

We also measured TOC and TN in order to confirm the marine origin of the organic carbon at each site. TOC ranges from 0.19 to 2.24 weight percent (wt %), with a mean value of 0.96 wt % TOC. Relatively high values of organic carbon are found in the highly productive cold pool, south of Saint Lawrence Island [*Grebmeier et al.*, 2006a] and in the Green Belt [*Springer et al.*, 1996] at the shelf-slope break [*Sharko,* 2010]. C/N values range between 4.0 and 11.81 with a mean value of 8.1, confirming a marine carbon source for most sites [*Meyers*, 1994]. The highest C/N ratio is observed in the Chukchi Sea [*Sharko,* 2010], relatively close to shore (12 km), indicating a mixed marine and terrigenous source [*Meyers*, 1994] for this site.

We then measured the median grain size of all samples in order to detect sea-ice rafted debris signatures [*Sakamoto et al.*, 2005]. The median grain size of samples ranged from silt (0.008 mm) to fine sand (0.3 mm). Similar to previous studies from the Bering Sea shelf [*Grebmeier*, 1993], grain size distribution closely follows TOC distributions with the smallest grain size being associated with the highest TOC sediment content.

5.5.2 Statistical Treatment of the Data

In order to determine the relationships between measured and environmental variables, we carried out a principal component analysis (PCA) on all 14 geochemical (IP_{25}, wt % TOC, wt % TN, C/N), sedimentary (median grain size), and MAMJ and annually averaged environmental variables (SST, SSS, NO_3, PO_4) (Figure 5.3). The first two principal components explain 80% of the variance, and the first three explain 88% of the variance. The first principal component shows that spring sea ice concentration is highly positively related to IP_{25} concentration, spring SSS and SST, and both spring and annual PO_4 concentrations. However, spring sea ice concentration is orthogonal to, and therefore not related to, the other

geochemical variables (C/N, TOC, TN) or grain size; these are largely explained by the second principal component.

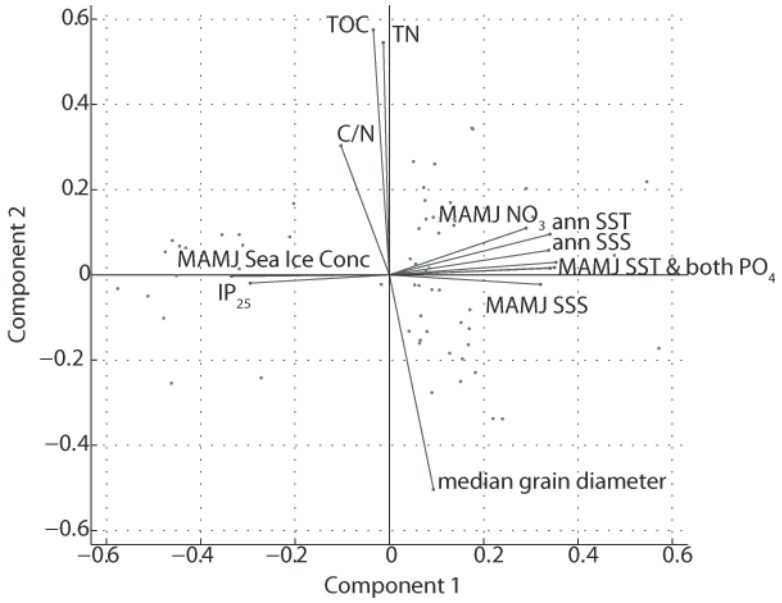

Figure 5.3. Principal component analysis of 13 environmental, sedimentological, and geochemical variables measured in the Bering and Chukchi seas.

We used correlation to identify variables with predictive power in relation to sea ice concentration (Table 5.1 and Figure 5.4) and used step-wise multiple linear regression to develop a predictive model of spring sea ice concentration. Spring sea ice concentration is significantly correlated with all environmental variables but shows a slightly higher correlation with most spring environmental conditions, in particular. Spring sea ice concentration shows the most significant correlation with spring SST (Figure 5.5a). The only geochemical variable that is significantly correlated with sea ice concentration is IP_{25} (Figure 5.5b; Table 5.1).

Step-wise regression tested linear combinations of all 13 independent variables until a combination with the highest regression coefficient and smallest residual was found. Although no constraint on the number of variables was added to the model, this regression contains only two independent variables: spring SST and IP_{25}:

$$[\text{MAMJ SI}] = 0.00647(IP_{25}) - 19.41(\text{SST}) + 52.45$$

This regression is highly significant (RMSE=4.77; r^2 =0.95; $p<0.01$) (Figure 5.6).

We propose that spring sea ice concentration can be predicted in the Bering and Chukchi seas using a combination of IP_{25} concentration and estimates of SST. Determination of past SST could be included in paleo-sea ice studies using methods such as the alkenone-based $U^{K'}_{37}$ temperature index [*Eglinton and Eglinton*, 2008], TEX_{86} temperature estimates derived from marine archaea [*Eglinton and Eglinton*, 2008], or Mg/Ca estimates of temperature derived from foraminifera tests [*Sagawa and Ikehara*, 2008].

Table 5.1: Correlation coefficients and resulting p-values between MAMJ sea ice concentration and possible predictive variables. Significant ($p<0.01$) correlations are in boldface, red type

	Correlation coefficient	p-value (2 tailed)
µg IP_{25}/g TOC	0.82	**0.0000**
wt % TOC	0.11	0.3982
wt % TN	0.07	0.6171
C/N ratio	0.18	0.1715
median grain diameter	-0.19	0.1390
NCEP MAMJ SST	-0.97	**0.0000**
NCEP Annual SST	-0.95	**0.0000**
WOA MAMJ SSS	-0.68	**0.0000**
WOA Annual SSS	-0.78	**0.0000**
WOA MAMJ NO_3	-0.63	**0.0000**
WOA Annual NO_3	-0.58	**0.0000**
WOA MAMJ PO_4	-0.87	**0.0000**
WOA Annual PO_4	-0.83	**0.0000**

5.5.3 Applicability of the proxy to other regions

It is difficult to compare IP_{25} concentration between different regions because it has been reported in at least four different ways: as relative abundance [*Massé et al.*, 2008], as a flux of IP_{25} (µg/cm^2/kyr) [*Müller et al.*, 2009], in µg of IP_{25} per gram of sediment [*Belt et al.*, 2010;

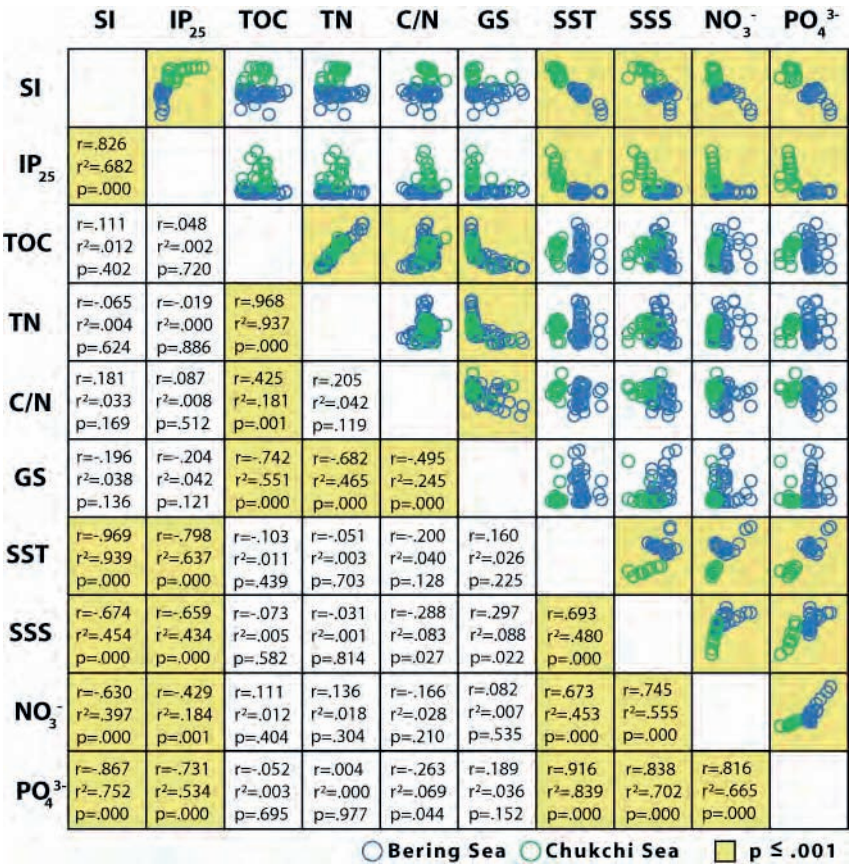

Figure 5.4. Correlation matrix of all spring (MAMJ) measured variables. Each square represents an x, y plot of the column and row variables that correspond with it. Statistics, including correlation coefficients and p-values can be found in the corresponding mirror image matrix. SI=sea ice concentration, GS=median grain size, SSS=sea surface salinty.

Vare et al., 2009], and normalized to total organic carbon [*Müller et al.*, 2011]. Values of IP_{25} per gram of sediment reported here are in line with those reported from the Canadian Arctic Archipelago [*Belt et al.*, 2010; *Vare et al.*, 2009]; whereas, concentrations normalized by TOC are up to two magnitudes higher than in the North Atlantic [*Müller et al.*, 2011] (Figure 5.7). Although the positive relationship between IP_{25} and sea ice concentration is also seen in the North Atlantic, the discrepancy in magnitude of IP_{25} concentration may be explained by differences in the abundances of phytoplankton contributors to the organic carbon pool [*Jin et al.*, 2006; *Lalande et al.*, 2007; *Takahashi et al.*, 2002], or perhaps the significant difference in

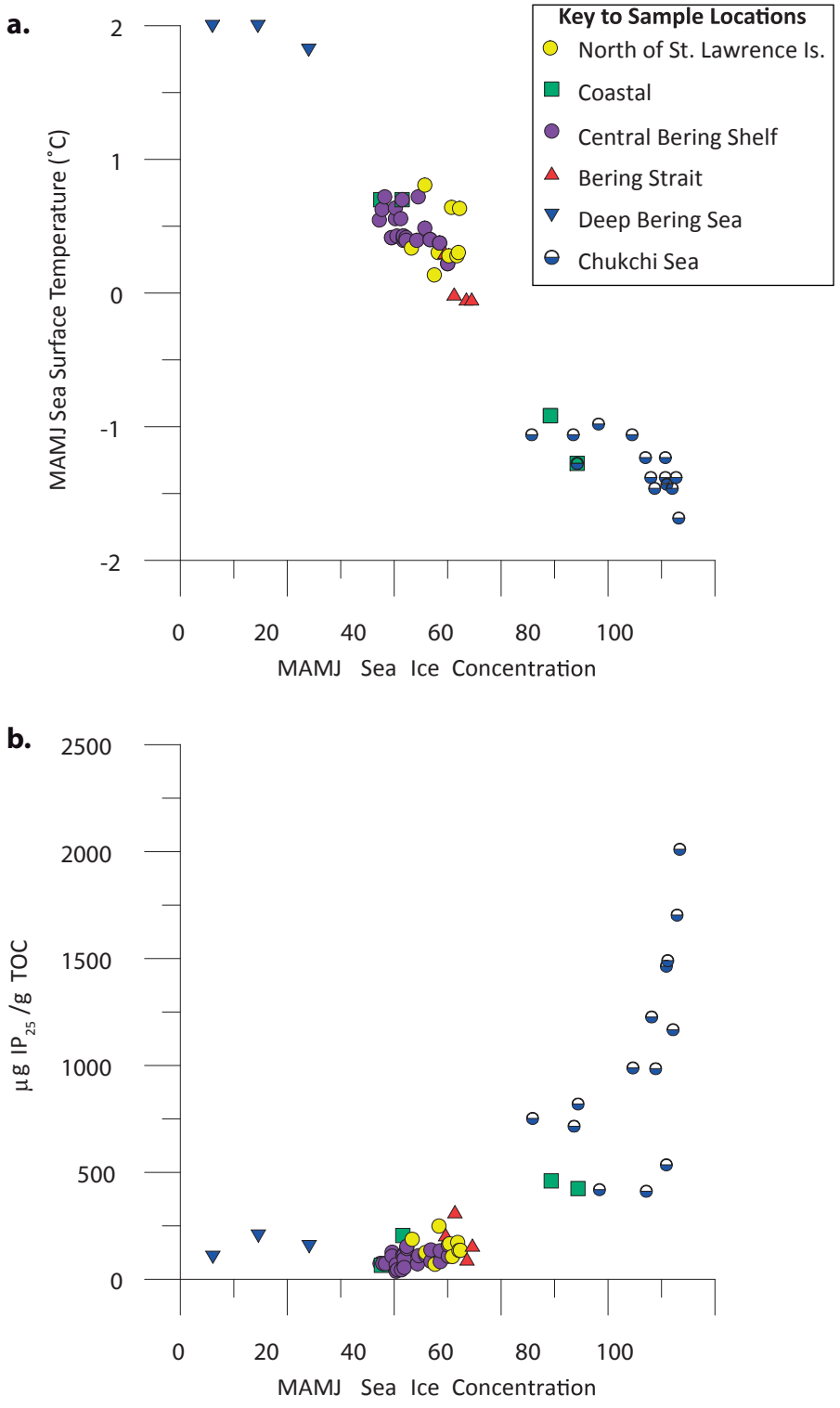

Figure 5.5. Plots showing the relationship between spring sea ice concentration (MAMJ) and a) spring sea surface temperature and b) IP25 concentration normalized to total organic carbon. Each site is coded by its generalized location (see key).

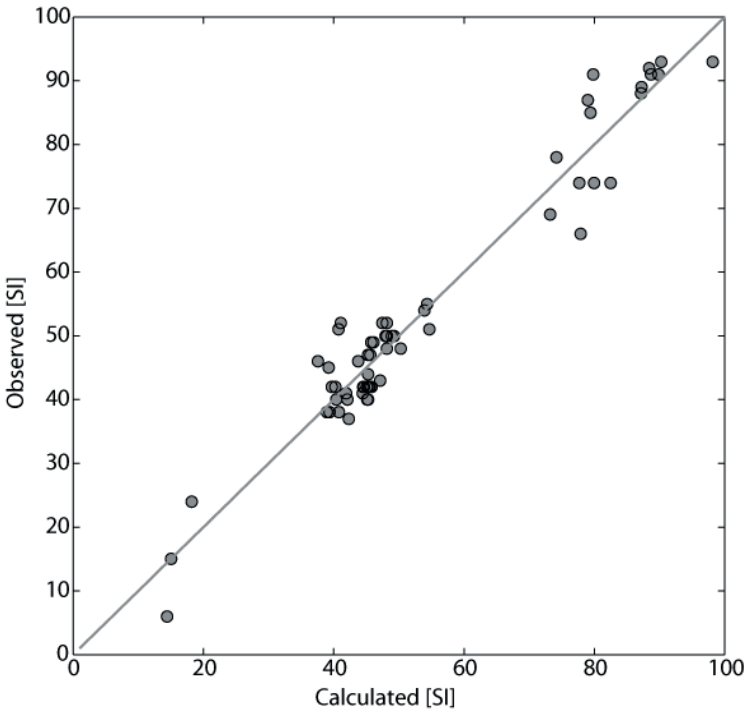

Figure 5.6. Plot of observed versus calculated sea ice concentration for the Bering and Chukchi seas stations in this study. Sea ice was calculated using the regression: [MAMJ SI] = 0.00647 (IP25) - 19.41(SST) + 52.45. The thin black line is the function f(x) = x.

water depth (>1000 m in the N. Atlantic vs. < 100 m on the Bering and Chukchi shelves). Although water depth varies across our study area, it is not possible to determine if water depth plays a role in IP_{25} preservation because all sites deeper than 1000 m also have very low concentrations of sea ice. It is important to identify areas of diverse water depth and sea ice concentrations to determine if there is a relationship between IP_{25} and water depth.

Ideally, measurements of IP_{25} concentration normalized to diatom-derived organic carbon could be compared between regions, but as yet quantitative measures of this component of OM are lacking. We caution that this discrepancy may bring up issues when using IP_{25} in different regions or back in time as the dominant contributors to productivity can change over time and space. Further work on this issue is clearly needed, and we suggest that IP_{25} studies be carried out as part of a multi-proxy study alongside other proxies for diatom or coccolithophorid productivity (e.g. the so-called PIP_{25} proxy which combines an open water phytoplankton biomarker with IP_{25} [*Müller et al.*, 2011]) in order to ascertain the contributors to the organic carbon pool. Although this calibration appears robust for the Bering and Chukchi

seas, further testing is necessary to determine its applicability for times and areas where coccolithophorids are the dominant phytoplankton.

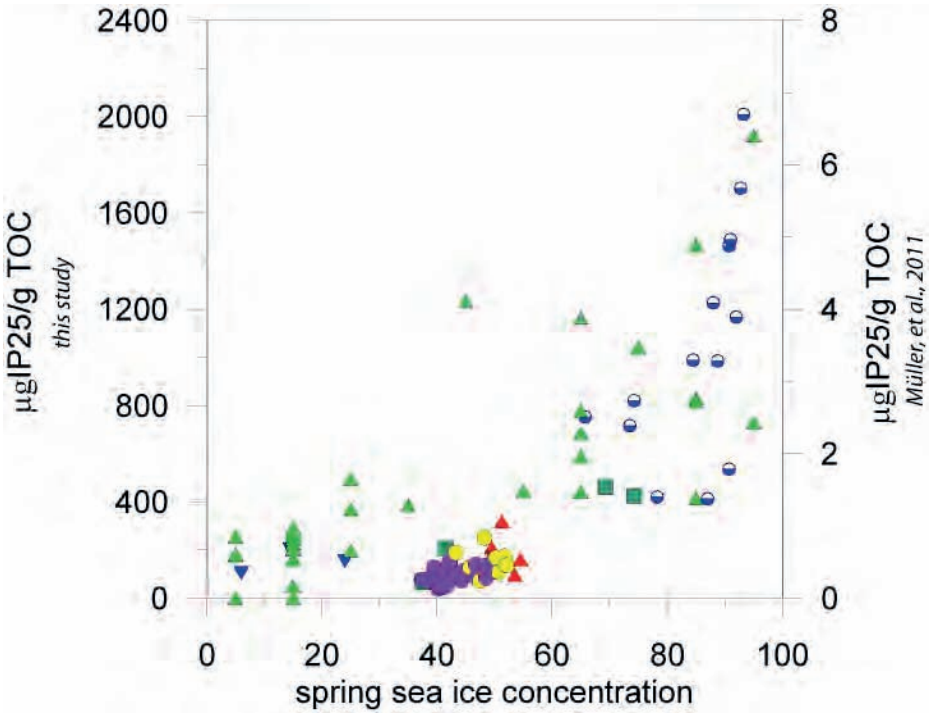

Figure 5.7. Spring sea ice concentration versus IP_{25} concentration normalized to total organic carbon. IP_{25} data is from this study and Müller [2011]. Blue triangles denote samples from the deep Bering Sea. Yellow circles are samples from north of St. Lawrence Island in the Bering Sea. Purple circles denote samples from coastal areas of the Bering and Chukchi seas. All of these samples are plotted on the left hand y-axis. Green triangles are samples from the North Atlantic [Müller et al., 2011] and plotted on the right hand y-axis.

5.6 Conclusions

IP_{25} shows a significant increase in TOC normalized concentration as spring sea ice concentration increases. We propose that this is driven by the length of time that the sub-ice bloom lasts. At the shelf-slope break in the Bering Sea where IP_{25} concentrations are low, the sub ice bloom lasts only a few weeks, whereas in the Chukchi Sea, where IP_{25} concentrations are an order of magnitude higher, the sub ice bloom may last a month or more before it is

succeeded by the marginal ice zone bloom. Further calibration is necessary to determine why the magnitude of IP_{25} concentration is strikingly different in various regions. We conclude that IP_{25} concentration can be used as a proxy for quantification of spring sea ice concentration if IP_{25} values are used in conjunction with estimates of SST. IP_{25} has the potential to become a powerful tool when used in conjunction with other proxies such as diatom assemblages, alkenones, or PIP_{25} that also indicate SST or diatom productivity changes. This calibration for the Bering and Chukchi seas represents a significant step forward in quantifying past sea ice concentrations.

CHAPTER 6

FUTURE DIRECTIONS

6.1 Introduction

As this dissertation evolved, several additional lines of work presented themselves. This chapter outlines some of the ideas that build on the work presented in the previous chapters. The first four sections are organized according to the chapters in the dissertation and outline plans for work that, in some cases, will need to be completed before publication. Other ideas in these sections are proposals for work that may be completed farther in the future. The final three sections outline projects that are separate from, but build upon the work presented in this dissertation. The sections detailing the quantitative diatom-based sea ice proxy and the Pliocene lamination study are more detailed than the other sections because significant work has already been completed for these two projects, and I plan to have manuscripts submitted for them within the next six months.

6.2 Taxonomy

The maps that are currently in Chapter 2 rely on diatom counts both from my own work and from Sancetta's [1981] study. These maps will be updated and expanded to the Chukchi Sea as I recount Sancetta's slides and complete counting slides for the sea ice proxy. Additionally, this chapter currently only has light microscope images and SEM images for the most common species found in the Bering Sea. Before publication, I will image all species (to the extent that this is possible) using both the light microscope and the SEM. This work would further be improved by adding a web component, after consideration of copyright issues, so that future Bering Sea diatom workers can more easily identify common species.

6.3 Modern Sedimentation on the Bering Sea shelf

Quantitative diatom slides have been made, but not analyzed, for down-core samples from sites HLY 0602 NEC5 (Area 2) and HLY 0601 SWC3a (Area 4) (see Figure 3.1 for Area locations). Before publication, I will analyze these slides to look for changes in the diatom assemblages. NEC5 shows the most promise for a site that is recording ecological change over a very short period of time (40 years), because it is located in the only area where differences between 1969 core top assemblages and 2006/2007 core top assemblages were significant (as discussed in Chapter 3). In addition, there are three more 1969 core top samples that have not been analyzed. Counting the diatoms in these samples would add two additional areas to this study. Area 6 north of St. Lawrence Island may not be appropriate to add, though, because it appears that there is a range of sea ice concentrations at the site and grain size profiles of these samples indicate that the sediments may be reworked (Figure 6.1).

6.4 Marine Isotope Stage 11

6.4.1 Additional Analyses

Before publication, Chapter 4 will be expanded to include several other methods for determining the different signatures of productivity and glacial ice versus sea ice. I will measure grain size in Exp 323 Site U1345A using the Laser Diffraction Particle Analyzer to look for varying contributions of coarse particles to the sediments and for changes in sediment sorting. Additionally, Alan Mix at Oregon State University has done CT scans of the whole rounds of Core U1345E. Once analyzed, these images will reveal the placement of large clasts throughout the interval as well as the three-dimensional structure of the laminations. Elena Colmenero Hidalgo at the Universidad de León, in Spain, has begun to count calcareous nannofossils in the same samples that diatom assemblages were counted in (see Chapter 4). This will provide more

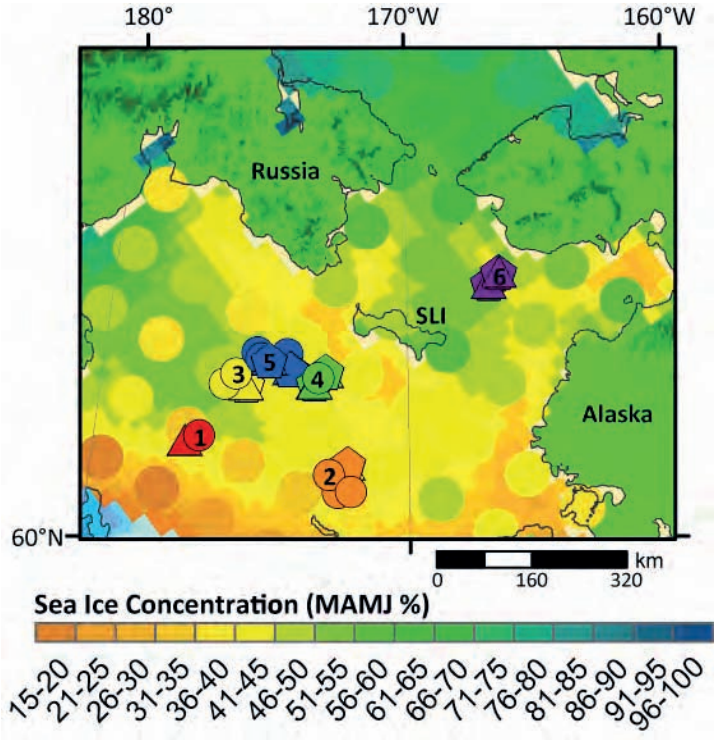

Figure 6.1. Map of the northern Bering Sea showing two additional areas that have core tops collected in 1969 and in 2006-2007. Sea ice concentration contours show MAMJ sea ice averaged over 1998-2007 [*Cavalieri et al.,* 1996] and large dots show MAMJ sea ice concentration averaged over 1960-1969 [*Chapman and Walsh,* 1991]. Circles are samples collected in 1969, pentagons are samples collected in 2006 and triangles are sample collected in 2007. Samples are color coded by area (1: Red; 2: Orange; 3: Yellow; 4: Green; 5: Blue; and 6: Purple). St. Lawrence Island is abbreviated as SLI.

information about primary productivity, both when environmental conditions triggered high productivity and the interplay between calcareous nannofossil and diatom productivity. Taoufik Radi at Université du Québec à Montréal (GEOTOP) plans to count dinoflagellate cysts in these same samples as well. Dinoflagellate cyst data would be especially informative, as transfer functions relating them to sea ice duration are quite robust. His reconstruction could be directly compared to the qualitative diatom-based sea ice reconstruction presented in Chapter 4.

I have also requested additional samples from the spliced core sequence of Exp 323 Site U1345 in order to fill in the gaps left by coring disturbance between cores, and the gap in

sampling near 374 ka. These few extra samples will complete the record and also add more information about diatom productivity during laminated intervals.

In the longer term, this site will be compared to other Exp 323 sites in the Bering Sea including U1339 on the Umnak Plateau, U1340 on Bowers Ridge, and U1343 also on the shelf-slope break (Figure 6.2). Diatom assemblages and grain size will be quantified for each of these sites and the diatom-based sea ice proxy that is in development will be applied to these four sites. Additionally, Jim Kocis, PhD Candidate at UMass Amherst, plans to submit a sample request to IODP in order to measure IP_{25}, and determine alkenone- and glycerol dialkyl glycerol tetraether-based temperatures ($U^{K'}_{37}$ and TEX86) in at least Site U1345, if not the other three as well. One of these cores may well become the subject of a sea ice proxy intercomparison project carried out by the Past Global Changes (PAGES) Sea Ice Proxies Working Group. This project aims to look at the differences between proxies based on diatom assemblages, dinoflagellate cyst assemblages, and IP_{25}.

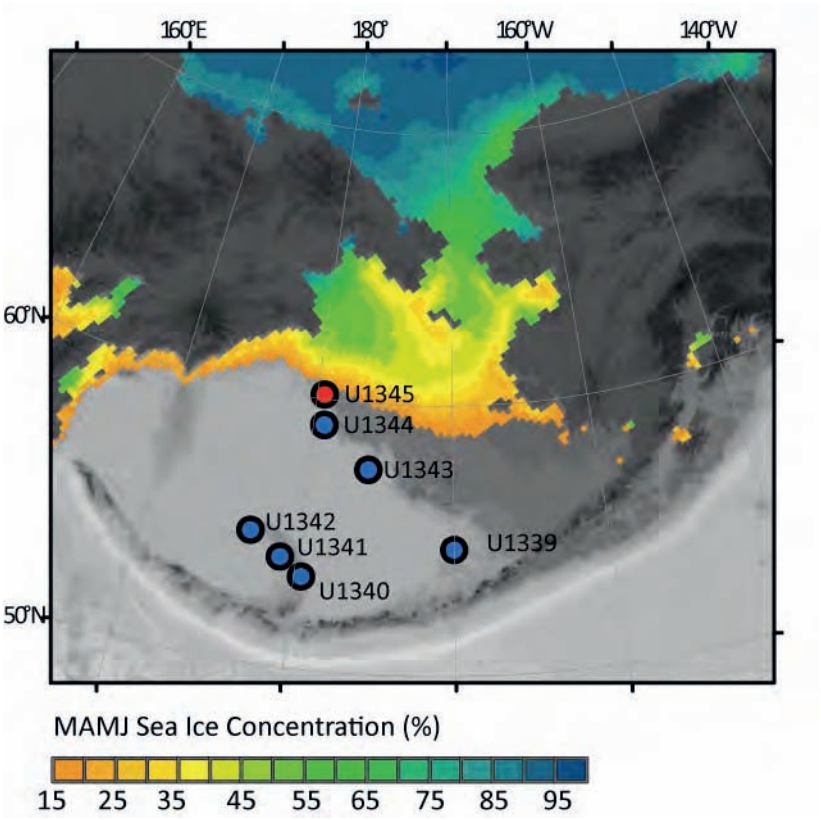

Figure 6.2. Map of the Bering and Chukchi seas showing the positions of all seven sites occupied during IODP's Exp. 323. The red dot depicts the site that is the focus of Chapter 4. Contours depict sea ice concentration averaged for March, April, May, and June over the years 1998-2007.

6.4.2 Additional Interpretation

There are several avenues of work that could expand upon this work in the future. One of the many open questions from IODP Exp 323 is what is controlling the magnetic susceptibility of the sediments. The shipboard interpretation of the magnetic susceptibility suggested that magnetic susceptibility was high during glacial intervals due the higher diatom content, with correspondingly low magnetic susceptibility during the interglacial periods [Takahashi et al., 2011]. However, after correlating the oxygen isotope values in benthic foraminifera to the global marine oxygen isotope stack, it was discovered that the highest magnetic susceptibility occurred during the interglacial periods [Cook, M.S., pers. comm.]. Additionally, there does not appear to be any relationship between diatom content, or ice rafted debris, and magnetic susceptibility (Figure 6.3.). There is however, an interesting decrease in color reflectance (a*), which reflects

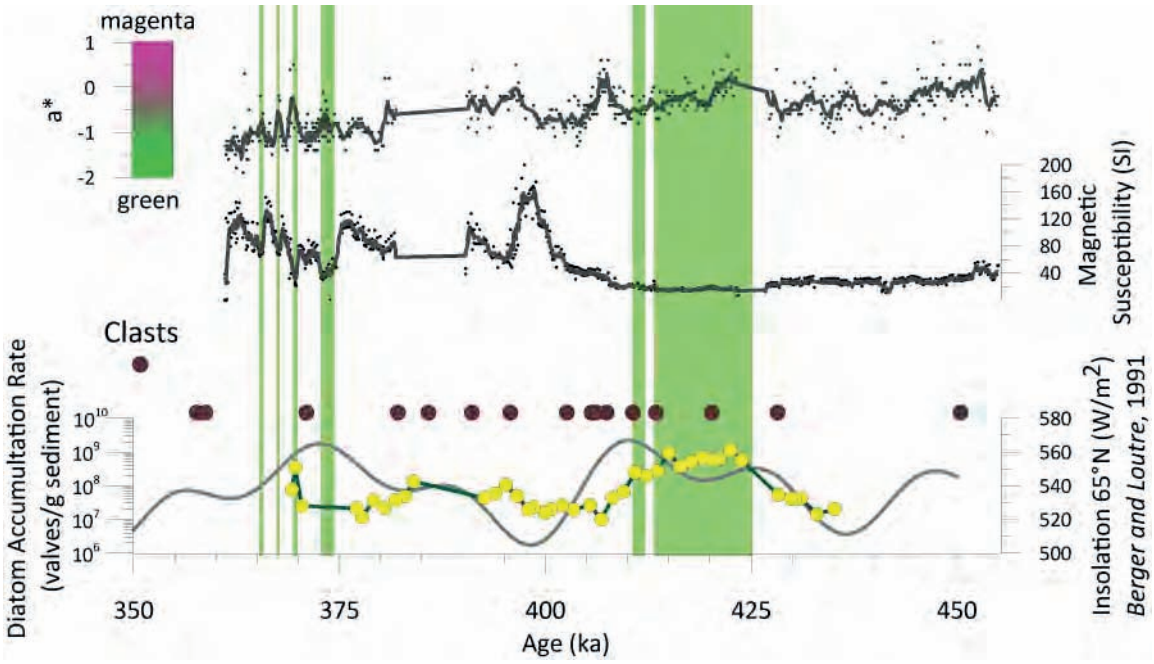

Figure 6.3. Plots showing color reflectance (a*), magnetic suceptibility, isolated clasts (IRD; brown dots), diatom accumulation rate (green line with yellow dots), and insolation (grey line) at U1345A during MIS 11. The green bars indicate the location of laminated intervals.

sediments becoming greener in color over MIS 11. One possible explanation that might tie both of these measurements together is that the sediments are becoming more oxidized over the course of the super-interglacial. Although the large laminated interval also supports this idea, a focused study to test this hypothesis would be necessary to fully explore the mechanisms responsible for anoxia, magnetic susceptibility, and sediment color.

The work presented in Chapter 4 highlights the need for independent measures of humidity and productivity during MIS 11. Because of the high concentrations of neritic and freshwater diatoms during part of MIS 11, and also the input of clay, silt, and sand, it is likely that there is terrigenous organic matter as well. Measuring the hydrogen isotopic composition (δD) of leaf wax lipids, if present in the core, might be a way to see if humidity was changing in the region [Liu and Yang, 2008]. At the very least, it might be a way of determining how much organic matter was being transported to the site from the coast. In addition, diatom assemblages from shallower cores should also reflect the changes in humidity and the closing of Bering Strait. I might propose collecting cores in ~200 to ~250 m of water both north and south of Bering Strait to see if assemblage changes similar to those seen in U1345 occur. I might expect an increase in fresh water diatoms during the MIS 11 Beringian glaciation and a sudden decrease in fresh water diatoms when humidity and sea level decreased to the point where glaciers retreated and were too distant from the coast to calve into the ocean. Finally, a multi-proxy study looking at sediment geochemistry, specifically total organic carbon, nitrogen, biogenic silica, and the ratio of carbon to nitrogen (C/N), would allow us to look more closely at productivity changes during Termination V. Variations in $CaCO_3$ may provide independent confirmation of carbonate productivity. Alternatively, high carbonate preservation coupled with high values of δ13C may reveal periods of proximal North Pacific Intermediate Water formation similar to records of NADW formation in the Atlantic [e.g. *Poli et al.*, 2010].

6.5 IP_{25}

A manuscript based on this chapter was submitted and rejected by *Nature Geoscience* and *Geophysical Research Letters.* Based on the reviews received from these journals, we are working in collaboration with Guillaume Massé to run IP_{25} and alkenone measurements on the downcore samples from either HLY 0601 NEC5 or HLY 0601 SWC4a, sub-Haps cores collected as part of the work presented in Chapter 3. We will estimate sea ice concentration from these analyses and compare our estimates to satellite observations of sea ice concentration for the past 34 years. Additionally, because the IP_{25} calibration presented in Chapter 5 is based on a subset of the surface samples collected in 2006-2008, James Kocis at UMass Amherst is working to measure IP_{25}, alkenones, and TEX_{86} in surface samples not used in the calibration. This is an additional way to validate our sea ice calibration. Without such a validation, it seems unlikely that this manuscript will be published.

Another way to attempt to strengthen this proxy might be to compare IP_{25} concentrations with diatom assemblages in surface sediments. Because sea ice diatoms likely produce IP_{25} [*Belt et al.*, 2007], it may be that there is a connection between sediment concentrations of certain diatoms, such as the epontic species, and IP_{25}.

6.6 Diatom Based Sea Ice Proxy

A quantitative, diatom-based sea ice proxy is a critical tool for understanding how sea ice responds to a warming climate. This dissertation builds the groundwork for such a proxy, but does not formally describe the proxy. Significant work has been completed towards this proxy, however, and I plan to submit a manuscript about it to a special *Quaternary Science Reviews* issue about sea ice proxies in July 2012.

The database for this proxy (Figure 6.4) contains a combination of surface sediments (Haps core and van Veen grabs) collected during the HLY 0601, HLY 0702, and Shell 2008 cruises and smear slides made in the 1980s from gravity core tops collected in the late 1960s [*Sancetta*, 1981].

All samples collected in 2006-2008 were processed and analyzed for grain size using a Laser Diffraction Particle Analyzer according to the methods described in Chapter 3. Three distinct patterns in grain size distribution emerged from this dataset (Figure 6.5). Type I sediments consist of poorly sorted clay and silt-sized sediments, characteristic of pelagic sedimentation. Type II sediments consist of well sorted sand sized sediments, and Type III sediments contain sand and gravel. Types II and III are typical for areas underlying strong currents and sediments exposed to transport and sorting. In most cases, samples with coarsely skewed grain size will be discarded as these sites are likely areas influenced by strong, erosional bottom currents [*Grebmeier*, 1993]. However, for some ranges of sea ice (i.e. 50-75% sea ice), there are few areas that lie over fine-grained, Type I sediments.

The work in Chapter 3 describing bioturbation, sedimentation and cesium dates on short, Haps cores confirms that the top 1 cm of shelf sediments likely contains less than 30 years of sedimentation. Furthermore, the top 1 cm of sediments are skewed towards very recent deposition, likely the last decade. In light of this, core tops are included in the sea ice database only if they can pass two tests of modernity [c.f.*Pichon et al.*, 1992]:

1) No fossil species, which would indicate reworking, are encountered during diatom analysis.
2) The sediment-water interface remained undisturbed during sediment recovery.

Criteria number two is difficult to confirm for older sediments, collected by others in the late 1960's, so we will only use older sediments in areas where no newer samples are available.

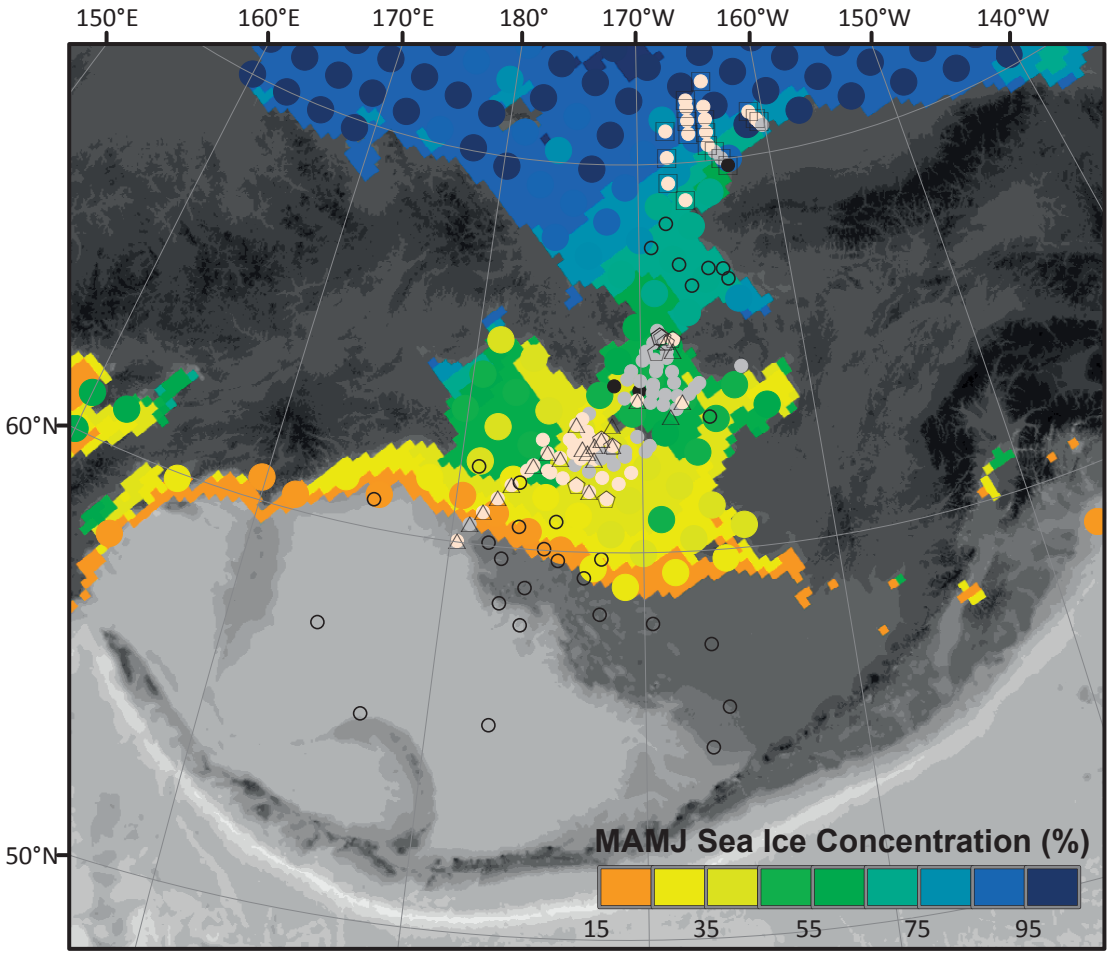

Figure 6.4. Map showing the location of the stations to be used as part of the diatom-based sea ice proxy. Open circles are samples collected in 1969, open pentagons are samples collected in 2006, open triangles are samples collected in 2007, and open squares are samples collected in 2008. Greyscale symbols depict average grain size of the recent samples. Silt is off-white, well-sorted sand is grey, and gravel is black. Sea ice concentration contours show MAMJ sea ice averaged over 1998-2007 [*Cavalieri et al.,* 1996] and large dots show MAMJ sea ice concentration averaged over 1960-1969 [*Chapman and Walsh,* 1991].

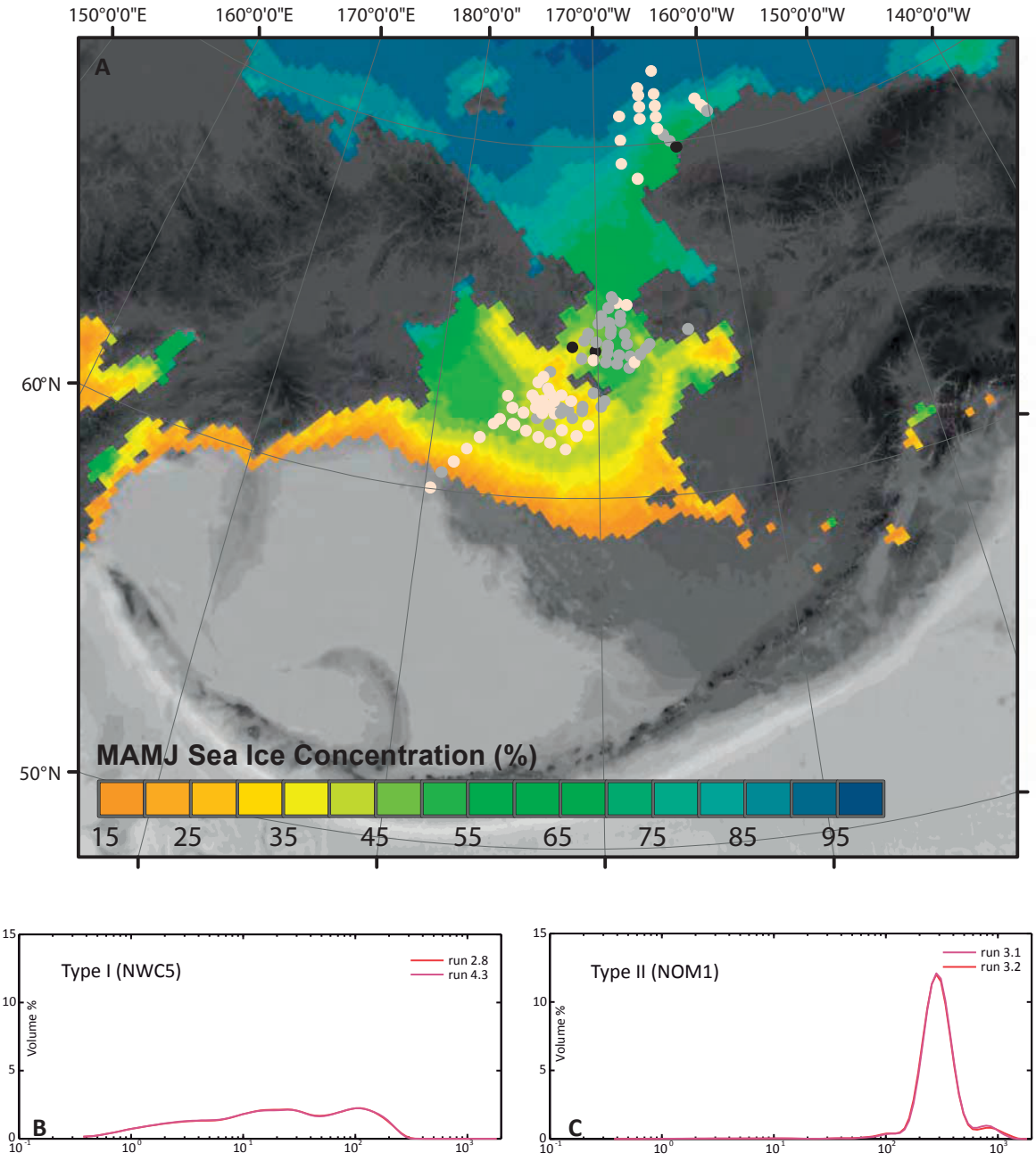

Figure 6.5. A. Sediment grain size plotted as greyscale symbols. Off-white symbols represent Type I sediments (poorly sorted clay to silt), grey and black symbols represent Type II sediments with sand-sized and gravel-sized modes respectively. Colored contours represent MAMJ sea ice concentration for the interval 1998-2007 [*Cavalieri et al.*, 1996]. B. Representative grain size distribution of Type I sediments. C. Representative grain size distribution of Type II sediments.

Modernity is further confirmed by using only samples with at least one independent verification of modern deposition made in the vicinity of the sample. For example, nearby sediment might contain:

- high sediment chlorophyll [e.g. *Pirtle-Levy et al.*, 2009],
- detectable ^{7}Be (half life = 53 days), generally deposited by recent precipitation [*Grebmeier and Cooper*, 1995],
- high total organic carbon [e.g. *Grebmeier and Cooper*, 1995],
- or long chain (>3 individuals) colonies of diatoms in the sample.

We compare this sediment dataset to two different time-averaged sea ice concentration datasets: 10 years prior to sample collection and 30 years prior to sample collection. For the older sea ice dataset, monthly sea ice concentrations were interpolated from Chapman and Walsh [1991]. This dataset compiles ship observations, interpolations from government ice charts, and calculated ice concentrations based on climatology [*Chapman and Walsh*, 1991]. Newer monthly sea ice concentrations were derived using brightness temperatures from the Special Sensor Microwave/Imager (SSM/I) passive microwave satellite data [*Cavalieri et al.*, 1996]. SSM/I data have been available since 1978 as either daily or monthly ice concentrations for 25 km^2 pixels. All sea ice concentration data was averaged over the sea ice bloom season (March, April, May, and June).

Finally, the database was culled randomly so that there was an equal number of samples (5) in each 5% sea ice concentration bin and the dataset spans a gradient of sea ice concentration (0-95%). Several bins of ice concentration remain that have fewer than five samples in them. A request for additional samples from these locations is pending.

Recently collected samples were analyzed for diatom assemblages following the protocols laid out in Chapters 3 and 4. Data from the 1969 archived smear slides show that

several diatom species were grouped together during analysis in the 1980s [e.g. *Sancetta*, 1982] that have distinct ecological preferences we recognize now for certain types of sea ice. For example, in earlier work, all *Fragilariopsis* species were grouped together. However, there are five *Fragilariopsis* species in the Bering Sea and some have a stronger affinity for the marginal ice zone than others [*Lundholm and Hasle*, 2010]. Additionally, many pennate benthic diatoms were grouped together in the past, but there are many pennate benthic diatoms that attach to sea ice and bloom with the epontic bloom, and others that live exclusively in the shallow, neritic zone. Because of this earlier grouping of species, smear slides are currently being recounted.

The final step in creating this proxy is to use machine learning techniques to create transfer functions that relate diatom assemblages to average sea ice concentration. Validation of this proxy will be done using additional Haps core tops from across the Bering and Chukchi seas that were not included in the transfer functions.

6.7 Diatom Morphology and Sea Ice Concentration

Recent findings in the Southern Ocean suggest that certain diatom species (i.e. *Thalassiosira antarctica* Comber) adjust the number of areolae per micron based on upon the type of ice they live in [*Taylor and McMinn*, 2001]. I am inspired by this to look for a link between the number of areolae per micron on centric diatoms such as *Thalassiosira trifulta* Fryxell and *Thalassiosira antarctica* var. *borealis* Fryxell, Doucette, and Hubbard as a function of mean annual duration of sea ice today in the Bering and Chukchi seas. Likewise, *Fragilariopsis oceanica* occurs in both plankton and ice and has been observed to be longer in length when living in the ice. In addition, there are two different morphologic clades of *F. oceanica,* [*Lundholm and Hasle*, 2010]. It's possible that one clade contains individuals which are longer than the other, and this is the morphotype that is associated with sea ice. I plan to measure the

length and width of several *Fragilariopsis* species in order to look for a connection between length and sea ice concentration. *Paralia sulcata* is a neritic species that forms long colonies [*Crawford*, 1979] that are often preserved in sediments even hundreds of thousands of years old. The valves are heterovalvular, meaning that the outer most valves on the colony have much less developed ridges and grooves on the valve face than their inner counterparts. So, it is easy to determine the average colony length by counting the relative number of outer valves vs. inner valves. In Antarctica, *Eucampia* varies the length of its colony based on SST [*Fryxell*, 1991]. Perhaps *Paralia sulcata* responds to changing temperature or sea ice in a similar way. This is another species whose morphology I will explore in the future.

6.8 Laminated Sediments in the Bering Sea

The sediments recovered during IODP Expedition 323 can provide centennial- to millennial-scale resolution of variability in sea-ice extent and duration across the region, and laminated intervals during both glacial and interglacial periods may provide the opportunity to reconstruct seasonal- to decadal-scale variability as well.

6.8.1 Pliocene Laminations from Bowers Ridge

Laminated sediments occur near the Pliocene-Pleistocene boundary at Site U1340 on Bowers Ridge. The laminations appeared as centimeter scale alternations of almost mono-specific diatom mats (*Lioloma pacificum*) with diatom-rich silt. X-radiographs and epoxy embedded thin sections revealed sub-millimeter scale laminations throughout the section. Work is in progress on a 60 cm long interval, dated to either 3.0 Ma or 2.5 Ma (due to uncertainties with the preliminary age model) from these Late Pliocene laminations. The primary methods used to characterize the laminations include scanning electron microscope (SEM) analyses, backscatter electron images (BSEI) and light microscope analysis of diatom assemblages.

Exp 323 Site U1340A was subsampled between 446.385 and 446.895 mbsf using a sediment slab cutter. The u-channel sections were freeze-dried and then epoxy embedded using a fluid displacement technique [e.g. *Ellis*, 2006; *Pike and Kemp*, 1996]. A total of nine sediment slabs were turned into polished thin sections and scanned at 2400 dpi under both plane polarized and cross polarized light (Figure 6.6) to aid in lamination and sedimentary fabric characterization. Scanned images will be analyzed using the software ImageJ to count laminae pairs or triplets and to determine the thickness of individual lamina. A mosaic of low magnification (60x) BSEI was used as a map of the core.

Small, 0.5 cm x 0.5 cm x 4 cm long, slabs were cut from two laminated sections of the U1340A core in order to image the laminations in finer detail. General species composition, degree of fragmentation, and clay content were recorded continuously along the slabs. In addition, two thick white layers within this core were sliced along the top contact of the layer. SEM analysis of these layers reveals the mono-specific mats of *Lioloma* sp. mentioned above. This genus is generally found in subtropical to temperate latitudes, especially the Mediterranean Sea [*Hasle*, 2001], and may be reflective of extreme Pliocene warmth here in the Bering Sea.

Thin sections and SEM analysis reveal sub-millimeter-scale laminations throughout the section. Laminations can be broadly categorized as one of four types (Figure 6.6):

1) *Lioloma* type lamina—dominated by mats of *Lioloma* sp. With rare *Neodenticulopsis seminae* (Pacific water tracer) and other species present.

2) *Coscinodiscus* (upwelling indicator) type lamina—dominated by *Coscinodiscus* sp. frustules stacked one on top of another with layers of other species above and below.

3) Mixed lamina—made up of higher diversity assemblages or very highly fragmented diatom pieces.

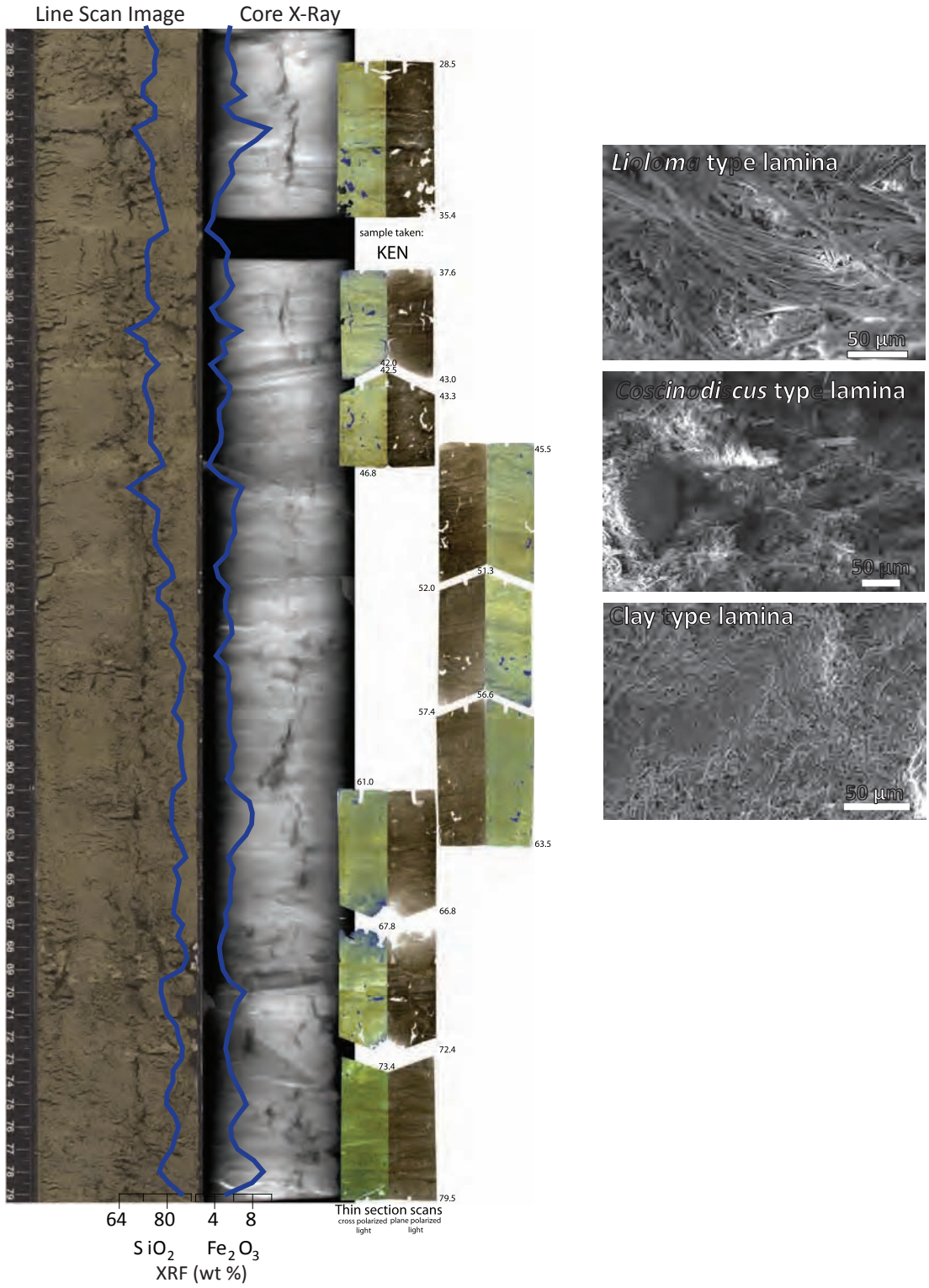

Figure 6.6. Preliminary investigations of a 60 cm long, Pliocene laminated interval collected in a sediment core from the Bowers Ridge (IODP Exp 323, Site U1340A, 52X-6H, 28.5-79.5 cm). We show the line scan image, core x-ray, and scans of thin sections. Low resolution SiO_2 and Fe_2O_3 from XRF scanning is overlaid on the core images. Representative scanning electron microscope images are shown for three of the characteristic laminae.

4) Clay type lamina—dominantly to entirely composed of clay minerals.

There are at least three very different mechanisms that may explain these laminations. They may be seasonally or decadally deposited. Repeating patterns of diatom assemblages and thick mats of *Lioloma* sp. support this scenario. Layer counting combined with high resolution age dating will be necessary to confirm this. Laminations may reflect changes in the direction of sea floor sediment transport. Instances of onlap and downlap, especially at the base of the section, support this scenario. Additionally, clay type lamina and laminations with high silt content may be due to increased sediment transport from the Aleutian Islands. Or, laminations may simply be related to soft sediment deformation. BSEI evidence for this includes folded and undulating layers of large centric diatoms, numerous examples of non-parallel laminations, and possible micro-burrow infilling by large centric diatoms.

Very little evidence of sea ice was found throughout the Plio-Pleistocene section. Sea ice diatoms are very rare (2-3 frustules were seen during detailed SEM analysis). However, the transport mechanism for the silt and clay remains unknown. Elemental data from XRF scanning is not yet fine enough resolution to reflect changes in individual laminations, however we expect that these three lamination types might have characteristic geochemical signatures or may even aid in clay mineral identification. Higher resolution XRF scanning, analysis of lamina thickness and periodicity, and detailed diatom assemblage counts are in progress.

6.8.2 Quaternary Laminations from the Shelf-Slope Break

During the IODP Exp 323, three types of Quaternary laminations were observed at Site U1345. A correlation was tentatively drawn between interglacials and biogenic-rich laminations and between glacial and siliciclastic-rich laminations. The first variety was proposed to be controlled by high productivity events, and the latter variety by changes in intermediate water

ventilation [*Takahashi et al.*, 2011]. I plan to collaborate with Mea Cook at Williams College to combine high resolution lamination investigations (similar to the procedures described above) with high resolution foraminiferal isotopic work and statistical methods such as wavelet analysis. The goals of this project are three-fold:

1) to determine the temporal frequency of laminated sediments,
2) to better understand the mechanisms controlling lamination deposition, whether it has to do with productivity, changes in ventilation, or a combination of the two, and
3) to characterize the sedimentological make-up of the laminations.

Preliminary work combining the age model in development by Cook and orbital parameters suggests that there may be a periodicity related to lamination development (Figure 6.7), although there is no single orbital configuration that is always present when laminations are deposited. It is plausible that during the glacial periods, laminations are deposited during Dansgaard-Oeschger events (Figure 6.x.), but again, this is not an absolute relationship. There are many D-O events that do not have an associated laminated interval.

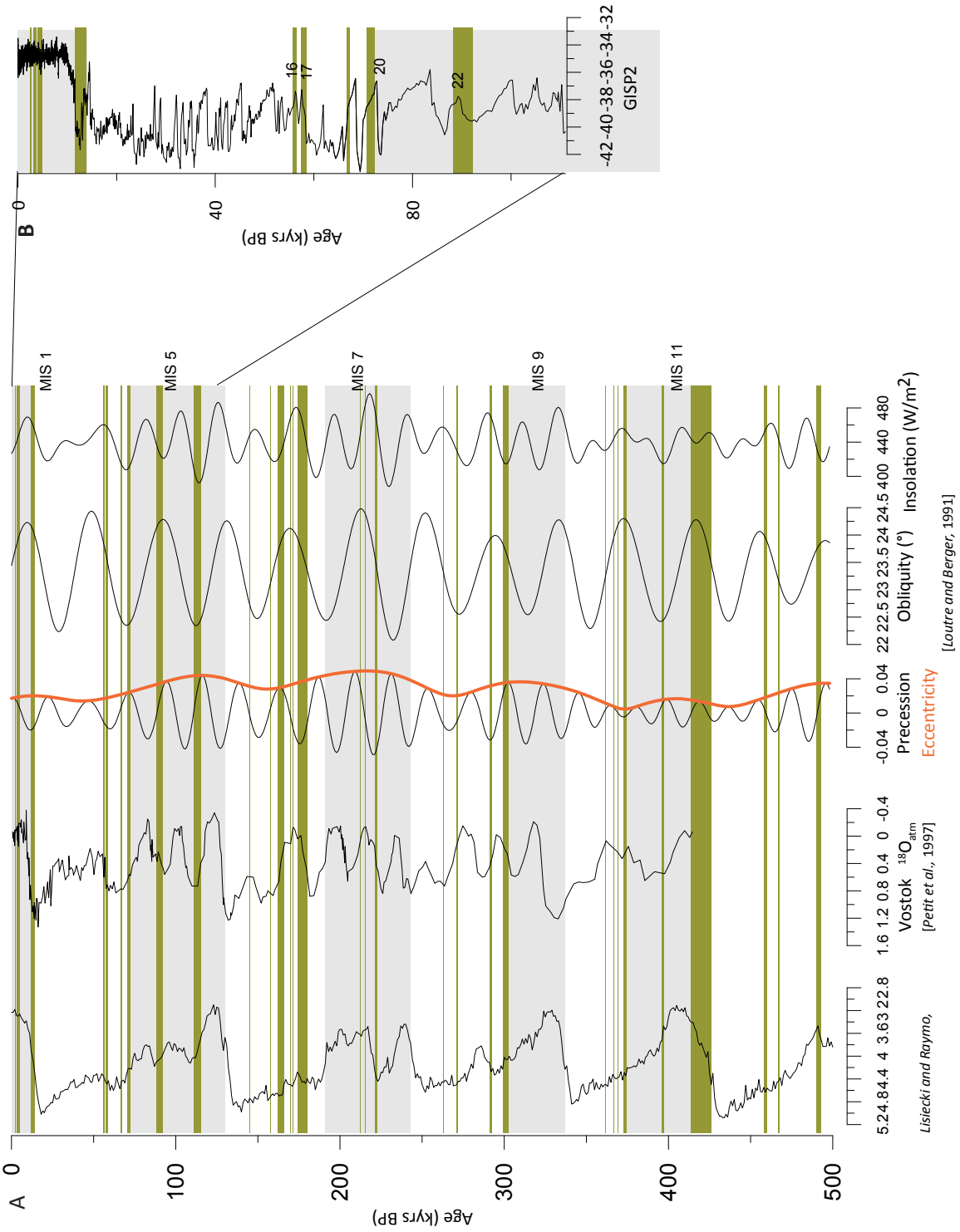

Figure 6.7. Laminated intervals in Exp 323, U1345 plotted under well-known climate records and orbital parameters. Note that in panel B, we zoon in to the last 100 ka. Grey bars represent interglaical periods. Select Dansgaard-Oeschgar events are numbered in panel B.

CHAPTER 7

CONCLUSIONS

This dissertation uses diatoms to investigate past changes in sea ice and related sea surface conditions in the Bering and Chukchi seas. One of the primary objectives was to document environmental change on various time scales. This was achieved by examining modern sedimentation, decadal-scale change in the very recent past, and centennial- to millennial-scale changes 400 ka. This thesis advances our understanding of how sea ice drives and interacts with the climate system and how primary producers react to and record climatic changes.

A solid foundation of knowledge concerning the diatom distribution across the Bering Sea shelf underlies the interpretations of climatic change presented. Currently, there is no central repository of diatom taxonomy; all descriptions and changes in classification are published in a wide array of journals and historical monographs. Chapter 2 collects these references into a single document that summarizes the taxonomic richness of the Bering Shelf. It builds on previous work by Sancetta [1982] by separating out groups of diatoms, specifically ice-related pennate diatoms and the *Chaetoceros* resting spore morphotaxa, and by updating taxa ranges. This work not only informs the rest of the dissertation, but will also be useful for training students in diatom identification in the future.

There were two main objectives for Chapter 3. The first was to determine if Bering Sea shelf sediments were appropriate recorders of the modern surface environments so that diatom assemblages and organic biomarkers found in these sediments could later be correlated with modern environmental conditions. Chapter 3 concludes that the top 1 cm of sediments on the Bering Sea shelf represent several years to decades of deposition and not hundreds to thousands of years. The second objective was to determine if the bioturbated shelf sediments

were recording the physical and biological changes occurring in the Bering Sea over the past several decades. It concludes that changes in the Pacific Decadal Oscillation and the strength of the Aleutian Low are reflected as subtle changes in diatom assemblages down-core and in samples collected 40 years apart. Specifically, changes in diatom accumulation rate, *Chaetoceros* resting spores, and sea-ice diatoms appear to reflect changing productivity and sea ice regimes.

One of the primary science questions that initiated this dissertation was, "What was the sea ice variability at finer than Milankovitch-scale temporal resolution in records older than marine isotope stage (MIS) 5?" Chapter 4 examined this question by presenting a record of sea surface changes during the transition from glacial stage 12 to glacial stage 10 at a site proximal to the current marginal ice zone. This chapter concludes that diatom assemblages at this site reflect changes in upwelling, sea ice, glacial ice, and potentially even current direction. It shows that in the Bering Sea, the glacial termination preceding MIS 11 was highly productive with reduced sea ice. At this time, shelf-derived nutrient pulses due to flooding of the Bering Land Bridge may have triggered the development of laminated sediments. Peak MIS 11 was marked by a brief, regional expansion of glaciers while sea level was at its highest point. This glaciation was driven by unusually humid conditions, decreasing insolation, and reduced seasonality. Finally, Chapter 4 concludes that when North Atlantic Deep Water (NADW) formation is vigorous in the North Atlantic, productivity is high in the Bering Sea. A short-term decrease in NADW strength at 410 ka may have triggered a reversal in the flow of water through Bering Strait.

Proxy development was a focal point of my dissertation and this thesis succeeds in building a solid foundation on which to base a diatom-based sea ice proxy for the Bering Sea in the near future. In Chapter 3, I suggested that studies using the top 1 cm of sediments for proxy calibration compare sediment characteristics to 10 to 30 years of climate data. The diatom-based sea ice proxy that is in development will calibrate surface sediments with two different

environmental databases to determine the best fit: a 10-year average of sea surface conditions, or the 30 year climatological mean. Chapter 5 begins this proxy calibration by comparing a 10-year average of sea surface temperature and sea ice concentration during the spring (March, April, May, June) with the molecular biomarker, IP_{25}. I propose that changes in the concentration of IP_{25} in the sediments may be related to the length of time that the epontic diatom bloom lasts.

BIBLIOGRAPHY

Aizawa, C., M. Tanimoto, and R.W. Jordan (2005), Living diatom assemblages from North Pacific and Bering Sea surface waters during summer 1999, *Deep-Sea Research II*, *52*, 2186-2205.

Alexander, V., and H.J. Niebauer (1981), Oceanography of the eastern Bering Sea ice-edge zone in spring, *Limnology and Oceanography*, *26*(6), 1111-1125.

Alexander, V., and T. Chapman (1981), The role of epontic algal communities in Bering Sea ice, in *The Eastern Bering Sea Shelf: Oceanography and Resources*, edited by D.W. Hood and J.A. Calder, pp. 773-780, University of Washington Press, Seattle, Washington.

Antonov, J.I., D. Seidov, T.P. Boyer, R.A. Locarnini, A.V. Mishonov, H.E. Garcia, O.K. Baranova, M.M. Zweng, and D.R. Johnson (2010), World Ocean Atlas 2009--Salinity, NOAA Atlas NESDIS 69, edited by S. Levitus, p. 184, U.S. Government Printing Office, Washington, DC.

Armand, L.K., X. Crosta, O. Romero, and J.J. Pichon (2005), The biogeography of major diatom taxa in Southern Ocean sediments: 1. Sea ice related species, *Palaeogeography, Palaeoclimatology, Palaeoecology*, *223*(1-2), 93-126.

Backman, J., M. Jakobsson, M. Frank, F. Sangiorgi, H. Brinkhuis, C. Stickley, M. O'Regan, R. Lovlie, H. Palike, D. Spofforth, J. Gattacecca, K. Moran, J. King, and C. Heil (2008), Age model and core-seismic integration for the Cenozoic Arctic coring expedition sediments from the Lomonosov Ridge, *Paleoceanography*, *23*(1), 10.1029/2007pa001476.

Barron, J., and A. Yu Gladenkov (1995), Early Miocene to Pleistocene diatom stratigraphy of Leg 145, *Proceedings of the ODP, Scientific Results*, *145*, 3-19.

Barron, J. A., D. Bukry, W. E. Dean, J. A. Addison, and B. Finney (2009), Paleoceanography of the Gulf of Alaska during the past 15,000 years: results from diatoms, silicoflagellates, and geochemistry, *Marine Micropaleontology*, *72*(3-4), 176-195.

Bassinot, F.C., L.D. Labeyrie, E. Vincent, X. Quidelleur, N. J. Shackleton, and Y. Lancelot (1994), (Table 4) Isotopic event stack. In supplement to: The astronomical theory of climate and the age of the Brunhes-Matuyama magnetic reversal, *Earth and Planetary Science Letters*, *126*(1-3), 91-108.

Belt, S.T., G. Massé, S.J. Rowland, M. Poulin, C. Michel, and B. LeBlanc (2007), A novel chemical fossil of palaeo sea ice: IP_{25}, *Organic Geochemistry*, *38*, 16-27.

Belt, S.T., G. Massé, L.L. Vare, S. J. Rowland, M. Poulin, M. A. Sicre, M. Sampei, and L. Fortier (2008), Distinctive C-13 isotopic signature distinguishes a novel sea ice biomarker in Arctic sediments and sediment traps, *Marine Chemistry*, *112*(3-4), 158-167.

Belt, S.T., L.L. Vare, G. Massé, H.R. Manners, J.C. Price, S.E. MacLachlan, J.T. Andrews, and S. Schmidt (2010), Striking similarities in temporal changes to spring sea ice occurrence across the central Canadian Arctic Archipelago over the last 7000 years, *Quaternary Science Reviews*, *29*(25-26), 3489-3504.

Berger, A., and M. F. Loutre (1991), Insolation Values for the Climate of the Last 10 Million Years, *Quaternary Science Reviews*, *10*, 297-317.

Bertrand, Philippe, Thomas F. Pedersen, Philippe Martinez, Stephen Calvert, and Graham Shimmield (2000), Sea level impact on nutrient cycling in coastal upwelling areas during deglaciation: evidence from nitrogen isotopes, *Global Biogeochemical Cycles*, *14*(1), 341-355.

Blasco, D., M. Estrada, and B. Jones (1980), Relationship between the phytoplankton distribution and composition and the hydrography in the Northwest African upwelling region near Cabo Carboeiro, *Deep Sea Research*, *27A*, 799-821.

Bond, N. A. (2003), Recent shifts in the state of the North Pacific, *Geophysical Research Letters*, *30*(23).

Bowen, D.Q. (2010), Sea level ~400 000 years ago (MIS 11): analogue for present and future sea-level?, *Climate of the Past*, *6*, 19-29.

Brigham-Grette, J., D.M. Hopkins, V.F. Ivanov, A.E. Basilyan, S.L. Benson, P.A. Heiser, and V.S. Pushkar (2001), Last Interglacial (isotope stage 5) glacial and sea-level history of coastal Chukotka Peninsula and St. Lawrence Island, Western Beringia, *Quaternary Science Reviews*, *20*, 419-436.

Brunelle, B.G., D.M. Sigman, M.S. Cook, L. Keigwin, G. H Haug, B. Plessen, G. Schettler, and S. L. Jaccard (2007), Evidence from diatom-bound nitrogen isotopes for subarctic Pacific stratification during the last ice age and a link to North Pacific denitrification changes, *Paleoceanography*, *22*(PA1215).

Caissie, B. E., J. Brigham-Grette, K. T. Lawrence, T. D. Herbert, and M. S. Cook (2010), Last Glacial Maximum to Holocene sea surface conditions at Umnak Plateau, Bering Sea, as inferred from diatom, alkenone, and stable isotope records, *Paleoceanography*, *25*, 10.1029/2008pa001671.

Carter, R.M. (2005), A New Zealand climatic template back to c. 3.9 Ma: ODP Site 1119, Canterbury Bight, south-west Pacific Ocean, and its relationship to onland successions, *Journal of the Royal Society of New Zealand*, *35*(1-2), 9-42.

Cavalieri, D.J., P. Parkinson, P. Gloersen, and Zwally (1996), Sea Ice Concentrations from Nimbus-7 SMMR and DMSP SSM/I Passive Microwave Data, 1996-2008, edited, National Snow and Ice Data Center, Boulder, CO.

Chaisson, W.P., M.S. Poli, and R.C. Thunell (2002), Gulf Stream and Western Boundary Undercurrent variations during MIS 10 -12 at Site 1056, Blake-Bahama Outer Ridge, *Marine Geology*, *189*, 79-105.

Chapman, W.L., and J.E. Walsh (1991), Arctic and Southern Ocean sea ice concentrations, 1959-1969, edited, National Snow and Ice Data Center/World Data Center for Glaciology, Boulder, CO.

Clarke, K.R. (1993), Non-parametric multivariate analyses of changes in community structure, *Australian Journal of Ecology*, *18*, 117-143.

Codispoti, L. A., C. N. Flagg, and J. H. Swift (2009), Hydrographic conditions during the 2004 SBI process experiments, *Deep Sea Research II*, *56*(17), 1144-1163.

Cooper, L.W., T.E. Whitledge, J.M. Grebmeier, and T. Wieingartner (1997), The nutrient, salinity, and stable oxygen isotope composition of Bering and Chukchi Seas waters in and near the Bering Strait, *Journal of Geophysical Research*, *102*(C6), 12563-12573.

Cooper, L.W., I.L. Larsen, J.M. Grebmeier, and S.B. Moran (2005), Detection of rapid deposition of sea ice-rafted material to the Arctic Ocean benthos using the cosmogenic tracer Be-7, *Deep Sea Research II*, *52*(24-26), 3452-3461.

Cooper, L.W., C. Lalande, R. Pirtle-Levy, I.L. Larsen, and J.M. Grebmeier (2009), Seasonal and decadal shifts in particulate organic matter processing and sedimentation in the Bering Strait Shelf region, *Deep Sea Research II*, *56*(17), 1316-1325.

Crawford, R.M. (1979), Taxonomy and Frustular Structure of the Marine Centric Diatom Paralia-Sulcata, *Journal of Phycology*, *15*, 200-210.

Crawford, R.M., P.A. Sims, and M. Hajós (1990), The morphology and taxonomy of the centric diatom genus *Paralia*: I. *Paralia siberica* comb. nov, *Diatom Research*, *5*(2), 241-252.

Cronin, T. M., L. Gemery, W. M. Briggs Jr, M. Jakobsson, L. Polyak, and E. M. Brouwers (2010), Quaternary sea-ice history in the Arctic Ocean based on a new ostracode sea-ice proxy, *Quaternary Science Reviews*, *29*(25-26), 3415-3429.

Crosta, X., J.J. Pichon, and L. H. Burckle (1998), Application of modern analog technique to marine Antarctic diatoms: reconstruction of maximum sea-ice extent at the Last Glacial Maximum, *Paleoceanography*, *13*, 284-297.

Cunningham, W. L., and A. Leventer (1998), Diatom assemblages in surface sediments of the Ross Sea: relationship to present oceanographic conditions, *Antarctic Science*, *10*(2), 134-146.

Damsté, J.S.S., G. Muyzer, B. Abbas, S.W. Rampen, G. Massé, W.G. Allard, S.T. Belt, J.M. Robert, S.J. Rowland, J.M. Moldowan, S.M. Barbanti, F.J. Fago, P. Denisevich, J. Dahl, L.A.F. Trindade, and S. Schouten (2004), The rise of the rhizosolenid diatoms, *Science*, *304*(5670), 584-587.

Darby, D. A. (2008), Arctic perennial ice cover over the last 14 million years, *Paleoceanography*, *23*(1), 10.1029/2007pa001479.

Davies, A., A. E. S. Kemp, and J. Pike (2009), Late Cretaceous seasonal ocean variability from the Arctic, *Nature*, *460*(7252), 254-259.

de Abreu, C., F. F. Abrantes, N. J. Shackleton, P. C. Tzedakis, J. F. McManus, D. W. Oppo, and M. A. Hall (2005), Ocean climate variability in the eastern North Atlantic during interglacial marine isotope stage 11: A partial analogue to the Holocene?, *Paleoceanography*, *20*(3), 10.1029/2004PA001091.

de Vernal, A., and C. Hillaire-Marcel (2008), Natural variability of Greenland climate, vegetation, and ice volume during the past million years, *Science*, *320*, 1622-1625.

de Vernal, A., C. Hillaire-Marcel, and D. A. Darby (2005), Variability of sea ice cover in the Chukchi Sea (western Arctic Ocean) during the Holocene, *Paleoceanography*, *20*(4), 10.1029/2005PA001157.

de Vernal, A., M. Henry, J. Mattiessen, P. J. Mudie, A. Rochon, K. P. Boessenkool, F. Eynaud, K. Grosfjeld, J. Guiot, D. Hamel, R. Harland, M. Head, M. Kunz-Pirrung, E. Levac, V. Loucheur, O. Peyron, V. Pospelova, T. Radi, J. Turon, and E. Voronina (2001), Dinoflagellate cyst assemblages as tracers of sea-surface conditions in the northern North Atlantic, Arctic and sub-Arctic seas: the new 'n=677' data base and its application for quantitative palaeoceanographic reconstruction, *Journal of Quaternary Science*, *16*(7), 681-698.

DeBoer, A.M., and D. Nof (2004), The Exhaust Valve of the North Atlantic, *Journal of Climate*, *17*(3), 417-422.

Dickson, A.J., C.J. Beer, C. Dempsey, M. A. Maslin, J.A. Bendle, E.L. McClymont, and R.D. Pancost (2009), Oceanic forcing of the Marine Isotope Stage 11 interglacial, *Nature Geoscience*, *2*, 428-433.

Droxler, A.W., R.B. Alley, W. R. Howard, R.Z. Poore, and L. H. Burckle (2003), Unique and exceptionally long interglacial Marine Isotope Stage 11: window into Earth's warm future climate, in *Earth's Climate and Orbital Eccentricity: The Marine Isotope Stage 11 Question*, edited by A.W. Droxler, R.Z. Poore and L.H. Burckle, pp. 1-14, American Geophysical Union, Washington, DC.

Eglinton, T. I., and G. Eglinton (2008), Molecular proxies for paleoclimatology, *Earth and Planetary Science Letters*, *275*, 1-16.

Ellis, E.A. (2006), Corrected formulation for Spurr low viscosity embedding medium using the replacement epoxide ERL 4221, *Microscopy and Microanalysis*, *12 (Supplement 12)*, 288-289.

EPICA community members (2004), Eight glacial cycles from an Antarctic ice core, *Nature*, *429*, 623-628.

Fawcett, P. J., J. P. Werne, R. S. Anderson, J. M. Heikoop, E. T. Brown, M. A. Berke, S. J. Smith, F. Goff, L. Donohoo-Hurley, L. M. Cisneros-Dozal, S. Schouten, J. S. Sinninghe Damste, Y. Huang, J. Toney, J. Fessenden, G. WoldeGabriel, V. Atudorei, J. W. Geissman, and C. D. Allen (2011), Extended megadroughts in the southwestern United States during Pleistocene interglacials, *Nature*, *470*(7335), 518-521.

Frank, M., J. Backman, M. Jakobsson, K. Moran, M. O'Regan, J. King, B. A. Haley, P. W. Kubik, and D. Garbe-Schonberg (2008), Beryllium isotopes in central Arctic Ocean sediments over the past 12.3 million years: stratigraphic and paleoclimatic implications, *Paleoceanography*, *23*(1), 10.1029/2007pa001478.

Fryxell, G. A., and G. R. Hasle (1972), *Thalassiosira eccentrica* (Ehreb.) Cleve, *T. symmetrica* sp. nov., and some related centric diatoms, *Journal of Phycology*, *8*, 297-317.

Fryxell, G.A. (1991), Comparison of winter and summer growth stages of the diatom *Eucampia antarctica* from the Kerguelen Plateau and south of the Antarctic Convergence Zone, in *Proceedings of the Ocean Drilling Program, Scientific Results, v. 119*, edited by J. Barron, B. Larsen, J.Q. Baldauf, et al., pp. 675-685, Ocean Drilling Program, College Station, TX.

Garcia, H.E., R.A. Locarnini, T.P. Boyer, and J.I. Antonov (2010), World Ocean Atlas 2009*Rep.*, 398 pp, U.S. Government Printing Office, Washington, DC.

Gardner, J.V., W. A. Dean, and T.L. Vallier (1980), Sedimentology and geochemistry of surface sediments, outer continental shelf, southern Bering Sea, *Marine Geology*, *35*, 299-329.

Glushkova, O. Y. (2001), Geomorphological correlation of Late Pleistocene glacial complexes of Western and Eastern Beringia, *Quaternary Science Reviews*, *20*(1-3), 405-417.

Gradinger, R. (2009), Sea-ice algae: Major contributors to primary production and algal biomass in the Chukchi and Beaufort Seas during May/June 2002, *Deep Sea Research II*, *56*(17), 1201-1212.

Gran, H.H. (1904), Diatomaceae from the ice-floes and plankton of the Arctic Ocean, in *The Norwegian North Polar Expedition 1893-1896*, edited by F. Nansen, pp. 1-74, Grondahl and Sons, Christiana.

Grebmeier, J.M. (1993), Studies of pelagic-benthic coupling extended onto the Soviet continental shelf in the northern Bering and Chukchi seas, *Continental Shelf Research*, *13*(5/6), 653-668.

Grebmeier, J.M. (2012), Shifting patterns of life in the Pacific Arctic and sub-Arctic seas, *Annual Reviews of Marine Science*, *4*, 63-78.

Grebmeier, J.M., and C.P. McRoy (1989), Pelagic-benthic coupling on the shelf of the Northern Bering and Chukchi seas. 3. Benthic food-supply and carbon cycling, *Marine Ecology-Progress Series*, *53*(1), 79-91.

Grebmeier, J.M., and L.W. Cooper (1995), Influence of the St. Lawrence Island polynya upon the Bering Sea benthos, *Journal of Geophysical Research-Oceans*, *100*(C3), 4439-4460.

Grebmeier, J.M., and J.P. Barry (2006), Benthic Processes in Polynyas, in *Polynyas: Windows to the World*, edited by W.O. Jr. Smith and D.G. Barber, p. 474, Elsevier B.V.

Grebmeier, J.M., L.W. Cooper, H.M. Feder, and B.I. Sirenko (2006a), Ecosystem dynamics of the Pacific-influenced Northern Bering and Chukchi Seas in the Amerasian Arctic, *Progress in Oceanography*, *71*(2-4), 331-361.

Grebmeier, J.M., S.E. Moore, J.E. Overland, K.E. Frey, and R. Gradinger (2010), Biological response to recent Pacific Arctic sea ice retreats, *Eos*, *91*(18), 161-162.

Grebmeier, J.M., J.E. Overland, S.E. Moore, E.V. Farley, E.C. Carmack, L.W. Cooper, K.E. Frey, J.H. Helle, F.A. McLaughlin, and S.L. McNutt (2006b), A major ecosystem shift in the northern Bering Sea, *Science*, *311*(5766), 1461-1464.

Gualtieri, L., and J. Brigham-Grette (2001), The age and origin of the Little Diomede Island upland surface, *Arctic*, *54*(1), 12-21.

Håkansson, H. (2002), A compilation and evaluation of species in the general *Stephanodiscus, Cyclostephanos,* and *Cyclotella* with a new genus in the family Stephanodiscaceae, *Diatom Research*, *17*(1), 1-139.

Halfar, J., B. Williams, S. Haetzinger, R.S. Steneck, P. Lebednik, C. Winsborough, A. Omar, P Chan, and A.D. Jr. Wanamaker (2011), 225 years of Bering Sea climate and ecosystem dynamics revealed by coralline algal growth-increment widths, *Geology*, *39*(6), 579-582.

Hasle, G. R., and G. Fryxell (1977), *Thalassiosira conferta* and *T. binata*, two new diatom species, *Norwegian Journal of Botany*, *24*, 239-248.

Hasle, G. R., E. E. Syvertsen, and C. von Quillfeldt (1996), *Fossula arctica* gen. nov., spec. nov., a marine Arctic pennate diatom, *Diatom Research*, *11*, 261-272.

Hasle, G.R. (2001), The marine, planktonic diatom family Thalassionemataceae: morphology, taxonomy and distribution, *Diatom Research*, *16*(1), 1-82.

Hasle, G.R., and B.R. Heimdal (1968), Morphology and distribution of the marine centric diatom *Thalassiosira antarctica* Comber, *Journal of the Royal Microscopical Society*, *88*(3), 357-369.

Hasle, G.R., and E.E. Syvertsen (1997), Marine Diatoms, in *Identifying Marine Phytoplankton*, edited by C.R. Tomas, pp. 5-386, Academic Press, Inc., San Diego, California.

Hay, Murray B., Audrey Dallimore, Richard E. Thomson, Stephen E. Calvert, and Reinhard Pienitz (2007), Siliceous microfossil record of late Holocene oceanography and climate along the west coast of Vancouver Island, British Columbia (Canada), *Quaternary Research*, *67*(1), 33-49.

Heimdal, B. R. (1971), Vegetative cells and resting spores of *Thalassiosira constrcta* Gaarder (Bacillariophyceae), *Norwegian Journal of Botany*, *18*, 153-159.

Holland, M.M., C.M. Bitz, and B. Tremblay (2006), Future abrupt reductions in the summer Arctic sea ice, *Geophysical Research Letters*, *33*(L23503), 1-5.

Honjo, S. (1990), Particle fluxes and modern sedimentation in the polar oceans, in *Polar Oceanography*, edited by W.O. Smith, pp. 687-739, Academic Press, San Diego, CA.

Hopkins, D.M. (1959), Cenozoic Hhistory of the Bering Land Bridge, *Science*, *129*, 1519-1528.

Hopkins, D.M. (1966), Pleistocene glaciation on St. George, Pribilof Islands, *Science*(152), 343-345.

Hopkins, D.M. (1967), Quaternary marine transgressions in Alaska, in *The Bering Land Bridge*, edited by D.M. Hopkins, pp. 121-143, Stanford University Press, Palo Alto, CA.

Hopkins, D.M. (1972), The paleogeography and climatic history of Beringia during late Cenozoic Time, *Internord*, *12*, 121-150.

Horner, R. (1985), *Sea Ice Biota*, 203 pp., CRC Press, Inc, Boca Raton, FL.

Horner, R., and G.C. Schrader (1982), Relative contributions of ice algae, phytoplankton, and benthic microalgae to primary production in nearshore regions of the Beaufort Sea, *Arctic*, *35*(4), 485-503.

Hu, A. X., G. A. Meehl, B. L. Otto-Bliesner, C. Waelbroeck, W. Q. Han, M. F. Loutre, K. Lambeck, J. X. Mitrovica, and N. Rosenbloom (2010), Influence of Bering Strait flow and North Atlantic circulation on glacial sea-level changes, *Nature Geoscience*, *3*(2), 118-121.

Huston, M.M., J. Brigham-Grette, and D.M. Hopkins (1990), Paleogeographic significance of middle Pleistocene glaciomarine deposits on Baldwin Peninsula, northwestern Alaska, *Annals of Glaciology*, *14*, 111-114.

Huybers, P., and C. Langmuir (2009), Feedback between deglaciation, volcanism, and atmospheric CO2, *Earth and Planetary Science Letters*, *286*(3-4), 479-491.

IPCC (2007), Summary for Policymakers, in *Climate Change 2007: The Physical Science Basis. Contribution of Working Group I to the Fourth Assessment Report of the Intergovernmental Panel on Climate Change*, edited by S. Solomon, D. Qin, M. Manning, Z. Chen, M. Marquis, K.B. Averyt, M. Tignor and H.L. Miller, Cambridge University Press, Cambridge, United Kingdom and New York, NY.

Jin, M. B., C. J. Deal, J. Wang, N. Tanaka, and M. Ikeda (2006), Vertical mixing effects on the phytoplankton bloom in the southeastern Bering Sea midshelf, *Journal of Geophysical Research-Oceans*, *111*(C3), 10.1029/2005jc002994.

Johnson, K.R., and C.H. Nelson (1984), Side-scan sonar assessment of gray whale feeding in the Bering Sea, *Science*, *225*, 1150-1152.

Jousé, A. P. (1968), Diatoms in Pleistocene Sediments from the Northern Pacific Ocean, in *The Micropaleontology of Oceans*, edited by W. R. Riedel and B. M. Funnell, pp. 407-421, Cambridge University Press, Cambridge.

Jouzel, J., V. Masson-Delmotte, O. Cattani, G. Dreyfus, S. Falourd, G. Hoffmann, B. Minster, J. Nouet, J. M. Barnola, J. Chappellaz, H. Fischer, J. C. Gallet, S. Johnsen, M. Leuenberger, L. Loulergue, D. Luethi, H. Oerter, F. Parrenin, G. Raisbeck, D. Raynaud, A. Schilt, J. Schwander, E. Selmo, R. Souchez, R. Spahni, B. Stauffer, J. P. Steffensen, B. Stenni, T. F. Stocker, J. L. Tison, M. Werner, and E. W. Wolff (2007), Orbital and millennial Antarctic climate variability over the past 800,000 years, *Science*, *317*(5839), 793-796.

Kanneworff, E., and W. Nicolaisen (1973), The "Haps", a frame supported bottom corer, *Ophelia*, *Supplement 10*, 119-129.

Kariya, Chie, Masayuki Hyodo, Koichiro Tanigawa, and Hiroshi Sato (2010), Sea-level variation during MIS 11 constrained by stepwise Osaka Bay extensions and its relation with climatic evolution, *Quaternary Science Reviews*, *29*(15-16), 1863-1879.

Katsuki, K., and K. Takahashi (2005), Diatoms as paleoenvironmental proxies for seasonal productivity, sea-ice and surface circulation in the Bering Sea during the late Quaternary, *Deep Sea Research II*, *52*, 2110-2130.

Kaufman, D.S. (1992), Aminostratigraphy of Pliocene-Pleistocene high-sea-level deposits, Nome coastal plain and adjacent nearshore area, Alaska, *Geological Society of America Bulletin*, *104*, 40-52.

Kaufman, D.S., and J. Brigham-Grette (1993), Aminostratigraphic correlations and paleotemperature implications, Pliocene-Pleistocene high sea-level deposits, Northwestern Alaska, *Quaternary Science Reviews*, *12*, 21-33.

Kaufman, D.S., R.C. Walter, J. Brigham-Grette, and D.M. Hopkins (1991), Middle Pleistocene age of the Nome River glaciation, northwestern Alaska, *Quaternary Research*, *36*(3), 277-293.

Kaufman, D.S., W.F. Manley, S.L. Forman, and P.W. Layer (2001), Pre-Late-Wisconsin glacial history, coastal Ahklun Mountains, southwestern Alaska - new amino acid, thermoluminescence, and $^{40}Ar/^{39}Ar$ results, *Quaternary Science Reviews*, *20*(1-3), 337-352.

Kazarina, G. K., and I. G. Yushina (1999), Diatoms in recent and Holocene sediments of the North Pacific and the Bering Sea, in *German-Russian cooperation; biogeographic and biostratigraphic investigations on selected sediment cores from the Eurasian continental margin and marginal seas to analyze the late Quaternary climatic variability*, edited by R. F. Spielhagen, M.S. Barash, G.I. Ivanov and J. Thiede, pp. 134-148, Kamloth, Bremerhaven, Germany.

Kindler, P., and P.J. Hearty (2000), Elevated marine terraces from Eleuthera (Bahamas) and Bermuda: sedimentological, petrographic, and geochronological evidence for important deglaciation events during the middle Pleistocene, *Global and Planetary Change*, *24*, 41-58.

Koç, N., and B.P. Flower (1998), High-resolution Pleistocene diatom biostratigraphy and paleoceanography of Site 919 from the Irminger Basin, in *Proceedings of the Ocean Drilling Program, Scientific Results, v. 152*, edited by A.D. Saunders, H.C. Larsen and S.W. Wise, Jr. , pp. 209-219, Ocean Drilling Program.

Koizumi, I. (1973), The Late Cenozoic diatoms of Sites 183-193, Leg 19 Deep Sea Drilling Project, *Initial Reports of the Deep Sea Drilling Project*, *19*, 805-855.

Kowalik, Z. (1999), Bering Sea Tides, in *Dynamics of the Bering Sea*, edited by T. R. Loughlin and K. Ohtani, pp. 93-127, Universtiy of Alaska Sea Grant, Fairbanks, AK.

Lalande, C., J.M. Grebmeier, P. Wassmann, L.W. Cooper, M.V. Flint, and V.M. Sergeeva (2007), Export fluxes of biogenic matter in the presence and absence of seasonal sea ice cover in the Chukchi Sea, *Continental Shelf Research*, *27*(15), 2051-2065.

Lee, S. H., T.E. Whitledge, and S. H. Kang (2008), Spring time production of bottom ice algae in the landfast sea ice zone at Barrow, Alaska, *Journal of Experimental Marine Biology and Ecology*, *367*, 204-212.

Lisiecki, L. E., and M. E. Raymo (2005), A Pliocene-Pleistocene stack of 57 globally distributed benthic delta O-18 records, *Paleoceanography*, *20*(1), 10.1029/2004PA001071.

Liu, W.G., and H. Yang (2008), Multiple controls for the variability of hydrogen isotopic compositions in higher plant n-alkanes from modern ecosystems, *Global Change Biology*, *14*, 2166-2177.

Lopes, C., A. C. Mix, and F. Abrantes (2006), Diatoms in northeast Pacific surface sediments as paleoceanographic proxies, *Marine Micropaleontology*, *60*(1), 45-65.

Loutre, M. F., and A. Berger (2003), Marine Isotope Stage 11 as an analogue for the present interglacial, *Global and Planetary Change*, *36*, 209-217.

Lozhkin, A.V., P. Anderson, T. Matrosova, and El'gygytgyn Scientific Party (in prep), Vegetation during Marine Isotope Stages 5.5, 11 and 31 at Lake El'gygytgyn and its comparison with Lake Baikal, *Climate of the Past*.

Lu, B., R. H. Chen, H. Y. Zhou, Z. P. Wang, J. F. Chen, and C. Zhu (2005), Oceanic environmental changes of subarctic Bering Sea in recent 100 years: Evidence from molecular fossils, *Science in China Series D-Earth Sciences*, *48*(4), 555-564.

Lundholm, N., and G. R. Hasle (2008), Are *Fragilariopsis cylindrus* and *Fragilariopsis nana* bipolar diatoms? Morphological and molecular analyses of two sympatric species, *Nova Hedwigia*, *133*, 231-250.

Lundholm, N., and G. R. Hasle (2010), *Fragilariopsis* (Bacillariophyceae) of the Northern Hemisphere--morphology, taxonomy, phylogeny and distribution, with a description of *F. pacifica* sp. nov., *Phycologia*, *49*(5), 438-460.

Lyle, M., L. Heusser, T. Herbert, A. C. Mix, and J. Barron (2001), Interglacial theme and variations: 500 k.y. of orbital forcing and associated responses from the terrestrial and marine biosphere, U.S. Pacific Northwest, *Geology*, *29*(12), 1115-1118.

Manley, W. F., D. S. Kaufman, and J. P. Briner (2001), Pleistocene glacial history of the southern Ahklun Mountains, southwestern Alaska: Soil-development, morphometric, and radiocarbon constraints, *Quaternary Science Reviews*, *20*(1-3), 353-370.

Manley, W.F. (2002), Digital Elevation Model (DEM) for the Bering Land Bridge, INSTAAR, University of Colorado, Boulder, CO.

Mantua, N.J. , S.R. Hare, Y. Zhang, J.M. Wallace, and R.C. Francis (1997), A Pacific interdecadal climate oscillation with impacts on salmon production, *Bulletin of the American Meteorological Society*, *78*, 1069-1079.

Massé, G., S. J. Rowland, M. A. Sicre, J. Jacob, E. Jansen, and S. T. Belt (2008), Abrupt climate changes for Iceland during the last millennium: evidence from high resolution sea ice reconstructions, *Earth and Planetary Science Letters*, *269*(3-4), 564-568.

Massé, G., S. T. Belt, X. Crosta, S. Schmidt, I. Snape, D. N. Thomas, and S. J. Rowland (2011), Highly branched isoprenoids as proxies for variable sea ice conditions in the Southern Ocean, *Antarctic Science*, *23*(5), 487-498.

Maurer, B.A., and B.J. McGill (2011), Chapter 5: measurement of species diversity, in *Biological Diversity*, edited by A.E. Magurran and B.J. McGill, pp. 55-65, Oxford University Press, New York.

McManus, J., D. W. Oppo, J. L. Cullen, and S. Healey (2003), Marine Isotope Stage 11 (MIS 11): analog for Holocene and future climate, in *Earth's Climate and Orbital Eccentricity: The Marine Isotope Stage 11*, edited by A. W. Droxler, R. Z. Poore and L.H. Burkle, pp. 69-85, American Geophysical Union, Washington, DC.

McQuoid, M. R., and L. A. Hobson (2001), A Holocene record of diatom and silicoflagellate microfossils in sediments of Saanich Inlet, ODP Leg 169S, *Marine Geology*, *174*, 111-123.

Medlin, L.K., and G.R. Hasle (1990), Some *Nitzschia* and related diatom species from fast ice samples in the Arctic and Antarctic, *Polar Biology*, *10*, 451-479.

Medlin, L.K., and J. Priddle (1990), *Polar Marine Diatoms*, 214 pp., British Antarctic Survey, Natural Environment Research Council, Cambridge.

Melnikov, I. A., E. G. Kolosova, H. E. Welch, and L. S. Zhitina (2002), Sea ice biological communities and nutrient dynamics in the Canada Basin of the Arctic Ocean, *Deep Sea Research I*, *49*(9), 1623-1649.

Merrill, T. E., B. Konar, and B. Bluhm (2010), A temporal comparison of a benthic infaunal community southwest of St. Lawrence Island, Bering Sea between 2006 and 1970-1974, *Polar Biology*, *33*(10), 1439-1444.

Meyers, P.A. (1994), Preservation of elemental and isotopic source identification of sedimentary organic matter, *Chemical Geology*, *114*, 289-302.

Miller, G. H., and A. De Vernal (1992), Will greenhouse warming lead to Northern Hemisphere ice-sheet growth?, *Nature*, *355*, 244-246.

Miller, G. H., J. Brigham-Grette, L. Anderson, H.A. Bauch, M.A. Douglas, M. E. Edwards, S.A. Elias, B.P. Finney, S. Funder, T. Herbert, L. D. Hinzman, D.K. Kaufman, G. M. MacDonald, A. Robock, M. C. Serreze, J. P. Smol, R. F. Spielhagen, A. P. Wolfe, and E. W. Wolff (2009), Temperature and precipitation history of the Arctic, in *Past Climate Variability and Change in the Arctic and at High Latitudes*, edited by U.S. Climate Change Program and Subcommittee on Global Change Research, pp. 77-246, U.S. Geological Survey, Reston, VA.

Müller, Juliane, Guillaume Massé, R. Stein, and S. T. Belt (2009), Variability of sea-ice conditions in the Fram Strait over the past 30,000 years, *Nature Geoscience*, *2*, 772-776.

Müller, Juliane, Axel Wagner, Kirsten Fahl, Ruediger Stein, Matthias Prange, and Gerrit Lohmann (2011), Towards quantitative sea ice reconstructions in the northern North Atlantic: A combined biomarker and numerical modelling approach, *Earth and Planetary Science Letters*, *306*, 137-148.

Murray, M.S., L. Anderson, G. Cherkashov, C. Cuyler, B. Forbes, J.C. Gascard, C. Haas, P. Schlosser, G. Shaver, K. Shimada, M. Tjernström, J. Walsh, J. Wandell, and Z. Zhao (2010), International Study of Arctic Change: Science Plan, edited by ISAC International Program Office, Stockholm.

Nelson, C.H., R.L. Phillips, J. Jr. McRea, J.H. Jr. Barber, M.W. McLaughlin, and J.L. Chin (1993), Gray Whale and Pacific Walrus Benthic Feeding Grounds and Sea Floor Interaction in the Chukchi Sea *Rep. MMS 93-0042*, 51 plus figures pp.

Niebauer, H.J., V. Alexander, and S.M. Henrichs (1995), A time-series study of the spring bloom at the Bering Sea ice edge I. Physical processes, chlorophyll and nutrient chemistry, *Continental Shelf Research*, *15*, 1859-1877.

Nittrouer, C.A., R.W. Sternberg, R. Carpenter, and J.T. Bennett (1979), The use of Pb-210 geochronology as a sedimentological tool: application to the Washington continental shelf, *Marine Geology*, *3/4*, 297-316.

Normack, W.R., and P.R. Carlson (2003), Giant submarine canyons: is size any clue to their importance in the rock record?, in *Geological Society of America Special Paper*, edited by M.A. Chan and A. W. Archer, pp. 1-15, Geological Society of America, Boulder, CO.

Oguri, K., N. Harada, and O. Tadai (2012), Excess ^{210}Pb and ^{137}Cs concentrations, mass accumulation rates, and sedimentary processes on the Bering Sea continental shelf, *Deep Sea Research II*, *61-64*, 193-204.

Onodera, J., and K. Takahashi (2007), Diatoms and siliceous flagellates (silicoflagellates, ebridians, and endoskeletal dinoflagellate *Actiniscus*) from the Subarctic Pacific, *Memoirs of the Faculty of Sciences Kyushu University., Series D, Earth and Planetary Sciences*, *31*(4), 105-136.

Overland, J. E., and C. H. Pease (1982), Cyclone climatology of the Bering Sea and its relation to sea ice extent, *Monthly Weather Review*, *110*, 5-13.

Pichon, J. J., M. Labracherie, L. D. Labeyrie, and J. Duprat (1987), Transfer functions between diatom assemblages and surface hydrology in the Southern Ocean, *Palaeogeography Palaeoclimatology Palaeoecology*, *61*(1-2), 79-95.

Pichon, J. J., L. D. Labeyrie, G. Bareille, M. Labracherie, J. Duprat, and J. Jouzel (1992), Surface water temperature changes in the high latitudes of the southern hemisphere over the last glacial-interglacial cycle, *Paleoceanography*, *7*(3), 289-318.

Pike, J., and A. E. S. Kemp (Eds.) (1996), *Preparation and analysis techniques for studies of laminated sediments*, 37-48 pp., Geological Society Special Publication.

Pike, J., X. Crosta, E. J. Maddison, C. E. Stickley, D. Denis, L. Barbara, and H. Renssen (2009), Observations on the relationship between the Antarctic coastal diatoms *Thalassiosira antarctica* Comber and *Porosira glacialis* (Grunow) Jorgensen and sea ice concentrations during the late Quaternary, *Marine Micropaleontology*, *73*(1-2), 14-25.

Pirtle-Levy, R., J.M. Grebmeier, L.W. Cooper, and I.L. Larsen (2009), Chlorophyll-*a* in Arctic sediments implies long persistence of algal pigments, *Deep Sea Research II*, *56*(17), 1326-1338.

Pol, K. (2011), Links between MIS 11 millennial to sub-millennial climate variability and long term trends as revealed by new high resolution EPICA Dome C deuterium data - A comparison with the Holocene, *Climate of the Past*, *7*(2), 437-450.

Poli, M.S., R.C. Thunell, and D. Rio (2000), Millenial-scale changes in North Atlantic Deep Water circulation during Marine Isotope Stages 11 and 12: linkage to Antarctic climate, *Geology*, *28*(9), 807-810.

Poli, M.S., Philip A. Meyers, and Robert C. Thunell (2010), The western North Atlantic record of MIS 13 to 10: Changes in primary productivity, organic carbon accumulation and benthic foraminiferal assemblages in sediments from the Blake Outer Ridge (ODP Site 1058), *Palaeogeography, Palaeoclimatology, Palaeoecology*, *295*(1-2), 89-101.

Polyak, L. (2010), Arctic sea-ice decline: a paleoclimatic perspective, Abstract A44B-07, in *2010 Fall Meeting, AGU*, edited, San Francisco, CA.

Polyak, L., R. B. Alley, J. T. Andrews, J. Brigham-Grette, T. M. Cronin, D. A. Darby, A. S. Dyke, J. J. Fitzpatrick, S. Funder, M. Holland, A. E. Jennings, G. H. Miller, M. O'Regan, J. Savelle, M. Serreze, K. St John, J. W. C. White, and E. Wolff (2010), History of sea ice in the Arctic, *Quaternary Science Reviews*, *29*(15-16), 1757-1778.

Preiss, N., M.-A. Melieres, and M. Pourchet (1996), A compilation of data on lead-210 concentration in surface air and fluxes at the air-surface and water-sediment interfaces, *Journal of Geophysical Research*, *101*(D22), 28847-28862.

Prokopenko, A.A., E.V. Bezrukova, G.K. Khursevich, E.P. Solotchina, M.I. Kuzmin, and P.E. Tarasov (2010), Climate in continental interior Asia during the longest interglacial of the past 500 000 years: the new MIS 11 records from Lake Baikal, SE Siberia, *Climate of the Past*, *6*, 31-48.

Pushkar, V.S., S.R. Roof, M. V. Cherepanova, D.M. Hopkins, and J. Brigham-Grette (1999), Paleogeographic and paleoclimatic significance of diatoms from Middle Pleistocene marine and glaciomarine deposits on Baldwin Peninsula, northwestern Alaska, *Palaeogeography, Palaeoclimatology, Palaeoecology*, *152*, 67-85.

Ray, G.C., J. McCormick-Ray, P. Berg, and H.E. Epstein (2006), Pacific walrus: Benthic bioturbator of Beringia, *Journal of Experimental Marine Biology and Ecology*, *330*, 403-419.

Raymo, M.E., and J.X. Mitrovica (2012), Collapse of polar ice sheets during the stage 11 interglacial, *Nature*, *483*, 453-456.

Raymo, M.E., J.X. Mitrovica, M.J. O'Leary, R.M. DeConto, and P. J. Hearty (2011), Departures from eustasy in Pliocene sea-level records, *Nature Geoscience*, *4*(5), 328-332.

Raynaud, D., J. M. Barnola, R. Souchez, R. Lorrain, J. R. Petit, P. Duval, and V. Y. Lipenkov (2005), The record for Marine Isotopic Stage 11, *Nature*, *436*, 39-40.

Reid, Philip C., David G. Johns, Martin Edwards, Michel Starr, Michel Poulin, and Pauli Snoeijs (2007), A biological consequence of reducing Arctic ice cover: arrival of the Pacific diatom *Neodenticula seminae* in the North Atlantic for the first time in 800,000 years, *Global Change Biology*, *13*(9), 1910-1921.

Reimnitz, E., M. McCormick, J. Bischof, and D. A. Darby (1998), Comparing sea-ice sediment load with Beaufort Sea shelf deposits: is entrainment selective?, *Journal of Sedimentary Research*, *68*(5), 777-787.

Reynolds, R.W., N.A. Rayner, T.M. Smith, D.C. Stokes, and W. Wang (2002), An improved *in situ* and satellite SST analysis for climate, *Journal of Climate*, *15*, 1609-1625.

Robbins, J.A. (1986), A model for particle selective transport of tracers in sediments with conveyor belt deposit feeders, *Journal of Geophysical Research*, *91*(C7), 8542-8558.

Rohling, E.J., M. Fenton, F.J. Jorissen, P. Bertrand, G. Ganssen, and J.P. Caulet (1998), Magnitudes of sea-level lowstands of the past 500,000 years, *Nature*, *394*, 162-165.

Rohling, E.J., K. Braun, K. Grant, M. Kucera, A. P. Roberts, M. Siddall, and G. Trommer (2010), Comparison between Holocene and Marine Isotope Stage-11 sea-level histories, *Earth and Planetary Science Letters*, *291*, 97-105.

Round, F.E., R.M. Crawford, and D.G. Mann (1990), *The diatoms: biology and morphology of the genera*, 747 pp., Cambridge University Press, Cambridge, UK.

Ryu, E., S.J. Lee, D.Y. Yang, and J.Y. Kim (2008), Paleoenvironmental studies of the Korean peninsula inferred from diatom assemblages, *Quaternary International*, *176-177*, 36-45.

Sagawa, T., and K. Ikehara (2008), Intermediate water ventilation change in the subarctic northwest Pacific during the last deglaciation, *Geophysical Research Letters*, *35*(24), 10.1029/2008GL035133.

Saitoh, K., and A. Taniguchi (1978), Phytoplankton communities in the Bering Sea and adjacent seas II: spring and summer communities in seasonally ice-covered areas, *Astarte*, *11*(1), 27-35.

Sakamoto, T., M. Ikehara, K. Aoki, K. Iijima, N. Kimura, T. Nakatsuka, and M. Wakatsuchi (2005), Ice-rafted debris (IRD)-based sea-ice expansion events during the past 100 kyrs in the Okhotsk Sea, *Deep Sea Research II*, *52*(16-18), 2275-2301.

Sancetta, C. A. (1979), Oceanography of the North Pacific during the Last 18,000 Years: Evidence from Fossil Diatoms, *Marine Micropaleontology*, *4*, 103-123.

Sancetta, C. A. (1981), Oceanographic and ecologic significance of diatoms in surface sediments of the Bering and Okhotsk seas, *Deep Sea Research*, *28A*(8), 789-817.

Sancetta, C. A. (1982), Distribution of diatom species in surface sediments of the Bering and Okhotsk seas, *Micropaleontology*, *28*, 221-257.

Sancetta, C. A. (1983), Effect of Pleistocene glaciation upon oceanographic characteristics of the North Pacific Ocean and Bering Sea, *Deep Sea Research*, *31A*(8), 851-869.

Sancetta, C. A. (1987), Three species of *Coscinodiscus* Ehrenberg from North Pacific sediments examined in the light and scanning electron microscopes, *Micropaleontology*, *33*(3), 230-241.

Sancetta, C. A., and S.W. Robinson (1983), Diatom evidence on Wisconsin and Holocene events in the Bering Sea, *Quaternary Research*, *20*, 232-245.

Sancetta, C. A., and S.M. Silvestri (1984), Diatom stratigraphy of the Late Pleistocene (Brunhes) Subarctic Pacific, *Marine Micropaleontology*, *9*, 263-274.

Sancetta, C. A., and S.M. Silvestri (1986), Pliocene-Pleistocene evolution of the North Pacific ocean-atmosphere system, interpreted from fossil diatoms, *Paleoceanography*, *1*(2), 163-180.

Schandelmeier, L., and V. Alexander (1981), An analysis of the influence of ice on spring phytoplankton population structure in the southeast Bering Sea, *Limnology and Oceanography*, *26*(5), 935-943.

Scherer, R. P. (1994), A new method for the determination of absolute abundance of diatoms and other silt-sized sedimentary particles, *Journal of Paleolimnology*, *12*, 171-179.

Scherer, R. P., A. Aldahan, S. Tulaczyk, G. Possnert, H. Engelhardt, and B. Kamb (1998), Pleistocene collapse of the West Antarctic Ice Sheet, *Science*, *281*, 82-85.

Schrader, H.J., and R. Gersonde (1978), Diatoms and silicoflagellates, in *Micropaleontological counting methods and techniques - an exercise on an eight metres section of the Lower Pliocene of Capo Rossello, Sicily*, edited by W.J. Zachariasse, W.R. Riedel, A. Sanfilippo, R.R. Schmidt, M.J. Brolsma, H.J. Schrader, R. Gersonde, M.M. Drooger and J.A. Broekman, pp. 129-176, Utrecht Micropaleontological Bulletin, Netherlands.

Schumacher, J.D., and P. J. Stabeno (1998), Continental shelf of the Bering Sea, in *The sea*, edited by A.R. Robinson and K.H. Brink, pp. 789-822, John Wiley and Sons, New York.

Seager, R., M. Ting, I. Held, Y. Kushnir, J. Lu, G. Vecchi, H. P. Huang, N. Harnik, A. Leetmaa, N. C. Lau, C. Li, J. Velez, and N. Naik (2007), Model projections of an imminent transition to a more arid climate in southwestern North America, *Science*, *316*(5828), 1181-1184.

SEARCH (2005), Study of Environmental Arctic Change: Plans for Implementation during the International Polar Year and beyond *Rep.*, 104 pp, Arctic Research Consortium of the United States (ARCUS), Fairbanks, AK.

Serreze, M.C., M.M. Holland, and J. Stroeve (2007), Perspectives on the Arctic's shrinking sea-ice cover, *Science*, *315*, 1533-1536.

Sharko, C.J. (2010), IP_{25}: a Molecular Proxy of Sea-Ice Duration in the Bering and Chukchi Seas, M.S. thesis thesis, 73 pp, University of Massachusetts Amherst, Amherst.

Shiga, K., and I. Koizumi (2000), Latest Quaternary oceanographic changes in the Okhotsk Sea based on diatom records, *Marine Micropaleontology*, *38*, 91-117.

Sigler, M. F., M. Renner, S. L. Danielson, L. B. Eisner, R. R. Lauth, K. J. Kuletz, E. A. Logerwell, and G. L. Hunt (2011), Fluxes, fins, and feathers: relationships among the Bering, Chukchi, and Beaufort seas in a time of climate change, *Oceanography*, *24*(3), 250-265.

Sims, P.A., and R.M. Crawford (2002), The morphology and taxonomy of the marine centric diatom genus *Paralia*: II.*Paralia crenulata, P. fausta* and the new species, *P. Hendeyi*, *Diatom Research*, *17*(2), 363-382.

Smol, J. P. (2002), The paleolimnologist's Rosetta Stone: calibrating indicators to environmental variables using surface-sediment training sets, in *Pollution of lakes and rivers: a paleoenvironmental perspective*, edited by J. P. Smol, Oxford University Press, New York.

Springer, A.M., C. P. McRoy, and M. V. Flint (1996), The Bering Sea green belt: shelf edge processes and ecosystem production, *Fisheries Oceanography*, *5*, 205-223.

St. John, K. (2008), Cenozoic ice-rafting history of the central Arctic Ocean: Terrigenous sands on the Lomonosov Ridge, *Paleoceanography*, *23*(1), 10.1029/2007pa001483.

Stabeno, P. J., J.D. Schumacher, and K. Ohtani (1999), The physical oceanography of the Bering Sea, in *Dynamics of the Bering Sea: a summary of physical, chemical, and biological characteristics, and a synopsis of research on the Bering Sea*, edited by T. R. Loughlin and K. Ohtani, pp. 1-28, University of Alaska Sea Grant, Fairbanks, AK.

Stabeno, P. J., N.A. Bond, N.B. Kachel, S.A. Salo, and J.D. Schumacher (2001), On the temporal variability of the physical environment over the south-eastern Bering Sea, *Fisheries Oceanography*, *10*(1), 81-98.

Stroeve, J., M. M. Holland, W. Meier, T. Scambos, and M. C. Serreze (2007), Arctic sea ice decline: faster than forecast, *Geophysical Research Letters*, *34*(9).

Suto, I. (2003), Taxonomy of the marine diatom resting spore genera *Dicladia* Ehrenberg, *Monocladia* gen. nov. and *Syndendrium* Ehrenberg and their stratigraphic significance in Miocene strata, *Diatom Research*, *18*(2), 331-356.

Suto, I. (2004a), *Dispinodiscus* gen. nov., a new diatom resting spore genus from the North Pacific and Norwegian Sea, *Diatom Research*, *20*, 70-94.

Suto, I. (2004b), Fossil marine diatom resting spore morpho-genus *Gemellodiscus* gen. nov. in the North Pacific and Norwegian Sea, *Paleontological Research*, *8*(4), 255-282.

Suto, I. (2004c), Fossil marine diatom resting spore morpho-genus *Xanthiopyxis* Ehrenberg in the Norrth Pacific and Norwegian Sea, *Paleontological Research*, *8*(4), 283-310.

Suto, I. (2005a), *Vallodiscus* gen. nov., a new fossil resting spore morpho-genus related to the marine diatom genus *Chaetoceros* (Bacillariophyceae), *Phycological Research*, *53*, 11-29.

Suto, I. (2005b), Taxonomy and biostratigraphy of the fossil marine diatom resting spore genera *Dicladia* Ehrenberg, *Monocladia* Suto and *Syndendrium* Ehrenberg in the North Pacific and Norwegian Sea, *Diatom Research*, *20*(2), 351-374.

Syvertsen, E.E. (1979), Resting Spore Formation in Clonal Cultures of *Thalassiosira antarctica* Comber, *T. nordenskioeldii* Cleve and *Detonula confervacea* (Cleve) Gran, *Nova Hedwigia*, *64*, 41-63.

Takahashi, K., N. Fujitani, and M. Yanada (2002), Long term monitoring of particle fluxes in the Bering Sea and the central subarctic Pacific Ocean, 1990-2000, *Progress in Oceanography*, *55*, 95-112.

Takahashi, K., A.C Ravelo, C.A. Alvarez Zarikian, and Expedition 323 Scientists (2011), Proceedings of the Integrated Ocean Drilling Program, edited, Tokyo.

Tarasov, Pavel E., Takeshi Nakagawa, Dieter Demske, Hermann Österle, Yaeko Igarashi, Junko Kitagawa, Lyudmila Mokhova, Valentina Bazarova, Masaaki Okuda, Katsuya Gotanda, Norio Miyoshi, Toshiyuki Fujiki, Keiji Takemura, Hitoshi Yonenobu, and Andreas Fleck (2011), Progress in the reconstruction of Quaternary climate dynamics in the Northwest Pacific: A new modern analogue reference dataset and its application to the 430-kyr pollen record from Lake Biwa, *Earth-Science Reviews*, *108*(1-2), 64-79.

Taylor, F., and A. McMinn (2001), Evidence from diatoms for Holocene climate fluctuation along the East Antarctic margin, *The Holocene*, *11*(4), 455-466.

Ternois, Y., K. Kawamura, L. Keigwin, N. Ohkouchi, and T. Nakatsuka (2001), A biomarker approach for assessing marine and terrigenous inputs to the sediments of Sea of Okhotsk for the last 27,000 years, *Geochimica et Cosmochimica Acta*, *65*(5), 791-802.

Thomas, D.N., and G.S. Dieckmann (2003), *Sea ice: an introduction to its physics chemistry biology and geology*.

Thomson, J., F. M. Dyer, and I. W. Croudace (2002), Records of radionuclide deposition in two salt marshes in the United Kingdom with contrasting redox and accumulation conditions, *Geochimica et Cosmochimica Acta*, *66*(6), 1011-1023.

Thunell, R., M.S. Poli, and D. Rio (2002), Changes in deep and intermediate water properties in the western North Atlantic during Marine Isotope Stages 11-12: evidence from ODP Leg 172, *Marine Geology*, *189*, 63-77.

Tomas, C.R. (1996), *Identifying marine diatoms and dinoflagellates*, Academic Press, Inc. Harcourt Brace and Co., Boston, U.S.A.

Tozzi, S., O. Schofield, and P. Falkowski (2004), Historical climate change and ocean turbulence as selective agents for two key phytoplankton functional groups, *Marine Ecology-Progress Series*, *274*, 123-132.

Tzedakis, P. C. (2010), The MIS 11 – MIS 1 analogy, southern European vegetation, atmospheric methane and the "early anthropogenic hypothesis", *Climate of the Past*, *6*, 131-144.

van Hengstum, Peter J., David B. Scott, and Emmanuelle J. Javaux (2009), Foraminifera in elevated Bermudian caves provide further evidence for +21m eustatic sea level during Marine Isotope Stage 11, *Quaternary Science Reviews*, *28*(19-20), 1850-1860.

Vare, L.L., G. Massé, T.R. Gregory, C.W. Smart, and S.T. Belt (2009), Sea ice variations in the central Canadian Arctic Archipelago during the Holocene, *Quaternary Science Reviews*, *28*(13-14), 1354-1366.

von Quillfeldt, C.H. (2000), Common diatom species in arctic spring blooms: their distribution and abundance, *Botanica Marina*, *43*(6), 499-516.

von Quillfeldt, C.H. (2001), Identification of some easily confused common diatom species in Arctic spring blooms, *Botanica Marina*, *44*, 375-389.

von Quillfeldt, C.H. (2004), The diatom *Fragilariopsis cylindrus* and its potential as an indicator species for cold water rather than for sea ice, *Vie Milieu*, *54*(2-3), 137-143.

von Quillfeldt, C.H., W.G. Jr. Ambrose, and L.M. Clough (2003), High number of diatom species in first-year ice from the Chukchi Sea, *Polar Biology*, *26*, 806-818.

Witkowski, A., H. Lange-Bertalot, and D. Metzeltin (2000), *Diatom Flora of Marine Coasts I*, 925 pp., A.R.G. Gantner Verlag K.G., Ruggell, Liechtenstein.

Wolff, E.W., H. Fischer, F. Fundel, U. Ruth, B. Twarloh, G. C. Littot, R. Mulvaney, R. Rothlisberger, M. de Angelis, C. F. Boutron, M. Hansson, U. Jonsell, M. A. Hutterli, F. Lambert, P. Kaufmann, B. Stauffer, T. F. Stocker, J. P. Steffensen, M. Bigler, M. L. Siggaard-Andersen, R. Udisti, S. Becagli, E. Castellano, M. Severi, D. Wagenbach, C. Barbante, P. Gabrielli, and V. Gaspari (2006), Southern Ocean sea-ice extent, productivity and iron flux over the past eight glacial cycles, *Nature*, *440*(7083), 491-496.

Zong, Y. (1997), Implications of *Paralia sulcata* abundance in Scottish isolation basins, *Diatom Research*, *12*, 125-150.